

# **X-RAY STUDIES OF ACTIVE GALACTIC NUCLEI**

*A Thesis*  
*Submitted for the Degree of*  
*Doctor of Philosophy in the Faculty of Science*  
**BANGALORE UNIVERSITY**

*By*  
**S. Soundararajaperumal**

INDIAN INSTITUTE OF ASTROPHYSICS  
BANGALORE 560034  
INDIA

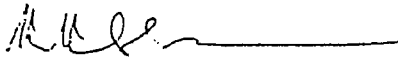
1999 JANUARY

# Declaration

I hereby declare that the matter contained in this Thesis is the result of the investigation carried out by me at the Indian Institute of Astrophysics, Bangalore and the Department of Physics, Bangalore University, Bangalore, under the supervision of Professor K. K. Ghosh. This work has not been submitted for the award of any Degree, Diploma, Associateship, Fellowship, etc. of any University or Institute.

*S. Soundararajaperumal.*  
S. Soundararajaperumal

(Candidate)



K. K. Ghosh

(Supervisor)

Bangalore 560 034

20 January 1999.

## Acknowledgement

I wish to express my sincere gratitude to Prof. K. K. Ghosh, under whose able guidance and supervision the present investigations were carried out. I was initiated into the field of active galaxies, observations, X-ray spectroscopy and data reductions by him. His constant encouragement and guidance were the main driving forces behind this work.

I thank the Director, Indian Institute of Astrophysics for providing all the facilities and for his kind support. My sincere thanks are also due to Dr. R. Srinivasan, Prof. Ch. V. Sastry, Prof. N. Kameswara Rao, Prof. T. P. Prabhu and Prof. C. Sivaram for their support and valuable help.

I am grateful to Prof. B. C. Chandrasekhara, Prof. Ragavendra Rao, Prof. M. N. Anandaram and Mr. V. H. Doddamani, Department of Physics, Bangalore University for their kind help.

My thanks to the Telescope Time Allocation Committee for allotting observing time on the Vainu Bappu telescope and the 102 cm telescope of VBO, Kavalur. It is a pleasure to acknowledge Mr. M. Appakutty, Mr. N. Dinakaran, Mr. M. Ganesan, Mr. M. Gopal, Mr. K. Jayakumar, Mr. K. Kuppuswamy, Mr. V. Moorthy, Mr. A. Muniyandi, Mr. M. Muniraj, Mr. S. Pukalenti, Mr. E. Ramachandran, Mr. V. Ramesh, Mr. A. K. V. Ramanan, Mr. R. Sadhanandan, Mr. G. Selvakumar, Mr. R. Sivakumar, Mr. C. Sundaravadivelu, Mr. N. Subramani, Mr. M. Vadivelu, and Mr. C. Velu and others for their kind help during observations at VBO.

I thank Mr. M. J. Rosario, Mr. S. Pukalenti and Mr. G. Selvakumar for their help at the computer centre of Vainu Bappu Observatory. Thanks also to Mr. K. N. Kutty, Mr. J. S. Nathan and Ms. T. Sivarani for their help at the computer centre of IIA, Bangalore. I express my thanks to Mr. P. Anbazhagan, Mr. K. Ravi, Mr. A. Ramachandran and Mr. S. Venkateswara Rao of VBT Electronics Lab for providing valuable support.

I gratefully acknowledge all the staff members of IIA for their encouragement and for the help they rendered.

I am immensely grateful to my uncle Mr. R. Sivashanmugam for his strong support, care, encouragement and affection. My sincere thanks to my mother, wife and family members for their encouragement and support.

## SUMMARY

Active Galactic Nuclei (AGNs), nuclei of active galaxies, are the most powerful compact objects in the Universe. AGNs emit radiation across the entire electromagnetic spectrum. This type of radiation can not come from stars, as they emit most of their radiation in a narrow band of frequencies, from UV to infrared. The very high energy outputs observed in a very concentrated volume and variability on time scales as short as minutes suggest that the radiation are produced through physical processes other than the nuclear fusion that powers stars. Thus studies on AGNs may help in verifying and developing many new theories in extreme physics. AGNs are natural laboratories in which a large variety of physical processes occur and as a result they emit radiation from radio to  $\gamma$ -rays. Therefore multifrequency observations are necessary in order to understand the energy generation mechanisms. Also it has been found that X-ray emission is a common property of AGNs and it can be considered as a defining characteristic of these sources. X-ray studies can have important consequences in our understanding of AGNs. X-rays are produced by highly energetic particles, such as thermal plasmas at several million degrees or relativistic non thermal plasmas, which might exist at the centre of the active nucleus. The shortest variability time scale observed in the X-rays indicates the association of X-ray emitting domain with the innermost regions of AGNs. Much of the observed luminosity in AGN is radiated in X-rays and  $\gamma$ -rays. It is shown that AGNs radiate at least 10% of their bolometric luminosity in the hard X-ray band ( $\sim 2 - 20$  keV). The reproduction of this energy by circumnuclear material causes much of the radiation in UV, optical and IR frequencies. The X-ray spectrum ( $\sim 0.1 - 100$  keV) of AGNs can be well approximated by a power-law. Deviations from this power-law form can be interpreted as the effects of X-ray reprocessing. A detailed study of this reprocessing yields direct information on the geometry and the nature of material in the central regions of AGNs, which is unresolvable even by the best telescope available today. In this thesis we present the X-ray (0.1-10 keV) spectral analysis, multifrequency studies and optical CCD imaging photometry results of several AGNs. A general introduction about AGNs is presented in **Chapter 1**.

The X-ray spectra (0.1-10 keV) of AGNs discussed in this thesis were obtained from the European X-ray Observational Satellite, EXOSAT. The X-ray Spectral Fitting software

(XSPEC) was used to analyze the X-ray spectra. The optical imaging photometric data were obtained using the 2.3 meter Vainu Bappu Telescope (VBT), the 1 meter telescope and the 0.75 meter telescope existing at the Vainu Bappu Observatory, Kavalur, India. For all the optical observations, Charge Coupled Devices (CCDs) were used as main detectors. The NOAO-IRAF (Image Reduction and Analysis Facility) software was used for processing the CCD images. The photometric analysis was carried out using the digital aperture reduction program DAOPHOT. **Chapter 2** describes about the instrumentation and data reduction procedures.

Results of the X-ray (0.1-10 keV) spectral analysis, multifrequency studies and optical CCD imaging photometry of a sample of AGNs are given in **Chapter 3**. We present the results of our studies on Seyfert galaxies in **Chapter 3.1**. An outline of our analysis is provided in Chapter 3.1.1. In Chapter 3.1.2. the X-ray spectral information on a sample of thirteen Seyfert galaxies are described. From the analysis it has been found that the ME (2-10 keV) X-ray spectra of Seyferts can be adequately described by a simple power-law. Our studies indicate that the soft X-ray excess emission is a common feature of Seyfert galaxies and the detection of soft excess depends on the low-energy absorption in the line-of-sight to the source. The differential variations between the low energy (0.1-2 keV) and the medium energy (2-10 keV) components detected in the Seyfert galaxies 3C382 and MCG 2-58-22 indicate that the soft and the hard X-rays originate from different regions of these galaxies. A significant emission line, (at energies around 6.0 keV) characteristic of iron  $K_{\alpha}$  line emission, is detected in majority (nine out of thirteen) of the sources in our sample. From the distribution of redshifted line energies of our analysis, it is noted that the data are consistent with 6.4 keV.

We participated in the International AGN Watch campaign on the luminous Seyfert 1 galaxy Fairall 9 and the results of this campaign are presented in Chapter 3.1.3. We monitored Fairall-9 in simultaneity with ultraviolet spectroscopic observations with the *IUE* satellite. We detected optical and ultraviolet continuum variations during the observing period. There is no measurable lag between the ultraviolet and optical continuum light curves. The  $H\beta$  emission line was also found to vary. The time lag between  $H\beta$  and ultraviolet continuum was found to be  $\sim 23$  days.

Results of our X-ray spectral analysis along with the radio through X-ray continuum studies and CCD imaging photometric studies of blazars are presented in **Chapter 3.2**. A brief introduction about blazars is given in Chapter 3.2.1. In Chapter 3.2.2 we present the results of the X-ray spectral analysis of the complete sample of twenty eight EXOSAT blazars. The X-ray spectra of the blazars are compared with the radio through ultraviolet multifrequency spectra. The blazars have been divided into two groups: radio-selected blazars (RBLs) and X-ray selected blazars (XBLs). X-ray results suggest that XBLs are steep spectrum sources and RBLs are relatively flat spectrum sources. Even though RBLs are, in general, higher redshift objects than XBLs, they are only slightly more luminous (by a factor of 4-7) in X-rays than XBLs. However, RBLs are much more luminous (by two or three orders of magnitude) in radio than the XBLs. The multifrequency spectra (radio through X-ray) can be well represented with a single parabolic curve for XBLs and with two parabolic curves for RBLs. One of the important differences between the multifrequency spectra of RBLs and XBLs is the spectral discontinuity in the UV-X-ray region of RBLs. Luminosities at different bands have also been computed for all the blazars in the present sample and bimodal character of distribution of these objects has been found in the radio and X-ray luminosity plane. All these results are discussed in the framework of a 'wide-jet' model. In the 'wide jet' model it is assumed that the flow velocity is constant but the degree of beaming increases with decreasing frequency, that is, the opening angle of the X-ray emitting region at the inner part of the jet is much wider than that of the radio emitting region at the outer part.

We participated in the international multifrequency monitoring campaigns to monitor six blazars (PKS0528+13, Mkn501, 3C390.3, BL Lac, 3C446 and CTA102) in the visual band simultaneously with multifrequency observations. Four of them (PKS0528+13, Mkn501, BL Lac, and CTA102) were monitored in simultaneity with *Compton Gamma Ray Observatory* observations. The blazars were observed during their flare states. Our results presented in Chapter 3.2.3., indicate night to night variations in all the sources, except CTA 102. We have detected intranight variations in two of them (Mkn501, BL Lac). The optical photometric and spectroscopic observations of 3C390.3 shows that the broad band fluxes (B, V, R and I), the spectrophotometric optical continuum flux  $F_{\lambda}$  ( at 5177 Å), and the integrated emission-line fluxes of H $\alpha$ , H $\beta$ , H $\gamma$ , He I ( $\lambda$ 5876) and He II  $\lambda$ 4686 show a nearly monotonic increase with

episodes of milder short-term variations superposed. The amplitude of the continuum variations increases with decreasing wavelength (4400-9000 Å). The optical continuum variations follow the variations in the ultraviolet and X-ray with time delays, measured from the centroids of the cross-correlation functions, typically around 5 days, but with uncertainties also typically around 5 days. Zero time delay between the high energy and low-energy continuum variations can not be ruled out. The strong optical emission lines H $\alpha$ , H $\beta$ , H $\gamma$  and He I ( $\lambda$ 5876) respond to the high-energy continuum variations with time delays typically about 20 $\pm$ 08 days.

To study the variations of the two blazars 3C66A and OJ287 in flare states we undertook a program to monitor these sources during 1995 December to 1996 March, when these two sources were in high states. Chapter 3.2.4. describes the outcomes of this program. Large amplitude night to night variations were found in 3C66A and OJ287. Our observations of flaring activity in the blazar OJ287 support the proposed periodicity of 11.6 years.

It is thought that non-periodic short term and periodic long term variabilities may be present in the case of radio-quiet quasars. Long term variability is the small and steady variations of the base level or quiescent state from which shorter and high/low amplitude events or flares apparently erupt. In order to study the long and short term variations, a sample of 20 radio-quiet quasars were observed in B, V and I photometric passbands, during 1995 to 1998 and the results are presented in **Chapter 3.3**. Our observations detected no long term variability in our sample of radio-quiet quasars. However, the radio-quiet quasars Q0101-304, PC0751+56 and Q1317-05 displayed intranight microvariations on a few nights.

Finally, the conclusions drawn in Chapters 3.1. to 3.3. are summarized in **Chapter 4** and at the end of this chapter the future prospects of this field have been highlighted. The references are given at the end. Tables and figures are given in different chapters with the chapter and section numbers indicated by suffixes.

## CONTENTS

<b>1. INTRODUCTION</b>	<b>1</b>
1.1 AGN Phenomenon	1
1.2 Historical Developments	1
1.3 Classification	4
1.3.1 Radio Galaxies	5
1.3.2 Seyfert 1 Galaxies	5
1.3.3 Narrow-line Seyfert 1 Galaxies	5
1.3.4 Seyfert 2 Galaxies	6
1.3.5 Radio-Loud Quasars	6
1.3.6 Radio-Quiet Quasars	7
1.3.7 Blazars	7
1.3.8 Low Ionization Emission-Line Regions	8
1.3.9 Star Burst Galaxies	9
1.3.10 Strong IRAS Galaxies	9
1.4 Structure of AGNs	9
1.4.1 Blackholes	10
1.4.2 Accretion Disks	10
1.4.3 Broad Line Regions	11
1.4.4 Molecular Torus	11
1.4.5 Narrow Line Regions	12
1.4.6 Jets	12
1.5 Radiation Processes	13
1.5.1 Synchrotron	13
1.5.2 Inverse Compton and SSC	14
1.5.3 Blackbody	15
1.5.4 Bremsstrahlung	15
1.6 Unified Theories	15
1.7 Multifrequency observations	16
1.7.1 Radio Observations	17



1.7.2	Infrared Observations	17
1.7.3	Visual Observations	18
1.7.4	Ultraviolet Observations	19
1.7.5	X-ray Observations	20
1.7.6	$\gamma$ - ray Observations	20
1.8	X-ray Studies	22
1.8.1	Need for X-ray Studies	22
1.8.2	History and Some Important Results of X-ray Observations of AGNs.	23
<b>2. INSTRUMENTATION AND DATA REDUCTION METHODS</b>		28
2.1	X-Ray Instrumentation and Reduction Methods	28
2.1.1	The Low Energy Imaging Telescopes	28
2.1.2	The Medium Energy Detector Array	32
2.1.3	X-ray Spectral Analysis	33
2.2	Optical Instrumentation and Reduction Methods	34
2.2.1	Telescopes and CCD detectors	34
2.2.2	Differential Photometric Analysis	37
<b>3. X-RAY AND OPTICAL OBSERVATIONS OF AGNs, RESULTS AND DISCUSSION</b>		40
3.1	Seyfert Galaxies	41
3.1.1	Introduction	41
3.1.2	X-ray Properties of a Sample of Seyfert Galaxies	41
3.1.3	International AGN Watch Campaign Results of Fairall-9	111
3.1.4	Discussion	115
3.1.5	Conclusions	120
3.2	Blazars	122
3.2.1	Introduction	122
3.2.2	X-ray properties and Multifrequency Spectra of a Sample of Blazars	123
3.2.3	International Multifrequency Monitoring Campaign Results of Blazars	161

3.2.4	CCD imaging photometry of the Blazars 3C66A and OJ287	181
3.2.5	Discussion	185
3.2.6	Conclusions	192
3.3	Radio-Quiet Quasars	194
3.3.1	Introduction	194
3.3.2	CCD Imaging Photometry of Radio-Quiet Quasars	194
3.3.3	Discussion	195
3.3.4	Conclusions	195
<b>4.</b>	<b>CONCLUSIONS AND FUTURE PROSPECTS</b>	<b>213</b>
4.1	Seyfert Galaxies	213
4.2	Blazars	215
4.3	Radio-Quiet Quasars	216
4.4	Future Prospects	217
	<b>List of Publications</b>	<b>219</b>
	<b>References</b>	<b>220</b>

# 1. INTRODUCTION

## 1.1. AGN Phenomenon

Only a very small fraction (~1 percent) of all galaxies in the universe have extremely bright compact central nuclei. The nuclear part of such galaxies emit radiation across the entire electromagnetic spectrum, from radio to  $\gamma$  - rays. This type of radiation can not come from stars, as they emit most of their radiation in a narrow band of frequencies, from UV to infrared. These galaxies with an extremely active nucleus are known as Active Galactic Nuclei (AGNs). The very high energy outputs which are observed in a very concentrated volume together with variability on time scales as short as minutes (Doxey et al. 1983; Feigelson et al. 1986) suggest that their radiation are produced through physical processes other than the nuclear fusion that powers stars. Thus studies on AGNs may help in verifying and developing many new theories in extreme physics. AGNs are the earliest assemblage of matter known. The discovery of high redshift quasars ( $z \sim 5$ ) implies that massive condensations occurred very early in the history of the universe (Efstathion & Rees 1988). The spectra of these objects (Schneider, Schmidt & Gunn 1989a,b, 1991) offer probes of the conditions of the early universe (when the universe was less than 10% of its current age). Consequently the studies of AGN are essential to understand the formation and evolution of large scale structures of the universe.

## 1.2. Historical Developments

In the beginning of this century, the presence of extragalactic sources was not known. A general belief at that time was the cosmos consisted only of our own galaxy, the milky way. However, several nebulous objects were known even at that time. Many of them were discovered by Williem Herschel of 18th century and many more were added later by his son John Herschel. Nearly 15000 objects have been included in the four famous catalogues, Messier Catalogue (M) of 1781, Herschel's General Catalogue of nebulae (GC) of 1864, Dreyer's New General Catalogue (NGC) of 1888 and Index Catalogues (IC I and IC II) of 1895 and 1908. Between 1912 and 1925 V. M. Slipher of Lowell Observatory, Arizona, measured the redshifts of many bright nebulous objects without knowing the nature of these sources. Slipher found that most of

these sources have very high line-of-sight recessional velocities. If the nebulae were within our own galaxy, it is too high a velocity to explain. A very few had velocities of approach. The anomalous velocities shown by these nebulae puzzled the astronomers of that time. This velocity puzzle was later solved by Edwin Hubble. In 1923-24 Edwin Hubble found Cepheid variables in Andromeda and other nearby nebulae. Using the period-luminosity relationship of Cepheids, he determined the distances to the nebulae and established that these nebulae were large galaxies of stars outside the Milky Way. During 1924-26 Hubble classified the galaxies based on their structure, which is usually depicted by a tuning fork diagram. In this system he morphologically classified them into ellipticals, lenticulars, normal and barred spirals and irregulars. Most galaxies can be fitted in this classification. The extragalactic nature of these nebulae has made it easy to explain their extraordinary velocities determined by Slipher. In 1929, with the help of Milton Humason in the observations with the 100 inch telescope on Mount Wilson; Hubble found a strong correlation between the recessional velocities and redshifts of these galaxies. This relation is known as Hubble's law. This very important discovery by Hubble and Humason formed the basis of the modern cosmological theories regarding the expanding universe. After the discovery of Hubble's law astronomers started obtaining the spectral information of several galaxies. Usually it was found that, these normal galaxies display continuous spectra with absorption lines like the stellar spectra. Spirals and irregular galaxies show very narrow emission lines also with stellar origin. The composite spectrum is the combination of contributions from various types of constituent stars of the galaxy. Around 1940 Milton Humason and Rudolph Minkowski of Mount Wilson observatory handed over the spectra of several spiral galaxies to a post doctoral student Carl K. Seyfert. Seyfert found that a small proportion of the galaxies (about 2%) show very broad emission lines (Full Width at Half Maximum -FWHM- of hydrogen lines  $\sim 1000 - 5000 \text{ km s}^{-1}$ ) and narrow absorption lines. These galaxies had very bright nuclei and very dim spiral arms, so they looked deceptively like stars in short photographic exposures. The nuclear regions appeared to be about a few light years in diameter (Seyfert 1943). Later galaxies of this type were named after Seyfert himself. This pioneering research by Seyfert was the first step towards the recognition of a new type of astronomical objects AGNs. Another important finding that helped in the eventual recognition of several AGNs was by Karl G. Jansky, a Bell Laboratories engineer. In 1932 Jansky accidentally discovered radio waves from space. In an

effort to find out the source of interference to the radio-telephone service, he built the first radio telescope and he detected radio signal coming from the centre of our galaxy. This was the first astronomical radio observation. The discovery by Jansky gave birth to radio astronomy. By 1960 radio astronomers detected several hundred radio sources. Some of them coincided with optical objects like nebulae and galaxies. Many of the radio sources coincided with star-like sources. These were called as “radio stars”. The very strong radio outputs from these radio stars puzzled the astronomers at that time. In 1960 at the Owens Valley Radio Astronomy Observatory of CIT, John Bolton and Tom Mathews obtained an accurate position of the radio source 3C48. As a follow-up, Palomar astronomer Allan Sandage later took a photograph of the field in September 1960, which showed a star-like object with nebulosity at the radio position. He also obtained the first spectra of this object which contained broad emission lines that could not be identified (Sandage 1960). A suggestion that it was a galaxy was dismissed, at that time, in favour of an interpretation in terms of a peculiar local radio star. Another ‘radio star’ 3C 273 provided the clue to the mystery of the ‘radio stars’. This object was occulted by the moon in 1962. Three Australian radio astronomers Cyril Hazard, M. Mackay and A. Shimmins took advantage of the occultation to establish 3C 273’s accurate coordinates. They found the radio source had two components separated by 19.5 seconds of arc. One of these, the fainter component, coincided with a star-like source from which a faint jet protruded and the brighter component coincided with the jet-like feature (Hazard et al. 1963). Maarten Schmidt took optical spectra of the star-like object 3C273. It was not a continuous spectrum with dark absorption lines like that of a normal star, but had bright, broad emission lines. He identified them with the Balmer series and a line of ionized Magnesium with redshift of 0.158 (Schmidt 1963). This result astonished the astronomers. A little later Schmidt and Jesse Greenstein identified the emission lines of the object 3C48 with the redshift of 0.36. The enormous luminosity of these radio stars calculated based on the redshift distances implied that these objects were not true ‘radio stars’, so the name ‘quasi-stellar radio source’ was coined by J. Greenstein to describe them (Green & Mathews 1963) and Hong-Yee Chiu, Shanghai born American astronomer gave the short form ‘quasar’. The next important discovery was by H. Smith and D. Hoffleit in 1963 when they found light variations in 3C273 of the order of one year (Smith & Hoffleit 1963). Considering the light travel time arguments it was estimated that the

size of the active region to be less than one parsec across, comparable to the size of galactic nuclei. This finding led to the recognition that quasars are the nuclear regions of very active galaxies at great distances. Thus the optical identification of 3C273 in the 1960s was crucial in the eventual recognition of a remarkable new type of extragalactic source. Quasars are the most luminous class of active galactic nuclei. The fore mentioned observational results along with many other broad-band observations prompted theoreticians to predict many new attractive models for the AGN phenomenon during this century. In 1969 Lynden-Bell (1969) first suggested the blackhole accretion disk model for the energy extraction mechanism in AGNs. A standard model which suggests accretion of matter on to a central supermassive, collapsed object has been widely accepted from about 1974 on. Description of this model is presented in Chapter 1.4.

### **1.3. Classification**

Some of the important properties of AGNs are: Compact nuclear region, brighter than that of galaxies of similar Hubble type, nonstellar nuclear continuum emission, nuclear emission lines excited by a nonstellar continuum, variable continuum, variable emission lines and strong X-ray emission.

Depending upon their characteristics, AGNs are classified under various names. The following classes of objects are referred to as AGNs.

1. Radio Galaxies
2. Seyfert 1 Galaxies
3. Narrow-line Seyfert 1 galaxies (NLS1s)
4. Seyfert 2 Galaxies
5. Radio-Loud Quasars (RLQs)
6. Radio-Quiet Quasars (RQQs)
7. Blazars
8. Low Ionization Emission-Line Regions (LINERS)
9. Star Burst Galaxies
10. Strong IRAS Galaxies

The natures of these classes are briefly described below.

### **1.3.1. Radio Galaxies**

The galaxies with strong radio emission are classified in this category. Powerful radio galaxies are usually associated with luminous ellipticals, frequently with pronounced peculiarities and with strong emission lines, whereas weak radio galaxies show weak or no emission lines. Radio maps of many of these objects show jets, a compact core with a flat spectrum that coincides with the nucleus of the galaxy and 'hot spots', the compact regions of high brightness embedded in extensive regions of much lower brightness on opposite sides of the central galaxy. Radio galaxies are classified using the ratio of the distance between the hot spots to the total extent of the source measured from the lowest contour. Those with this ratio less than 0.5 are placed in FR I and the rest in FR II (Fanaroff and Riley 1974; FR I & FR II). The study of this type of radio source is important because it may shed light on the nature of energy-supply mechanisms for double radio sources. The radio structures of giant radio sources are likely to be strongly affected by their environments. Therefore, they can be used as probes of the intergalactic medium.

### **1.3.2 Seyfert 1 Galaxies**

The spectral properties of Seyfert 1 galaxies (Seyfert 1943) resemble that of Radio Quiet Quasars (RQQs) but their luminosity is lower. They show strong, broad permitted emission lines. The typical line widths of these sources (Full Width at Zero Intensity -FWZI  $\sim 3000-5000$  km s<sup>-1</sup>) indicate gas motions at high velocities. Seyfert 1 galaxies also show strong, narrow (FWZI  $\sim 400 - 1000$  km s<sup>-1</sup>) permitted and forbidden lines. The high velocities indicated by the broad lines in Seyfert 1 galaxies are taken to be good evidence of a compact, massive object. The strong and variable hard X-ray emission that is generally observed in these objects is also an indicator for the presence of a compact supermassive central object

### **1.3.3. Narrow-line Seyfert 1 galaxies (NLS1s)**

NLS1s are a peculiar group of AGNs with the following properties (Boller, Brandt & Fink 1996). Most NLS1s show unusually strong Fe II lines relative to H $\beta$  and relatively narrow optical lines of hydrogen. The Balmer lines of hydrogen are having comparable line widths of the forbidden lines such as [O III], [N II] and [S II]. Emission lines from higher ionization iron lines

### **1.3.1. Radio Galaxies**

The galaxies with strong radio emission are classified in this category. Powerful radio galaxies are usually associated with luminous ellipticals, frequently with pronounced peculiarities and with strong emission lines, whereas weak radio galaxies show weak or no emission lines. Radio maps of many of these objects show jets, a compact core with a flat spectrum that coincides with the nucleus of the galaxy and 'hot spots', the compact regions of high brightness embedded in extensive regions of much lower brightness on opposite sides of the central galaxy. Radio galaxies are classified using the ratio of the distance between the hot spots to the total extent of the source measured from the lowest contour. Those with this ratio less than 0.5 are placed in FR I and the rest in FR II (Fanaroff and Riley 1974; FR I & FR II). The study of this type of radio source is important because it may shed light on the nature of energy-supply mechanisms for double radio sources. The radio structures of giant radio sources are likely to be strongly affected by their environments. Therefore, they can be used as probes of the intergalactic medium.

### **1.3.2 Seyfert 1 Galaxies**

The spectral properties of Seyfert 1 galaxies (Seyfert 1943) resemble that of Radio Quiet Quasars (RQQs) but their luminosity is lower. They show strong, broad permitted emission lines. The typical line widths of these sources (Full Width at Zero Intensity -FWZI  $\sim 3000$ - $5000$  km s<sup>-1</sup>) indicate gas motions at high velocities. Seyfert 1 galaxies also show strong, narrow (FWZI  $\sim 400$  -  $1000$  km s<sup>-1</sup>) permitted and forbidden lines. The high velocities indicated by the broad lines in Seyfert 1 galaxies are taken to be good evidence of a compact, massive object. The strong and variable hard X-ray emission that is generally observed in these objects is also an indicator for the presence of a compact supermassive central object.

### **1.3.3. Narrow-line Seyfert 1 galaxies (NLS1s)**

NLS1s are a peculiar group of AGNs with the following properties (Boller, Brandt & Fink 1996). Most NLS1s show unusually strong Fe II lines relative to H $\beta$  and relatively narrow optical lines of hydrogen. The Balmer lines of hydrogen are having comparable line widths of the forbidden lines such as [O III], [N II] and [S II]. Emission lines from higher ionization iron lines



such as [Fe VII] 6087Å and [Fe X] 6375Å are often present in the spectra of NLS1s. The ratio of [O III] 5007 Å to H $\beta$  is  $< 3$ , a level found to discriminate well Seyfert 1s from Seyfert 2s (Shuder & Osterbrock 1981). The FWHM of NLS1 hydrogen Balmer lines is usually in the range  $\sim 500$ - $1500 \text{ km s}^{-1}$ . There is a suggestion that NLS1s are Seyfert 1s with small line-of-sight velocity dispersions in the Broad Line emitting Region (BLR) (Goodrich 1989). Nearly 10 per cent of the optically selected Seyfert 1s and 15-50 per cent of the soft X-ray selected Seyfert 1s are NLS1s. It has been found that NLS1s are generally steeper soft X-ray continuum slopes than normal Seyfert 1s (Boller, Brandt & Fink 1996).

#### **1.3.4. Seyfert 2 Galaxies**

Seyfert 2 galaxies (Seyfert 1943) are less luminous than Seyfert 1 galaxies and generally they do not show broad emission lines. The narrow lines (FWZI  $\sim 400 - 1000 \text{ km s}^{-1}$ ) are similar in width and excitation to the narrow lines of Seyfert 1 galaxies. The discovery of the polarized broad lines from the typical Seyfert 1 galaxy NGC 1068 via spectropolarimetry (Antonucci & Miller 1985) suggested that the central parts of NGC1068 have characteristics of a Seyfert 1 galaxy, but they are obscured by the optically thick material in the line-of-sight presumably the molecular torus. The non-thermal continuum and broad lines can be explained as features of the nuclear region that have been scattered over the top of the torus by ionized material. This model has been referred to as the unified Seyfert model. The discovery of broad lines in the polarization spectra of several Seyfert 2 galaxies (Miller & Goodrich 1990), the perpendicularity of the angle between the direction of polarization and the axis of the radio jet (Brindal et al. 1990) are among the observational evidence in support of this model.

#### **1.3.5. Radio-Loud Quasars (RLQs)**

The quasi-stellar radio sources for which the logarithm of the ratio of the radio and B-band flux is greater than 1 ( $\log F_{5\text{GHz}}/F_B > 1$ ) (Lawson et al. 1992) are classified as radio-loud quasars. Less than 1% of quasars only have radio fluxes comparable to the optical flux (Weedman 1986). Radio-loud quasars are divided into two groups, those with their radio spectral index ( $\alpha_r$ ) greater than 0.5 are called steep spectrum radio quasars (SSRQs) and the flatter ones are called flat spectrum radio quasars (FSRQs). The radio characteristics of the RLQs resemble

those of powerful radio galaxies, but the optical image is dominated by a bluish unresolved luminous nucleus with strong broad emission lines in its optical spectrum (Woltjer 1990). Apparent superluminal motions were found in many radio-loud quasars.

### **1.3.6. Radio-Quiet Quasars (RQQs)**

Radio-quiet and radio-loud quasars have very similar properties in the ultraviolet, optical and near infrared bands, but their radio powers differ by several orders of magnitude. RLQs are more luminous in radio by a factor of  $10^4$  or so for a given far-IR luminosity (Lawson & Turner 1997). Also RLQs are generally relatively brighter at X-rays than RQQs (Worrall et al. 1987; Zamorani et al. 1981; Lawson & Turner 1997). The UV to optical continuum of RQQs usually show a flat power-law, suggesting a non-thermal origin. The convex shaped infrared continuum normally seen in RQQs has been explained by a combination of two thermal components. One is due to the warm dust present in the nuclear region heated by the optical/UV continuum (Rees et al. 1969) and the other one is thermal emission from stars and cool dust in the host galaxy's disk (Barvainis 1990). X-ray spectra of RQQs are, in general, steeper than the RLQs (Lawson et al. 1992).

### **1.3.7 Blazars**

The term 'blazar' was coined by E. Spiegel in a banquet speech at the Pittsburgh meeting on BL Lacertae objects (Wolfe 1978), which was the topic of the first conference after the discovery of the first example of a BL Lacertae object (Schmidt 1968). Around that time the characteristics of BL Lac objects were reviewed by Kinman (1975), Stein, O'Dell & Strittmatter (1976), and Stein (1978), and more than 50 objects were classified as BL Lac objects based on the following characteristics : (1) strong variability at radio, optical, infrared and X-ray frequencies; (2) strong and variable linear polarization in the radio, infrared, and optical bands; and (3) featureless (or weak emission and/or absorption) optical spectrum. The featureless optical continuum may be due to the absence of gas around the BL Lac objects, which was suggested based on the radio (Jones & O'Dell 1977), optical (Strittmatter et al. 1974; Wills & Wills 1976; Miller, French & Hawley 1978), ultraviolet (Bosenberg et al. 1978), and X-ray (Mushotzky et al. 1978) observations. However, several BL Lac objects which are embedded in the nuclei of galaxies

were also detected (Ulrich et al. 1975). The above listed characteristics of blazars suggest that the overall electromagnetic spectra are dominated by Doppler-boosted (details of Doppler-boosting can be seen in Chapter 1.4.6) radiation from relativistic jet pointing closely to our line-of-sight. The VLBI maps of several blazars show jets that consist of discrete emitting blobs which exhibit superluminal motion: apparent speeds greater than that of light. This phenomenon occurs for emitting regions moving at very high speeds at small angle to the line-of-sight (Rees 1966). Thus the detection of superluminal motions in blazars is an observational evidence for the presence of relativistic jets pointing closely to our line-of-sight. It is shown that Doppler-boosted Synchrotron Self Compton (SSC) emission is responsible for the high energy  $\gamma$  - ray emission in AGNs (e.g. Kubo et al 1998 and references therein). Since blazar jets are aligned closely to the line of sight, the expected Doppler factor is more for them and hence their  $\gamma$  - ray emission is enhanced many folds by this mechanism. This may be the reason that almost all of the AGNs detected so far with EGRET, the highest energy (20 MeV to 30 GeV) instrument on *Compton Gamma Ray Observatory* (CGRO) are blazars. Almost all the EGRET blazars exhibit superluminal motion (Hartman et al. 1993), indicating that the jet is the source of  $\gamma$  - ray emission. In 1980 Angel & Stockman (1980) made a list of blazars which were usually variable and highly polarized objects. Later Moore & Stockman (1981, 1984) produced a list of highly polarized quasars (HPQs) and around that time the term 'optically violent variable' (OVV) was also introduced (Angel & Stockman 1980); Ledden & O'Dell 1985). Presently, BL Lac objects, HPQs and OVVs are classed as blazars. They are core dominated sources, displaying rapid variability, and relatively high optical polarization.

### **1.3.8. Low Ionization Nuclear Emission Line Region (LINER)**

LINERs are the least luminous AGNs. Over 30% of all spirals show this phenomenon. The non stellar luminosity of most LINERs is small compared with the stellar continuum (Netzer 1990; and references therein). The strongest emission lines are of low ionization species and are narrower ( $200 - 400 \text{ km s}^{-1}$ ) than the narrow lines of Seyfert galaxies

### **1.3.9. Starburst Galaxies**

A very high rate of star-formation, far greater than the average during a galactic life time, takes place in starburst galaxies. It has been estimated from the study of  $H_{\alpha}$  flux in interacting galaxies, that the star-formation rate is 6 times higher than the normal galaxies (Bushouse 1987). A general feature is that star formation is more concentrated towards the centre (Hummel 1981). Huge starbursts are found almost always towards nuclei (Bushouse 1987; Kennicutt et al. 1986). In starburst galaxies, unlike quasars and Seyferts, BLR is absent for the emission lines. No part of the continuum is variable, so there is no evidence for relativistic beaming effects. UV continuum shows absorption lines, characteristic of hot and massive stars. This gives the evidence that hot stars, forming and dying in great numbers, provide the fundamental power source. There is additional evidence that other AGN also may have sometimes high rates of star formation in the host galaxies.

### **1.3.10. Strong IRAS Galaxies**

The Infrared Astronomical Satellite, IRAS, discovered a class of luminous infrared galaxies, some of which emit over 90% of their energy in the far infrared (FIR) region of the spectrum. Much of this radiation is believed to be re-radiation from dust which is heated by an AGN or by a burst of star formation. Since their discovery, strong IRAS galaxies ( $L_{\text{FIR}} \geq 10^{12} L_{\odot}$ ) have become key targets to study the relationship between galaxy interactions, enhanced circumnuclear star formation, and to investigate the creation of a massive blackhole in their nucleus as the end product of the starburst (Heckman 1990; Norman & Scoville 1988).

## **1.4. Structure of AGN**

Multifrequency observational studies (Krolik & Begelman 1986; Blandford & Rees 1978) and certain theoretical considerations (Rees 1984) provide a cylindrically symmetric, heterogeneous, unified model for AGN. The widely accepted, approximate structure is described below.

At the centre there is a supermassive blackhole whose gravitational potential energy is the source of the AGN luminosity. The X-ray source whose nature is unknown is very close to the

blackhole. This X-ray source illuminates an optically thick, geometrically thin accretion disk, situated at a few milli pc from the centre, giving rise to a Compton reflected spectrum and many emission lines (iron  $K_{\alpha}$  is one of the strongest lines). Further out, about a few parsecs from the nucleus are clouds of gas moving rapidly in the potential of blackhole, this is the broad line region (BLR). A thick obscuring molecular torus ( $\sim 1$  kpc from the centre) is situated beyond the BLR. Slower moving clouds of gas that produce narrow emission lines were found in the Narrow Line emitting Region (NLR) about 100 pc from the blackhole. A column of highly ionized material, possibly formed by irradiation of the inner edge of molecular torus fills the central hole portion of the torus. Highly energetic particles escaping along the poles of the torus or accretion disk form collimated radio-emitting jets which extend upto 1 Mpc (also sub-parsec jets have been observed in many AGNs).

#### **1.4.1. Blackholes**

Rapid variability, high efficiency of conversion of rest mass into energy (Soltan 1982), the recent discovery of broadened and skewed iron  $K_{\alpha}$  emission lines in the X-ray spectra of AGNs (Nandra et al. 1997) are among the several observational evidences that favour the supermassive blackhole model. The observational and circumstantial evidences favours that a blackhole of mass  $10^6$ - $10^8 M_{\odot}$  lie at the centre of a typical AGN. It has been deduced that a central mass  $M$  will have a gravitational radius,

$$r_g = \frac{GM}{c^2}$$

for a blackhole with  $10^8 M_{\odot}$   $r_g = 1.5 \times 10^{13}$  cm. Hence, usually, in an AGN the region of blackhole and its magnetosphere engulfs a spherical volume with radius of the order of  $10^{13}$  cm.

#### **1.4.2. Accretion Disks**

The fast time variations of the optical and UV continuum observed in several AGN are not consistent with their being caused by variations of the accretion rate. Possible origin of the fast variations would be either the instabilities in the innermost region of the disk or the irradiation of the disk surface by the variable X-ray source (Ulrich 1990). Jets and ionization cones provide indirect evidence for a durable symmetry axis, most probably, associated with the angular

momentum of accreting gas. It is suggested, based on the observed broad Fe K $\alpha$  emission in AGN (Ghosh & S.Soundararajaperumal 1992c; and references therein), that the line emission is primarily due to the bulk plasma motions in a Keplerian disk irradiated with X-rays emitted near the central collapsed object. The 'big blue bump' (see Chapter 1.7.3.) and the soft X-ray excess (Arnaud et al. 1985; Ghosh & Soundararajaperumal, 1992a,b) are the other indicators of the presence of an accretion disk in AGN. The observed spectral properties suggest that the inner and outer radii of the accretion disk (R) may lie in the range  $10r_g < R < 10^3 r_g$  (Collin-Souffrin 1992; and references therein).

#### **1.4.3. Broad Line Region (BLR)**

The observed properties of AGNs, described below, lead to the conclusion that the broad-line emissions originate in a complex ensemble of clouds of cold and dense gas concentrations. The region in which these clouds are common in an AGN is called BLR. The broad line variability found in AGNs suggests that the size of the BLR to be 10-100 light days in Seyfert 1 galaxies and up to a few light years in bright quasars (Netzer 1990; and references therein). The absence of strong, broad forbidden lines indicate the electron density to be at least  $10^8 \text{ cm}^{-3}$ . The typical gas velocity is  $300 \text{ km s}^{-1}$  to  $1000 \text{ km s}^{-1}$ . Variations in line profile parameters such as asymmetry and width can place constraints on the kinematics of the BLR clouds. For instance, a systematic red and blue asymmetry may imply radial motion in BLR clouds. An increase in line width during a continuum outburst suggests rotational motion and no change in width implies chaotic bulk motion. Different models for BLR and NLR are described by Netzer (1990). The basic challenge for BLR models is to explain the physical mechanism that protects the clouds from disintegration in the extreme environment of an AGN.

#### **1.4.4. Molecular Torus**

The unified scheme of Seyfert galaxies assume that a geometrically thick molecular torus or (warped disk) surrounds the active nucleus (Antonucci & Miller 1985; Krolik & Begelman 1988). A great deal of observational evidence suggests the existence of such dusty material present in the zone between the broad and narrow emission line regions. Spectropolarimetric and polarimetric observations of type 2 Seyferts (Antonucci & Miller 1985; Miller and Goodrich

1990) have shown that a torus of obscuring material hides a probable type 1 Seyfert nucleus in these objects. This obscuring torus must possess a high degree of dust extinction in order to block the nuclear light effectively. In a large sample of 48 Seyferts studied by Edelson, Malkan & Rieke (1987) the infrared spectra of most of the Seyfert galaxies have far-infrared excesses which can be interpreted as reradiation of nuclear emission by the dust surrounding the nucleus. Theoretical models and observations predict the size of the molecular torus to be typically of the order of a few kpc.

#### **1.4.5. Narrow Line Region (NLR)**

The observed nonvariability of the narrow emission lines in objects undergoing continuum variations suggest that the NLR must be much larger than the BLR. Ground based observations of many Seyfert galaxies have resolved the NLR. These observations show that the NLR dimension to be of the order of 100 - 300 pc. The signatures of the presence of NLR in quasars is not well established by the observations. Yet there are theoretical reasons to believe that the size of NLR to be of the order of few kpc in quasars. The typical density of a narrow line cloud is  $10^3 - 10^6 \text{ cm}^{-3}$  and the gas velocity is  $300-1000 \text{ km s}^{-1}$  (Netzer 1990; and references therein).

#### **1.4.6. Jets**

In 1953 Jennison and Das Gupta (1953) discovered that the radio emission from Cygnus A originated from the two lobes of the associated optical galaxy rather than the galaxy itself. Subsequent observations of other powerful radio sources showed that this was a general phenomenon (Blandford 1990; and references therein). The idea that the lobes were continuously fueled along the channels, called jets, was proposed by Rees (Rees 1971). Jets had already been seen in sources like M87 and 3C273. In 1918 H.D.Curtis found M87 to have a visible jet which is the first discovery of jet emission in an astronomical object. Baade and Minkowski (1954) were the first to use the terminology jet while describing the elongated optical emission structure in the nucleus of M87 (Bridle & Perley 1984). Many powerful radio sources show only one jet though they usually have two lobes. Another curious phenomenon is superluminal motion in which jets appear to travel outwards from the nucleus with apparent velocities as high as 20 times the speed of light. In addition to these two phenomena a wide

range of observations of compact core sources can be explained in the framework of relativistic beaming scenario. In this model the observed flux density  $F_o$  of a relativistic jet is related to its emitted flux density  $F_e$  via

$$F_o = \delta^p F_e$$

Where  $\delta$ , the kinematic Doppler factor for the jet, is defined by  $\delta = [\gamma(1 - \beta \cos \theta)]^{-1}$ ,  $\beta = v/c$ ,  $v$  is the velocity of the jet,  $\gamma = (1 - \beta^2)^{-1/2}$  is the Lorentz factor, and  $\theta$  is the angle between the velocity vector and the line of sight (Urry & Shafer 1984). The exponent  $p$  depends on assumptions about the spectrum of jet emission, the structure of the jet and the frequencies at which comparisons are made (Urry & Shafer 1984; references therein). The one sidedness of jet emission is a natural consequence of bulk relativistic motion since the flux density of the approaching jet is enhanced while that of the receding one is diminished. The new observational evidence for the presence of relativistic bipolar plasma motion comes from the discovery, made using the EGRET, that bright compact, flat-spectrum radio sources are frequently associated with unexpectedly large hard ( $\sim 100$  MeV - 10 GeV)  $\gamma$  - ray fluxes. The interpretation of these  $\gamma$  - ray sources is that they involve inverse Compton scattering of UV and X-ray soft photons by relativistic electrons or positrons accelerated within the outflowing jet (Blandford 1994; and references therein). In a few cases jets up to Mpc scales have been observed.

## 1.5. Radiation Processes

The nature of physical processes occurring deep inside the AGNs can be understood by studying the radiation they emit. This is produced by a wide variety of mechanisms within AGNs. Some of the dominant radiation processes of AGNs are briefly outlined described in this section.

### 1.5.1. Synchrotron

Electrically charged particles emit electromagnetic radiation whenever they change their speed or direction of motion. The radiation produced by non-relativistic charged particles circling around a magnetic field is known as cyclotron radiation. The frequency of emission is simply the frequency of gyration of these particles in the magnetic field. However, for extreme relativistic



particles the frequency of emitted radiation can extend many times the gyration frequency. This radiation is known as synchrotron radiation. Synchrotron radiation is continuous and highly polarized. Synchrotron emission is responsible for the radio emission from jets and lobes. If the electrons are accelerated to high enough energies then it can emit radiation even at X-ray frequencies. Since the spectra of AGNs at different energy ranges display the characteristics of synchrotron radiation, the determination of the spectrum makes possible a calculation of the concentration and energy spectrum of the relativistic electrons in the emission sources, as illustrated below.

The electrons in the emitting regions in AGNs have a wide range of energies. The number density of electrons with energies between  $E$  and  $E+dE$  can be approximately expressed in the power-law form,

$$N(E)dE \propto E^{-p} dE$$

For such a power-law distribution of electrons it is shown that (e.g. Rybicki & Lightman 1979)

$$P_{\text{tot}}(\omega) \propto \omega^{-(p-1)/2}$$

Where  $P_{\text{tot}}(\omega)$  is the total power emitted per unit volume per unit frequency. Often the AGN spectrum can be approximated by a power-law, over a range of frequency, in the form

$$P(\omega) \propto \omega^{-s}$$

Where  $s$  is the spectral index of the radiation. Hence for power-law distribution of particle energies with index  $p$ , over a sufficiently broad energy range, the spectral index of the radiation

is

$$s = \frac{p-1}{2}$$

### **1.5.2. Inverse Compton and SSC**

This process also involves relativistic charged particles. In this process the highly accelerated charged particle imparts a part of its energy to the interacting ambient photon. In this case the energy of the photon is much less than rest mass energy of the electron. i.e.  $\gamma h\nu \ll m_e c^2$ . When a synchrotron source is sufficiently compact that the synchrotron radiation photons are inverse Compton scattered by the relativistic electrons, then the emergent spectrum is known as synchrotron-self-Compton (SSC) radiation (Band & Grindlay 1985).

### **1.5.3. Blackbody**

The electromagnetic radiation from a blackbody, a perfect absorber, in thermodynamic equilibrium at a given temperature (T) is known as blackbody radiation or thermal radiation. Blackbody radiation is the maximum amount of radiation that can be emitted by hot solid bodies. It is of theoretical importance in the history of Physics because through the study of its properties Planck was lead to the initial ideas of the quantum theory (Planck 1901). The brightness of the radiation from a blackbody at the temperature T is

$$B_{\nu}(T) = \frac{2h\nu^3}{c^2} \frac{n_{\nu}^2}{[\exp(h\nu / kT) - 1]} \text{ erg cm}^{-2} \text{ s}^{-1} \text{ Hz}^{-1} \text{ Str.}^{-1}$$

where  $n_{\nu}$  is the refractive index of the medium at frequency  $\nu$  and  $h$  and  $k$  are the Planck and Boltzman constants respectively. The above expression is known as Planck's law. Blackbody radiation is isotropic and unpolarized and has a continuous distribution of frequencies.

### **1.5.4. Thermal Bremsstrahlung**

Radiation due to the acceleration of a charge in the Coulomb field of another charge is called bremsstrahlung or free-free radiation. This radiation is emitted when electrons interact with ions or positrons. When the energy radiated by the single speed electron is averaged over a thermal distribution of speeds in an emitting plasma, it is known as thermal bremsstrahlung.

## **1.6. Unified Theories of AGN**

Based on the characteristics of anisotropic spectral emissions, active galactic nuclei have been divided into many categories. There have been several attempts to unify the AGN classes. The following theory is considered to be favourable as it satisfies most of the observed properties of different classes of AGNs. In this model there are two basic types of AGNs: the radio-quiets and the radio-louds. For each type there is a range of intrinsic luminosities. However, their basic structure, mentioned earlier, assumed to be similar for all these classes. This means that intrinsically identical AGNs at a given intrinsic luminosity display different spectral properties when observed at different orientations (Barthel 1989; Antonucci 1993; and references therein). Since the plasma in jets moves at nearly the speed of light, its radio emission is boosted many

fold because of relativistic beaming (Rees 1966). Thus the approaching jet appears very bright, the receding one undetectably faint. When an AGN is viewed from the side, the thick molecular torus obscures the galaxy's nucleus at visible wavelengths but has no effect on the radio jets; thus, the object looks like a radio galaxy. When viewed obliquely, the torus does not hide the central source and the object looks like a quasar. Its radio emitting regions are foreshortened due to perspective. Those with one jet pointed almost along the line of sight are blazars (either RBLs or XBLs), the most rapidly varying, highly polarized, highly luminous type of AGN. The strongest case for unification originates from relativistic beaming. An essential step in establishing a unification scheme is the correct association of parent with beamed object, usually this is done through comparison of other properties assumed to be independent of orientation. The unification of Seyfert 1 and Seyfert 2 galaxies also based on the argument of obscuration by the dust torus. The spectropolarimetric studies of hidden Seyfert 1 nuclei within several Seyfert 2 galaxies gives the strongest evidence for this unification model. Hence according to this unification theory the observed properties of AGN are highly dependent on the viewing angle. Both relativistic beaming and obscuration are instrumental in causing the differences in properties of parent and beamed sources.

## **1.7. Multifrequency Observations**

AGNs radiate over the entire electromagnetic spectrum from radio to  $\gamma$  - rays. Therefore it becomes an important problem to understand the emission and energy generation mechanisms that produce the overall spectral energy distributions. These distributions may arise from a combination of different emission mechanisms like, thermal and nonthermal. It may also be noted that the classification of AGN also heavily dependent on the overall spectral behaviour of these sources. Understanding the physics of these objects therefore requires the observational data from many different spectral regions. Until the beginning of the space era, only ground-based optical, near infrared and some radio observations were possible. Now, thanks to the advent of spacecraft and to the fast development of technologies, it becomes possible to observe almost in the entire electromagnetic spectrum. The absorption of the interstellar medium in the extreme ultraviolet (EUV) range and the absorption of the interstellar and interplanetary medium

in the radio range are the only two exceptions. The multifrequency data of several AGNs showed differential variability in flux and in shape of the emitted spectra which indicate that different processes are involved in the production of anisotropic emission in different bands of the AGN electromagnetic spectrum. Therefore multifrequency observations are necessary for the actual comprehension of the intriguing physics governing the behaviour of AGN. Though the present work reported in this thesis started with an intention to analyze only the X-ray data of AGNs, the scientific justifications mentioned above compelled the inclusion of data from other bands too. Hence this thesis outlines the multifrequency behaviour of AGNs also, along with the detailed X-ray spectroscopic results.

### **1.7.1 Radio Observations**

Radio emission from extragalactic radio sources is essentially due to the synchrotron process. Thermal emission is a minor contributor in spiral galaxies and is negligible in elliptical galaxies and quasars. The very large array (VLA) is the most sensitive device for determining fluxes of AGNs at wavelengths ranging 2 to 20 cm. In the VLA the individual antennas are wired together for data acquisition. This limits, the separation of the baseline. The angular resolution is dependent on baseline separation. So to get improved resolution, radio astronomers devised a new idea of using disconnected telescopes that take reference to local clocks. Data are combined after observation. This is the principle of Very Long Baseline Interferometry (VLBI) which can use antennas separated by thousand of kilometers.

### **1.7.2. Infrared observations**

Almost all known radio-quiet AGN emit a large fraction of their total energy at infrared wavelengths. Mainly thermal reradiation of incident optical and ultraviolet continuum by the dust is the cause for the IR continuum (Rees et al. 1969). The thermal emission produces a very steep spectrum which curves downwards at shorter wavelengths as a result of Wien cutoff. Thermal far-infrared emission is also mostly associated with dust reddening of the nuclear emission lines and nonstellar continuum. Some AGNs produce their IR continua by nonthermal processes. Rapid variability in the infrared and high polarization observed in blazars evidently show that the IR continuum is of nonthermal origin (Angel & Stockman 1980). They also display flat infrared

spectra (Ghosh & Soundararajaperumal 1994; Impey & Neugebauer 1987) which favours a nonthermal model. Flat power law infrared continuum is seen in many quasars also (Edelson 1986). Though lot of study has been done on AGNs in their near infrared region, using ground based telescopes, the complete far-infrared (FIR) study was not possible until the launch of the *Infrared Astronomical Satellite (IRAS)*. Obscuration by the Earth's atmosphere and thermal emission from warm telescopes were the main hurdles for the infrared spectroscopy. IRAS contained a cryogenically cooled telescope orbiting above the Earth's atmosphere which made an unbiased all-sky survey at 12, 25, 60 and 100  $\mu\text{m}$  (Neugebauer et al. 1984). In September 1995, the European Space Agency (ESA) launched the Infrared Space Observatory (ISO). ISO is designed to observe astronomical objects in the range 2.5 - 200  $\mu\text{m}$ .

### **1.7.3. Visual observations**

Several mechanisms have been proposed for the origin of visual wavelength continua of AGNs. It is usually assumed that visual spectral emission comes from a thermal accretion disk at temperatures  $10^4 - 10^5$  K (Shields 1978; Malkan & Sargent 1982). It has been noticed that in most of the AGNs the power generally peaks in the optical to soft X-ray region. The most prominent feature in multifrequency continuum of AGNs is this excess power, known as, the 'big blue bump' (BBB) which extends from optical to the extreme ultraviolet band. It is theoretically derived that for geometrically thin and optically thick accretion disks (Shakura & Sunyaev 1973), the emergent spectrum, of the blackbody radiation from different radii along the disk, will have the form  $F_\nu \propto \nu^{1/3}$ . It was observationally proved that (Malkan & Sargent 1982) the UV through optical continuum of several AGNs is the combination of this underlying power-law of the form  $F_\nu \propto \nu^{1/3}$  and a pseudo-continuum bump around 3000  $\text{\AA}$  (UV bump). This UV bump is created by the combination of Balmer continuum and blended Fe II lines. Synchrotron emission would be a possible physical mechanism for explaining the featureless power-law continuum found in blazars and some quasars. The correlated luminosity relation of visual continuum of blazars with radio and X-ray bands (e.g. Ghosh & Soundararajaperumal 1995) indicate that same or related mechanisms are responsible for producing these radiations. A substantial fraction of all the presently known AGNs exhibit variability in the optical domain. At

least two types of variability may be simultaneously present in a source, comprising a superposition of short and long term variabilities (Wallinder et al. 1992). Kinematical, hydrodynamical, thermal and radiative transfer effects may be responsible for the observed variability patterns. Over a period of 3 years (1995 - 1998) the CCD photometric data for a sample of 30 AGNs have been collected for the study of variability using the 0.75m, 1m and 2.34m Vainu Bappu telescope of Vainu Bappu Observatory, Kavalur, India and the results are discussed in the Chapter 3. The study of variability is instrumental for understanding the physical conditions in the central regions of AGNs.

#### **1.7.4. Ultraviolet observations**

A well known property of AGNs is the flux and shape variability in all wavebands. It is especially useful to study the ultraviolet variability of AGNs because the large amplitude continuum variations can be compared with variations in the emission lines. Also the relationship of the ultraviolet continuum variation with the variations of spectral properties in other bands can provide clear picture of the geometry of the emitting region. To study the UV spectral properties of astronomical objects, the International Ultraviolet Explorer (IUE) satellite was launched in 1978 January. The unpredicted very long (15 years) life span of the satellite has provided several thousands of spectra of many sources from 1200 Å to 3300 Å. IUE has gathered over 4500 spectra of some 500 AGNs in this period. IUE observations of AGNs have led to a number of important findings, including the discovery of the “UV bump” and the estimation of the BLR size in Seyfert 1s. (e.g. Malkan, Alloin & Shore 1989; Clavel et al. 1991). IUE observations provided, for the first time, a view of the UV spectrum of Seyfert 1 galaxies. The studies of the Fe II lines and the evaluation of the extension of the “Baldwin relation” towards lower luminosities (Wamsteker & Colina 1986) provided clues to the connection between the Seyfert 1s and QSOs. The Hubble Space Telescope (HST) was launched in 1990 and is providing a good quality UV data. With comparatively more collecting area HST has reached more than eight magnitudes fainter objects with comparable resolution to that of IUE. Low and moderate resolution spectroscopy are achieved with the faint object spectrograph (FOS) and the high resolution spectrograph (HRS) can provide high resolution spectroscopy of brighter sources. To study the extreme ultraviolet (EUV), the Extreme Ultraviolet Explorer

(EUVE) satellite was launched from US in 1992. It conducted all-sky all-band survey for EUV sources. In 1993 it began spectroscopic observations using three spectral channels covering 70 - 760 Å region at a spectral resolving power of  $\sim 250$  (Bower 1994). EUV observations of the blazar PKS 2155-304 revealed it to be a detectable source of EUV emission. EUV light curve show about 10% variation in output over a 1.3 day observing period, in contrast to the more extreme variability of this object at both hard X-ray and UV wavelengths (Marshall et al. 1993; Bower 1994). The all-sky survey detected a total of six extragalactic objects (Mkn279, 1H 0419-577, Mkn421, Mkn180, Mkn501 and PKS2155-304) in the 50 Å - 180 Å band. All of them are AGNs which include 4 blazars. The detection of extragalactic sources in EUV range indicates that there must be several low column density lines of sight that extend into the galactic halo.

#### **1.7.5. X-ray observations**

During the last four decades X-ray astronomy has taken a very important place in the observational astrophysics. We also see large concentration of relativistic electrons interacting with photon fields or magnetic fields. AGNs are the predominant category of X-ray sources in the sky. Majority of the X-ray sources detected by the all-sky surveys of several X-ray satellites are AGNs. Early X-ray studies of AGNs were conducted in late 1960s, by means of sounding rockets. Now X-ray astronomy has taken new dimensions with the flight of several advanced new generation space observatories. A detailed account on the history of X-ray studies and present day advancements in the field of AGN research is given in section 1.8.

#### **1.7.6. $\gamma$ - ray observations**

$\gamma$  - rays are the most energetic photons having energies ranging from  $10^7$  eV to more than  $10^{15}$  eV. The interaction of  $\gamma$  - rays with the gases in the terrestrial atmosphere prevents the detection of low energy ( $< 10^{12}$  eV)  $\gamma$  - rays from the ground based observations. However, the most energetic  $\gamma$  - rays can be observed from the ground. The interaction of such high energy photons with the atmosphere produces electron-positron pairs at an altitude of about 20 km from the mean sea level. The annihilation of positron and bremsstrahlung electrons produces  $\gamma$  - ray photons. This process cascades into a shower of relativistic electrons which emit Cerenkov

radiation in the direction of motion. This optical radiation can be collected by an array of telescopes. Such a system of atmospheric Cerenkov telescopes is being operated at several observatories for the study of TeV  $\gamma$  - rays. Also satellites have been flown to monitor the  $\gamma$  - radiation of the celestial objects from the space. The OSO-3 was the first satellite to detect  $\gamma$  - rays from the outer space in 1972. Later several missions have been sent to space for the study of  $\gamma$  - ray emitters, like the Indian mission of a series of satellites called SROSS (Marar 1996; and references therein). The Arthur Holly Compton Gamma Ray Observatory (CGRO) is a major mission for the extensive studies of astronomical  $\gamma$  - ray sources in a wide range of frequencies. It was launched by NASA on 5 April 1991. CGRO represents a dramatic increase in capability over previous  $\gamma$  - ray missions. The four scientific instruments on CGRO covers the hard X-ray and  $\gamma$  - ray energy regimes from 15 keV to 30 GeV. The four instruments are (1) Burst And Transient Source Experiment (BATSE : 15 keV - 2 MeV), (2) Oriented Scintillation Spectrometer Experiment (OSSE : 0.1 - 10 MeV), (3) Imaging Compton Telescope (COMPTEL : 1- 30 MeV) and (4) Energetic Gamma Ray Experiment Telescope (EGRET : 20 MeV - 30 GeV). A new and more sensitive instrument named Gamma ray Large-Area Space Telescope (GLAST) is now under study and development by a large international collaboration is in progress (Tau et al. 1996; Leonard 1996). Already prior to the launch of CGRO, AGNs had been expected to have their peak luminosities at  $\gamma$  - ray energies. This prediction is now confirmed with the experiments by the CGRO. Almost all the AGNs detected by EGRET are blazars (or grazars, the gamma ray blazars) (Mayer-Hasselwander 1996). The observations of these grazars at other wavelengths indicate the alignment of jet axis in the line of sight to these sources. There is an indication of a rapid time variability in these objects in the  $\gamma$  - ray regime. The blazar PKS0528+134 and 3C279 showed variability on the order of a few days. EGRET observed 3C279 to increase its emission by a factor of 5 within a week which decreased over two days (MPE report 1992). The results derived from the EGRET observations suggest that the high energy  $\gamma$  - radiation originates from the jets. EGRET could not detect  $\gamma$  - radiation from any Seyfert galaxy, so far, in its high energy band width. However, almost all the sources detected in the energy range of 50 keV - 1 MeV by OSSE are Seyfert and radio galaxies (Kniffen et al. 1994).



Based on the comprehensive studies of the observed behaviour of the radio through  $\gamma$  - ray spectral energy distributions of AGNs, released by a wide range of physical processes, several theoretical models are being proposed and tested. With the advent of more sensitive instruments and coordinated simultaneous multifrequency observations the knowledge of the AGN phenomenon is developing steadily.

## **1.8. X-ray studies**

### ***1.8.1. Need for X-ray studies***

X-ray emission is an extremely common property of active galactic nuclei (Elvis et al. 1978; Zamorani et al. 1981). X-ray studies can have important consequences for our understanding of AGNs, for many reasons. X-rays are produced by highly energetic particles, such as thermal plasmas at several million degrees or relativistic non-thermal plasmas, which might exist at the centre of the active nucleus. The shortest variability time scale observed in the X-ray wavelengths indicates the association of X-ray emitting domain with the innermost regions of AGNs (McHardy 1990). Much of the observed luminosity in AGN is radiated in X-rays and  $\gamma$  - rays. It is shown that AGN radiate at least 10% of their bolometric luminosity in the hard X-ray band ( $\sim 2 - 20$  keV) (Pounds et al. 1990; and references therein). The reproduction of this energy by circumnuclear material causes much of the radiations in UV, optical and IR frequencies. The X-ray spectrum ( $\sim 0.1 - 100$  keV) of AGNs can be well approximated by a power-law. Deviations from this power-law form can be interpreted as the effects of X-ray reprocessing. A detailed study of this reprocessing yields direct information on the geometry and the nature of material in the central regions of AGNs, which is unresolvable even by the best telescope available today. The EXOSAT (European X-ray Observatory Satellite) observations of Seyferts found evidences for the fluorescent  $K_{\alpha}$  emission line at 6.4 keV (detailed references can be seen in Ghosh & Soundararajaperumal 1993). Spectral flattening above 10 keV also been noted in AGNs (Nandra, Pounds & Stewart 1990; Nandra & Pounds 1994). These features are the evidences for the reflection of the X-ray continuum by cold optically thick material (Guilbert & Rees 1988; Lightman & White 1988; George & Fabian 1991, Matt, Perola & Piro 1991).

Recent high resolution X-ray observations of many AGNs have found the iron  $K_{\alpha}$  line at 6.4 keV to be broadened and skewed towards low energies (Mushotzky et al. 1995; Tanaka et al. 1995; Nandra et al. 1997). The line profile is usually found to be in good agreement with that expected, if it were to originate from the inner regions of an accretion disk around a black hole (Reynolds & Fabian 1997). The study of X-ray spectra of AGNs is also important in order to set constraints to the integrated contribution of these objects to the extragalactic X-ray background. Thus the X-ray studies of AGNs are gaining importance day by day in revealing the secrets of the unresolved, compact nuclear regions of active galaxies.

### **1.8.2. History and some important results of X-ray observations of AGN**

The detection of X-ray emission from the bright quasar 3C 273 by means of rocket and balloon experiments in 1967 was the first successful X-ray observation of an AGN. The first suggestion of X-rays from 3C273 was obtained from rocket data by H. Friedman and E.T. Byram in 1967. It was confirmed later with the X-ray satellites. Thus 3C273 was the first known quasar to be observed in all three domains; optical, radio, and X-ray (Bradt & Margon 1978). The precise position of the X-ray source detected by *Ariel-V* was measured by G. Ricker and his colleagues with the rotating modulation collimator on SAS-3 X-ray satellite (Bradt & Margon 1978). Later with the ground based optical observations this source was identified as an AGN (MR2251-178). The second AGN discovered from X-ray survey was 4U0241+61 ( $z=0.044$ ). A series of observations by Indian, Italian and American researchers led to this discovery. During 23-30, November 1977 Krishna Apparao, Helmken and Rick Dower used SAS-3 satellite to measure the X-ray source's position to 30 seconds of arc. Within this error circle only a few stars were seen. On 4th December 1977 using the 3m reflector at Lick observatory the brightest object within the error circle of SAS-3 was identified as the X-ray quasar by means of spectroscopy (Apparao et al. 1978; Bradt & Margon 1978). The radio observations using VLA observations by Bob Hjellming on the very next day confirmed the identification. The radio spectrum was typical of AGNs. After this discovery the optical identifications of X-ray sources were continued and now it is found that the majority of the X-ray sources seen in the sky are AGNs. Several new X-ray sources were discovered by different X-ray satellites. The imaging

and spectral resolution capabilities of these skyborne observatories grew with time. Details of some important X-ray missions are sketched below:

The *UHURU* was the first Earth-orbiting X-ray satellite launched on 12 December 1970. It operated continuously for four years. The long time available for observations, and better temporal and spatial resolutions, compared to rocket flights, resulted in the better understanding of the X-ray sky. The final *UHURU* X-ray catalog contains 339 objects which includes a few AGNs. The AGN X-ray luminosities assessed by this mission is about  $10^{42} - 10^{46}$  erg s<sup>-1</sup> (Giacconi 1976). Several new discoveries and numerous other pioneering studies by *UHURU* brought X-ray astronomy solidly into the mainstream of astronomy. The first catalog from *Ariel-V* (1974 - 1980), the British X-ray mission, provided the clue that the X-ray emission is a common property of Seyfert 1 galaxies (Elvis et al. 1978). Also *Ariel-V* survey indicated that X-ray variability scales of the order of days to be a character of AGNs (Marshall et al. 1981). The first X-ray spectral results for the brightest AGNs were published (Tucker et al. 1973; Winkler & White 1975; Mushotzky et al. 1976) from *UHURU* and OSO-7 observations (Orbiting Solar Observatory -7, 1971-1973). Winkler and White (1975), and Davidson et al. (1975) reported the X-ray variability measurements of AGN, for the first time, based on OSO-7 and Copernicus (1972-1981). The power-law shape of the X-ray continuum, low energy absorption and 6.4 keV iron K $\alpha$  line were found in the spectra of NGC 4151 and Cen-A from OSO-8 (1975-1978) and *Ariel-V* observations (Mushotzky, Done & Pounds 1993; and references therein). A series of very large satellites called High Energy Astronomy Observatories (HEAO) were put in to space by NASA. Two of them, HEAO-1 (1977-1979) and HEAO-2 or *Einstein* (1978-1981), were dedicated to X-ray astronomy, in which *Einstein* was a pioneering imaging mission, the first satellite borne X-ray telescope with improved sensitivity and angular resolution (Giacconi et al. 1971). HEAO-3 was a cosmic ray and  $\gamma$  - ray mission (Bradt, Ohashi & Pounds 1992). The first large spectral samples of AGNs, obtained with HEAO-1 satellite (Mushotzky, Done & Fabian 1993; and references therein) were well modeled by a power-law in the 2-20 keV band with intrinsic absorption and the observed range of photon index was narrowly distributed around 1.7. The HEAO-2 data has shown that all types of AGN are powerful emitters of X-ray (Zamorani et al. 1981).

The European Space Agency's X-ray observatory EXOSAT was operational from May 1983 to April 1986 and in that time it made 1780 detailed observations of a wide variety of objects including AGN. A description of EXOSAT instrumentation is provided in Chapter 2. Based on the EXOSAT data it was discovered that many Seyferts have 'soft excess' below 1 keV (Arnaud et al. 1985; Turner & Pounds 1989; detail references can be seen in Ghosh & Soundararajaperumal 1992a,b). The term 'soft excess' means the observed excess emission above the extrapolation of ME power-law at low energies (Arnaud et al. 1985). The brightest object in the universe, the radio-loud, high redshift quasar ( $z= 3.27$ ) PKS 2126-158 ( $\sim 10^{48}$  erg s $^{-1}$ ), was discovered by Ghosh & Soundararajaperumal (1992) using the EXOSAT spectra of this source. EXOSAT provided the best data to study X-ray variability in AGNs since the satellite was able to observe a source continuously for up to 3 days. The EXOSAT observations showed that rapid, large amplitude variability was a common feature of Seyferts. Thus the EXOSAT program of obtaining the X-ray spectra of an increased sample of hard X-ray selected AGN from *Ariel V* and HEAO-1 catalogs provided many new interesting results (detail references can be seen in Ghosh & Soundararajaperumal, 1991a,b, 1992a,b,c,d,e,f, 1993).

*Ginga* the Japanese mission was launched in 1987. It had a large area (0.4 m $^2$ ) of proportional counters sensitive from 1.5 - 37 keV. The *Ginga* mission also carried a wide-field sky monitor detection system (Tsunemi et al. 1989) and a US-built gamma-burst detector. Since the satellite was launched just before the 1987 supernova (SN1987A), it could help in the detection and studies of X-rays from the supernova. The discovery of two absorption lines each of two GRB spectra at  $\sim 20$  keV and 40 keV was another major result obtained from the *Ginga* observations. This result suggested that the origin of the bursts may be from a highly magnetized neutron star (Murakami et al. 1988; Fenimore et al. 1988). Several bright galaxies observed by *Ginga* have shown the presence of a spectral flattening above 8 keV and an iron line at 6.4 keV with a typical equivalent width  $\sim 150$  eV (Piro et al. 1990; Piro, Yamauchi & Matsuoka 1990). These features are now attributed to the reprocessing of the intrinsic emission by a cold and optically thick medium, producing an iron line by fluorescence and a reflected component by Compton scattering and photoelectric absorption.

The German mission ROSAT (Rontgen Satellite) was launched in 1990. It is devoted largely to imaging observations with few arc-second resolution. The satellite comprises a German large X-ray telescope sensitive to photon energies from 0.1-3 keV and a smaller British EUV telescope covering the adjacent band between 25 and 100 eV. The first six months of the mission was devoted to an all sky survey. This program detected a large number of X-ray sources (may be more than 60000 sources). The largest fraction of these survey sources is AGNs (> 25000). New results have been obtained with ROSAT on nearby galaxies. In Andromeda some 400 X-ray sources were found. Another important finding of ROSAT is the discovery of a class of sources in nearby galaxies characterized by very low temperatures (< 40000 K) but luminosities close to the Eddington limit ( $\sim 10^{38}$  erg s<sup>-1</sup>). These sources may be probable white dwarfs in binary system accreting matter at a rate just sufficient to sustain steady nuclear burning on their surface (Trumper 1994). In the Seyfert galaxy NGC6814 the existence of the  $\sim 12100$  s period was first detected in the EXOSAT ME detector which was later confirmed by the *Ginga* observations (Done et al. 1992). These observations have motivated a number of exotic models for the active nucleus. Later the high resolution imaging with the ROSAT PSPC detector revealed that although the nucleus of NGC6814 is an X-ray emitter, the periodicity is due to another source, most likely a Galactic accreting binary system separated by  $\sim 37$  arc min away.

ASCA (Advanced Satellite for Cosmology & Astrophysics) was launched by Japan's University group in the year 1993. ASCA has two sets of major imaging and spectral instruments. The telescope has four sets of multilayer thin-foil X-ray mirror system. The focal plane instruments at the foci of four sets of mirrors are two sets of solid-state imaging spectrometer (SIS) with X-ray CCD cameras and two sets of gas imaging spectrometer (GIS). Spectroscopic line profile studies are major objective of this mission (Oda 1994). The superior spectral resolution of the SIS allowed dramatic advances to be made in the line profile studies of AGNs. Many Seyfert galaxies were found to have broad iron lines (FWHM  $\sim 0.1-0.2c$  Mushotzky et al 1995). The ASCA observations of the Seyfert 1 galaxy MCG-6-30-15 (Tanaka et al. 1995) has revealed an asymmetry in the iron K $\alpha$  line profile confirming theoretical models which attribute the iron line emission to an accretion disc orbiting around a black hole.

The recent major missions planned to be launched in the near future are the American AXAF (Advanced X-ray Astrophysics Facility), which will carry out sub arc-second X-ray imaging, the Russian led multinational *Spektrum-X-Gamma*, the European XMM (X-ray Multi-Mirror Mission) and the Japanese-American joint venture Astro-E.

With the flights of modern X-ray observatories, using improved detector systems, X-ray astronomy is approaching the sensitivity of optical astronomy. *Einstein* Observatory provided an angular resolution (Half Power Diameter - HPD) of 16 arc-second, the high resolution optics of ROSAT provided 5 arc-second, the AXAF will have HPD < 1 arc-second. Having achieved high angular resolutions, the future missions will concentrate on attaining very high resolution spectroscopy. The High Throughput X-ray Spectroscopy (HTXS) is a next generation X-ray observatory dedicated to high spectral resolution imaging. HTXS is under study by NASA for flight during the first decade of the next century (Ramsey 1996). The future high resolution high energy spectroscopic studies and the coordinated multiband simultaneous observational (radio through  $\gamma$ -rays) studies will be certainly useful to understand the nature of active galactic nuclei.

## 2. INSTRUMENTATION AND DATA REDUCTION METHODS

### 2.1. X-ray Instrumentation and Data Reduction

X-ray spectra of the sample of AGNs discussed in this thesis were obtained mainly from the European X-ray Observational Satellite, EXOSAT (Fig.2.1.1). The mission consisted of three instrument packages : (1) two identical Low Energy Imaging Telescopes (LEITs), (2) the Medium Energy Detector Array (MEDA) and (3) the Gas Scintillation Proportional Counter (GSPC). The GSPC was used for the spectroscopy of strong sources. For our studies only the data from the MEDA and LEITs were used.

#### 2.1.1. *The Low Energy Imaging Telescopes*

The EXOSAT mission carried two identical, independent Wolter Type 1 (Fraser 1989; and references therein) low energy imaging telescopes. These telescopes consisted of double nested gold coated Wolter type 1 grazing incidence optics (Fig.2.1.2), comprising four mirror shells, with a focal length of 1.090m and an outer diameter of 0.3m (Fig.2.1.3). The telescope parameters give a high energy cut-off of  $\sim 2\text{keV}$ . Each telescope was designed to use in either of two principal modes: (1) an imaging mode with either a position sensitive proportional counter detector (PSD) or a channel multiplier array (CMA) plate in the focal plane. CMA is an array of compact electron multipliers of high gain (Fraser 1989) (2) a spectrometer mode which features a  $500\text{ lines mm}^{-1}$  and a  $1000\text{ lines mm}^{-1}$  transmission grating as dispersive element.

However, both the PSDs failed during the early phase of the mission and no PSD data were available for the objects in our sample. Also no spectral data of AGNs were obtained using the transmission grating. The LE data of all the AGNs in our sample were obtained using the CMAs. The field of view of each CMA covered a diameter of  $2^\circ.2$ . The detection efficiency of the CMAs decrease from 30% at 0.15 keV to 7% at 1.5 keV. The minimum particle background count rate of the CMA is  $8 \times 10^{-6}\text{ counts s}^{-1}\text{ pixel}^{-2}$  in the central region. One pixel covers  $\sim 4$  arcseconds on the sky. CMA has no intrinsic energy resolution in the X-ray band. So a number of filters were used to get a rough spectral information in the low energy band. Also CMAs are

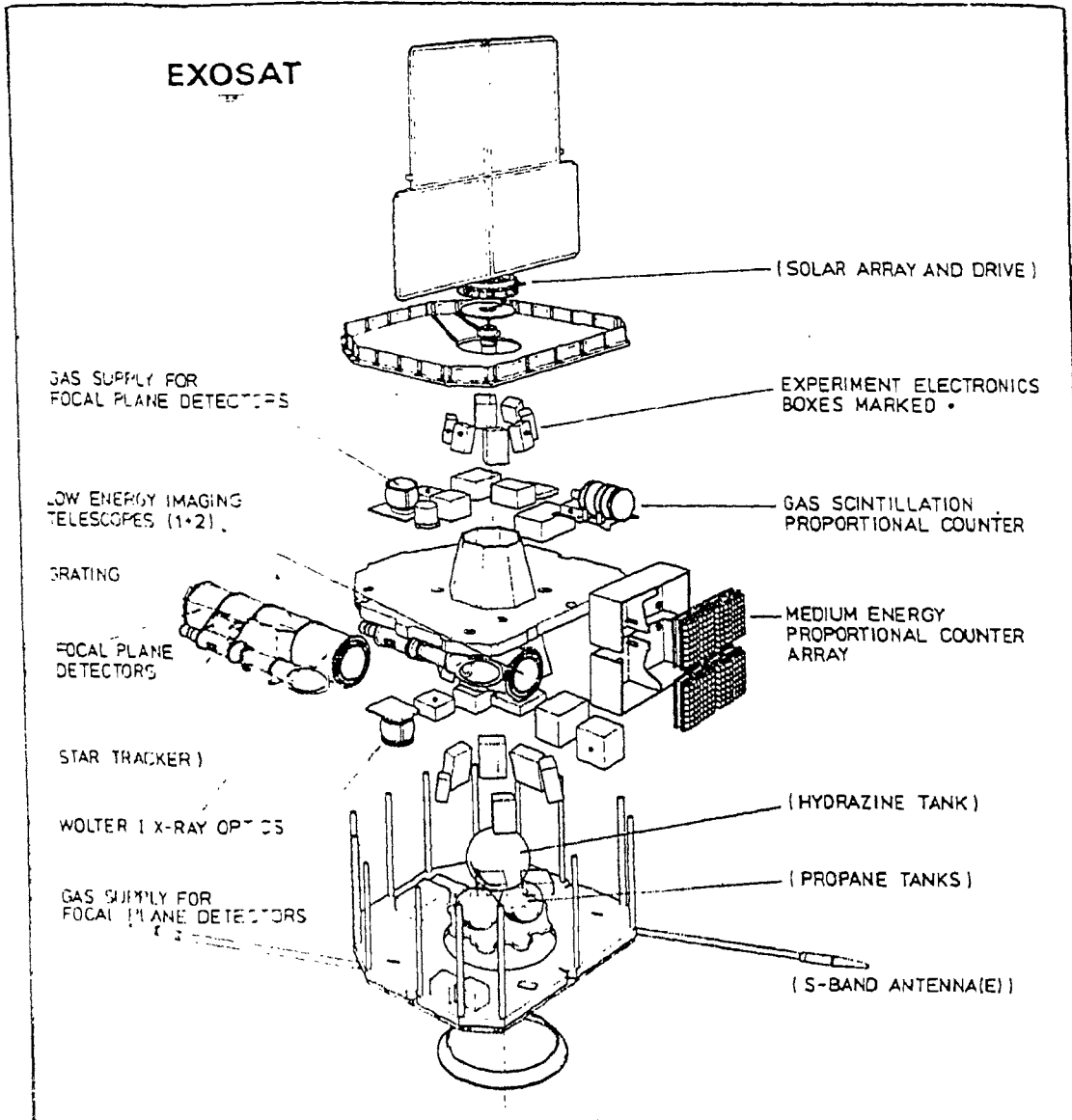


Fig. 2.1.1 Exploded view of EXOSAT showing the scientific instruments and the principal spacecraft subsystems (White & Peacock 1988).



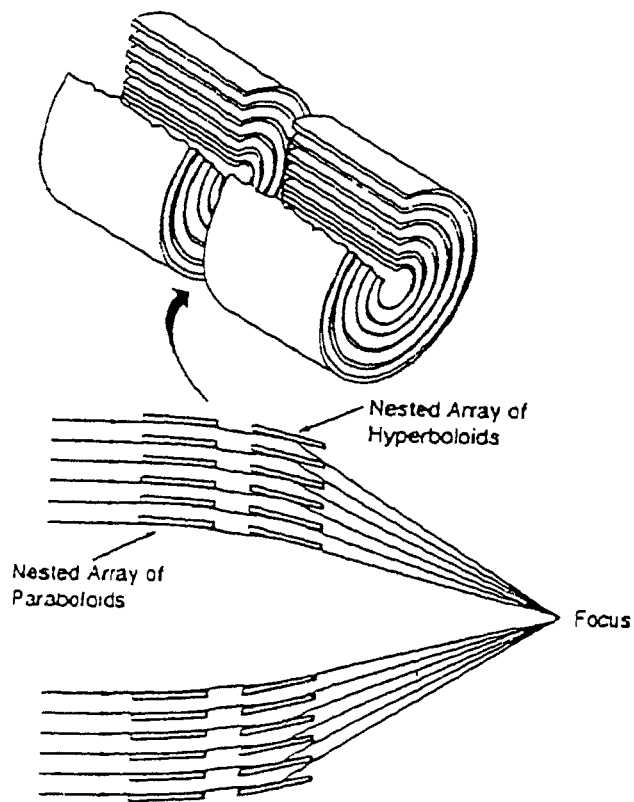
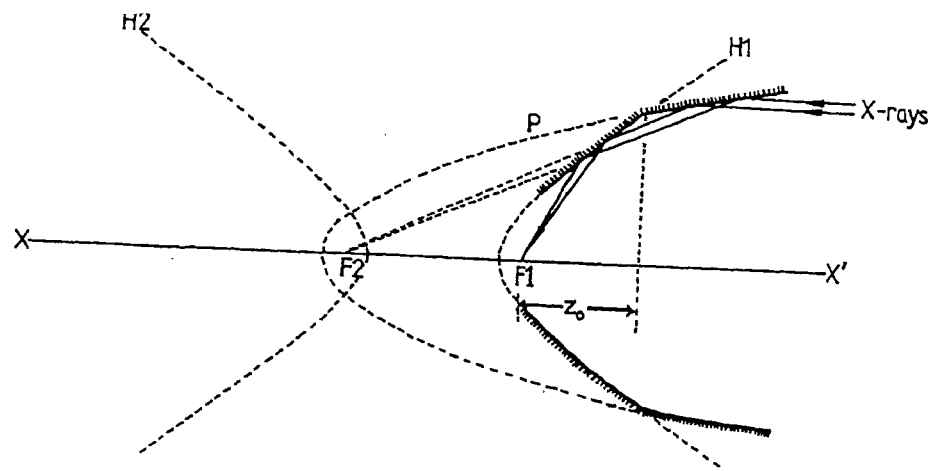


Fig. 2.1.2a (Top) Cross section of Wolter Type 1 grazing incidence mirror. The focal length of the combination of the parabolic section (P) and hyperbolic (H1) sections is measured from the join of the conic sections (Fraser 1989).

Fig. 2.1.2b (Bottom) A schematic of a typical Wolter Type 1 grazing incidence optics, comprising five mirror shells (Ramsey 1997).

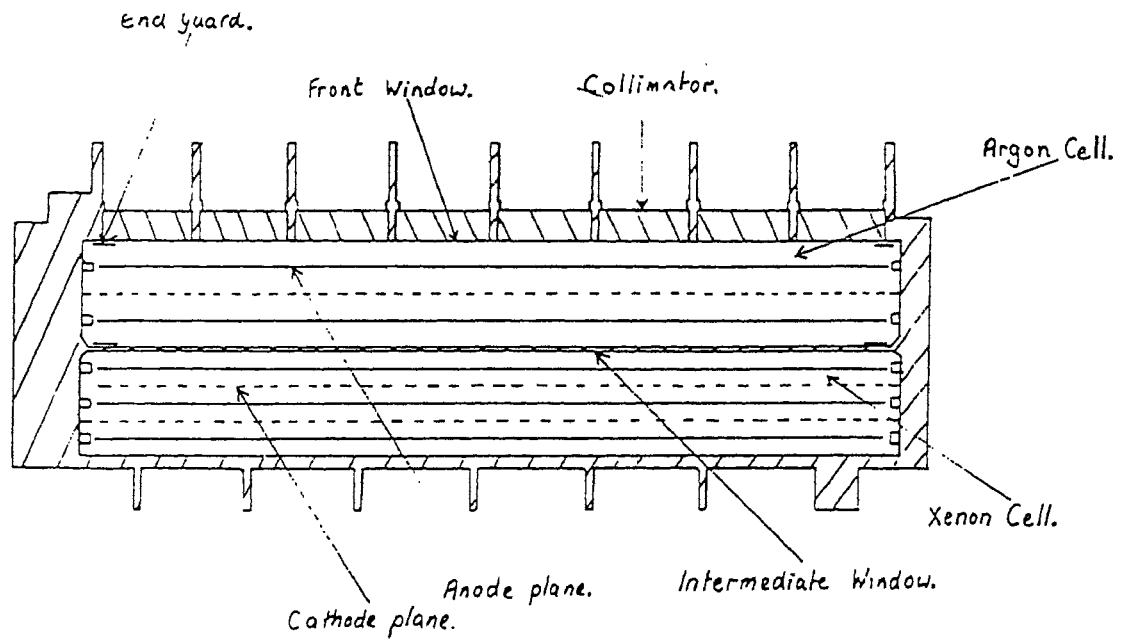
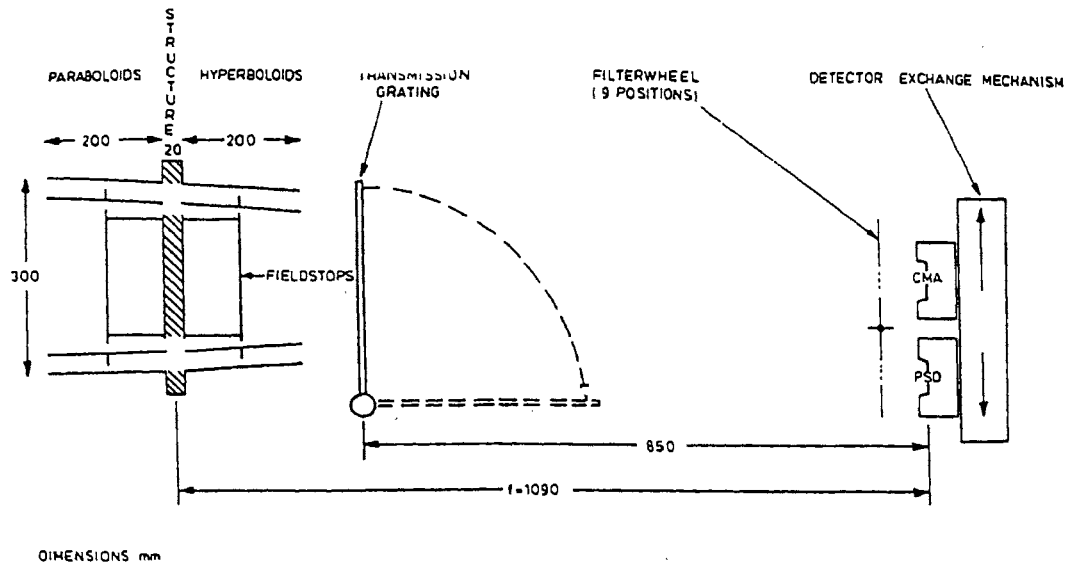


Fig. 2.1.3 (Top) A schematic of a low energy imaging telescope system of EXOSAT (de Korte et al. 1981).

Fig. 2.1.4 (Bottom) Schematic cross section of a medium energy detector of EXOSAT (Turner et al. 1981).

sensitive to UV photons so it was necessary to use CMAs in association with a filter in order to absorb the diffuse UV-sky background. Throughout the mission the most commonly used filters were 3000Å Lexan, Aluminum/Parelene and Boron. Combining these filters with the better resolution ME data provides a powerful method of investigating the low energy properties of X-ray sources. A more detailed description of the LEIT is given by de Korte et al. (1981) and White and Peacock (1988).

### **2.1.2. The Medium Energy Detector Array**

EXOSAT's MEDA (Turner et al. 1981; White and Peacock 1988; Fraser 1989) was proposed to ESA by the X-ray Astronomy Group at Leicester, the Max Planck Institute at Garching and the University of Tübingen in 1973. MEDA consisted of an array of eight proportional counters with a total geometric area ( $A_g$ ) of  $\sim 2500 \text{ cm}^2$  (all eight modules aligned). The ME experiment provided spectral and temporal data in the 1-50 keV band. Each proportional counter consisted of two layered gas cells with an argon chamber on top of a Xenon chamber separated by a 1.5mm beryllium window (Fig.2.1.4). The upper cell pressurized with an argon-CO<sub>2</sub> mixture to 2 bar, contained two planes of anode wires with an interleaved cathode plane. The lower chamber filled with Xe-CO<sub>2</sub> to the same pressure contained three anode planes. The entrance windows to the argon chambers were also beryllium with a thickness of 32  $\mu\text{m}$  for a four detectors and 62  $\mu\text{m}$  for the other four detectors. Lead glass channel multiplier arrays were used as the collimators with a square field of view of  $45 \times 45$  arcmin FWHM. All the 8 detectors were multiwire proportional counters with energy resolutions ( $\Delta E/E$ ) of  $21(E/6\text{keV})^{-0.5} \%$  FWHM for the argon chambers and  $18(E/22\text{keV})^{-0.5} \%$  FWHM for the xenon chambers. The output count or pulse height is proportional to the energy of the original incident X-ray photon. The output from each chamber was pulse height analyzed to 128 PHA (Pulse Height Analyzer) channels. The energy range is 1.3-15 keV for argon and 5-55 keV for xenon. The ME experiment provided only 1-10 keV good quality spectra for AGNs. The eight proportional counter modules of the MEDA were grouped in four pairs with each pair occupying one of the four quadrants. Each pair of detectors were pivoted around the line joining opposite corners of a quadrant. The quadrants can be moved in opposite directions to monitor the source and the source free regions of the sky simultaneously to record the source and background counts. Half

of the detectors were aligned to the source and the remaining half were offset by upto  $2^\circ$  to monitor the background. The source and background halves of the arrays were swapped ('nodded') during each observation in order to account for small systematic differences between individual modules. Background correction is performed on the ME spectra of AGNs by subtracting the offset spectrum from the aligned spectrum of each detector. The observations with significant background variations were discarded. This kind of occasional background variations were caused mainly by the enhancements in the solar wind. Systematic background subtracted LE and ME spectra were extracted from the EXOSAT database.

### ***2.1.3. X-ray Spectral Analysis***

The XSPEC (X-ray Spectral Fitting) package (Shafer, Haberl, Arnaud & Tennant 1991) was used to analyze the background subtracted PHA spectra. XSPEC is a command-driven, interactive, detector-independent X-ray spectral fitting program. The observed data is called as count or PHA (Pulse Height Analyzer) spectrum. Using the XSPEC a suitable range of ME PHA channels were selected for spectral fitting. Usually ME channels 6-30 (2-8 keV) were chosen to have clean source spectrum. The selected spectrum is a convolution of the response function of the detectors with the true source spectrum. The detector response function is described in the form of a matrix, in a response matrix file corresponding to the PHA file, with each row describing the response to a monoenergetic flux as a function of PHA channels. To derive the source spectrum, a model spectral shape is initially assumed, which can be described using a few parameters. Usually a simple power-law plus galactic absorption (values of the effective photoelectric cross-sections were obtained from Morrison & McCammon 1983) model is initially selected for this purpose. Then the detector response characteristics, given in the response matrix, is used to convert this model spectrum into a folded model (convolved through the detector response matrix) that can be compared to the observed data. The goodness of the fit is evaluated using the  $\chi^2$  statistics. The parameters of the fit are then varied or additional components are added to minimize the  $\chi^2$  value and hence to obtain a model spectrum that closely resembles the observed spectrum. The iterative process is stopped at a point where the  $\chi^2$  value is minimum. The best fit spectral parameters are then considered as the final result. The 90 % confidence errors on each parameters were calculated following Lampton, Margon &

Bowyer (1976). Observed X-ray spectra were fitted using different models and the components of the models are:

power-law :	$F_1 (E) = c_1 E^{-\Gamma}$
blackbody :	$F_2 (E) = c_2 E^2 / [(kT_b)^4 (\exp(E/ kT_b)-1)]$
thermal bremsstrahlung :	$F_3 (E) = c_3 \exp(-E/T) G(E,T)/E$
Gaussian line :	$F_4 (E) = c_4 [1/(2\pi\sigma_L^2)^{1/2} \exp(-(E-E_{Line})/2\sigma_L^2)]$
broken power-law :	$F_5 (E) = c_5 E_{break}^{(\Gamma_2-\Gamma_1)} E^{-\Gamma_2}$
absorption edge :	$F_6 (E) = \exp(-\tau (E/E_{edge})^3)$

where  $F_i (E)$  denotes the spectrum in photon  $\text{cm}^{-2} \text{s}^{-1} \text{keV}^{-1}$ ,  $E$  is the photon energy in keV,  $\Gamma$  is the photon index,  $E_{edge}$ ,  $E_{break}$ ,  $E_{line}$ ,  $E_{edge}$  and  $kT_b$  are all in keV,  $G(E,T)$  is the Gaunt factor,  $\tau$  is the optical depth and  $c_i$  are the normalization constants.  $\Gamma_1$  and  $\Gamma_2$  are the photon indices below and above the break point energy,  $E_{break}$ , respectively. All these spectral components have to be corrected for the low-energy absorption, mainly due to the absorption within our own galaxy. This can be done by multiplying the above spectral components by  $\exp(-\sigma(E)N_H)$ , where  $\sigma(E)$  is the photo-electric cross section (not including Thompson scattering) and  $N_H$  is the absorbing column density. The data reduction works were performed using the VAX - 11/780 computer system at the Vainu Bappu Observatory, Kavalur.

## 2.2. Optical Instrumentation and Data Reduction

### 2.2.1 Telescopes and CCD Detectors

The optical imaging photometric data were obtained using the 2.3 meter Vainu Bappu Telescope (VBT), the 1 meter telescope and the 0.75 meter telescope existing at the Vainu Bappu Observatory, Kavalur, India. The indigenously built VBT has a parabolic primary of focal ratio 3.25. The telescope is used at the prime focus for the photography of very faint objects. The telescope is equatorially mounted with the polar axis pointing due north on a horse-shoe-yoke structure to facilitate easy observations of low latitude objects as well as the objects near the north celestial pole. VBT has a prime focus image scale of about  $27 \text{ arcsec mm}^{-1}$ . The 1m telescope, by Carl Zeiss Jena, is of Ritchey-Chretien design with a coma-free field of 40 arcmin

diameter at the F/13 Cassegrain focus. The image scale at the Cassegrain focus is  $15.6 \text{ arcsec mm}^{-1}$ . Observations of two blazars (3C66A and OJ287) were made using the 0.75m Cassegrain reflector. For all the observations, Charge Coupled Devices (CCDs) were used as main detectors. CCDs are 2-dimensional detectors made up of silicon. When a photon is absorbed in silicon, an electron-hole pair is created. Sets of three polysilicon electrodes cover the surface of the CCD. These electrodes collect and transfer the electrons to output registers. One of the three electrodes is biased more positively than the other two. Under this electrode electrons are accumulated and by supplying appropriate voltages to the electrodes the accumulated charges are transferred and read out at the output registers. The electrons are restrained from moving along the length of the electrodes by 'channel stops'. These are narrow regions of heavily doped P-type material. Their negative charge repel electrons and therefore prevents electron movement across the channel stops. The extent of each set of three electrodes and the length between two channel stops define the size of each picture element or pixel (Mackay 1986). CCDs are operated at temperatures around  $-120^\circ \text{ C}$  to minimize the image noise caused by the thermal agitation of electrons within the semiconductor. A DC offset (bias) voltage is applied to avoid negative signals caused by fluctuations due to noise. The bias values over the entire frame need not be the same and hence it has to be estimated for every pixel in the array. This is done by reading the charges, over the smallest integration time, without allowing any light to fall on the CCD. The bias frame thus obtained is subtracted pixel by pixel from the object frame. Also the quantum efficiency of CCD pixels differs from pixel to pixel. Exposing the CCD to a flat uniform field will result in a frame that indicate relative responses of different pixels. This exposure is used to correct (flat-fielding) the non uniformity of the response in the object frame. Twilight sky is considered as a good flat source. Sky flats were obtained with each filter for flat-fielding the images taken with the corresponding filter. Normally a few flat frames were taken using the evening and morning twilight sky and were stacked. When more than 2 flats were available, stacking was done with median option. The stacked flat frame was used for the flat-fielding. The bias subtracted, flat fielded images were used for performing the final photometric analysis. The NOAO-IRAF (Image Reduction and Analysis Facility) software was used for the processes of bias subtraction and flat-fielding. A blue coated Astromed GEC P8603 CCD detector and a back illuminated, UV coated and thinned Tektronics 1k CCD were

used as detectors at the  $f/3.25$  prime focus of VBT. The GEC P8603 chip was used with the 0.75m telescope also for the observations of the two bright blazars, 3C66A and OJ 287 (Chapter 3.2.2). The GEC P8603 chip has  $385 \times 578$  pixels of dimensions  $22 \times 22 \mu\text{m}^2$ ; each pixel thus corresponds to  $0.61 \times 0.61 \text{ arcsec}^2$  on the sky and the total area covered by the CCD chip is about  $4 \times 6 \text{ arcmin}^2$ . The Tektronics 1k chip has  $1024 \times 1024$  pixels of  $24 \times 24 \mu\text{m}^2$  dimensions. Each pixel corresponds to  $0.66 \times 0.66 \text{ arcsec}^2$  and the total area covered is about  $11 \times 11 \text{ arcmin}^2$  on the sky. For the observations with the 1m telescope at the  $f/13$  Cassegrain focus a Thomson CSF TH7882 CCD chip, obtained from the Photometrics Limited, USA, was used as the detector. This chip has  $384 \times 576$  pixels with each pixel having  $23 \mu\text{m}^2$  dimension. At the Cassegrain focus this chip provided a total field of  $137 \times 206 \text{ arcsec}^2$  with an image scale of  $0.357 \text{ arcsec pixel}^{-1}$ . The readout noise and gain for the Tek 1k system were, 9.8 electron rms and 8.97 electron ADU<sup>-1</sup>; for P8603, 7.7 electron rms and 4 electron ADU<sup>-1</sup>; and for TH7882, 6.5 electron rms and 27.3 electron ADU<sup>-1</sup>. The following system of coated filters were used for our observations, the central wavelength and the passband are indicated within the brackets: B (4400/1050), V (5425/1050), R (6550/1300) and I (8150/1700). More than one frame of each object were obtained on each night during the observations. For the multi-epoch studies, to improve the signal-to-noise ratio, the processed images were stacked after aligning them. For aligning the frames for stacking, the centroid pixel positions (or pixel coordinates) of more than 4 stars which were found common to all the frames were determined. The coordinates of these reference stars in the best image of the night were considered as the reference coordinates. The transformation required for mapping the other input images with the reference image was computed using the coordinates of the reference stars, in the reference image and the other input images, using the GEOMAP program in IRAF. The transformation has the following form.

$$x_{in} = f(x_{ref}, y_{ref})$$

$$y_{in} = g(x_{ref}, y_{ref})$$

The functions  $f$  and  $g$  are either a power series polynomial or a Legendre or Chebyshev polynomial (IRAF Reference Manual 1992). The final fit - the coordinate transformation - is stored in a text file, called 'database', in a format suitable for use by the program GEOTRAN which corrects the input images for geometric distortion and transformation with respect to the reference image. The transformed coordinates at intermediate pixel values were determined by

bilinear interpolation in the coordinate surface. The aligned images of each night were then stacked and averaged for the aperture photometric analysis.

### ***2.2.2. Differential Photometric Analysis***

In differential photometric method, the magnitude differences between the program AGN and the standard field stars of similar brightness are compared and plotted as a function of time. This method is a powerful and easy tool to detect even minute variations. At the start, concentric aperture photometry was done to determine the instrumental magnitudes of the program AGNs and the other standard stars in the same field. The photometric analysis was carried out using the digital aperture reduction program DAOPHOT (Stetson 1987) installed on the SUN Workstations at VBO. Initially the processed images were examined using IRAF and the approximate FWHM of the point spread function (PSF) of the objects of our interest were estimated. This indicates the value of radius of the object aperture to be used and the inner radius and width of the annular sky region to be used to fit the background. Also a list of object centres, in terms of pixel coordinates, were prepared by using the FIND subroutine. The PHOTOMETRY program was then executed. It computes accurate centre, sky values and magnitudes for the objects in the input IRAF images whose coordinates were listed in the output text file of FIND subroutine. PHOTOMETRY program determines a constant background value by analysis of an annular region surrounding the objects. The defects and contaminating objects in the selected background annular region is eliminated by the fitting algorithm. Then the program determines the integral of object minus background within the given aperture, centred upon the object. On doing this, it adds up the observed flux in pixels within the specified radial distance of the centroid of a star and subtracts the contribution from the diffuse sky background to get an estimate of the total flux from the star alone. The PHOTOMETRY routine produces instrumental magnitudes measured through up to 12 concentric apertures of differing radii. The aperture size is kept the same for all the frames. Also it estimates standard error of each aperture magnitude based on the readout noise and gain of the CCD and the observed sky background in the vicinity of the star. This method of synthetic aperture photometry could yield correct results when no other objects are contained within the aperture and the sky-brightness estimate is correct. Also it is necessary that the seeing, tracking and focus errors should not cause fraction



of the object's flux to fall outside the aperture. A more accurate method to improve the measurement accuracy is the growth-curve method (Rich et al. 1984; Stetson 1990). The growth-curve method was employed, by means of DAOGROW program (Stetson 1990). In this method the magnitude differences between successive apertures for each star are plotted as a function of radius and a smooth curve is drafted through them to get the average growth curve of the frame. The average magnitude differences between successive apertures are then read from this curve and summed from the outside inward to yield cumulative corrections from each of the smaller apertures to the system of the largest (Stetson 1990). For example the average magnitude difference between 12th and 11th apertures is summed with the magnitude of 11th aperture of each object; and the sum of average differences between 12th and 11th apertures and 11th and 10th apertures is summed with the magnitude of 10th aperture of each object and so on. This multiple-aperture technique offers several advantages. If some stars include a companion star or a cosmic ray event situated very close to the star which contributes some unknown amount of flux, or if a pixel flaw or image blemish which would obstruct some flux, or if the signal-to-noise ratio of the measurement in the largest aperture may be too poor to be useful for fainter stars or if a star is located close to the edge of the frame for which the largest aperture would extend outside the frame, then the simple synthetic aperture method can not give accurate results. Conversely such stars may be measurable through several of smaller apertures. Here the magnitude differences of successive apertures of all the stars, that can be reliably measured alone, were estimated and averaged. High magnitude differences caused by the defects such as those mentioned above will not be included for the estimation. To do this the upper limit of magnitude difference is fed interactively to DAOGROW program. Determining the mean magnitude difference between each successive pair of apertures from all the stars and then summing the mean differences from the outside in for all the objects in the frame yields a more precise determination. DAOGROW also makes necessary corrections for the differences caused by the variations in the air mass. A file containing the details of names of all the input IRAF image files, air masses, filters and integration times of all the processed files is supplied to make necessary corrections. Air mass correction is done despite the fact that the program AGN and the standard field stars were observed through identical atmospheric layers. The total, integrated instrumental magnitudes of the sources were estimated using the fore mentioned

growth-curve method and redirected to an output file by the DAOGROW program. Two nearby non-variable stars with comparable magnitudes were selected as comparison sources. The magnitude differences between program AGN and the standard stars were plotted as a function of time to find out the possible variations.

### **3. X-RAY AND OPTICAL OBSERVATIONS OF AGNs, RESULTS AND DISCUSSION**

X-ray flux variability results suggest that these radiation are emitted from the very close to the putative supermassive black hole at the core of AGNs. The emitted X-ray spectrum of AGNs can be approximated by a power-law. Deviations from a power-law form can usually be interpreted as the effects of X-ray reprocessing by the circumnuclear matter. Thus a detailed study of the X-ray spectral properties of AGNs can yield direct information on the geometry and state of matter in the nuclear regions of these sources.

The anisotropic emission from AGNs originate from different regions for different wavebands. Although it is widely believed that much of observed UV, optical and infrared luminosities originate from the reprocessing of the primary X-ray emission by the circumnuclear material. The multifrequency data of several AGNs showed differential variability in flux and in shape of the emitted spectra which indicate that different processes are involved in the production of anisotropic emission in different band of AGN electromagnetic spectrum. Therefore multifrequency observations are necessary for the comprehension of emission mechanisms and structure of AGN.

In this Chapter the results of EXOSAT X-ray spectral analysis of a sample of 13 Seyfert galaxies and 28 blazars are presented. The X-ray spectra of all the blazars are compared with the radio through UV multifrequency continua. Results of the optical differential photometric CCD observations of 20 radio-quiet quasars and two blazars are also presented in this chapter. Optical observations of one Seyfert and 6 blazars were carried out in collaboration with the International AGN Watch Program. Brief mention of the results of these observations are also presented in this chapter .

## 3.1. Seyfert Galaxies

### 3.1.1. Introduction

X-ray spectroscopy of Seyfert galaxies that were carried out with the EXOSAT, the GINGA and the ASCA has revealed many interesting results (Turner & Pounds 1989; Turner et al. 1989; Nandra et al. 1997; Turner et al. 1997 and references therein). First, the spectral indices of the power-law spectra have a gaussian distribution with mean intrinsic photon index  $\Gamma=1.9$ . Secondly, in many spectra there is a soft excess and low-energy absorption and absorption-edges of OVII and OVIII. Thirdly, structured  $K_{\alpha}$  emission of fluorescent cold iron and bump above 8 keV (may be due to reflection from the accretion disk). However, it is true that all the Seyferts did not display all these characteristics. Thus it is important to study more such objects in order to understand the nature of these objects and its environment. In this Section spectral information of a sample of 13 Seyfert galaxies observed with the EXOSAT are presented.

The continuum source and the BLR in AGNs are too small regions to be resolved spatially even with the very large ground and space-based telescopes. However, coordinated observations of continuum and emission-line variations can be a powerful tool to probe the inner structure of AGNs. This idea led to the formation of a large consortia to carry out multiwavelength coordinated spectroscopic monitoring programs on AGNs. We participated in such a program of International AGN Watch (Santos-Lleo et al. 1997) to monitor the variability of one Seyfert 1 galaxy (Fairall-9) in the optical band. The results obtained from this program are also presented in this Chapter.

### 3.1.2. X-ray Properties of a Sample of Seyfert Galaxies

In this Section X-ray spectral results of a sample of 13 Seyfert galaxies are presented. To select the sample we thoroughly searched the EXOSAT database and isolated the Seyfert galaxies for which no spectral information is available in the literature or no detailed modeling has been done earlier. A number of criteria were then imposed on this sample to make sure that the spectra

analyzed were good and uncontaminated. The criteria followed to reject the spectra are as follows: (1) observations that were carried out with the EXOSAT but not published, (2) a flux less than 4 times its error, (3) a data-quality factor less than 3 (the data-quality flag takes account of solar contamination, high background and other factors that would affect the quality of detection) and (4) the objects that were contaminated by other bright sources in the field. After screening the sources in this manner, we were left with 13 Seyferts galaxies (ESO 012-G21, Mkn352, Mkn374, NGC3516, NGC3783, Mkn766, NGC4593, Mkn279, Mkn464, Mkn290, 3C382, ESO140-G43 and MCG-2-58-22). Their redshift and coordinate are listed in Table 3.1.2A. A log of EXOSAT observations and count rates are given in Table 3.1.2B. Brief information about the individual galaxies is given below.

### Notes on Individual Objects

#### *ESO 012-G21*

This is a Seyfert 1 galaxy (West 1979) with  $m_v = 14.73$ ,  $M = -21.6$ ,  $B-V = 0.57$ ,  $U-B = -0.25$  (West, Grobsol & Sterken 1980). Prior to EXOSAT the first X-ray (2-10 keV) spectrum was obtained with the MSSL proportional counter spectrometer on *Ariel V* (Hayes, Culhane & Bell Burnell 1980). X-ray detection with *Uhuru* (3U0055-79) was doubtful (Giacconi et al. 1974), but the galaxy was detected with *Ariel V* (Bell Burnell & Chiappetti 1984).

#### *Mkn352*

This Seyfert 1 galaxy ( $m_v = 14.81$ ,  $M = -20.0$ ,  $B-V = 0.44$ ,  $U-B = -0.66$ ; Markarian & Lipovetski 1971; Osterbrock 1977) was observed with *Einstein* in the 0.2-4 keV range (Kriss, Canizares & Ricker 1980; Urry et al. 1989). The first X-ray observation beyond 4 keV was with EXOSAT in the 0.1-10 keV range. Later this source was observed with ROSAT (Walter & Fink 1993).

#### *Mkn374*

No spectral information in the X-ray region except for the *Einstein* Imaging Proportional Counter (0.2-4 keV) results (Urry et al. 1987), is available for this Seyfert 1 galaxy ( $m_v = 14.61$ ,  $M = -22.5$ ,  $B-V = 0.7$ ,  $U-B = -0.38$ ; Markarian & Lipovetski 1971; Weedman 1973; Osterbrock 1977). The EXOSAT spectrum was obtained on 1984 November 5.

**TABLE 3.1 2^ SOURCE LOG OF SEYFERT GALAXIES**

Source	Position (1950)		Redshift z
	R.A.	Dec.	
ESO 012-G21	00 39 16	-79 30 54	0.033
Mkn352	00 57 09	+31 33 28	0.015
Fairall-9	01 21 51	-59 03 59	0.046
Mkn374	06 55 34	+54 15 57	0.044
NGC3516	11 03 23	+72 50 20	0.009
NGC3783	11 36 33	-37 27 41	0.009
Mkn766	12 15 56	+30 05 26	0.012
NGC4593	12 37 04	-05 04 11	0.009
Mkn279	13 51 54	+69 33 13	0.031
Mkn464	13 53 45	+38 49 07	0.051
Mkn290	15 34 45	+58 04 00	0.030
3C382	18 33 12	+32 39 18	0.059
ESO140-G43	18 40 14	-62 24 58	0.014
MCG-2-58-22	23 02 07	-08 57 20	0.047

TABLE 3.1.2B LOG OF EXOSAT OBSERVATIONS AND COUNT RATES OF SEYFERT GALAXIES

Source	Start time <sup>a</sup>	End time <sup>b</sup>	LE count rate ( $10^4 \text{cm}^{-2} \text{s}^{-1}$ )			ME count rate <sup>c</sup> ( $10^3 \text{cm}^{-2} \text{s}^{-1}$ )
			(LX3)	(Al/P)	(B)	
ESO012-G21	1985,108,09:12	108,12:49	01.85±0.24	00.69±0.15		0.61±0.06
Mkn352	1983,319,02:46	319,03:47	00.37±0.05	00.28±0.07		1.34±0.12
Mkn374	1984,310,18:44	311,02:13	00.22±0.03			0.59±0.04
NGC3516	1985,308,21:00	309,07:25	00.61±0.11	00.35±0.07		1.48±0.04
NGC3516	1985,311,16:56	312,03:55	00.47±0.07	00.31±0.08		1.46±0.03
NGC3516	1985,330,12:05	330,19:10	00.45±0.07			1.37±0.05
NGC3516	1985,340,15:46	341,11:03	00.44±0.15			0.92±0.03
NGC3783	1983,347,10:44	347,18:42	02.53±0.33			4.24±0.06
NGC3783	1984,162,17:08	162,23:00	010.6±0.77	06.37±0.42	01.68±0.20	7.92±0.07
NGC3783	1985,005,05:38	005,12:07	03.62±0.32	02.68±0.28	00.95±0.16	5.16±0.05
Mkn766 <sup>d</sup>	1985,363,18:17	364,04:02	02.65±0.23			3.10±0.09
Mkn766 <sup>d</sup>	1985,364,04:16	364,13:27	02.30±0.21			2.70±0.08
Mkn766 <sup>d</sup>	1985,364,13:45	365,00:57	01.95±0.19			2.43±0.07
Mkn766 <sup>d</sup>	1985,365,01:04	365,11:19	02.88±0.23			3.01±0.08
Mkn766	1985,365,11:36	366,00:08	03.45±0.26			3.80±0.07
NGC4593	1984,154,06:30	154,12:20	22.20±1.30	10.20±0.90	10.60±0.20	3.45±0.05
NGC4593	1984,183,00:55	183,06:37	21.51±1.52	09.50±0.61	01.43±0.11	4.20±0.05
NGC4593	1985,176,06:05	176,14:30	04.33±0.30	02.14±0.22		1.36±0.04
NGC4593	1985,180,17:25	180,23:09	05.90±0.30	02.21±0.30		1.64±0.05
NGC4593	1985,185,15:48	186,03:00	05.90±0.40	02.60±0.20		1.68±0.03
NGC4593	1986,009,23:50	010,11:58	21.70±0.70			3.47±0.04
NGC4593 <sup>d</sup>	1986,010,00:09	011,02:11	21.70±0.70			3.06±0.04
Mkn279	1983,320,16:52	320,20:48	01.32±0.11	00.51±0.06	00.11±0.02	2.17±0.09
Mkn279 <sup>c</sup>	1984,028,18:29	028,21:47	01.20±0.08	00.55±0.04	00.13±0.02	1.78±0.11
Mkn464	1985,178,23:21	199,04:30	05.26±0.46	02.31±0.19		1.04±0.05
Mkn290 <sup>d</sup>	1986,056,00:05	056,07:01	04.43±0.32	02.10±0.29		0.75±0.04
3C382	1983,255,03:16	255,09:10	03.76±0.21			2.73±0.06
3C382	1984,130,19:24	130,22:58	08.07±0.60			4.85±0.14
3C382	1985,109,07:20	109,11:03	04.09±0.31			2.57±0.10
3C382	1985,109,23:28	110,03:11	04.09±0.31			2.51±0.09
3C382	1985,116,17:50	117,00:18	04.13±0.40			2.36±0.11
3C382	1985,117,16:27	117,21:29	04.13±0.40			2.25±0.06
3C382	1985,147,01:46	147,05:10	05.05±0.46			3.31±0.07
3C382	1985,153,13:10	153,16:50	06.90±0.58			4.12±0.07
3C382	1985,161,05:50	161,11:45	06.49±0.55			3.61±0.05
3C382	1985,171,21:05	172,01:56	06.77±0.39			4.28±0.06
3C382	1985,178,05:40	178,12:01	06.47±0.42			3.97±0.14
3C382	1985,195,05:01	195,07:30	07.08±0.40			4.38±0.08
3C382	1985,204,21:26	204,23:10	04.23±0.36			3.28±0.15
3C382	1985,211,21:29	212,09:20	06.21±0.39			3.44±0.05
3C382	1985,223,16:00	223,18:49	07.51±0.52			3.67±0.07
3C382	1985,233,10:36	233,13:15	07.85±0.50			4.81±0.08
3C382	1985,246,19:36	247,00:50	08.17±0.49			4.52±0.06
3C382	1985,256,13:12	256,19:26	08.57±0.50			4.13±0.06
3C382	1985,273,03:44	273,09:39	08.97±0.52			4.69±0.12

TABLE 3.1.2B - continued

Source	Start time <sup>a</sup>	End time <sup>b</sup>	LE count rate ( $10^{-4}\text{cm}^{-2}\text{s}^{-1}$ )			ME count rate <sup>c</sup> ( $10^{-3}\text{cm}^{-2}\text{s}^{-1}$ )
			(LX3)	(A/P)	(B)	
ESO140-G43	1985,105,13:30	105,16:22	01.29±0.36			2.12±0.10
MCG2-58-22	1984,321,06:26	321,12:32	08.78±0.83	04.23±0.50		2.75±0.05
MCG2-58-22	1984,322,23:39	323,02:51	06.98±0.56	04.42±0.37		2.65±0.06
MCG2-58-22	1984,325,19:30	325,22:46	07.62±0.61	04.20±0.39		2.90±0.07
MCG2-58-22	1984,327,03:08	327,06:17	08.80±0.62	04.87±0.40		2.95±0.06
MCG2-58-22	1984,329,10:43	329,14:17	07.41±0.57	05.10±0.38		2.95±0.06
MCG2-58-22	1984,331,15:08	331,22:34	08.28±0.57	04.59±0.41	01.23±0.14	2.63±0.05

<sup>a</sup> Format: year,day,hour:minutes.

<sup>b</sup> Format : day,hour:minutes.

<sup>c</sup> The count rates are for PHA channels 6-35 corresponding to the energy range 2-10 with the best signal-to-noise ratio.

<sup>d</sup> Detector 3 was off during ME observations.

<sup>e</sup> Only half of detector 2 was on during ME observations.



### ***Mkn766***

Prior to the EXOSAT observations of this Narrow-line Seyfert 1 galaxy (Boller, Brandt & Fink 1996;  $m_v = 14.0$ ,  $M = -20.4$ ; Markarian & Lipovetski 1976), the only X-ray observation was with the *Einstein* IPC (Kriss et al. 1980; Urry et al. 1987). It was observed with EXOSAT at five epochs between 1985/363 and 1985/365. Later this source was observed with ROSAT (Boller et al. 1996) and ASCA (Nandra et al. 1997).

### ***Mkn279***

Mkn279 (MCG 12-13-22; 3A 1348+700) is a type 1 Seyfert galaxy ( $m_v = 14.46$ ,  $M = -21.9$ ,  $B-V = 0.69$ ,  $U-B = -0.45$ ; Walker & Chincarini 1967; Markarian 1969). Infrared (Lonsdale et al. 1985) and weak radio (de Bruyn & Wilson 1976) emission has been detected. Prior to EXOSAT, X-ray observations were made with *Uhuru* (Tananbaum et al. 1978), *Ariel V* (Cooke et al. 1978; Elvis et al. 1978), *HEAO-1* (Dower et al. 1980) and *Einstein* (Kriss & Doxey 1983). It was observed with EXOSAT at two epochs between 1983 and 1984. ROSAT spectral information of this source has been presented by Rush et al. (1996).

### ***Mkn464***

By spectroscopy, Denisyuk & Lipovetsky (1974) classified Mkn464 as a type 1 Seyfert galaxy ( $m_v = 16.1$ ,  $M = -21.3$ ; Markarian & Lipovetski 1972; Denisyuk & Lipovetski 1974). Weak radio emission ( $\sim 0.006$  Jy) was detected by Ulvested & Wilson (1984). X-ray observations were made with *HEAO-1* (Marshall et al. 1979), *Ariel V* (Hayes, Culhane & Bell Burnell 1980) and EXOSAT.

### ***Mkn290***

This type 1 Seyfert galaxy ( $m_v = 14.96$ ,  $B-V = 0.6$ ,  $U-B = -0.62$  and  $M = -21.3$ ; Markarian 1969; Arakelian et al. 1971) was detected with *HEAO-1* (Wood et al. 1984) and spectra were obtained with *Einstein* (Kriss et al. 1980; Kruper, Urry & Canizares 1990), EXOSAT (Turner & Pounds 1989) and ROSAT (Walter & Fink 1993).

### ***ESO140-G43***

ESO140-G43 is a compact IRAS Seyfert 1 galaxy ( $m_v = 14.1$ ,  $B-V = 0.73$ ,  $U-B = -0.17$  and  $M = -20.5$ ; West, Dank & Alcaino 1978). Prior to EXOSAT no X-ray spectra was obtained for this Seyfert galaxy. Later this source was observed with ROSAT (Malaguti 1994).

### **NGC3516**

NGC3516 (MCG 12-11-009, UGC6153,  $m_v = 12.40$ ,  $B-V=0.72$ ,  $U-B=-0.23$  and  $M=-21.2$ ; Adams 1977; Osterbrock 1977) is an original Seyfert galaxy (Seyfert 1943) which has been classified as RSBO type galaxy with heliocentric radial velocity as  $2664 \pm 22 \text{ km s}^{-1}$  (Sandage & Tammann 1981). This galaxy was observed in 1979 with *Einstein* IPC and it displayed flux variations by a factor of 3.2 over a time scale of 5 months (Maccacaro et al. 1987). This source was observed with EXOSAT on four occasions in 1985. Later *Ginga* (Nandra & Pounds 1994), ROSAT (Rush et al. 1996) and ASCA (Nandra et al. 1997) made extensive observations of this Seyfert galaxy.

### **NGC3783**

NGC3783 is one of the nearest ( $z=0.009$ ) and brightest ( $m_v = 13.43$ ,  $B-V=0.56$ ,  $U-B=-0.70$  and  $M=-20.2$ ) Seyfert 1 galaxy (Osmer et al. 1974). This galaxy has displayed both optical continuum and emission line variability (Penfold 1979; Menzies & Feast 1983; de Ruiter & Lub 1986). This is the first X-ray Seyfert galaxy identified from *Ariel V* survey (Cooke et al. 1976). Later this galaxy was observed with *Einstein* (Kruiper et al. 1990), HEAO-1 (Mushotzky 1984), EXOSAT (Turner & Pounds 1989), *Ginga* (Nandra & Pounds 1994), ROSAT (Alloin et al. 1995) and ASCA (Nandra et al. 1997) satellites. This galaxy was observed on 3 epochs with EXOSAT between 1983 and 1985.

### **NGC4593**

NGC4593 also is a nearby ( $z=0.009$ ) and bright ( $m_v=13.15$ ,  $B-V=0.8$ ,  $U-B=-0.19$  and  $M=-20.5$ ; Veron et al. 1982) Seyfert 1 galaxy (Simkin et al. 1980) with strong broad allowed, and narrow forbidden optical emission lines and weak radio emission (Ulvestad & Wilson 1984). This galaxy was first observed in the X-ray spectral region with Uhuru satellite and it was proposed that the X-ray source 4U1240-05 is associated with the cluster Abell 1588. Later on HEAO-1 observations with small error box, have identified this X-ray source (H1238-049) with the Seyfert galaxy NGC4593 (Marshall et al. 1978; Wood et al. 1984). *Ariel V* (Bell Burnell & Culhane 1979; Hayes et al. 1981) and *Einstein* SSS+MPC (Holt et al. 1989) were the other instruments that studied this source prior to EXOSAT. EXOSAT observed this galaxy on seven epochs between 1984 and 1986. Later this source was observed with *Ginga* (Nandra & Pounds 1994), ROSAT (Rush et al. 1993) and ASCA (Nandra et al. 1997).

### **3C382**

Optical and ultraviolet observations of the Seyfert 1 galaxy 3C382 ( $m_v=15.39$ ;  $M=-22.4$ ) displayed the presence of narrow and very broad variable emission lines (Osterbrock et al. 1975, 1976; Tadhunter et al. 1986, Reichert et al. 1985). Ultraviolet and infrared excesses (O'Dell et al. 1978; Puschell 1981) are present in the continuum energy distribution of this galaxy. It is a strong radio source with double radio lobes (MacDonald et al. 1968; Preuss & Fosbury 1983). Prior to EXOSAT, 3C382 was observed with Ariel V (Elvis et al 1978), HEAO-1 (Marshall et al. 1979, Dower et al. 1980), and Einstein (Petre et al. 1984; Urry et al. 1989) X-ray satellites. This radio-loud galaxy was observed with EXOSAT on many occasions between 1983 and 1985. Later it was also observed with Ginga (Kaastra et al. 1991; Nandra & Pounds 1994) and ROSAT (Walter & Fink 1993).

### **MCG-2-58-22**

This is a bright type 1 Seyfert galaxy ( $m_v=13.76$ ,  $B-V=0.36$ ,  $U-B=-0.98$  and  $M=-23.1$ ; Veron-Cetty & Veron 1993). Optical spectra of this galaxy display extremely broad Balmer lines and a weak broad [O III] wing (Vrtilek & Carleton 1985; van Groningen & de Bruyen 1989). X-ray spectra of MCG 2-58-22 obtained from Einstein (Holt et al. 1989), HEAO 1, and HEAO-2 (Mushotzky 1984) observations showed no evidence of soft excess in it. This source was observed with EXOSAT on six epochs during 1984 November 16-26. Later on Ginga (Nandra & Pounds 1994) and ASCA (Nandra et al. 1997) satellites monitored this source.

### **Analysis of LE and ME spectra**

Analysis of the combined LE and ME spectra were carried out using XSPEC software package. Initially a simple power-law model with uniform absorption (using the absorption cross sections given by Morrison & McCammon 1983) in the line-of-sight to the source ( $N_H$ ) was used to fit the spectra. The parameters of this model are presented in Table 3.1.2C. The best-fit parameters of of this model show that the derived values of  $N_H$  are smaller than the corresponding Galactic  $N_H$  values, except for the two sources NGC3516 and ESO 140-G43. Thus, in the next model, we have frozen the values of  $N_H$  with the corresponding galactic values for the sources showing  $N_H$  deficiency (Table 3.1.2D). Since we do not know the galactic  $N_H$  values towards ESO 021-G21 and ESO 140-G43, we have assumed  $N_H$  to be  $2.0 \times 10^{20} \text{ cm}^{-2}$ . The best-fitting parameters

TABLE 3.1.2C POWER-LAW + ABSORPTION

Source	Date (year,day)	$\Gamma^a$	$N^b$	$N_H$ (observed)	$N_H$ (galactic)	$\chi^2_\tau$ /d.o.f.
ESO012-G21	1985,108	1.21 <sup>+0.18</sup> <sub>-0.15</sub>	00.80 <sup>+0.62</sup> <sub>-0.30</sub>	0-0.50	2.00	1.10/30
Mkn352	1983,319	1.82 <sup>+0.30</sup> <sub>-0.28</sub>	01.58 <sup>+2.05</sup> <sub>-1.43</sub>	03.01 <sup>+3.72</sup> <sub>-1.88</sub>	5.60	1.24/31
Mkn374	1984,310	1.80 <sup>+0.26</sup> <sub>-0.28</sub>	01.95 <sup>+0.80</sup> <sub>-0.60</sub>	02.00 <sup>+2.37</sup> <sub>-1.32</sub>	6.30	1.18/29
NGC3516	1985,308	1.33	02.83	107	3.00	2.85/28
NGC3516	1985,311	1.32	03.08	282	3.00	2.32/29
NGC3516	1985,330	1.14	02.07	238 <sup>+120</sup> <sub>-129</sub>	3.00	2.53/30
NGC3516	1985,340	1.18 <sup>+0.32</sup> <sub>-0.30</sub>	01.60 <sup>+1.49</sup> <sub>-0.66</sub>	228 <sup>+149</sup> <sub>-131</sub>	3.00	1.43/27
NGC3783	1983,347	1.32 <sup>+0.07</sup> <sub>-0.07</sub>	06.50 <sup>+0.67</sup> <sub>-0.61</sub>	06.41 <sup>+4.00</sup> <sub>-2.30</sub>	9.40	1.48/28
NGC3783	1984,162	1.40 <sup>+0.03</sup> <sub>-0.04</sub>	13.60 <sup>+0.60</sup> <sub>-0.70</sub>	02.12 <sup>+0.58</sup> <sub>-0.45</sub>	9.40	1.08/32
NGC3783	1985,005	1.40 <sup>+0.05</sup> <sub>-0.04</sub>	08.95 <sup>+0.58</sup> <sub>-0.53</sub>	06.93 <sup>+2.35</sup> <sub>-1.72</sub>	9.40	1.75/32
Mkn766	1985,363	1.81 <sup>+0.11</sup> <sub>-0.12</sub>	08.96 <sup>+1.44</sup> <sub>-1.25</sub>	0-0.80	1.60	1.24/29
Mkn766	1985,364	1.98 <sup>+0.13</sup> <sub>-0.11</sub>	11.77 <sup>+1.79</sup> <sub>-1.57</sub>	0-1.80	1.60	1.34/27
Mkn766	1985,364	2.14 <sup>+0.11</sup> <sub>-0.12</sub>	11.17 <sup>+1.53</sup> <sub>-1.40</sub>	01.74 <sup>+0.72</sup> <sub>-0.54</sub>	1.60	1.06/32
Mkn766	1985,365	1.95 <sup>+0.10</sup> <sub>-0.11</sub>	10.30 <sup>+1.40</sup> <sub>-1.24</sub>	0-1.05	1.60	1.25/32
Mkn766	1985,365	2.07 <sup>+0.07</sup> <sub>-0.07</sub>	15.72 <sup>+1.44</sup> <sub>-1.34</sub>	0-1.57	1.60	1.10/32
NGC4593	1984,154	1.85 <sup>+0.07</sup> <sub>-0.07</sub>	10.92 <sup>+0.96</sup> <sub>-0.92</sub>	01.04 <sup>+0.32</sup> <sub>-0.27</sub>	2.30	1.79/27
NGC4593	1984,183	1.76	11.96	01.33	2.30	3.45/27
NGC4593	1985,176	1.22	01.73	0.00	2.30	2.70/27
NGC4593	1985,180	1.66 <sup>+0.12</sup> <sub>-0.11</sub>	04.06 <sup>+0.69</sup> <sub>-0.58</sub>	01.09 <sup>+0.64</sup> <sub>-0.45</sub>	2.30	1.27/27
NGC4593	1985,185	1.64 <sup>+0.07</sup> <sub>-0.09</sub>	04.06 <sup>+0.43</sup> <sub>-0.38</sub>	01.04 <sup>+0.46</sup> <sub>-0.34</sub>	2.30	0.98/27
NGC4593	1986,009	1.98 <sup>+0.05</sup> <sub>-0.05</sub>	13.65 <sup>+0.91</sup> <sub>-0.83</sub>	01.58 <sup>+0.28</sup> <sub>-0.25</sub>	2.30	1.94/27
NGC4593	1986,010	1.97	11.79	01.29	2.30	3.89/27
Mkn279	1983,320	1.84 <sup>+0.09</sup> <sub>-0.09</sub>	06.90 <sup>+0.84</sup> <sub>-0.77</sub>	01.10 <sup>+0.50</sup> <sub>-0.40</sub>	1.90	1.48/34
Mkn279	1984,028	1.40 <sup>+0.06</sup> <sub>-0.04</sub>	03.43 <sup>+0.32</sup> <sub>-0.20</sub>	0.00	1.90	1.54/34
Mkn464	1985,178	1.33 <sup>+0.09</sup> <sub>-0.07</sub>	01.69 <sup>+0.60</sup> <sub>-0.45</sub>	0-0.30	1.70	1.32/26
Mkn290	1986,056	1.33 <sup>+0.07</sup> <sub>-0.05</sub>	01.43 <sup>+0.17</sup> <sub>-0.09</sub>	0-0.90	1.80	0.80/29

TABLE 3.1.2C - continued

Source	Date (year,day)	$\Gamma^a$	$N^b$	$N_H^c$ (observed)	$N_H^c$ (galactic)	$\chi^2_r$ /d.o.f.
3C382	1983,255	1.65 <sup>+0.09</sup> <sub>-0.09</sub>	06.28 <sup>+0.78</sup> <sub>-0.69</sub>	04.10 <sup>+1.40</sup> <sub>-1.10</sub>	7.40	0.79/33
3C382	1985,116	1.85 <sup>+0.18</sup> <sub>-0.18</sub>	07.65 <sup>+1.93</sup> <sub>-1.55</sub>	05.68 <sup>+3.61</sup> <sub>-2.35</sub>	7.40	0.90/33
3C382	1985,117	1.66 <sup>+0.09</sup> <sub>-0.10</sub>	05.70 <sup>+0.75</sup> <sub>-0.07</sub>	03.11 <sup>+1.48</sup> <sub>-1.00</sub>	7.40	1.93/33
3C382	1985,147	1.62 <sup>+0.08</sup> <sub>-0.08</sub>	07.59 <sup>+0.90</sup> <sub>-0.08</sub>	03.40 <sup>+1.51</sup> <sub>-1.02</sub>	7.40	0.98/33
3C382	1985,153	1.75 <sup>+0.07</sup> <sub>-0.07</sub>	11.05 <sup>+1.10</sup> <sub>-1.00</sub>	04.23 <sup>+1.49</sup> <sub>-1.07</sub>	7.40	0.94/33
3C382	1985,161	1.76 <sup>+0.06</sup> <sub>-0.06</sub>	09.97 <sup>+0.75</sup> <sub>-0.70</sub>	04.04 <sup>+1.29</sup> <sub>-0.92</sub>	7.40	1.37/33
3C382	1985,171	1.67 <sup>+0.06</sup> <sub>-0.06</sub>	10.31 <sup>+0.83</sup> <sub>-0.76</sub>	03.66 <sup>+0.95</sup> <sub>-0.75</sub>	7.40	0.85/33
3C382	1985,195	1.66 <sup>+0.08</sup> <sub>-0.09</sub>	10.09 <sup>+1.15</sup> <sub>-1.03</sub>	03.25 <sup>+1.07</sup> <sub>-0.83</sub>	7.40	1.30/33
3C382	1985,211	1.48 <sup>+0.07</sup> <sub>-0.06</sub>	06.35 <sup>+0.58</sup> <sub>-0.54</sub>	01.54 <sup>+0.53</sup> <sub>-0.32</sub>	7.40	0.96/33
3C382	1985,223	1.84 <sup>+0.08</sup> <sub>-0.08</sub>	10.95 <sup>+1.14</sup> <sub>-1.04</sub>	04.02 <sup>+1.23</sup> <sub>-0.94</sub>	7.40	1.15/33
3C382	1985,233	1.83 <sup>+0.08</sup> <sub>-0.07</sub>	14.54 <sup>+1.46</sup> <sub>-1.32</sub>	05.60 <sup>+1.60</sup> <sub>-1.24</sub>	7.40	1.17/33
3C382	1985,246	1.66 <sup>+0.05</sup> <sub>-0.05</sub>	10.75 <sup>+0.75</sup> <sub>-0.70</sub>	02.89 <sup>+0.71</sup> <sub>-0.57</sub>	7.40	0.92/33
3C382	1985,256	1.67 <sup>+0.06</sup> <sub>-0.05</sub>	09.99 <sup>+0.78</sup> <sub>-0.72</sub>	02.46 <sup>+0.63</sup> <sub>-0.51</sub>	7.40	0.60/33
ESO140-G43	1985,105	1.46 <sup>+0.21</sup> <sub>-0.21</sub>	04.28 <sup>+1.49</sup> <sub>-1.08</sub>	11.00 <sup>+17.8</sup> <sub>-6.90</sub>	2.00	0.70/28
MCG2-58-22	1984,321	1.52 <sup>+0.07</sup> <sub>-0.06</sub>	06.00 <sup>+0.56</sup> <sub>-0.52</sub>	00.80 <sup>+0.39</sup> <sub>-0.28</sub>	3.40	0.82/29
MCG2-58-22	1984,322	1.58 <sup>+0.08</sup> <sub>-0.09</sub>	06.32 <sup>+0.75</sup> <sub>-0.68</sub>	01.35 <sup>+0.60</sup> <sub>-0.45</sub>	3.40	1.11/29
MCG2-58-22	1984,325	1.52 <sup>+0.09</sup> <sub>-0.08</sub>	06.25 <sup>+0.78</sup> <sub>-0.70</sub>	01.08 <sup>+0.55</sup> <sub>-0.40</sub>	3.40	0.83/29
MCG2-58-22	1984,327	1.19	03.98	02.81	3.40	2.20/29
MCG2-58-22	1984,329	1.63 <sup>+0.08</sup> <sub>-0.08</sub>	07.35 <sup>+0.78</sup> <sub>-0.75</sub>	01.64 <sup>+0.56</sup> <sub>-0.48</sub>	3.40	1.31/29
MCG2-58-22	1984,331	1.62 <sup>+0.07</sup> <sub>-0.07</sub>	06.58 <sup>+0.86</sup> <sub>-0.61</sub>	01.24 <sup>+0.47</sup> <sub>-0.37</sub>	3.40	0.88/30

<sup>a</sup> Photon index.

<sup>b</sup> Normalization in  $10^{-3}$  photons  $\text{cm}^{-2} \text{s}^{-1} \text{keV}^{-1}$  at 1 keV.

<sup>c</sup> Column density in  $10^{20} \text{cm}^{-2}$ .

TABLE 3.1.2D POWER-LAW + FIXED ABSORPTION †

Source	Date (year,day)	$\Gamma^a$	$N^b$	Flux <sup>c</sup>		$L_x^d$		$\chi^2_\nu$ /d.o.f.
				(0.1-2keV)	(2-10 keV)	(0.1-2keV)	(2-10 keV)	
ESO012-G21	1985,108	1.87 <sup>+0.13</sup> <sub>-0.14</sub>	01.89 <sup>+0.26</sup> <sub>-0.24</sub>	00.46±0.06	00.58±0.06	02.00±0.26	02.50±0.26	1.30/31
Mkn352	1983,319	2.03 <sup>+0.12</sup> <sub>-0.13</sub>	05.95 <sup>+0.78</sup> <sub>-0.81</sub>	01.36±0.18	01.46±0.13	01.34±0.18	01.43±0.13	1.25/32
Mkn374	1984,310	2.16 <sup>+0.13</sup> <sub>-0.15</sub>	03.11 <sup>+0.46</sup> <sub>-0.50</sub>	00.69±0.09	00.62±0.04	06.00±0.78	05.39±0.35	1.35/30
Mkn766	1985,363	2.06 <sup>+0.07</sup> <sub>-0.08</sub>	12.30 <sup>+1.00</sup> <sub>-1.10</sub>	03.91±0.34	02.88±0.08	02.45±0.21	01.80±0.05	1.78/30
Mkn766	1985,364	2.06 <sup>+0.05</sup> <sub>-0.07</sub>	12.76 <sup>+0.90</sup> <sub>-0.93</sub>	04.05±0.37	03.02±0.09	02.54±0.23	01.89±0.06	1.34/28
Mkn766	1985,364	2.11 <sup>+0.06</sup> <sub>-0.06</sub>	10.88 <sup>+0.76</sup> <sub>-0.79</sub>	03.53±0.34	02.34±0.07	02.22±0.21	01.48±0.04	1.02/33
Mkn766	1985,365	2.14 <sup>+0.06</sup> <sub>-0.07</sub>	12.95 <sup>+0.91</sup> <sub>-0.95</sub>	04.24±0.34	02.71±0.07	02.66±0.21	01.70±0.04	1.59/33
Mkn766	1985,365	2.13 <sup>+0.04</sup> <sub>-0.05</sub>	16.91 <sup>+0.95</sup> <sub>-0.97</sub>	05.52±0.42	03.58±0.07	03.46±0.26	02.24±0.04	1.16/33
Mkn279	1983,320	1.95 <sup>+0.05</sup> <sub>-0.05</sub>	07.90 <sup>+0.50</sup> <sub>-0.50</sub>	02.34±0.19	02.20±0.09	09.97±0.81	09.37±0.38	1.64/35
Mkn279	1984,028	2.04 <sup>+0.05</sup> <sub>-0.06</sub>	07.69 <sup>+0.45</sup> <sub>-0.44</sub>	02.34±0.19	01.87±0.11	09.97±0.68	07.97±0.47	1.67/35
Mkn464	1985,178	2.12 <sup>+0.06</sup> <sub>-0.07</sub>	04.66 <sup>+0.33</sup> <sub>-0.34</sub>	01.20±0.10	01.00±0.05	14.10±1.20	11.80±0.60	1.50/27
Mkn290	1986,056	2.18 <sup>+0.07</sup> <sub>-0.08</sub>	04.14 <sup>+0.31</sup> <sub>-0.32</sub>	00.91±0.06	00.90±0.05	03.40±0.22	03.40±0.20	1.65/30
ESO140-G43 <sup>c</sup>	1985,105			00.80±0.20	02.55±0.12	00.70±0.17	02.20±0.10	
NGC3516 <sup>c</sup>	1985,308			00.15±0.03	01.96±0.05	0.057±0.010	00.73±0.02	
NGC3516 <sup>c</sup>	1985,311			00.05±0.01	01.94±0.04	0.018±0.003	00.72±0.01	
NGC3516 <sup>c</sup>	1985,330			00.04±0.01	01.83±0.07	0.017±0.003	00.68±0.03	
NGC3516 <sup>c</sup>	1985,340			00.04±0.01	01.31±0.04	0.014±0.004	00.49±0.01	
NGC3783	1983,347	1.35 <sup>+0.06</sup> <sub>-0.06</sub>	06.79 <sup>+0.58</sup> <sub>-0.55</sub>	01.33±0.17	04.81±0.07	00.58±0.07	02.10±0.03	1.49/29
NGC3783	1984,162	1.50	15.70	03.04±0.22	08.78±0.08	01.32±0.09	03.83±0.03	3.59/33
NGC3783	1985,005	1.43 <sup>+0.03</sup> <sub>-0.04</sub>	09.34 <sup>+0.46</sup> <sub>-0.46</sub>	01.81±0.16	05.83±0.06	00.79±0.07	02.54±0.03	1.78/33
NGC4593	1984,154	2.01	13.48	03.88±0.23	03.40±0.05	01.36±0.08	01.19±0.02	2.76/28
NGC4593	1984,183	1.84	13.27	03.66±0.25	04.33±0.05	01.28±0.09	01.52±0.02	3.86/28
NGC4593	1985,176	1.82 <sup>+0.05</sup> <sub>-0.04</sub>	03.96 <sup>+0.21</sup> <sub>-0.22</sub>	01.08±0.07	01.32±0.04	00.38±0.02	00.46±0.01	0.83/28
NGC4593	1985,180	1.85 <sup>+0.05</sup> <sub>-0.05</sub>	05.20 <sup>+0.28</sup> <sub>-0.29</sub>	01.43±0.07	01.68±0.05	00.50±0.02	00.59±0.02	1.50/28
NGC4593	1985,185	1.77 <sup>+0.05</sup> <sub>-0.04</sub>	04.95 <sup>+0.26</sup> <sub>-0.26</sub>	01.35±0.09	01.78±0.03	00.47±0.03	00.62±0.01	1.44/28
NGC4593	1986,009	2.09	15.64	04.62±0.15	03.51±0.04	01.62±0.05	01.23±0.01	2.48/28
NGC4593	1986,010	2.14	14.61	04.39±0.14	03.04±0.04	01.54±0.05	01.06±0.01	4.93/28
3C382	1983,255	1.80 <sup>+0.05</sup> <sub>-0.06</sub>	07.65 <sup>+0.51</sup> <sub>-0.61</sub>	01.41±0.08	02.77±0.06	21.40±1.20	42.10±0.90	1.10/34
3C382	1985,116	1.93 <sup>+0.09</sup> <sub>-0.10</sub>	08.50 <sup>+0.90</sup> <sub>-0.93</sub>	01.33±0.13	02.66±0.12	20.50±1.90	40.40±1.80	0.92/34
3C382	1985,117	1.78	06.75	01.25±0.12	02.48±0.07	19.00±1.80	37.70±1.10	2.25/34
3C382	1985,147	1.73 <sup>+0.07</sup> <sub>-0.07</sub>	08.80 <sup>+0.80</sup> <sub>-0.80</sub>	01.74±0.16	03.44±0.07	26.40±2.40	52.30±1.10	1.30/34
3C382	1985,153	1.83 <sup>+0.06</sup> <sub>-0.06</sub>	12.33 <sup>+0.96</sup> <sub>-0.93</sub>	02.16±0.18	04.26±0.07	32.80±2.70	64.80±1.10	1.18/34

TABLE 3.1.2D - continued

Source	Date (year,day)	$\Gamma^a$	$N^b$	Flux <sup>c</sup>		$L_x^d$		$\chi^2_r$ /d.o.f.
				(0.1-2keV)	(2-10 keV)	(0.1-2keV)	(2-10 keV)	
3C382	1985,161	1.82 <sup>+0.05</sup> <sub>-0.06</sub>	10.82 <sup>+0.70</sup> <sub>-0.68</sub>	01.93±0.16	03.80±0.05	29.30±2.40	57.80±0.80	1.67/34
3C382	1985,171	1.79 <sup>+0.05</sup> <sub>-0.05</sub>	12.03 <sup>+0.73</sup> <sub>-0.72</sub>	02.22±0.13	04.38±0.06	33.80±2.00	66.60±0.90	1.54/34
3C382	1985,195	1.85 <sup>+0.06</sup> <sub>-0.06</sub>	13.01 <sup>+0.89</sup> <sub>-0.90</sub>	02.24±0.13	04.43±0.08	34.10±2.00	67.30±1.20	1.96/34
3C382	1985,211	1.66	08.07	01.75±0.11	03.45±0.05	26.60±1.70	52.50±0.80	3.00/34
3C382	1985,223	1.96 <sup>+0.07</sup> <sub>-0.06</sub>	12.90 <sup>+0.93</sup> <sub>-0.94</sub>	01.93±0.13	03.80±0.07	29.40±2.00	57.80±1.10	1.54/34
3C382	1985,233	1.89 <sup>+0.06</sup> <sub>-0.05</sub>	15.78 <sup>+0.99</sup> <sub>-0.98</sub>	02.57±0.16	05.08±0.09	39.10±2.40	77.30±1.40	1.25/34
3C382	1985,246	1.77	12.54	02.35±0.14	04.65±0.06	35.70±2.10	70.70±0.90	2.16/34
3C382	1985,256	1.82	12.22	02.16±0.13	04.26±0.06	32.90±1.90	64.80±0.90	2.23/34
MCG2-58-22 <sup>f</sup>	1984,321	1.66 <sup>+0.06</sup> <sub>-0.07</sub>	07.22 <sup>+0.61</sup> <sub>-0.59</sub>	01.84±0.17	03.24±0.38	18.30±1.70	32.20±3.80	1.99/30
MCG2-58-22 <sup>f</sup>	1984,322	1.76 <sup>+0.06</sup> <sub>-0.06</sub>	08.05 <sup>+0.56</sup> <sub>-0.57</sub>	01.91±0.15	03.15±0.26	19.00±1.50	31.30±2.60	1.67/30
MCG2-58-22 <sup>f</sup>	1984,325	1.74 <sup>+0.05</sup> <sub>-0.06</sub>	08.33 <sup>+0.60</sup> <sub>-0.63</sub>	01.96±0.16	03.41±0.32	19.50±1.60	33.90±3.20	1.57/30
MCG2-58-22 <sup>f</sup>	1984,327	1.81 <sup>+0.05</sup> <sub>-0.06</sub>	09.46 <sup>+0.60</sup> <sub>-0.63</sub>	02.16±0.15	03.47±0.28	21.40±1.50	34.50±2.80	1.95/30
MCG2-58-22 <sup>f</sup>	1984,329	1.78 <sup>+0.05</sup> <sub>-0.05</sub>	08.97 <sup>+0.55</sup> <sub>-0.57</sub>	02.29±0.18	03.43±0.25	22.80±1.80	34.10±2.50	1.76/30
MCG2-58-22 <sup>f</sup>	1984,331	1.81 <sup>+0.05</sup> <sub>-0.05</sub>	08.47 <sup>+0.51</sup> <sub>-0.51</sub>	02.02±0.14	03.03±0.27	20.10±1.40	30.10±2.70	1.78/31

<sup>e</sup> Fixed with corresponding galactic  $N_H$  value for the sources with observed  $N_H < \text{galactic value}$ .

<sup>a</sup> Photon index.

<sup>b</sup> Normalization in  $10^{-3}$  photon  $\text{cm}^{-2} \text{s}^{-1} \text{keV}^{-1}$ .

<sup>c</sup> Flux in  $10^{-11}$  erg  $\text{cm}^{-2} \text{s}^{-1}$ .

<sup>d</sup> Luminosity in  $10^{43}$  erg  $\text{s}^{-1}$ .

<sup>e</sup> Flux and  $L_x$  values derived from the Power-law +absorption model (Table 3.1.1c).

<sup>f</sup> Flux and  $L_x$  values derived from the Two power-law +fixed absorption model (Table 3.1.1g).

of the power-law and fixed absorption model are shown in Table 3.1.2D along with the 90 per cent confidence errors computed as described by Lampton, Margon & Bowyer (1976). The reduced  $\chi^2$  ( $\chi_r^2$ ) values in this Table are large ( $>1.0$ ) and show that this model is unacceptable. For the unacceptable fits, with  $\chi_r^2 > 2$ , the software restrained from estimating the 90 per cent confidence uncertainty ranges and for such fits the error range has not been provided in the Tables 3.1.2C-3.1.2H. To estimate the luminosities presented in Table 3.1.2D the values of  $H_0 = 50 \text{ km s}^{-1} \text{ Mpc}^{-1}$  and  $q_0=0$  have been used. The X-ray spectra of all the sources in our sample are presented in this section along with the power-law plus absorption model. Residuals between the model and the spectra are shown in the lower panels of these figures.

The deficiency in  $N_H$  implies source spectra with more emission than the power-law predictions at low-energies, i.e. a ‘soft excess’. It is shown that (Wilkes & Elvis 1987) forcing a column density in the presence of a soft excess always steepens the spectral slope. Comparison of models without and with frozen  $N_H$  values shows that the spectral slopes of the model with frozen  $N_H$  are steeper, thus suggesting the presence of soft excesses in all the sources other than ESO140-G43. In the case of NGC3516, even though the observed column density is greater (by two orders of magnitude) than the galactic  $N_H$  value, the presence of a weak soft excess emission is detected. The presence/absence of soft excesses can be seen in the residual plots of these sources. To fit the soft excesses, two power-law (Table 3.1.2G), thermal bremsstrahlung (Table 3.1.2E) and broken power-law (Table 3.1.2E ; break energy fixed at 0.6 keV following Wilkes et al. 1989) models were tried.

It was mentioned earlier in this section that there is evidence for the presence of iron K-shell emission and absorption lines in the X-ray spectra of Seyfert galaxies, and the residual plots of the 9 Seyferts NGC3516, NGC3783, Mkn766, NGC4593, Mkn464, Mkn290, 3C382, ESO012-G43 and MCG-2-58-22 indeed indicate the presence of an emission feature near 6.0 keV. Thus a Gaussian component was added to the power-law model and used to fit the spectra of these sources (Tables 3.1.2H and 3.1.2I). The  $\chi^2$  statistics suggest that the fit is better than that with the power-law model. F-test calculations show that the inclusion of the emission line is highly



TABLE 3.1.2E THERMAL BREMSSTRAHLUNG + ABSORPTION

Source	Date (year,day)	kT <sup>a</sup>	N <sup>b</sup>	$\chi^2_r$ /d.o.f.
ESO012-G21	1985,108	04.56 <sup>+2.47</sup> <sub>-1.29</sub>	1.01 <sup>+0.37</sup> <sub>-0.31</sub>	1.14/31
Mkn352	1983,319	03.60 <sup>+1.57</sup> <sub>-0.90</sub>	3.74 <sup>+1.58</sup> <sub>-1.20</sub>	1.75/32
Mkn374	1984,310	04.26	1.33	2.14/30
NGC3783	1983,347	50.45 <sup>+45.10</sup> <sub>-17.98</sub>	1.77 <sup>+0.31</sup> <sub>-0.31</sub>	1.69/29
NGC3783	1984,162	22.54	4.63	5.05/33
NGC3783	1985,005	25.88 <sup>+6.07</sup> <sub>-4.32</sub>	2.84 <sup>+0.24</sup> <sub>-0.25</sub>	1.80/33
Mkn766	1985,363	06.30	3.95	4.00/30
Mkn766	1985,364	04.43	5.82	3.30/28
Mkn766	1985,364	03.83	5.48	2.14/33
Mkn766	1985,365	04.92	4.83	4.13/33
Mkn766	1985,365	04.44	7.10	3.92/33
NGC4593	1984,154	05.64	5.07	8.90/28
NGC4593	1984,183	07.17	5.00	7.00/28
NGC4593	1985,176	03.85	2.86	2.60/28
NGC4593	1985,180	04.29	3.24	4.10/28
NGC4593	1985,185	06.92	2.10	4.70/28
NGC4593	1986,009	04.38	6.95	20.0/28
NGC4593	1986,010	04.40	6.07	22.6/28
Mkn279	1983,320	05.32	3.44	3.76/35
Mkn279	1984,028	02.34	8.40	3.65/35
Mkn464	1985,178	02.96	3.08	2.29/27
Mkn290	1986,056	03.47	2.25	3.25/30
3C382	1983,255	07.78	2.88	3.00/34
3C382	1985,116	4.83 <sup>+1.45</sup> <sub>-0.95</sub>	4.15 <sup>+1.06</sup> <sub>-0.89</sub>	1.40/34
3C382	1985,117	8.51	2.40	2.57/34
3C382	1985,147	9.93 <sup>+2.57</sup> <sub>-1.77</sub>	2.99 <sup>+0.45</sup> <sub>-0.41</sub>	1.90/34
3C382	1985,153	7.80	4.39	2.25/34
3C382	1985,161	7.89	3.89	2.52/34
3C382	1985,171	8.89	4.11	3.71/34
3C382	1985,195	7.77	4.58	4.38/34
3C382	1985,211	15.82	2.32	4.48/34
3C382	1985,223	6.03	4.84	3.32/34
3C382	1985,233	6.15	6.37	2.88/74
3C382	1985,246	9.67	4.11	4.49/34
3C382	1985,256	8.93	3.97	4.69/34
ESO140-G43	1985,105	98.23 <sup>+7.60</sup> <sub>-4.20</sub>	0.77	0.90/29

<sup>a</sup> Plasma temperature in keV.

<sup>b</sup> Normalization in  $10^{-3}$  photons  $\text{cm}^{-2} \text{s}^{-1} \text{keV}^{-1}$  at 1 keV.

TABLE 3.1.2F BROKEN POWER-LAW\* + FIXED ABSORPTION†

Source	Date (year,day)	$\Gamma_1^a$	$\Gamma_2^a$	$N^b$	$\chi^2_\nu/\text{d.o.f.}$
ESO012-G21	1985,108	4.47 <sup>+0.97</sup> <sub>-1.13</sub>	1.25 <sup>+0.34</sup> <sub>-0.35</sub>	00.16 <sup>+0.36</sup> <sub>-0.11</sub>	1.06/30
Mkn352	1983,319	3.30 <sup>+1.16</sup> <sub>-1.68</sub>	1.81 <sup>+0.30</sup> <sub>-0.30</sub>	02.10 <sup>+6.00</sup> <sub>-1.42</sub>	1.23/31
Mkn374	1984,310	4.17 <sup>+0.95</sup> <sub>-1.18</sub>	1.81 <sup>+0.27</sup> <sub>-0.27</sub>	00.60 <sup>+1.09</sup> <sub>-0.23</sub>	1.18/29
NGC3783	1983,347	2.70 <sup>+0.80</sup> <sub>-0.80</sub>	1.33 <sup>+0.07</sup> <sub>-0.06</sub>	03.26 <sup>+8.64</sup> <sub>-1.54</sub>	1.49/28
NGC3783	1984,162	5.09 <sup>+0.28</sup> <sub>-0.33</sub>	1.42 <sup>+0.04</sup> <sub>-0.03</sub>	02.18 <sup>+0.51</sup> <sub>-0.39</sub>	0.85/32
NGC3783	1985/005	2.90 <sup>+0.68</sup> <sub>-0.98</sub>	1.40 <sup>+0.04</sup> <sub>-0.04</sub>	04.21 <sup>+2.98</sup> <sub>-1.37</sub>	1.68/32
Mkn766	1985,363	2.90 <sup>+0.30</sup> <sub>-0.30</sub>	1.81 <sup>+0.11</sup> <sub>-0.12</sub>	05.17 <sup>+2.13</sup> <sub>-1.47</sub>	1.23/29
Mkn766	1985,364	2.28 <sup>+0.32</sup> <sub>-0.35</sub>	1.99 <sup>+0.12</sup> <sub>-0.11</sub>	10.15 <sup>+4.35</sup> <sub>-2.95</sub>	1.34/27
Mkn766	1985,364	3.04 <sup>+0.33</sup> <sub>-0.39</sub>	1.85 <sup>+0.10</sup> <sub>-0.12</sub>	11.69 <sup>+4.88</sup> <sub>-3.31</sub>	1.02/32
Mkn766	1985,365	2.76 <sup>+0.26</sup> <sub>-0.28</sub>	1.94 <sup>+0.11</sup> <sub>-0.09</sub>	06.85 <sup>+2.40</sup> <sub>-1.76</sub>	1.25/32
Mkn766	1985,365	2.40 <sup>+0.20</sup> <sub>-0.25</sub>	2.07 <sup>+0.07</sup> <sub>-0.07</sub>	13.40 <sup>+3.30</sup> <sub>-2.60</sub>	1.09/32
NGC4593	1984,154	2.97 <sup>+0.20</sup> <sub>-0.22</sub>	1.82 <sup>+0.06</sup> <sub>-0.06</sub>	05.86 <sup>+1.39</sup> <sub>-1.11</sub>	1.24/27
NGC4593	1984,183	2.77	1.72	06.67	2.70/27
NGC4593	1985,176	2.04 <sup>+0.47</sup> <sub>-0.54</sub>	1.77 <sup>+0.14</sup> <sub>-0.13</sub>	03.23 <sup>+2.14</sup> <sub>-1.20</sub>	0.84/27
NGC4593	1985,180	2.08 <sup>+0.38</sup> <sub>-0.42</sub>	1.68 <sup>+0.12</sup> <sub>-0.13</sub>	02.74 <sup>+1.48</sup> <sub>-0.94</sub>	1.34/27
NGC4593	1985,185	2.03 <sup>+0.30</sup> <sub>-0.33</sub>	1.62 <sup>+0.08</sup> <sub>-0.09</sub>	02.51 <sup>+0.92</sup> <sub>-0.65</sub>	1.01/27
NGC4593	1986,009	2.78 <sup>+0.15</sup> <sub>-0.16</sub>	1.78 <sup>+0.05</sup> <sub>-0.05</sub>	10.63 <sup>+1.90</sup> <sub>-1.58</sub>	1.93/27
NGC4593	1986,010	2.94	1.77	08.12	3.87/27
Mkn279	1983,320	2.51 <sup>+0.31</sup> <sub>-0.33</sub>	1.83 <sup>+0.09</sup> <sub>-0.10</sub>	04.81 <sup>+1.76</sup> <sub>-1.26</sub>	1.48/34
Mkn279	1984,028	2.74 <sup>+0.42</sup> <sub>-0.46</sub>	1.80 <sup>+0.17</sup> <sub>-0.17</sub>	03.63 <sup>+2.34</sup> <sub>-1.45</sub>	1.54/34
Mkn464	1985,178	3.83 <sup>+0.55</sup> <sub>-0.63</sub>	1.76 <sup>+0.18</sup> <sub>-0.18</sub>	01.00 <sup>+0.86</sup> <sub>-0.45</sub>	1.05/26
Mkn290	1986,056	4.12 <sup>+0.51</sup> <sub>-0.54</sub>	1.65 <sup>+0.18</sup> <sub>-0.19</sub>	00.63 <sup>+0.50</sup> <sub>-0.28</sub>	0.75/29
3C382	1983,255	3.04 <sup>+0.33</sup> <sub>-0.40</sub>	1.70 <sup>c</sup>	03.88 <sup>+0.33</sup> <sub>-1.05</sub>	0.80/34
3C382	1985,116	3.54 <sup>+0.46</sup> <sub>-0.63</sub>	1.70 <sup>c</sup>	02.49 <sup>+1.03</sup> <sub>-0.58</sub>	0.95/34
3C382	1985,117	3.71 <sup>+0.39</sup> <sub>-0.58</sub>	1.70 <sup>c</sup>	02.17 <sup>+0.76</sup> <sub>-0.43</sub>	1.87/34
3C382	1985,147	3.30 <sup>+0.45</sup> <sub>-0.63</sub>	1.70 <sup>c</sup>	03.72 <sup>+1.45</sup> <sub>-0.79</sub>	1.05/34
3C382	1985,153	3.61 <sup>+0.38</sup> <sub>-0.50</sub>	1.70 <sup>c</sup>	03.94 <sup>+1.17</sup> <sub>-0.71</sub>	0.98/34
3C382	1985,161	3.76 <sup>+0.35</sup> <sub>-0.48</sub>	1.70 <sup>c</sup>	03.26 <sup>+0.91</sup> <sub>-0.56</sub>	1.45/34
3C382	1985,171	3.46 <sup>+0.29</sup> <sub>-0.35</sub>	1.70 <sup>c</sup>	04.35 <sup>+0.87</sup> <sub>-0.61</sub>	0.85/34
3C382	1985,195	3.60 <sup>+0.26</sup> <sub>-0.33</sub>	1.70 <sup>c</sup>	04.05 <sup>+0.78</sup> <sub>-0.56</sub>	1.29/34
3C382	1985,211	3.92 <sup>+0.27</sup> <sub>-0.32</sub>	1.70 <sup>c</sup>	02.70 <sup>+0.50</sup> <sub>-0.36</sub>	1.72/34

Table 3.1.1f - continued

Source	Date (year,day)	$\Gamma_1^a$	$\Gamma_2^a$	$N^b$	$\chi^2_\nu/\text{d.o.f.}$
3C382	1985,223	$4.17^{+0.27}_{-0.33}$	$1.70^c$	$02.60^{+0.50}_{-0.36}$	1.46/34
3C382	1985,233	$3.47^{+0.31}_{-0.39}$	$1.70^c$	$05.00^{+1.14}_{-0.76}$	1.45/34
3C382	1985,246	$3.84^{+0.26}_{-0.30}$	$1.70^c$	$03.80^{+0.66}_{-0.48}$	0.94/34
3C382	1985,256	$4.21^{+0.23}_{-0.27}$	$1.70^c$	$02.87^{+0.44}_{-0.33}$	0.61/34

<sup>\*</sup> Break energy fixed at 0.6 keV.

<sup>†</sup> Fixed with corresponding galactic  $N_H$  value.

<sup>a</sup> Photon index.

<sup>b</sup> Normalization in  $10^{-3}$  photon  $\text{cm}^{-2} \text{s}^{-1} \text{keV}^{-1}$  at 1 keV.

<sup>c</sup>  $\Gamma_2$  fixed with the canonical value 1.7

TABLE 3.1.2G TWO POWER-LAW + FIXED ABSORPTION †

Source	Date (year,day)	$\Gamma_1^a$	$N_1^b$	$\Gamma_2^a$	$N_2^b$	$\chi^2_r/\text{d.o.f.}$
NGC3783	1983,347	1.58	7.36	1.33	07.40	1.35/27
NGC3783	1984,162	5.94	0.47	1.42	14.20	0.97/31
NGC3783	1985,005	1.43	4.67	1.43	04.67	1.90/31
NGC4593	1984,154	3.91 <sup>+1.10</sup> <sub>-0.90</sub>	0.89 <sup>+2.52</sup> <sub>-0.74</sub>	1.80 <sup>+0.08</sup> <sub>-0.10</sub>	10.22 <sup>+1.08</sup> <sub>-1.75</sub>	1.45/27
NGC4593	1984,183	4.17	0.59	1.71	11.48	3.00/27
NGC4593	1985,176	2.11 <sup>+0.54</sup> <sub>-0.47</sub>	1.29 <sup>+0.77</sup> <sub>-0.61</sub>	1.71 <sup>+0.44</sup> <sub>-0.38</sub>	02.58 <sup>+0.31</sup> <sub>-0.33</sub>	0.83/27
NGC4593	1985,180	2.29 <sup>+0.58</sup> <sub>-0.52</sub>	0.77 <sup>+0.52</sup> <sub>-0.47</sub>	1.69 <sup>+0.41</sup> <sub>-0.40</sub>	04.22 <sup>+0.67</sup> <sub>-0.56</sub>	1.25/27
NGC4593	1985,185	2.37 <sup>+0.49</sup> <sub>-0.44</sub>	0.89 <sup>+0.41</sup> <sub>-0.40</sub>	1.64 <sup>+0.33</sup> <sub>-0.30</sub>	04.11 <sup>+0.41</sup> <sub>-0.39</sub>	0.96/27
NGC4593	1986,009	4.68 <sup>+1.03</sup> <sub>-0.95</sub>	0.36 <sup>+0.24</sup> <sub>-0.19</sub>	1.77 <sup>+0.37</sup> <sub>-0.34</sub>	13.70 <sup>+1.54</sup> <sub>-1.42</sub>	1.78/27
NGC4593	1986,010	4.94	0.39	1.78	11.90	3.81/27
3C382	1983,255	3.91	0.51	1.70 <sup>c</sup>	06.69	0.80/34
3C382	1985,116	2.41	3.39	1.70 <sup>c</sup>	04.93	0.90/34
3C382	1985,117	4.90	0.32	1.70 <sup>c</sup>	06.04	1.88/34
3C382	1985,147	5.51	0.19	1.70 <sup>c</sup>	07.69	0.95/34
3C382	1985,153	3.59	1.69	1.70 <sup>c</sup>	10.60	0.91/34
3C382	1985,161	3.41 <sup>+6.59</sup> <sub>-0.72</sub>	2.19 <sup>+1.51</sup> <sub>-2.19</sub>	1.70 <sup>c</sup>	09.02 <sup>+0.40</sup> <sub>-0.74</sub>	1.38/34
3C382	1985,171	2.71	5.62	1.70 <sup>c</sup>	06.99	0.80/34
3C382	1985,195	4.76 <sup>+5.24</sup> <sub>-1.68</sub>	0.60 <sup>+2.37</sup> <sub>-0.50</sub>	1.70 <sup>c</sup>	10.70 <sup>+0.31</sup> <sub>-0.62</sub>	1.29/34
3C382	1985,211	5.71	0.26	1.70 <sup>c</sup>	07.44	1.16/34
3C382	1985,223	2.94 <sup>+0.56</sup> <sub>-0.42</sub>	4.85 <sup>+2.04</sup> <sub>-1.90</sub>	1.70 <sup>c</sup>	08.10 <sup>+0.80</sup> <sub>-1.36</sub>	1.15/34
3C382	1985,233	2.28 <sup>+0.36</sup> <sub>-0.37</sub>	8.95 <sup>+6.21</sup> <sub>-2.73</sub>	1.70 <sup>c</sup>	07.00 <sup>+2.07</sup> <sub>-6.32</sub>	1.16/34
3C382	1985,246	2.72 <sup>+1.37</sup> <sub>-0.45</sub>	8.04 <sup>+5.25</sup> <sub>-6.31</sub>	1.70 <sup>c</sup>	06.17 <sup>+4.50</sup> <sub>-4.42</sub>	0.80/34
3C382	1985,256	4.73 <sup>+5.27</sup> <sub>-1.13</sub>	1.02 <sup>+2.02</sup> <sub>-0.72</sub>	1.70 <sup>c</sup>	10.35 <sup>+0.23</sup> <sub>-0.37</sub>	0.60/34
MCG2-58-22	1984,321	5.03 <sup>+4.98</sup> <sub>-1.97</sub>	0.17 <sup>+2.00</sup> <sub>-0.14</sub>	1.52 <sup>+0.07</sup> <sub>-0.10</sub>	5.98 <sup>+0.59</sup> <sub>-0.98</sub>	0.80/29
MCG2-58-22	1984,322	3.37 <sup>+2.00</sup> <sub>-1.08</sub>	1.11 <sup>+3.82</sup> <sub>-1.09</sub>	1.51 <sup>+0.11</sup> <sub>-0.20</sub>	5.62 <sup>+1.06</sup> <sub>-2.92</sub>	0.99/29
MCG2-58-22	1984,325	3.36 <sup>+3.17</sup> <sub>-2.68</sub>	1.27 <sup>+6.26</sup> <sub>-1.07</sub>	1.45 <sup>+0.13</sup> <sub>-0.20</sub>	5.53 <sup>+1.22</sup> <sub>-4.75</sub>	0.79/29
MCG2-58-22	1984,327	3.46 <sup>+2.21</sup> <sub>-1.23</sub>	1.37 <sup>+5.76</sup> <sub>-1.08</sub>	1.48 <sup>+0.13</sup> <sub>-0.10</sub>	5.98 <sup>+1.24</sup> <sub>-4.21</sub>	0.97/29
MCG2-58-22	1984,329	2.31 <sup>+1.44</sup> <sub>-0.38</sub>	5.40 <sup>+1.66</sup> <sub>-4.73</sub>	1.26 <sup>+0.64</sup> <sub>-0.50</sub>	3.10 <sup>+3.96</sup> <sub>-2.59</sub>	1.10/29
MCG2-58-22	1984,331	3.96 <sup>+3.09</sup> <sub>-1.28</sub>	0.59 <sup>+2.66</sup> <sub>-0.48</sub>	1.60 <sup>+0.08</sup> <sub>-0.16</sub>	6.36 <sup>+0.80</sup> <sub>-1.81</sub>	0.84/30

† Fixed with corresponding galactic  $N_H$  value.

<sup>a</sup> Photon index.

<sup>b</sup> Normalization in  $10^{-3}$  photon  $\text{cm}^{-2} \text{s}^{-1} \text{keV}^{-1}$  at 1 keV.

<sup>c</sup>  $\Gamma_2$  fixed with the canonical value 1.7

TABLE 3.1.2H POWER-LAW + ABSORPTION + GAUSSIAN LINE

Source	Date (year,day)	$\Gamma^a$	$N^b$	$N_H^c$	$E_L^d$	$E_N^e$	$EW^f$	$\chi^2/d.o.f.$
NGC3516	1985,308	1.61 <sup>+0.40</sup> <sub>-0.28</sub>	03.36 <sup>+1.83</sup> <sub>-1.13</sub>	107 <sup>+110</sup> <sub>-051</sub>	5.05 <sup>+0.32</sup> <sub>-0.25</sub>	2.76 <sup>+0.78</sup> <sub>-0.77</sub>	678±189	1.08/26
NGC3516	1985,311	1.33 <sup>+0.49</sup> <sub>-0.41</sub>	02.75 <sup>+2.41</sup> <sub>-1.96</sub>	242 <sup>+194</sup> <sub>-138</sub>	5.06 <sup>+0.59</sup> <sub>-0.51</sub>	1.61 <sup>+1.24</sup> <sub>-1.21</sub>	424±318	1.58/27
NGC3516	1985,330	1.36 <sup>+1.36</sup> <sub>-0.47</sub>	02.42 <sup>+3.14</sup> <sub>-1.71</sub>	215 <sup>+1.89</sup> <sub>-1.43</sub>	5.95 <sup>+0.51</sup> <sub>-0.48</sub>	2.65 <sup>+1.23</sup> <sub>-1.21</sub>	852±389	1.47/28
NGC3516	1985,340	1.63 <sup>+0.61</sup> <sub>-0.49</sub>	02.65 <sup>+4.60</sup> <sub>-1.98</sub>	260 <sup>+200</sup> <sub>-173</sub>	5.98 <sup>+0.38</sup> <sub>-0.41</sub>	1.84 <sup>+0.80</sup> <sub>-0.80</sub>	758±330	0.91/25
NGC3783	1983,347	1.42 <sup>+0.07</sup> <sub>-0.07</sub>	07.22 <sup>+0.67</sup> <sub>-0.63</sub>	9.40 <sup>g</sup>	5.32 <sup>+0.25</sup> <sub>-0.26</sub>	1.55 <sup>+0.78</sup> <sub>-0.78</sub>	169±085	1.10/27
NGC3783	1985,005	1.47 <sup>+0.04</sup> <sub>-0.05</sub>	09.63 <sup>+0.51</sup> <sub>-0.49</sub>	9.40 <sup>g</sup>	5.60 <sup>+0.54</sup> <sub>-0.72</sub>	1.21 <sup>+0.69</sup> <sub>-0.69</sub>	124±070	0.60/31
Mkn766	1985,363	2.17 <sup>+0.06</sup> <sub>-0.07</sub>	12.76 <sup>+0.91</sup> <sub>-0.95</sub>	1.60 <sup>g</sup>	5.20 <sup>+0.24</sup> <sub>-0.23</sub>	3.21 <sup>+0.95</sup> <sub>-0.95</sub>	371±110	0.82/28
Mkn766	1985,364	2.10 <sup>+0.05</sup> <sub>-0.08</sub>	12.94 <sup>+0.86</sup> <sub>-0.90</sub>	1.60 <sup>g</sup>	6.10 <sup>+0.52</sup> <sub>-0.58</sub>	2.42 <sup>+1.47</sup> <sub>-1.44</sub>	357±214	1.15/25
NGC4593	1985,185	1.81 <sup>+0.04</sup> <sub>-0.05</sub>	05.02 <sup>+0.25</sup> <sub>-0.26</sub>	2.30 <sup>g</sup>	6.04 <sup>+0.49</sup> <sub>-1.26</sub>	0.81 <sup>+0.41</sup> <sub>-0.40</sub>	380±190	1.10/26
NGC4593	1986,009	2.12 <sup>+0.03</sup> <sub>-0.02</sub>	15.92 <sup>+0.45</sup> <sub>-0.45</sub>	2.30 <sup>g</sup>	5.08 <sup>+0.30</sup> <sub>-0.26</sub>	0.89 <sup>+0.55</sup> <sub>-0.55</sub>	190±095	1.78/26
NGC4593	1986,010	2.17	14.67	2.30 <sup>g</sup>	5.70	1.58	439	2.64/26
Mkn464	1985,178	2.19 <sup>+0.08</sup> <sub>-0.08</sub>	04.59 <sup>+0.30</sup> <sub>-0.30</sub>	1.70 <sup>g</sup>	6.43 <sup>+0.90</sup> <sub>-0.77</sub>	0.85 <sup>+0.72</sup> <sub>-0.70</sub>	524±437	1.20/25
Mkn290	1986,056	2.28 <sup>+0.07</sup> <sub>-0.08</sub>	04.12 <sup>+0.29</sup> <sub>-0.30</sub>	1.80 <sup>g</sup>	6.05 <sup>+0.30</sup> <sub>-0.31</sub>	2.12 <sup>+0.66</sup> <sub>-0.66</sub>	424±132	0.72/28
3C382	1983,255	1.85 <sup>+0.06</sup> <sub>-0.06</sub>	07.92 <sup>+0.52</sup> <sub>-0.53</sub>	7.40 <sup>g</sup>	5.45 <sup>+0.39</sup> <sub>-0.34</sub>	1.28 <sup>+0.63</sup> <sub>-0.62</sub>	240±120	0.81/32
3C382	1985,116	1.98 <sup>+0.09</sup> <sub>-0.11</sub>	08.64 <sup>+0.86</sup> <sub>-0.91</sub>	7.40 <sup>g</sup>	5.62 <sup>+0.40</sup> <sub>-0.40</sub>	1.32 <sup>+0.62</sup> <sub>-0.62</sub>	280±125	0.86/32
3C382	1985,117	1.88 <sup>+0.06</sup> <sub>-0.06</sub>	07.28 <sup>+0.50</sup> <sub>-0.50</sub>	7.40 <sup>g</sup>	5.62 <sup>+1.07</sup> <sub>-3.36</sub>	1.38 <sup>+1.21</sup> <sub>-1.37</sub>	270±255	1.87/32
3C382	1985,147	1.77 <sup>+0.08</sup> <sub>-0.08</sub>	09.14 <sup>+0.86</sup> <sub>-0.87</sub>	7.40 <sup>g</sup>	7.06 <sup>+0.62</sup> <sub>-1.11</sub>	1.18 <sup>+1.10</sup> <sub>-1.10</sub>	300±280	1.20/32
3C382	1985,153	1.86 <sup>+0.07</sup> <sub>-0.06</sub>	12.67 <sup>+1.02</sup> <sub>-1.00</sub>	7.40 <sup>g</sup>	7.13 <sup>+14.9</sup> <sub>-7.13</sub>	1.08 <sup>+1.12</sup> <sub>-1.08</sub>	250±250	1.11/32
3C382	1985,161	1.86 <sup>+0.06</sup> <sub>-0.06</sub>	11.20 <sup>+0.78</sup> <sub>-0.76</sub>	7.40 <sup>g</sup>	5.51 <sup>+0.85</sup> <sub>-0.57</sub>	0.76 <sup>+0.64</sup> <sub>-0.62</sub>	165±135	1.60/32
3C382	1985,171	1.82 <sup>+0.05</sup> <sub>-0.05</sub>	12.41 <sup>+0.77</sup> <sub>-0.77</sub>	7.40 <sup>g</sup>	7.26 <sup>+1.28</sup> <sub>-1.14</sub>	1.36 <sup>+1.01</sup> <sub>-0.96</sub>	310±225	1.43/32
3C382	1985,195	1.87 <sup>+0.06</sup> <sub>-0.06</sub>	13.23 <sup>+1.10</sup> <sub>-1.00</sub>	7.40 <sup>g</sup>	5.32 <sup>+0.50</sup> <sub>-0.50</sub>	0.79 <sup>+0.62</sup> <sub>-0.62</sub>	115±090	1.84/32
3C382	1985,211	1.78 <sup>+0.07</sup> <sub>-0.08</sub>	09.11 <sup>+0.07</sup> <sub>-0.08</sub>	7.40 <sup>g</sup>	6.54 <sup>+0.07</sup> <sub>-0.08</sub>	2.35 <sup>+0.07</sup> <sub>-0.08</sub>	740±410	2.43/32
3C382	1985,223	2.03 <sup>+0.07</sup> <sub>-0.07</sub>	13.36 <sup>+0.98</sup> <sub>-0.97</sub>	7.40 <sup>g</sup>	4.58 <sup>+0.44</sup> <sub>-0.41</sub>	1.35 <sup>+0.80</sup> <sub>-0.80</sub>	225±130	1.34/32
3C382	1985,233	1.91 <sup>+0.06</sup> <sub>-0.05</sub>	15.87 <sup>+1.01</sup> <sub>-0.99</sub>	7.40 <sup>g</sup>	4.07 <sup>+1.44</sup> <sub>-0.81</sub>	0.76 <sup>+1.01</sup> <sub>-0.76</sub>	060±060	1.12/32
3C382	1985,246	1.84 <sup>+0.06</sup> <sub>-0.05</sub>	13.41 <sup>+0.84</sup> <sub>-0.80</sub>	7.40 <sup>g</sup>	6.76 <sup>+0.42</sup> <sub>-0.38</sub>	2.16 <sup>+0.82</sup> <sub>-0.83</sub>	370±140	1.71/32
3C382	1985,256	1.89 <sup>+0.07</sup> <sub>-0.07</sub>	12.96 <sup>+0.90</sup> <sub>-0.90</sub>	7.40 <sup>g</sup>	6.57 <sup>+0.40</sup> <sub>-0.40</sub>	1.63 <sup>+0.75</sup> <sub>-0.75</sub>	315±145	1.82/32
ESO140-G43	1985,105	1.67 <sup>+0.29</sup> <sub>-0.26</sub>	05.42 <sup>+2.43</sup> <sub>-1.59</sub>	17.00 <sup>+24.0</sup> <sub>-10.0</sub>	6.00 <sup>+0.55</sup> <sub>-0.47</sub>	2.10 <sup>+1.48</sup> <sub>-1.43</sub>	354±244	0.50/26

<sup>a</sup> Photon index.

<sup>b</sup> Normalization in  $10^{-3}$  photon  $\text{cm}^{-2}$   $\text{s}^{-1}$   $\text{keV}^{-1}$  at 1 keV.

<sup>c</sup> Column density in  $10^{20}$   $\text{cm}^{-2}$ .

<sup>d</sup> Line energy in keV.

<sup>e</sup> Line intensity in  $10^{-4}$  photons  $\text{cm}^{-2}$   $\text{s}^{-1}$ .

<sup>f</sup> Equivalent width in eV.

<sup>g</sup> Fixed with corresponding Galactic  $N_H$  value.

TABLE 3.1.21 SPECTRAL FITS TO THE SPECTRA OF MCG2-58-22:  
POWER-LAW + FIXED ABSORPTION<sup>c</sup> + GAUSSIAN LINE

Date (year,day)	$\Gamma_1^a$	$N_1^b$	$\Gamma_2^a$	$N_2^b$	$E_L^d$	$E_N^e$	EW <sup>f</sup>	$\chi^2/d.o.f.$
1984,321	5.12 <sup>+4.72</sup> <sub>-2.14</sub>	0.18 <sup>+1.75</sup> <sub>-0.09</sub>	1.56 <sup>+0.09</sup> <sub>-0.10</sub>	6.34 <sup>+0.70</sup> <sub>-0.90</sub>	6.13 <sup>+1.08</sup> <sub>-1.05</sub>	0.72 <sup>+0.53</sup> <sub>-0.52</sub>	154±110	0.50/27
1984,322	3.33 <sup>+2.69</sup> <sub>-2.49</sub>	1.82 <sup>+6.17</sup> <sub>-1.68</sub>	1.54 <sup>+0.18</sup> <sub>-1.11</sub>	5.39 <sup>+1.78</sup> <sub>-5.18</sub>	4.81 <sup>+0.41</sup> <sub>-0.32</sub>	1.48 <sup>+0.78</sup> <sub>-0.76</sub>	198±103	0.61/27
1984,325	3.46 <sup>+3.90</sup> <sub>-3.28</sub>	1.05 <sup>+0.10</sup> <sub>-0.95</sub>	1.49 <sup>+0.15</sup> <sub>-1.31</sub>	5.83 <sup>+1.33</sup> <sub>-4.97</sub>	6.47 <sup>+0.84</sup> <sub>-0.63</sub>	0.54 <sup>+0.41</sup> <sub>-0.42</sub>	122±095	0.64/27
1984,327	3.06 <sup>+2.46</sup> <sub>-2.85</sub>	2.28 <sup>+4.26</sup> <sub>-1.93</sub>	1.45 <sup>+0.17</sup> <sub>-0.29</sub>	5.42 <sup>+2.31</sup> <sub>-5.24</sub>	5.81 <sup>+0.88</sup> <sub>-0.76</sub>	0.57 <sup>+0.45</sup> <sub>-0.47</sub>	132±109	0.82/27
1984,329	2.51 <sup>+1.88</sup> <sub>-1.96</sub>	5.97 <sup>+2.37</sup> <sub>-3.22</sub>	1.32 <sup>+0.31</sup> <sub>-0.46</sub>	2.82 <sup>+0.43</sup> <sub>-1.32</sub>	5.60 <sup>+0.62</sup> <sub>-0.50</sub>	1.30 <sup>+0.80</sup> <sub>-0.80</sub>	206±126	0.78/27
1984,331	4.23 <sup>+3.72</sup> <sub>-2.60</sub>	0.37 <sup>+2.62</sup> <sub>-0.34</sub>	1.66 <sup>+0.10</sup> <sub>-0.16</sub>	6.78 <sup>+0.88</sup> <sub>-1.84</sub>	5.67 <sup>+0.68</sup> <sub>-0.83</sub>	0.69 <sup>+0.64</sup> <sub>-0.64</sub>	145±134	0.76/28

<sup>a</sup> Photon index.

<sup>b</sup> Normalization in  $10^{-3}$  photon  $\text{cm}^{-2} \text{s}^{-1} \text{keV}^{-1}$  at 1 keV.

<sup>c</sup> Column density fixed at the Galactic  $N_H$  value ( $3.4 \times 10^{20} \text{cm}^{-2}$ ).

<sup>d</sup> Line energy in keV.

<sup>e</sup> Line intensity in  $10^{-4}$  photons  $\text{cm}^{-2} \text{s}^{-1}$ .

<sup>f</sup> E±ivalent width in eV.

significant. Measured equivalent widths are also given in these two tables. To compute the error ranges of the equivalent widths, only the statistical errors have been considered.

## Results

### 3.1.2a. ESO 012-G21

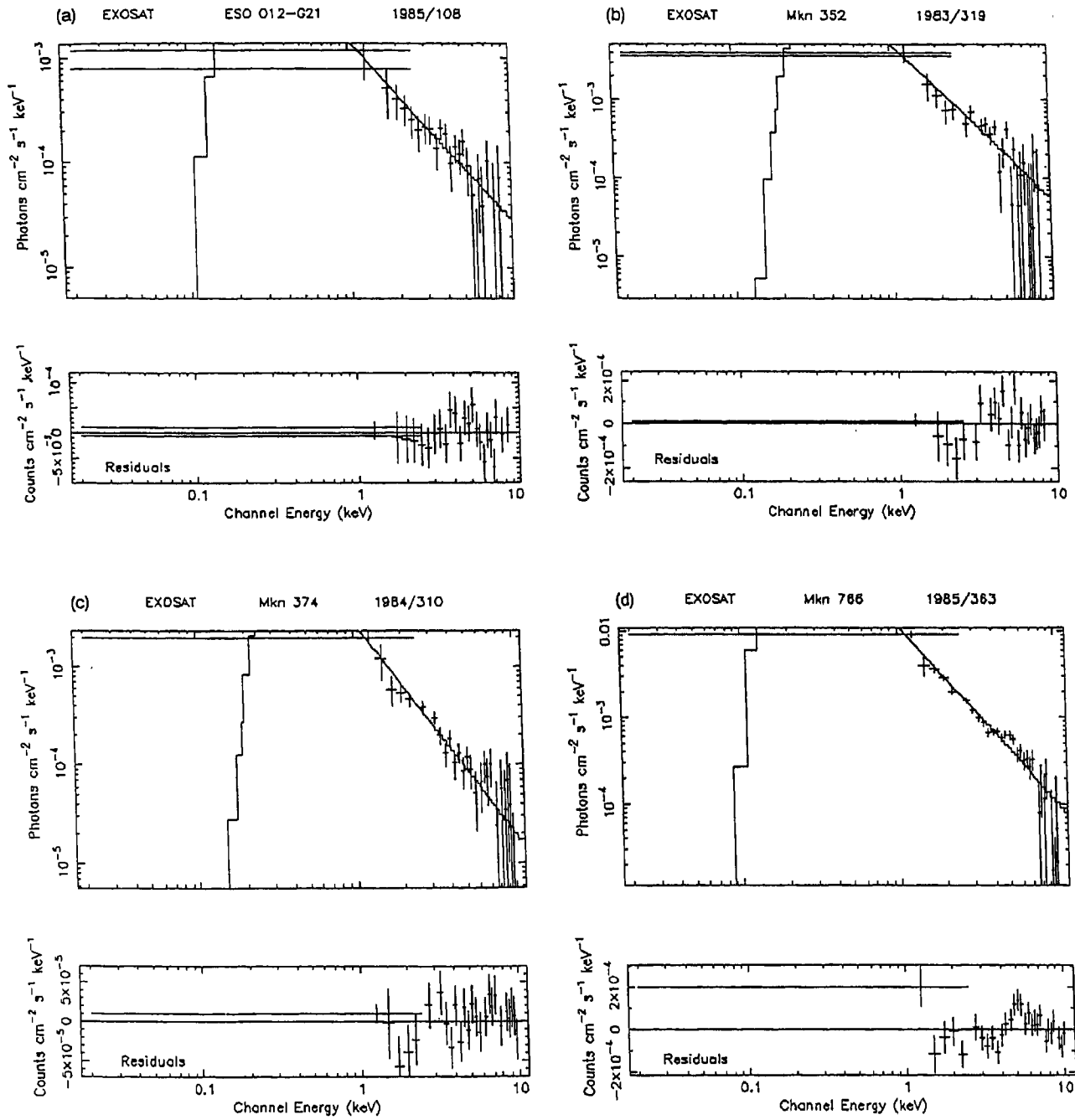
The EXOSAT results show the presence of a soft excess in the spectrum of ESO 012-G21 (Fig.3.1.1a). This soft excess fits well with the broken power-law model, which indicates that two components (soft and hard) are required to fit the spectrum. However, the spectrum from *ArielV* observations fitted best with the single power-law model ( $\Gamma = 1.80$ , Hayes et al. 1980). the hard X-ray (2-10 keV) flux of this source decreased by a factor of  $\sim 7$  between 1976 August [ $F_{2-10} \sim (3.8 \pm 0.6) \times 10^{-11} \text{ erg cm}^{-2} \text{ s}^{-1}$ , *Ariel V* observation] and 1985 April [ $F_{2-10} \sim (0.58 \pm 0.06) \times 10^{-11} \text{ erg cm}^{-2} \text{ s}^{-1}$ , EXOSAT observation]. The derived EXOSAT soft photon index ( $\Gamma \sim 4.47$ ; Table 3.1.2F) is consistent with the ROSAT value ( $\Gamma \sim 4.2$ ; Malaguti 1994). The soft X-ray luminosity displayed a decrement by a factor of  $\sim 2.5$  between the 1985 observation of EXOSAT [ $L_{2-10} \sim 2 \times 10^{43} \text{ erg s}^{-1}$ ; (1985)] and 1990 observation of ROSAT [ $L_{2-10} \sim 0.77 \times 10^{43} \text{ erg s}^{-1}$ ; (Rush et al. 1996)]. The derived plasma temperature, obtained from the fits of the thermal bremsstrahlung model, is  $\sim 4.6 \text{ keV}$  (Table 3.1.2E).

### 3.1.2b. Mkn352

From the comparison of the soft fluxes (0.2-4 keV) measured with *Einstein* [ $(3.34 \pm 0.05) \times 10^{-11} \text{ erg cm}^{-2} \text{ s}^{-1}$ ; Kruper et al. 1990] and EXOSAT [ $(2.0 \pm 0.15) \times 10^{-11} \text{ erg cm}^{-2} \text{ s}^{-1}$ ], it appears that the luminosity did not vary significantly between 1980 January and 1983 November. Fig. 3.1.1b shows that the soft excess stands above the extrapolation of the hard (ME) power-law. The soft power-law index of 1990 observation of ROSAT ( $\Gamma = 2.43 \pm 0.19$ ; Walter & Fink 1993) lies within the uncertainty range of the 1985 EXOSAT observational value ( $\Gamma = 3.30^{+1.16}_{-1.68}$ ; Table 3.1.2F). The thermal bremsstrahlung model (Table 3.1.2E) also fits well with the spectra of this galaxy, and the derived plasma temperature is  $\sim 3.6 \text{ keV}$ .

### 3.1.2c. Mkn374

The X-ray (0.2-4 keV) luminosity did not vary significantly between the *Einstein* [ $(0.70 \pm 0.05) \times 10^{-11} \text{ erg cm}^{-2} \text{ s}^{-1}$  measured on 1979 April; Kruper et al. 1990 and references therein] and



Incident photon spectra of the Seyfert galaxies (a) ESO 012-G21, (b) Mkn 352, (c) Mkn 374, (d) Mkn 766, (e) Mkn 279, (f) Mkn 464, (g) Mkn 290, and (h) ESO 140-G43. The spectra have been fitted with a simple power-law and fixed-absorption model. The lower panel of each part shows the residuals between the spectrum and the model.

Fig. 3.1.1



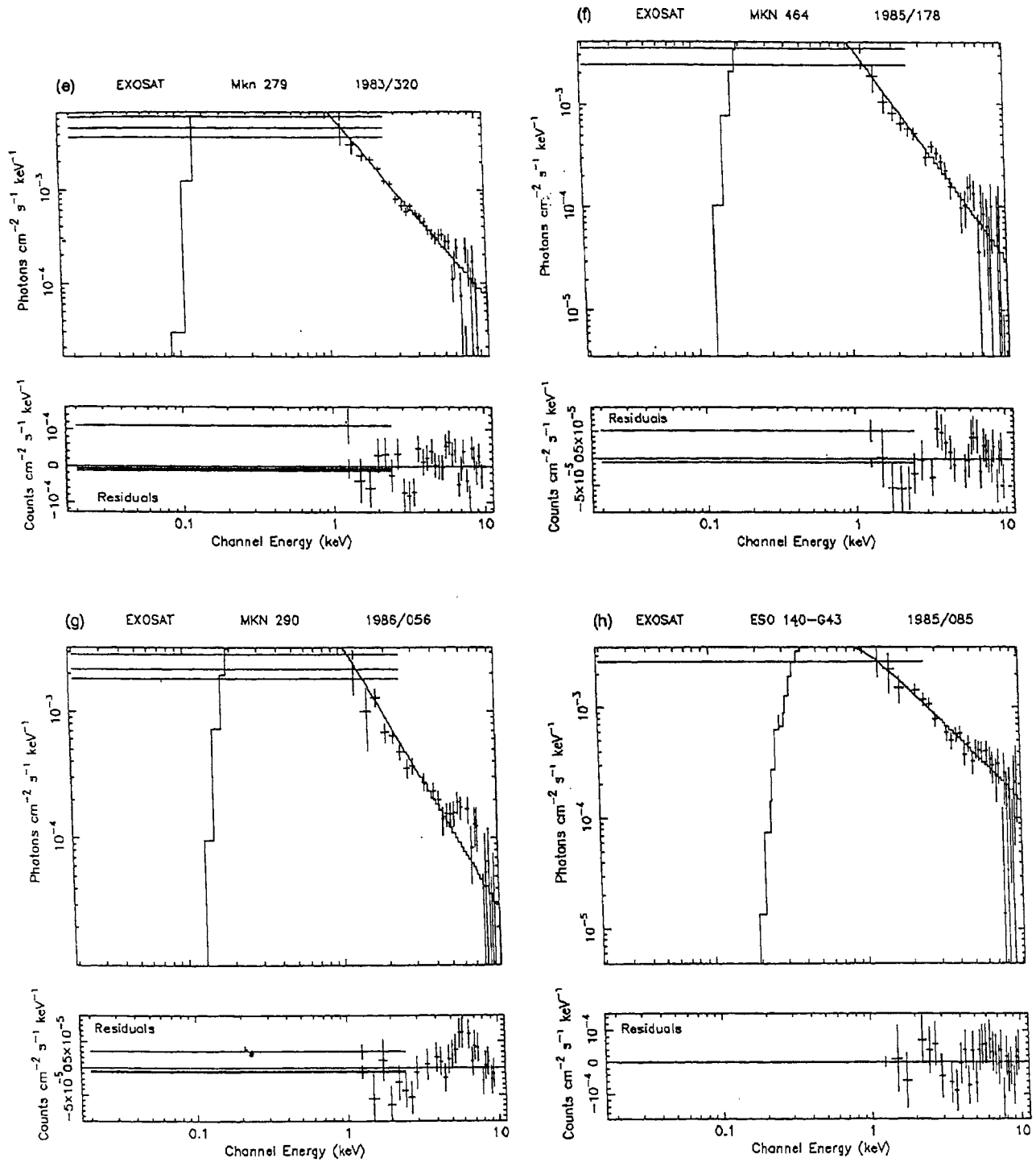


Fig. 3.1.1 (continued)

EXOSAT  $[(0.98 \pm 0.06) \times 10^{-11} \text{ erg cm}^{-2} \text{ s}^{-1}]$  measured on 1984 November] observations. There is a weak soft excess in the spectrum (Fig.3.1.1c) and the value of  $\Gamma_1$  is larger than  $\Gamma_2$  as obtained from the broken power-law fits (Table 3.1.2F).

### 3.1.2d. *Mkn766*

The LE and ME count rates, obtained with EXOSAT between 1985/363 and 1985/365 are plotted in Fig.3.1.2. Table 3.1.2A and Fig.3.1.2 show the LE and ME fluxes varied by 32 and 20 per cent, respectively, within 11 hours. Also it can be seen from Fig.3.1.3 that the LE and ME variations are correlated (the correlation coefficient is 0.97 for five observations which suggests that probability of the fit being random is 0.5 per cent). The soft excess detected in this ultrasoft excess source (Urry et al. 1989) has displayed weak variability on a time-scale of hours (Fig.3.1.4). and is correlated with the variations of the LE and ME fluxes, the linear correlation coefficients being 0.87 and 0.84 respectively (Fig.3.1.5), the soft excess being stronger when the galaxy was brighter. This type of correlated variability has already been seen in other Seyfert galaxies, such as NGC3783 (Ghosh et al. 1991), 3C382 (Ghosh & Soundararajaperumal 1992A), MCG 2-58-22 (Ghosh & Soundararajaperumal 1992B) etc, but is not understood. Based on ROSAT all-sky survey and pointed observations, Molendi et al. (1993) and Molendi & Maccacaro (1994) studied the flux and spectral variability of Mkn766. This source was found to be variable by a factor of about 3 on timescales of a few hours. Molendi & Maccacaro have found spectral variability in which 0.1-0.9 keV part of the spectrum hardens as the source brightens while the 0.9-2.0 keV part of the spectrum does not change significantly. They claim that emission from an accretion disc can explain the observed spectral behaviour (Boller et al. 1996). From the comparison of the ROSAT all-sky survey (1990) data ( $\langle \Gamma \rangle \sim 2.5$ ; Boller et al. 1996) and EXOSAT (1985 December) data ( $\langle \Gamma_1 \rangle \sim 2.6$ ; Table 3.1.2F), it is found that the LE power-law photon index remained almost unchanged. However, the LE luminosity (EXOSAT  $\langle L_{0.1-2} \rangle \sim 2.66 \times 10^{43}$ ; ROSAT  $\langle L_{0.1-2.4} \rangle \sim 9.7 \times 10^{43}$ ) varied by a factor of 3.6. Whereas the EXOSAT ( $\langle L_{2-10} \rangle \sim 1.8 \times 10^{43}$ ; 1985 December; Table 3.1.2D) and ASCA ( $L_{2-10} \sim 1.2 \times 10^{43}$ ; 1993 December; Nandra et al. 1997) observations of 2-10 keV band of this source displayed slight (factor of 0.67) decrement in luminosity. However, the photon index remained unchanged [EXOSAT  $\langle \Gamma \rangle \sim 2.1$  (Table 3.1.2D); ASCA  $\Gamma_{3-10} \sim 2.16$  (Nandra et al. 1997)]. Considering

EXOSAT

Mkn 766

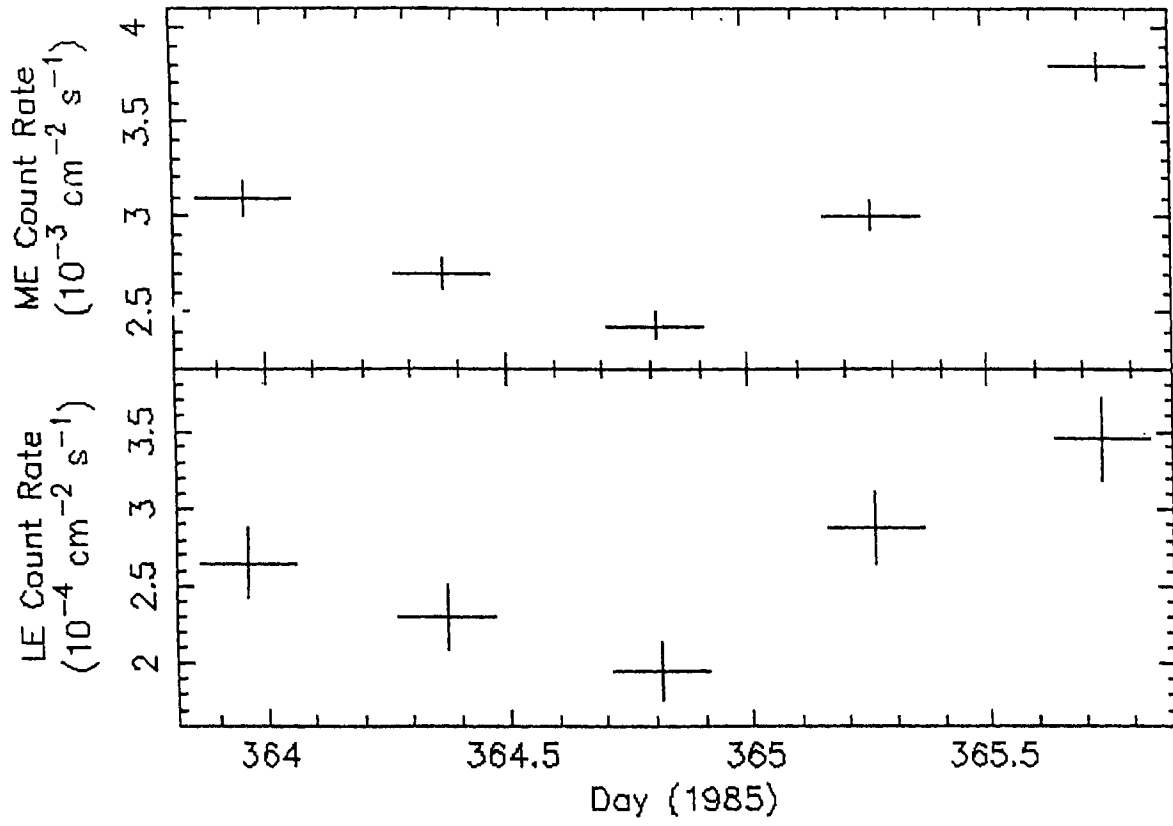


Fig. 3.1.2. Plot of the LE and ME count rates of Mkn 766 versus the date of observations.

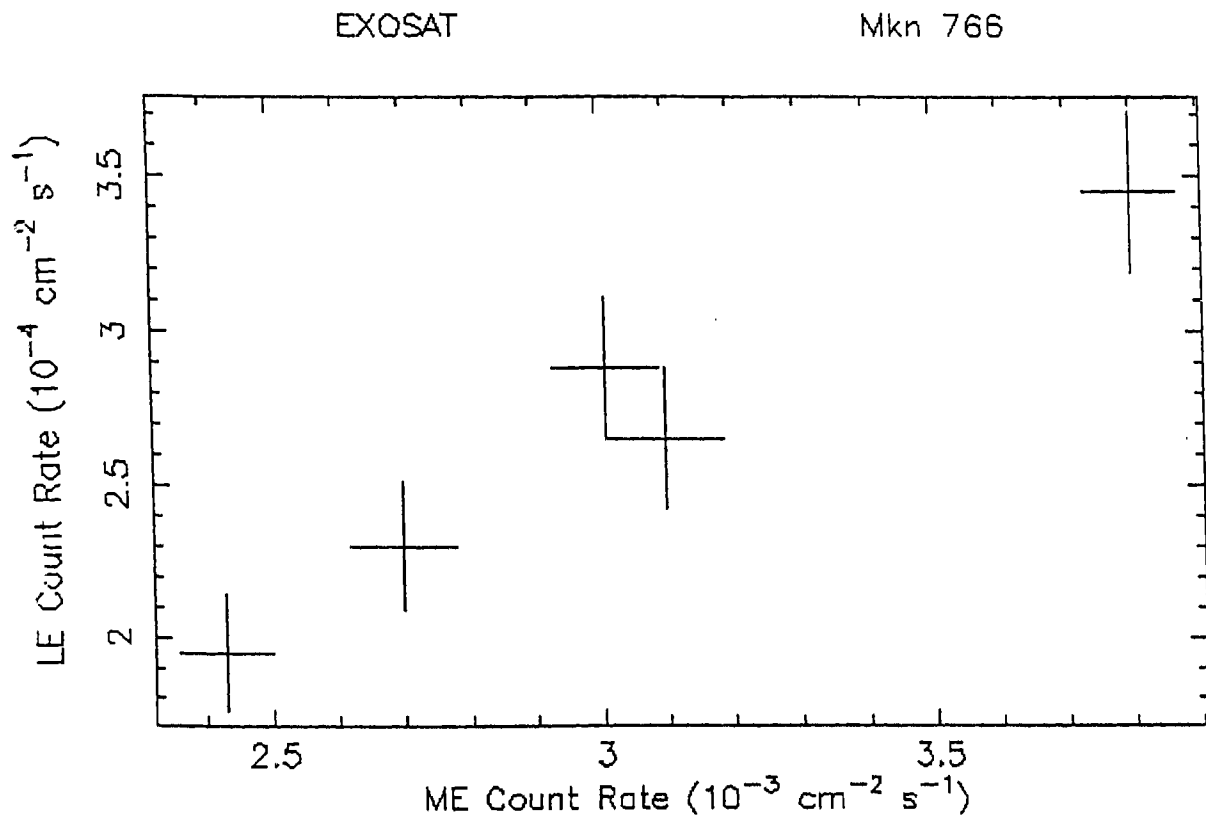
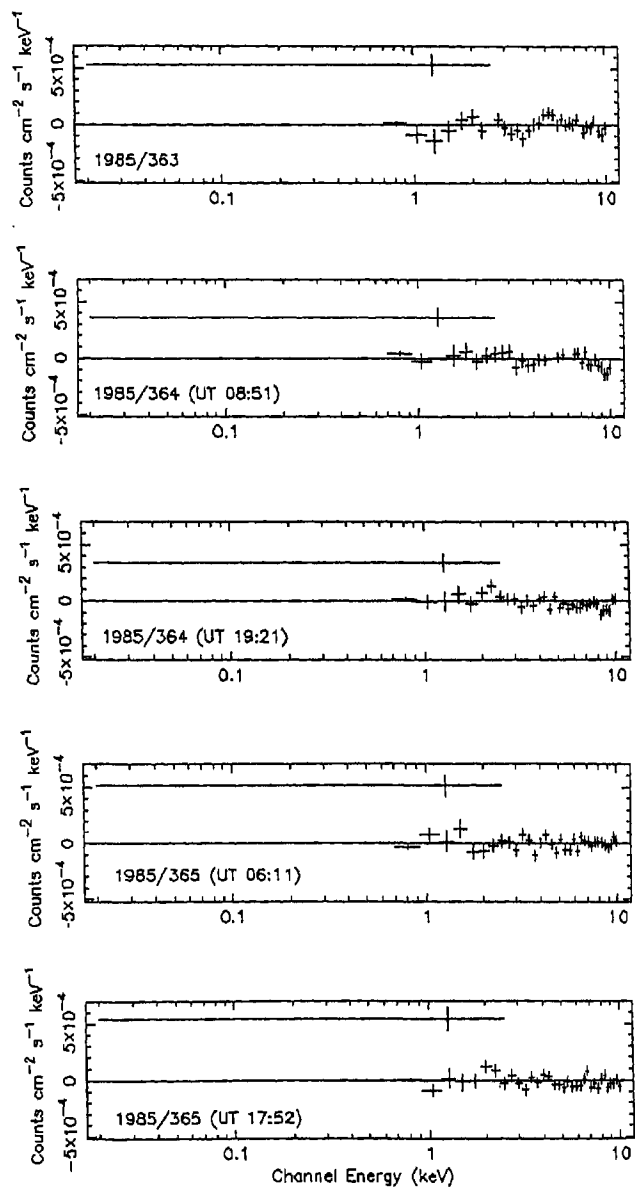


Fig. 3.1.3. Observed count rates of the LE versus ME of Mkn 766



Residuals between different spectra of Mkn 766 and model

Fig. 3.1.4

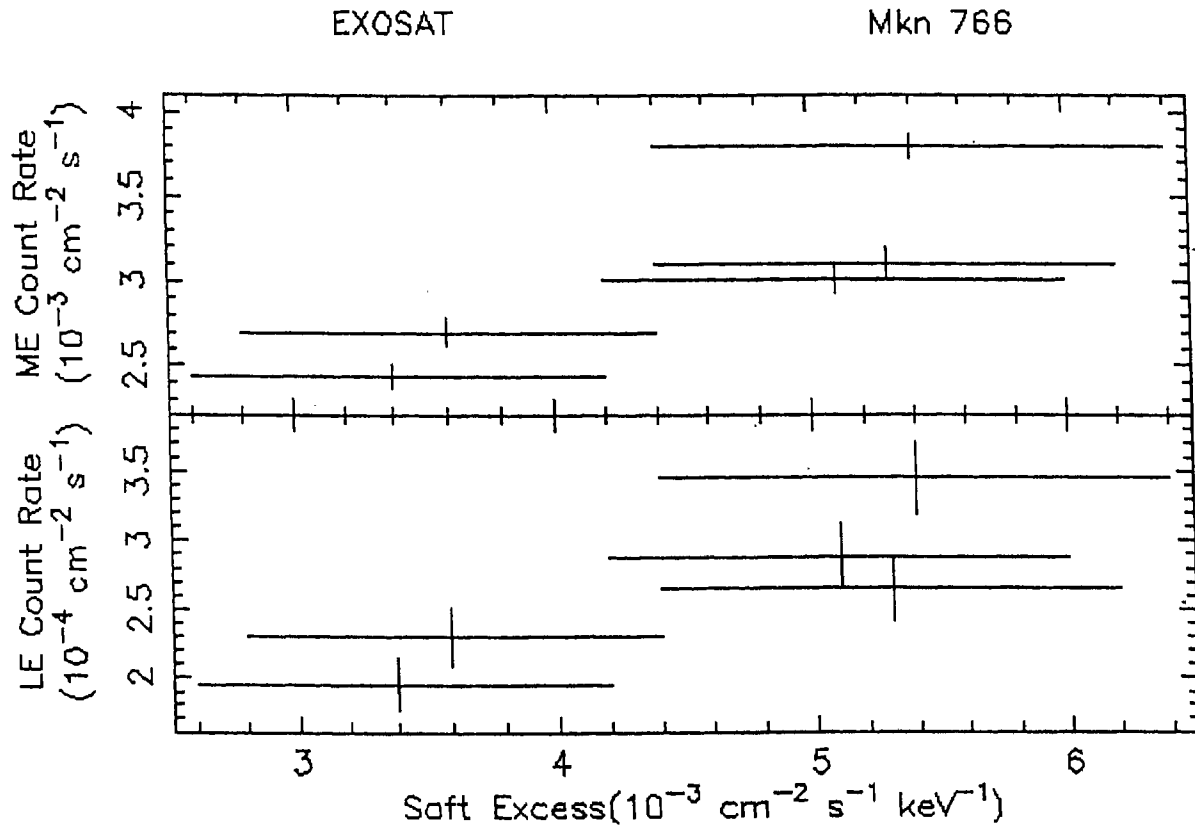


Fig. 3.1.5. Plots of the LE and ME count rates versus soft excesses of Mkn 766.

the uncertainty range, the equivalent widths of the Fe  $K_{\alpha}$  line detected by both EXOSAT and ASCA are consistent.

### 3.1.2e. *Mkn279*

The soft excess emissions measured in the spectra of this source showed no marked variations between 1983/320  $[(2.2 \pm 1.0) \times 10^{-4} \text{ counts cm}^{-2} \text{ s}^{-1}]$  and 1984/028  $[(1.8 \pm 0.4) \times 10^{-4} \text{ counts cm}^{-2} \text{ s}^{-1}]$ . No significant Fe  $K_{\alpha}$  emission is detected in this source. The LE luminosity decreased by a factor of  $\sim 1.7$  between EXOSAT (1984; Table 3.1.2D) and ROSAT (1990; Rush et al. 1996) observations. However the LE photon index value remained unchanged during these observations (Malaguti 1994 and Table 3.1.2F).

### 3.1.2f. *Mkn464*

The X-ray flux measured by Ariel V on 1977 January in the 2-10 keV band was  $(2.7 \pm 0.5) \times 10^{-11} \text{ erg cm}^{-2} \text{ s}^{-1}$  (Hayes et al. 1980), while the fluxes from HEAO-1 on 1977 December (Marshall et al. 1979) and 1978 October (Dower et al. 1980) were  $(2.6 \pm 0.5)$  and  $(0.8 \pm 0.4) \times 10^{-11} \text{ erg cm}^{-2} \text{ s}^{-1}$ , respectively. The 2-10 keV flux thus decreased by a factor of 3 between 1977 December and 1978 October (HEAO-1 observation) and 1985 June (EXOSAT observation). Ariel V detected a steep photon index ( $\Gamma = 3.0$ ) and high  $N_{\text{H}}$  ( $\sim 2.5 \times 10^{23} \text{ cm}^{-2}$ ) in the 2-10 keV range (Hayes et al. 1980), and the values from HEAO-1 in the 2-40 keV range were  $\Gamma = 1.39_{-0.11}^{+0.19}$  and  $N_{\text{H}} \sim (0-0.9) \times 10^{23} \text{ cm}^{-2}$  (Mushotzky 1984), whereas from the EXOSAT results we found no low energy absorption in this galaxy. The EXOSAT results indeed reveal the presence of a soft excess and the values of the soft and hard photon indices are  $3.83 \pm 0.60$  and  $1.76 \pm 0.18$ , respectively (Table 3.1.2F). The residuals of Fig. 3.1.1f show an emission feature around 6 keV. Introduction of the Gaussian component to the power-law fit reduced the  $\chi^2$  value significantly (Tables 3.1.2D and 3.1.2h). The measured line centre energy ( $\sim 6.42 \text{ keV}$ ) is consistent with the fluorescent Fe  $K_{\alpha}$  emission from a cold material.

### 3.1.2g. *Mkn290*

A soft excess and an emission line (Fig. 3.1.1g) were detected in the EXOSAT spectrum of this source observed in 1985/056. From a comparison of the X-ray fluxes obtained with Einstein (Kruiper et al. 1990) and EXOSAT, we find no significant variation between 1979/210 and 1985/056. The source was observed during the ROSAT all-sky survey. The EXOSAT LE photon index ( $\Gamma_1 \sim 4.12$ ; Table 3.1.2F) is very much steeper than the ROSAT value ( $\Gamma_{0.1-2.4} \sim$

2.44; Walter & Fink 1993). A highly significant emission line was detected around 6 keV (Fig. 3.1.1g & Table 3.1.2h).

### 3.1.2h. *ESO 140-G43*

This is a flat spectrum ( $\Gamma = 1.46 \pm 0.21$ ; Table 3.1.2C) source with a weak low-energy absorption. (Table 3.1.2C). No soft excess is present, but there is an emission line at about 6.0 keV (Table 3.1.2h & Fig.3.1.1i). This source was observed during the ROSAT all-sky survey ( $\Gamma = 2.06^{+0.58}_{-0.62}$ ) considering the error range there is no significant variation in the photon indices of ROSAT and EXOSAT.

### 3.1.2i. *NGC3516*

A simple power-law model with uniform absorption was used to fit the spectra. Table 3.1.2C presents the best fit parameters of the above model with 90% confidence error bars. Table 3.1.2D and Fig. 3.1.7 show that this galaxy displayed soft X-ray (0.1-2 keV) flux variation by a factor of  $\sim 3$  on a time scale of 2 days and the hard X-ray (2-10 keV) flux of this source varied by a factor of  $\sim 1.5$  over a period of a month. However, considering the 90% error bars, the values of the photon index indicate that there were no changes of  $\Gamma$  during the EXOSAT observations. Values of the column densities of the equivalent hydrogen along the line-of-sight of NGC3516 which are presented in Table 3.1.2C suggest that the average  $N_H$  value is very much greater, nearly by two orders of magnitude, than the galactic column density value ( $3 \times 10^{20}$ ; Stark et al. 1992). This means that probably there is a significant absorption in this galaxy. But our results do not show any variation of  $N_H$ . In Figs 3.1.8 the observed LE + ME spectra of NGC3516 are shown with the best fit power-law with uniform absorption model convolved through the detector response, and the lower panels of these two figures show the residuals between the spectra and the model. From the residuals of Fig.3.1.8b, it can be seen that this galaxy displays weak soft excess in its spectrum. Weak soft excesses have also been detected in the spectra of this source which were observed on 1985/311 and 1985/330. However, no variations of the soft excesses were found in this source from the EXOSAT observations. Two power-laws, broken power-law and thermal bremsstrahlung models were tried to fit the soft excesses. But there were no improvements in the  $\chi^2$  statistics than that obtained from the simple power-law and uniform absorption model.



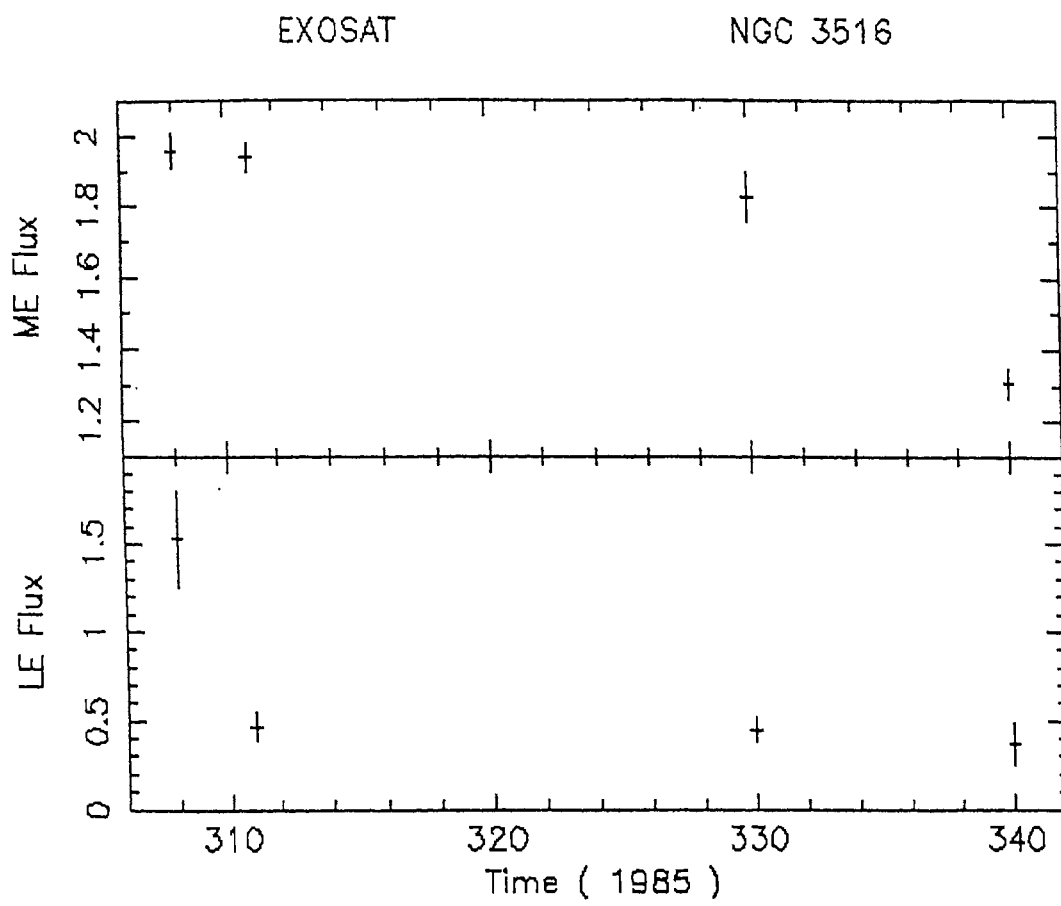


Fig. 3.1.7. Plot of the LE and ME fluxes versus date of observations.

EXOSAT

1985/308

NGC 3516

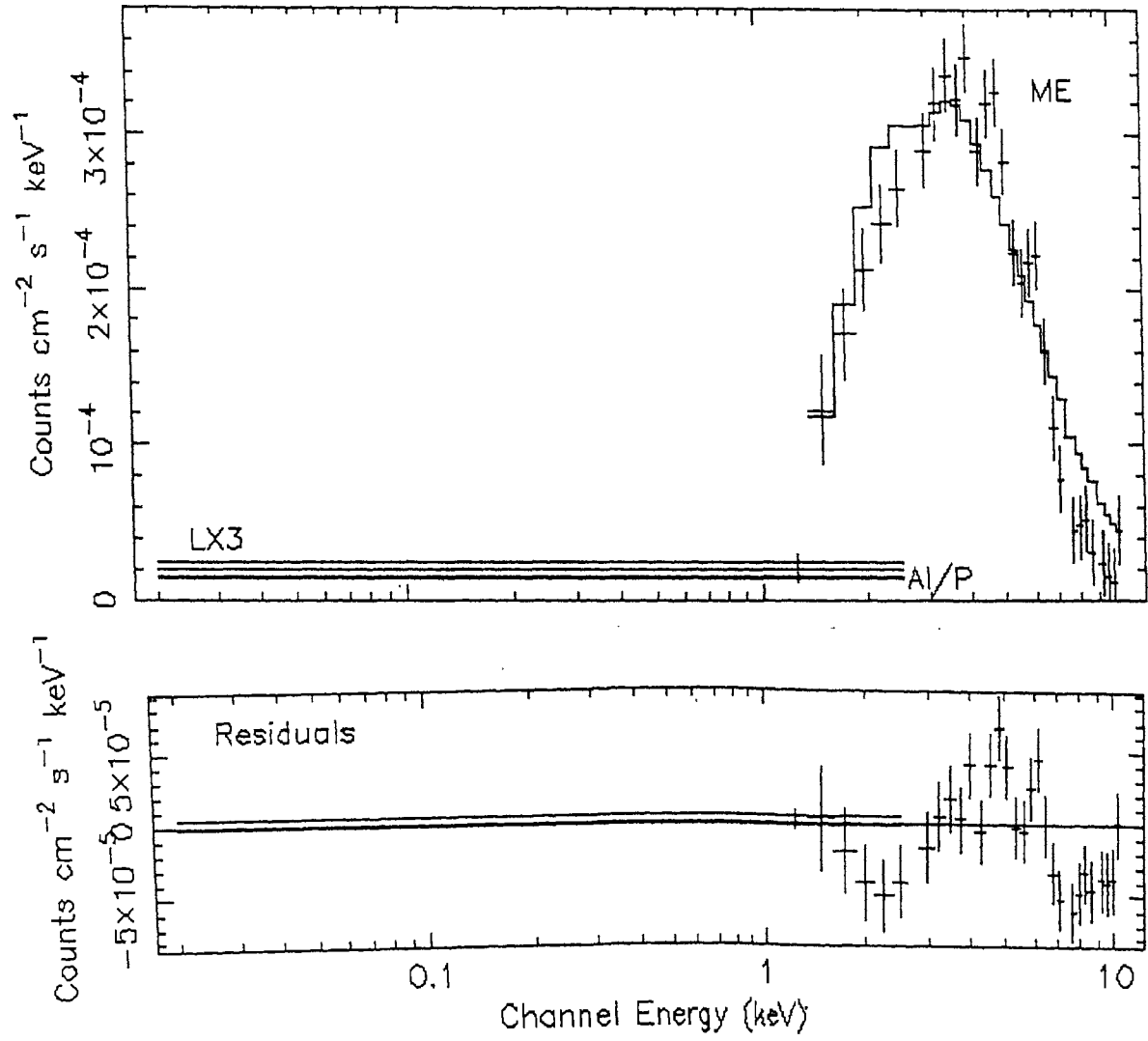


Fig. 3.1.8a Observed spectrum of NGC3516 for 1985/308 fitted with a simple power-law and uniform absorption model.

EXOSAT

1985/340

NGC 3516

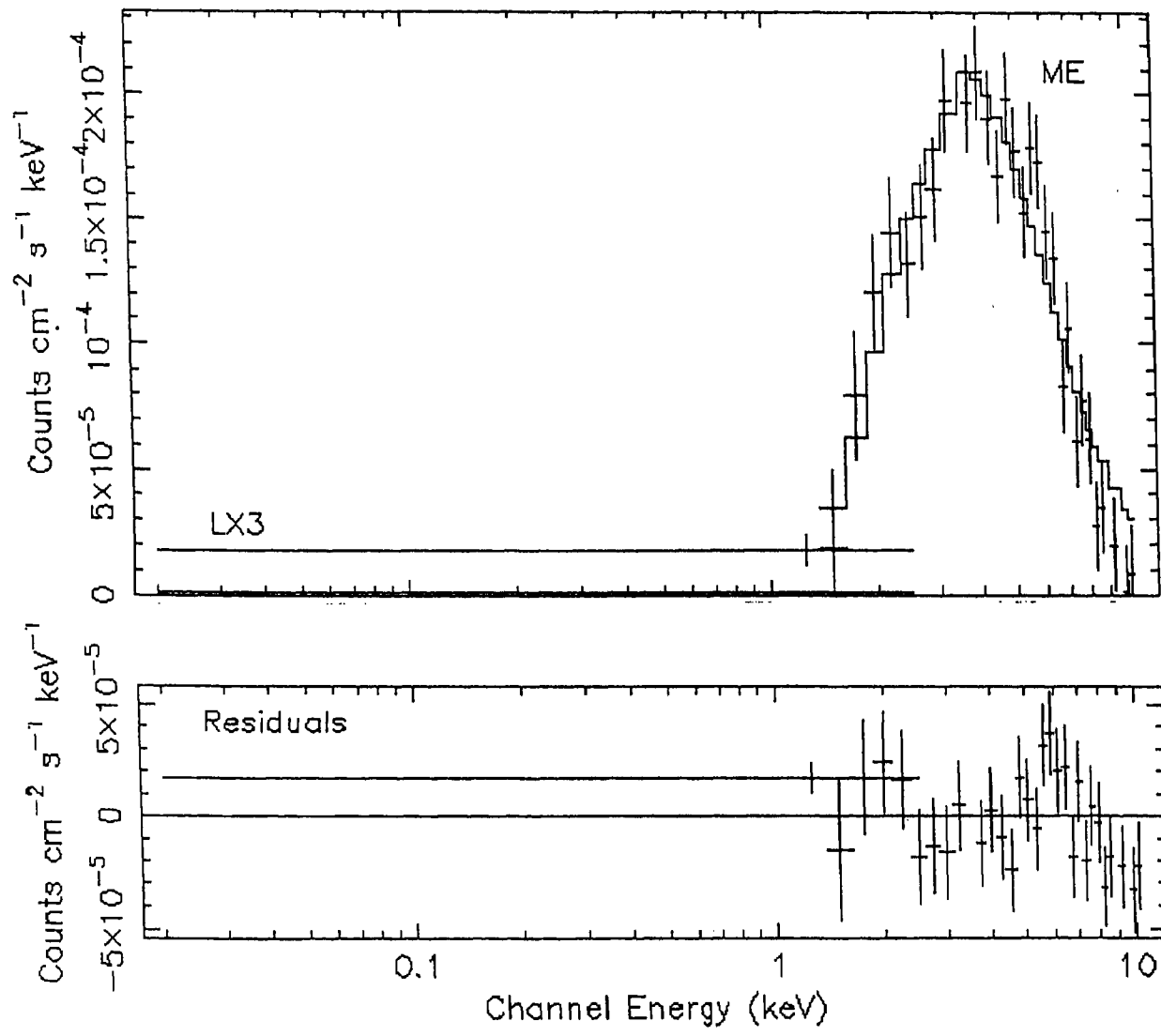


Fig. 3.1.8b Same as Fig. 3.1.8a but for 1985/340

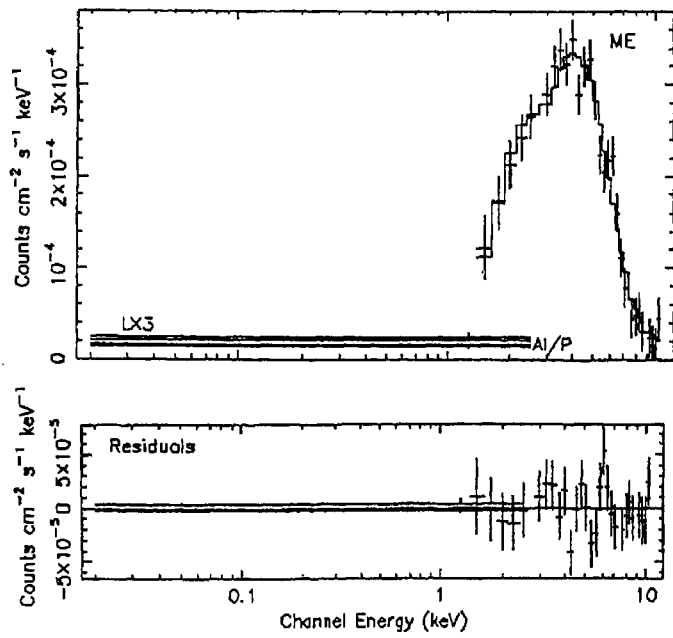


FIG. 4a

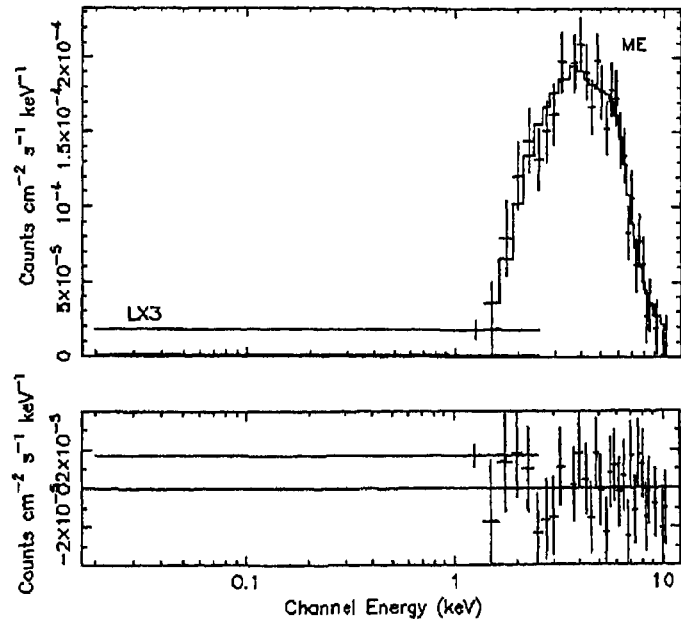


FIG. 4b

Observed spectrum of NGC 3516 for (a) 1985/308, (b) 1985/340 fitted with power law, uniform absorption, and Gaussian line model. Residuals between the spectra and the model are shown in the lower panel.

Fig. 3.1.9

Presence of an emission feature around 6.0 keV is also clearly evident from the residuals, presented in the lower panels of Figs 3.1.8. Also the  $\chi^2_r$  statistics (Table 3.1.2C) show that the simple power-law model does not provide good fits to the spectra. Therefore, a Gaussian line feature with variable line centre energy and variable line width was added with the power-law model and were fitted with the spectra. The best fitting model was obtained with line width value as 1.0 keV. The best-fit parameters with 90% confidence error bars are presented in Table 3.1.2h. After the addition of the Gaussian line feature around 6.0 keV, a very significant reduction in  $\chi^2_r$  ( $\Delta\chi^2 > 10$  for all the spectra) was obtained which provides a very high significance (>99.9%) for justifying the presence of the line using the F- statistics. LE + ME spectra with the best fit, power-law plus Gaussian line plus uniform absorption model convolved through the detector response are shown in Figs 3.1.9. Later observations of this source by Ginga on October 1989 ( $\Gamma_{2-18} \sim 1.72$ ; Nandra & Pounds 1994) and ASCA on 1994 ( $\Gamma_{3-10} \sim 1.83$ ; Nandra et al. 1997) showed steeper photon indices than EXOSAT ( $\langle \Gamma \rangle \sim 1.2$ ; Table 3.1.2C). Also the equivalent widths of the line emission around 6 keV were lower for the Ginga ( $\langle \text{EW} \rangle \sim 307 \pm 107$  eV) and ASCA ( $\text{EW} \sim 340 \pm 120$  eV) compared to the EXOSAT value ( $\langle \text{EW} \rangle \sim 678 \pm 306$ ). However, the error range is high for EXOSAT fits. There is no substantial variation in the 2-10 keV luminosity between the EXOSAT ( $\langle L_{2-10} \rangle \sim 0.67 \times 10^{43}$  erg s<sup>-1</sup>; Table 3.1.2D) observations of 1985 and Ginga ( $L_{2-10} \sim 0.73 \times 10^{43}$  erg s<sup>-1</sup>; ) observations of 19 October 1989. However, a factor of  $\sim 4$  change is detected between EXOSAT observations (1985) and ASCA ( $L_{2-10} \sim 2.7 \times 10^{43}$  erg s<sup>-1</sup>; Nandra et al. 1997) observation of this source on 1994 April 2.

### 3.1.2j. NGC3783

All the three spectra of this source observed between 1983 and 1985 were initially fitted with simple power-law plus uniform absorption model. This model provided the  $N_H$  values smaller than the galactic value towards this source (Table 3.1.2C). So the value of  $N_H$  was fixed with the galactic value and the best-fitting parameters presented in Table 3.1.2D. A plot of the observed spectrum of 1983/347 along with the power-law plus fixed absorption model convolved through the detector response is provided in Fig.3.1.10 lower panel of the figure shows the residuals between the spectra and model. Fig.3.1.11 presents the residuals of 1983/347, 1984/162 and 1985/005 which shows the presence of variable soft excess in this galaxy. Two power-law,

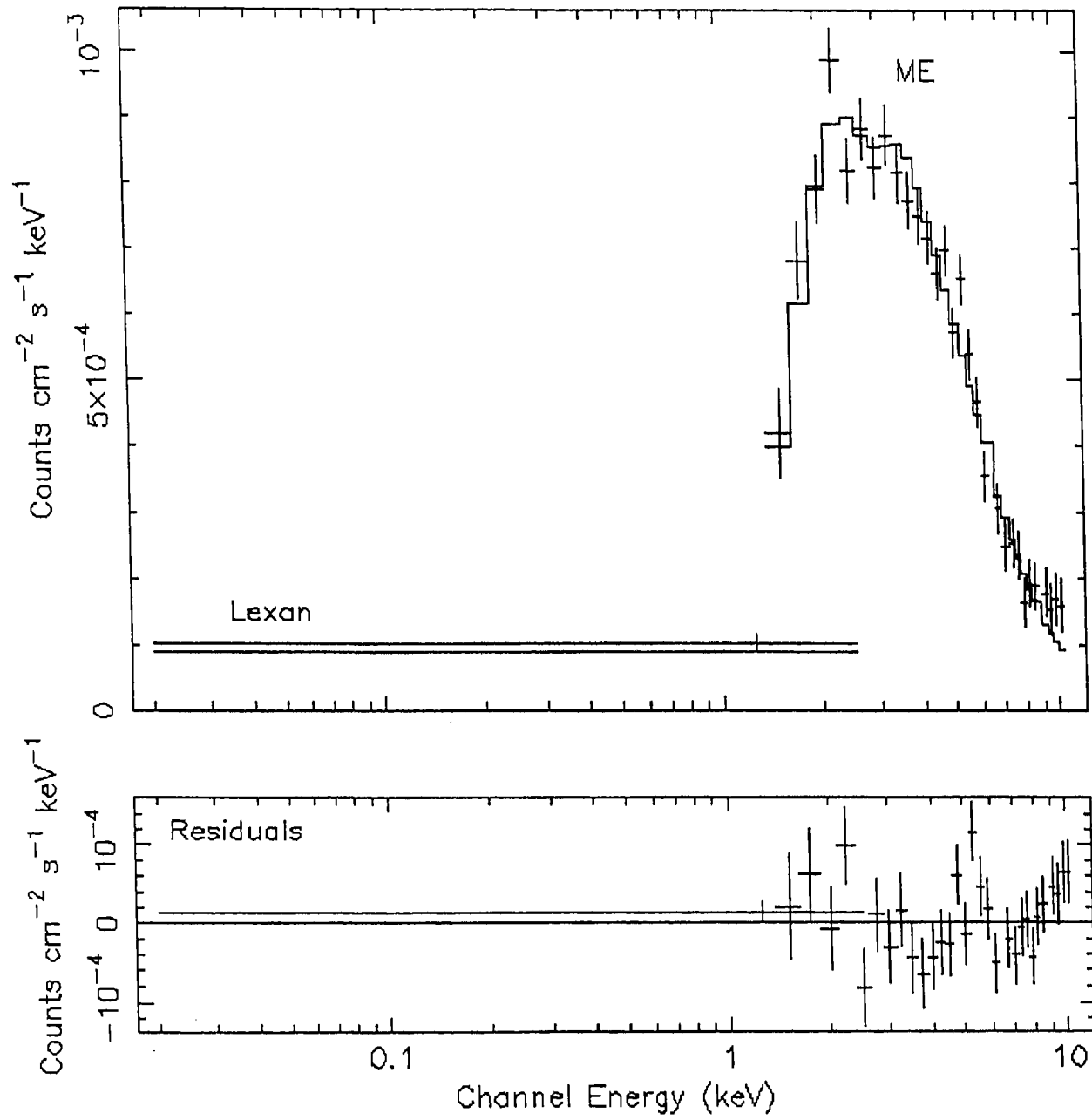


Fig. 3.1.10. Observed spectrum of NGC3783 fitted with a power-law plus fixed absorption model.

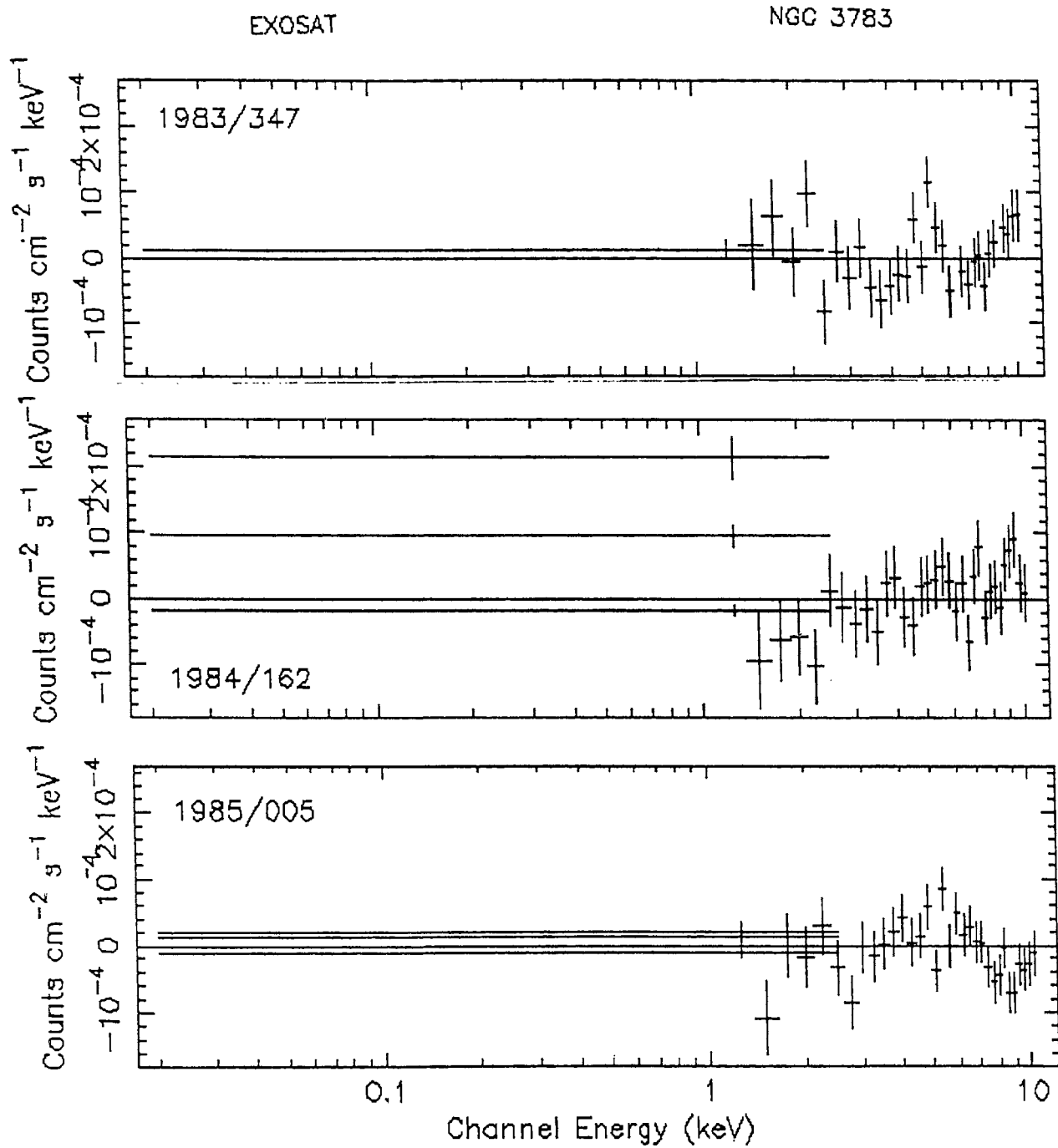


Fig. 3.1.11. Residuals between the model (power-law + fixed absorption) and the spectra of NGC 3783 which were observed on three epochs. This figure shows the presence of variable soft excess.

EXOSAT

1983/347

NGC 3783

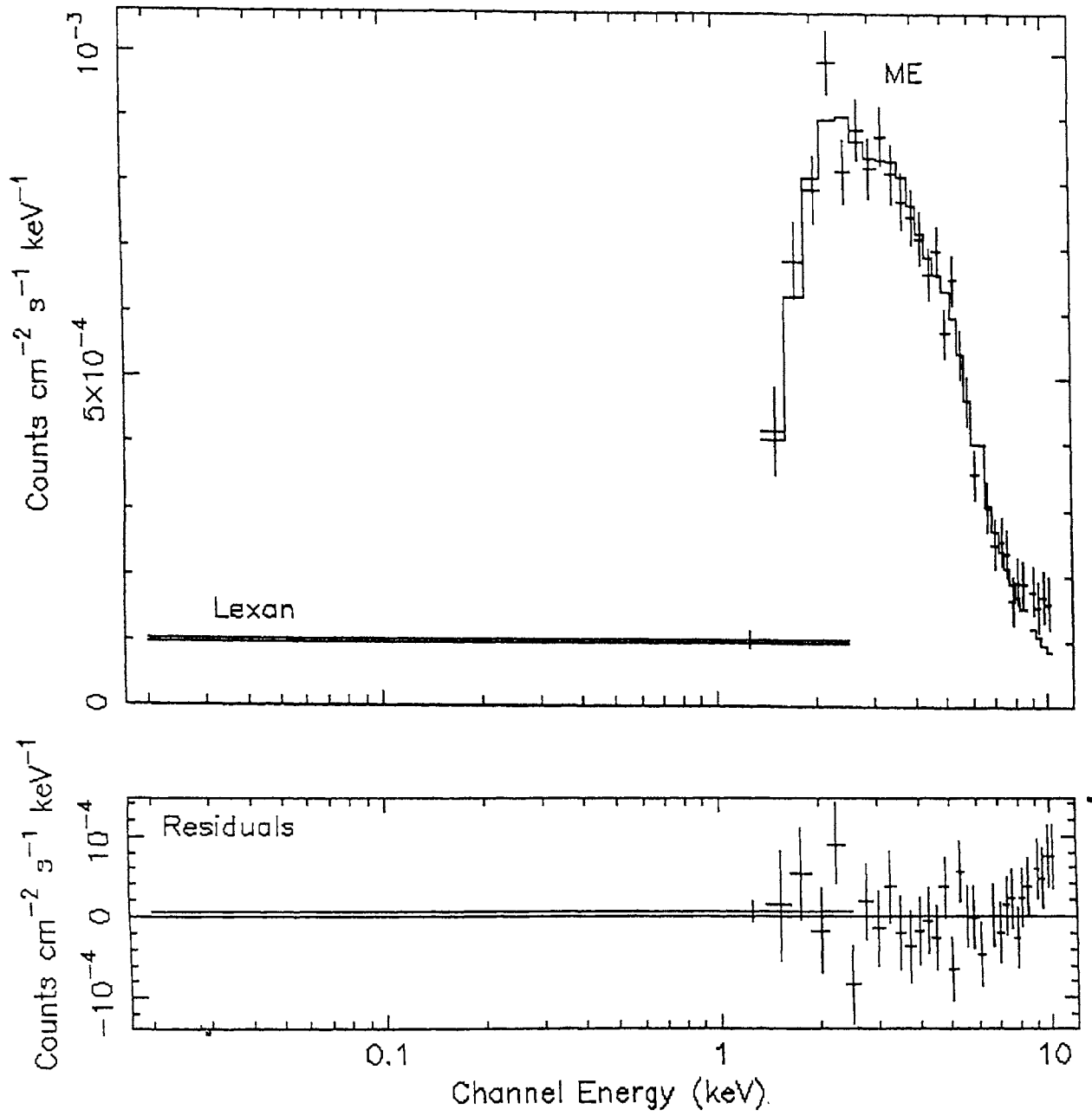


Fig. 3.1.12. Observed spectrum of NGC3783 fitted with the power-law + fixed absorption + Gaussian line model.



thermal bremsstrahlung and broken power-law models were used to fit the soft excess detected in this galaxy. Two power-law model (Table 3.1.2G) provides acceptable fits to the data sets but the model is insensitive to compute the errors and there were no improvements in the  $\chi^2$  values of the thermal bremsstrahlung model (Table 3.1.2E) over the power-law plus fixed absorption model (Table 3.1.2D). Broken power-law model provides good fit to the soft excess. The best-fit parameters of the broken power-law model are presented in Table 3.1.2F. The soft photon index ( $\Gamma_1$ ) values are correlated with the soft excess values. However, hard photon index ( $\Gamma_2$ ) remained unchanged in response to the flux variations. The residuals of the spectra of NGC3783 presented in Fig.3.1.11 show the presence of an emission feature around 6 keV. A Gaussian line component with variable line centre energy was added with the power-law plus fixed absorption model. Best-fit parameters are presented in Table 3.1.2h. In Fig. 3.1.12 the observed LE+ME spectra with the best fit power-law plus fixed absorption plus Gaussian line model convolved through the detector response are shown. The comparison of the 1992 July 23 observations of ROSAT ( $\Gamma \sim 2.5$ ;  $F_{0.1-2} \sim 5 \times 10^{-11}$  erg cm<sup>-2</sup> s<sup>-1</sup>; Alloin et al. 1995) and the EXOSAT observations (Table 3.1.2D, Table 3.1.2F and Fig. 3.1.11) reveals the correlated variability of LE flux and photon index. NGC3783 was also observed with Ginga (1990, Jan 13; Nandra & Pounds 1994) and ASCA (1993 December 19; Nandra et al. 1997). The measured equivalent widths of EXOSAT, Ginga and ASCA observations are consistent.

### 3.1.2k. NGC4593

The spectral fits using simple power-law with uniform absorption model yielded the  $N_H$  values smaller than the galactic  $N_H$  value towards this source (Table 3.1.2C). Hence all the 7 EXOSAT spectra of NGC4593 observed between 1984 and 1986 were fitted with power-law plus fixed absorption model (Table 3.1.2D). Fig.3.1.13 shows the plot of the LE+ME photon spectra of NGC4593 observed on 1985/185 with best fit power-law + fixed absorption model convolved through the detector response. The residuals shown in the lower panel of this figure indicate the presence of soft excess emission and an emission feature around 6 keV. Figures 3.1.14a and b show the plots of residuals between spectra and power-law + fixed absorption model which shows the variable nature of the soft excess emission. Two power-law (Table 3.1.2G), broken power-law (Table 3.1.2F) and thermal bremsstrahlung (Table 3.1.2E) models were used to fit the soft excess emissions of the source. Reduced  $\chi^2$  values show that the broken power-law model

EXOSAT

NGC 4593

1985/185

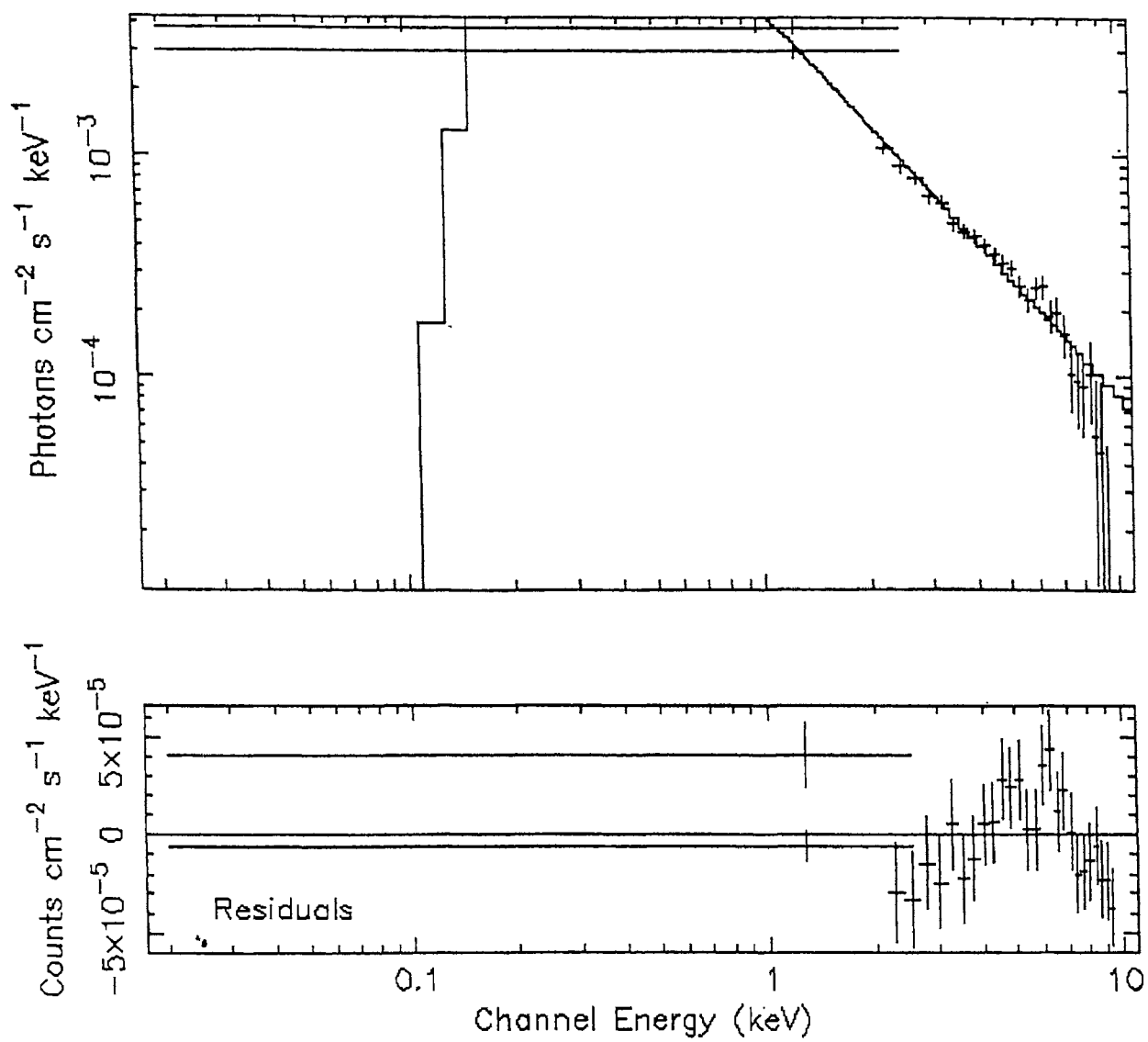


Fig. 3.1. 13 LE + ME photon spectrum of NGC 4593 for 1985/185 fitted with a power-law plus fixed absorption model.

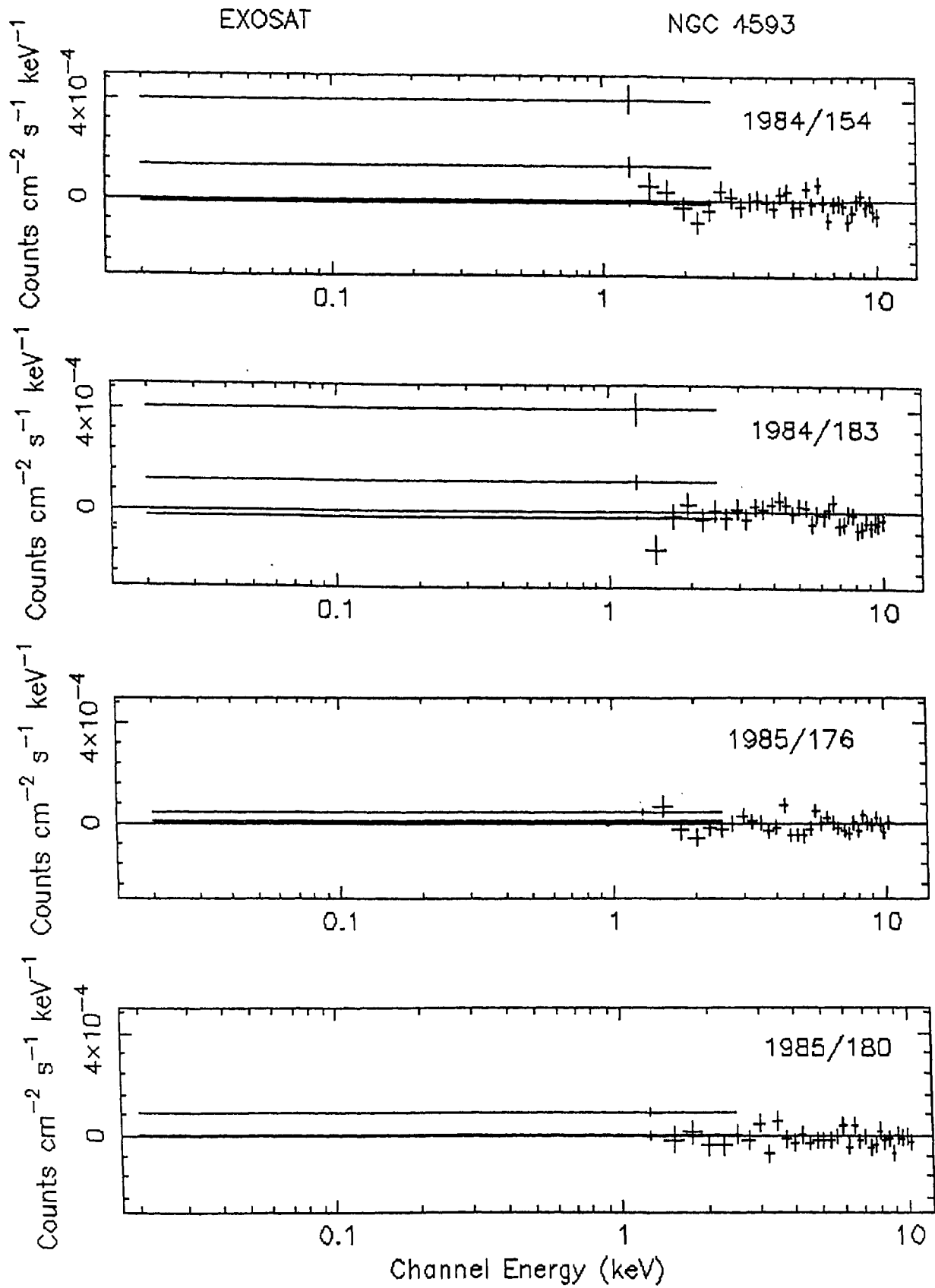


Fig. 3.1.14a Residuals between the observed spectra and the model (fixed power-law+ fixed absorption) for different dates.

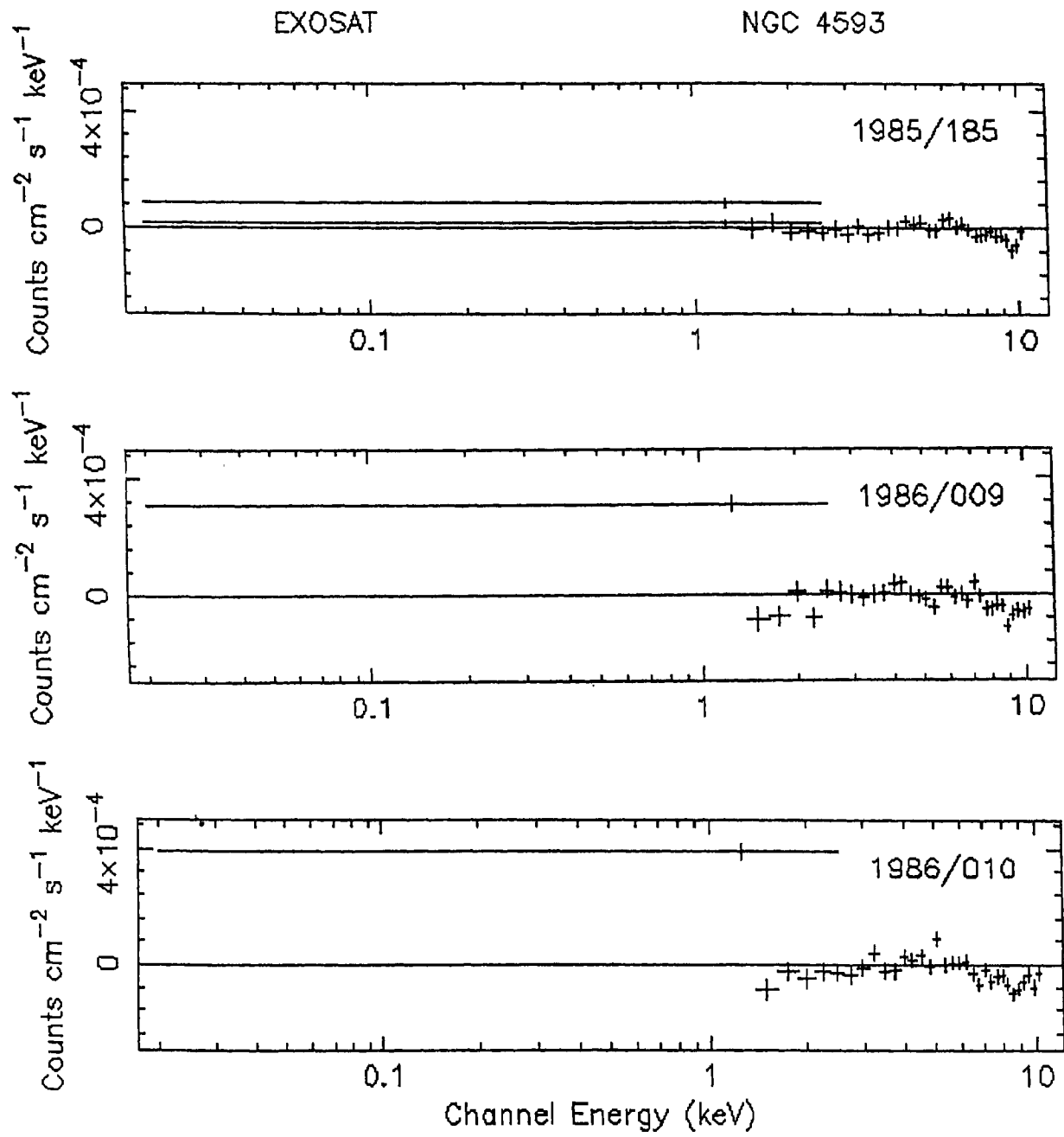


Fig. 3.1.14b. Same as Fig. 3.1.14a but for different dates of observations.

fits better than that obtained from the two power-law and the thermal bremsstrahlung models. Power-law plus fixed absorption plus Gaussian line model was used to fit the line emission around 6 keV and the results are given in Table 3.1.2h. Fig. 3.1.15 shows the photon spectra of NGC4593 fitted with Gaussian component.

This galaxy displayed remarkable intensity variations during EXOSAT observations between 1984 and 1986. In particular the LE count rates show a factor of 5 decrease in a year (between 1984/183 and 1985/185 and 1986/009; Table 3.1.2B). In a year interval the ME count rates also decreased, although only by a factor of 3 and increased in 189 days only by a factor 2. Both the LE and ME count rates increased by factors 1.4 and 1.2 respectively, in 4 days (between 1985/176 and 1985/180) time interval. This differential and uncorrelated (Fig. 3.1.16) variability of LE and ME count rates on short and long time scales indicate that low and medium energy X-ray emissions are from different sources.

No significant variations of  $\Gamma$  was found during the EXOSAT observations. The values of  $\Gamma$  for the LE+ME fits are steeper than the average ME slope. This is because of the presence of soft excess emission in the spectra. Broken power-law model describes significantly better fits to the data, over the energy range 0.1-10 keV than the single power-law model (Tables 3.1.1d and Table 3.1.2F). No remarkable variations of LE photon index ( $\Gamma_1$ ) between 1984 and 1986. The steep power-law slopes ( $\Gamma_1$ ) are relatively less steeper than usually found in other Seyfert galaxies (Ghosh & Soundararajaperumal 1992c) in which soft excesses are present. These low values of  $\Gamma_1$  can not completely fit the soft excess emissions present in this galaxy and as a result of this we still find the presence of some more soft emissions in the residuals of broken power-law fits (Figs 3.1.17a and b). These results suggest that, most probably, two soft emission components are present in NGC4593. However, runs made with broken power-law plus blackbody or thermal bremsstrahlung model do not significantly improve the fits. From the Fig.3.1.16 it can be seen that during the brighter state of NGC4593 the ME count rates varied with, almost, non variable LE count rates. The LE count rates and soft excess emissions display correlated variability (Fig. 3.1.18). However, during the brighter state of this source the soft excess became non variable (Fig.3.1.18). The hard power-law slope was almost constant even though the source brightness varied (Fig.3.1.19). Also  $N_H$  values remained nearly constant during the observations (Table 3.1.2C) which suggest that the absorbing columns did not vary

EXOSAT

NGC 4593

1985/185

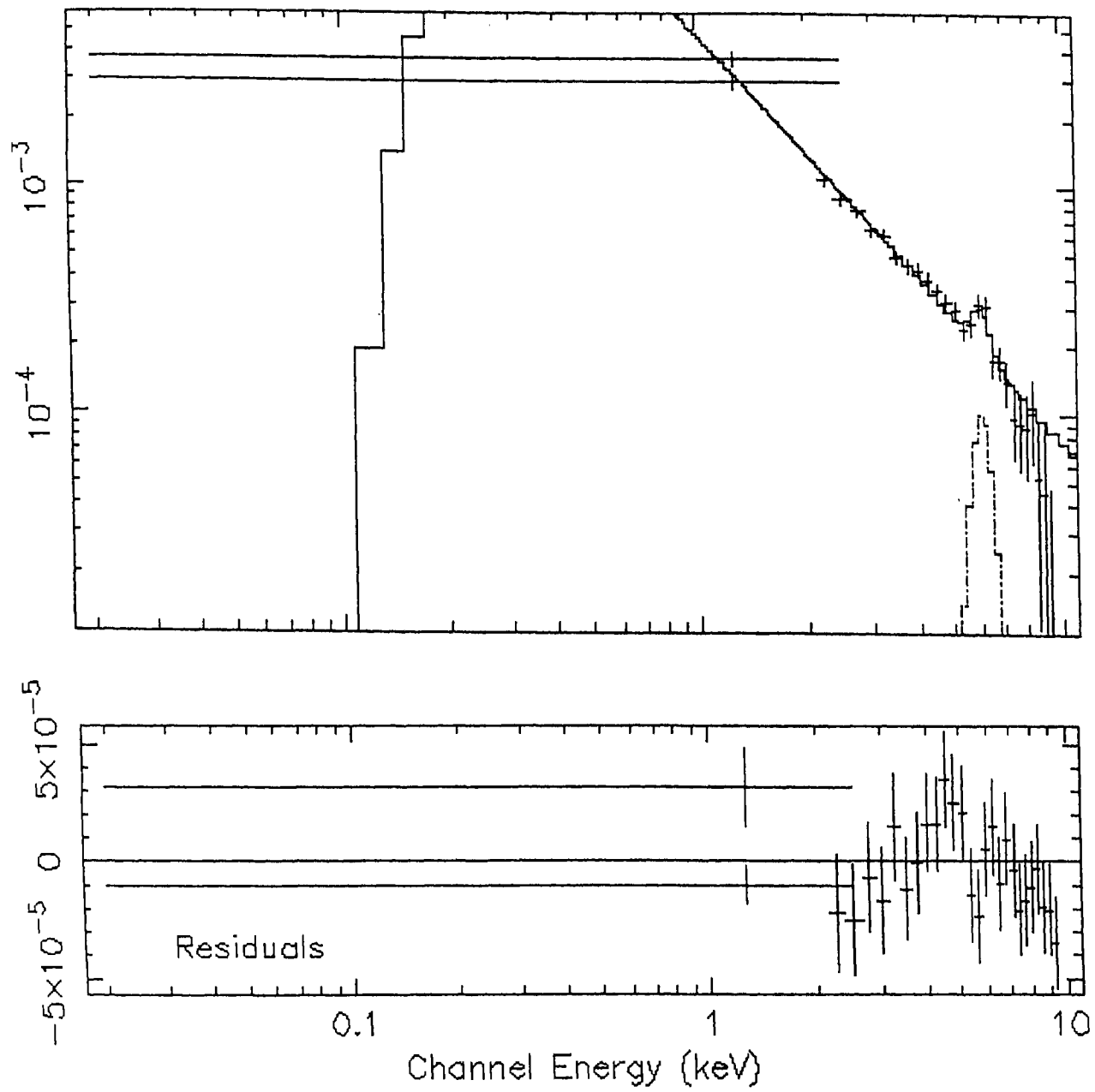


Fig. 3.1.15. Photon spectrum of NGC4593 for 1985/185 fitted with the power-law + fixed absorption + Gaussian line model.

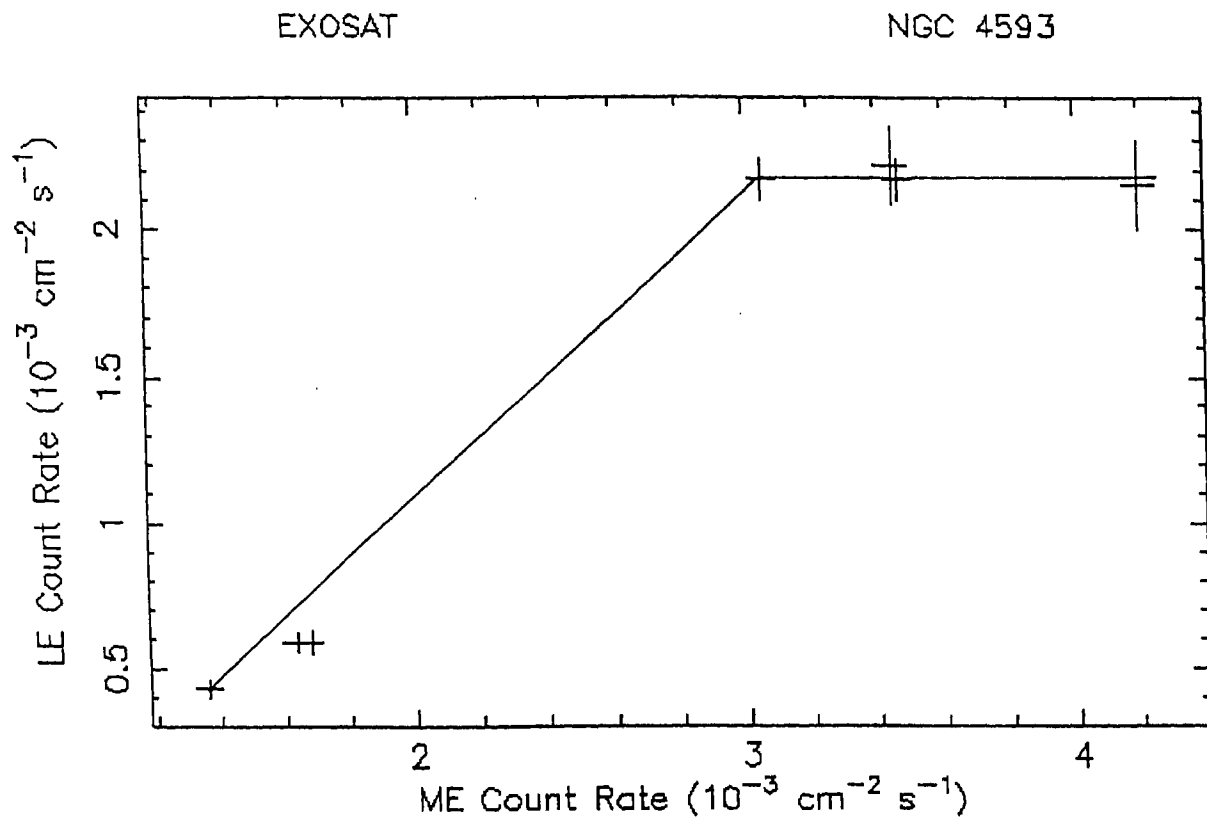


Fig. 3.1.16. Plot of the LE versus ME count rates.

EXOSAT

NGC 4593

1984/183

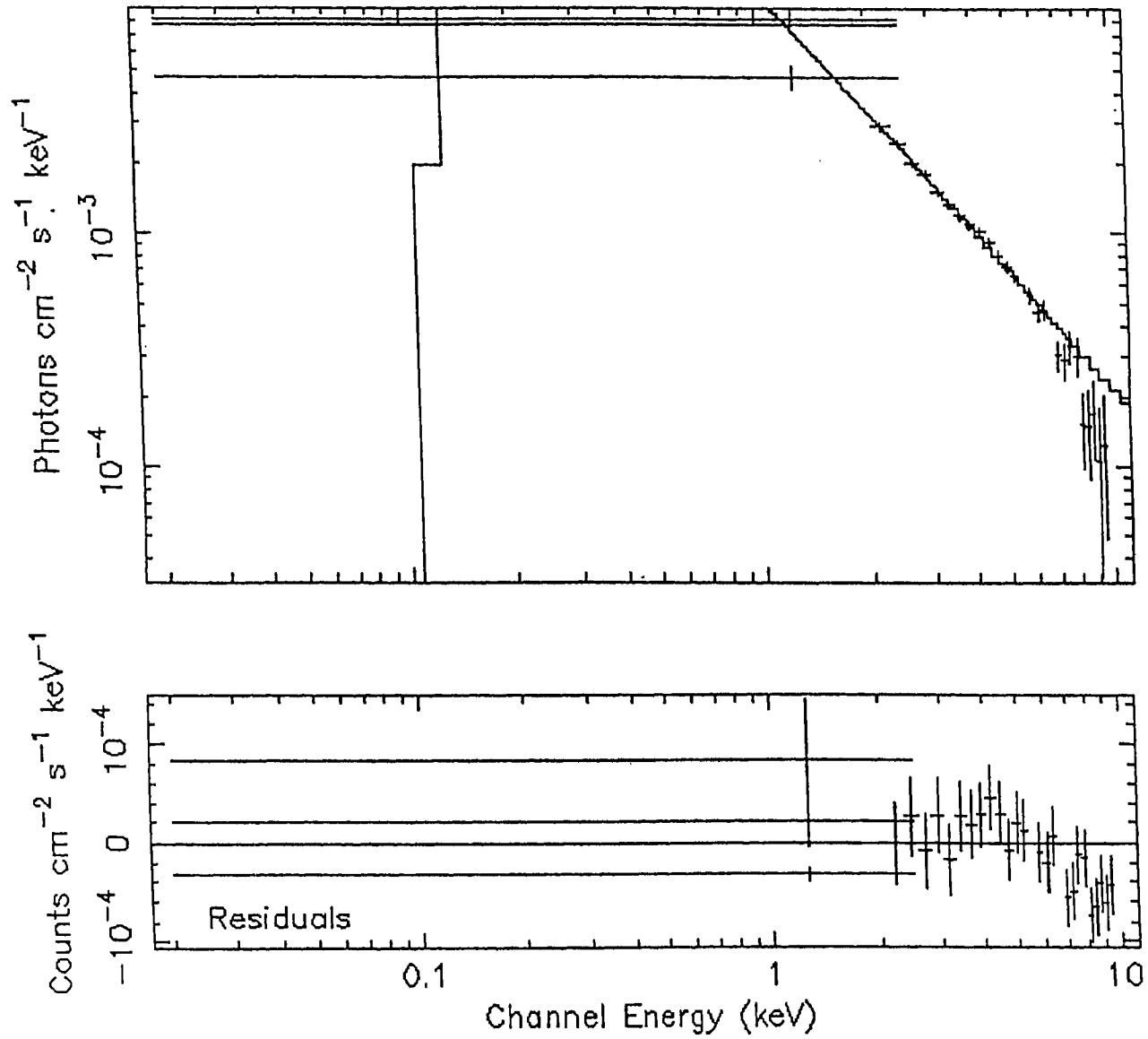


Fig. 3.1.17a LE + ME photon spectrum of NGC4593 for 1984/183 fitted with the broken power-law model. Still the presence of soft excess emission can be seen from the residuals between the model and the spectrum shown in the lower-panel



EXOSAT

NGC 4593

1984/154

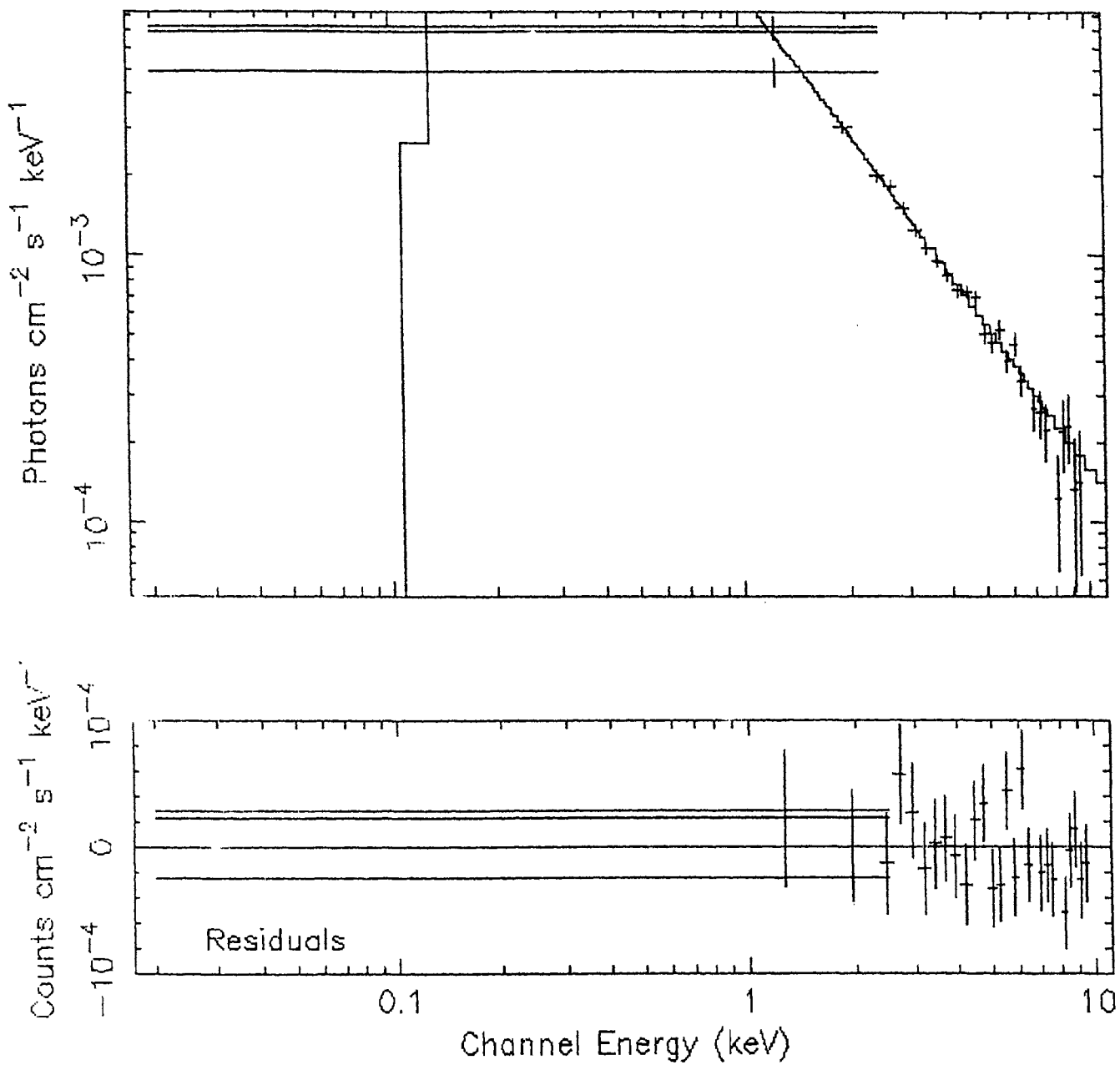


Fig. 3.1.17b Same as Fig. 3.1.17a but for 1984/154

EXOSAT

NGC 4593

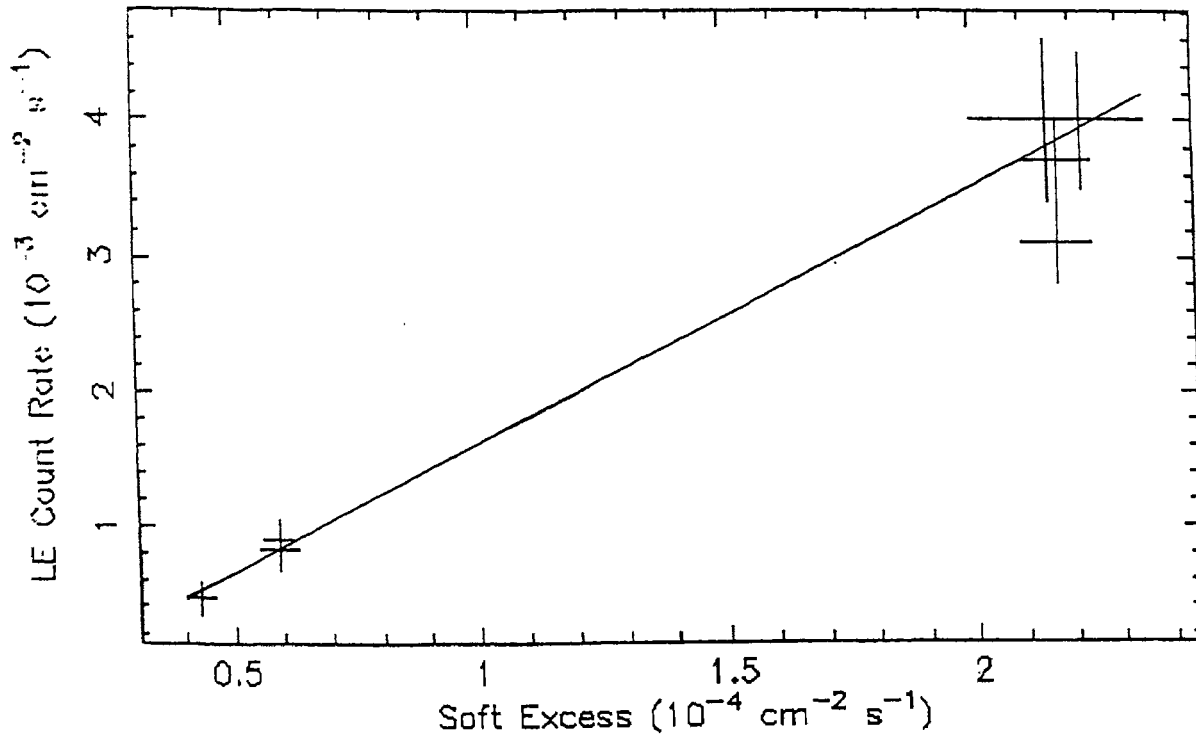


Fig. 3.1.18. Measured soft excess values are plotted against the observed LE count rates. Solid line shows that these two parameters are correlated.

with the source brightness. In certain galaxies it was found that their spectra become softer as they get brighter (Grandi et al. 1992). However we do not find any such relation in NGC 4593 even though the brightness varied dramatically during EXOSAT observations (Fig.3.1.19). The results of our EXOSAT X-ray spectral analysis of NGC4593 are also published (Ghosh & S.Soundararajaperumal 1993)

1984-1986 observations of EXOSAT ( $\langle \Gamma \rangle \sim 1.8$ ;  $\langle L_{2-10} \rangle \sim 0.95 \times 10^{43}$  erg s<sup>-1</sup>; Ghosh & Soundararajaperumal 1993), 1987 December observation of Ginga ( $\Gamma \sim 1.73$ ;  $\langle L_{2-10} \rangle \sim 1.07 \times 10^{43}$  erg s<sup>-1</sup>; Nandra & Pounds 1994) and 1994 January observations of ASCA ( $\Gamma \sim 1.78$ ;  $\langle L_{2-10} \rangle \sim 1.1 \times 10^{43}$  erg s<sup>-1</sup>; Nandra et al. 1997) all show nearly identical ME photon indices and 2-10 keV luminosities.

### 3.1.21. 3C382

EXOSAT observations of 3C382 were carried out on many (>20) epochs between 1983 and 1985). A log of observations of 3C382 is given in Table 3.1.2B. Observed LE and ME count rates are plotted in Fig. 3.1.20. This figure shows the dramatic variations of the LE and ME count rates of this galaxy during its major outburst (Kastral et al. 1991). In the present analysis 13 good quality spectra were selected and used. Since the spectral fits using simple power-law with uniform absorption model yielded the  $N_H$  values smaller than the galactic  $N_H$  value towards this source (Table 3.1.2C), all the 13 EXOSAT spectra of 3C382 were fitted with power-law plus fixed absorption model (Table 3.1.2D). ME spectral indices (obtained from the power-law + fixed absorption fits to the ME spectra alone) are plotted in Figs 3.1.21 and 3.1.22 against the date of observations and ME count rates respectively. From these figures it is evident that the hard spectral slope of 3C382 did not vary during the major out burst of this galaxy. Average value of  $\Gamma$  is around 1.7 (Figs 3.1.21 & 3.1.22) and this value is steeper than the Ginga value ( $\Gamma \sim 1.50$ ; Kastral et al. 1991).

The LE and ME spectrum of 3C382 observed on 1985/246 is plotted in Fig. 3.1.23. Figures 3.1.24a-c plot the residuals of different dates and these figures show the presence of variable soft excess and the presence of an emission feature around 6 keV is also seen in some of them. The soft excess variability is found to vary in correlation with the LE count rates (Fig.3.1.25; coefficient of the linear regression fit is 0.89 for 12 observations which implies the probability of

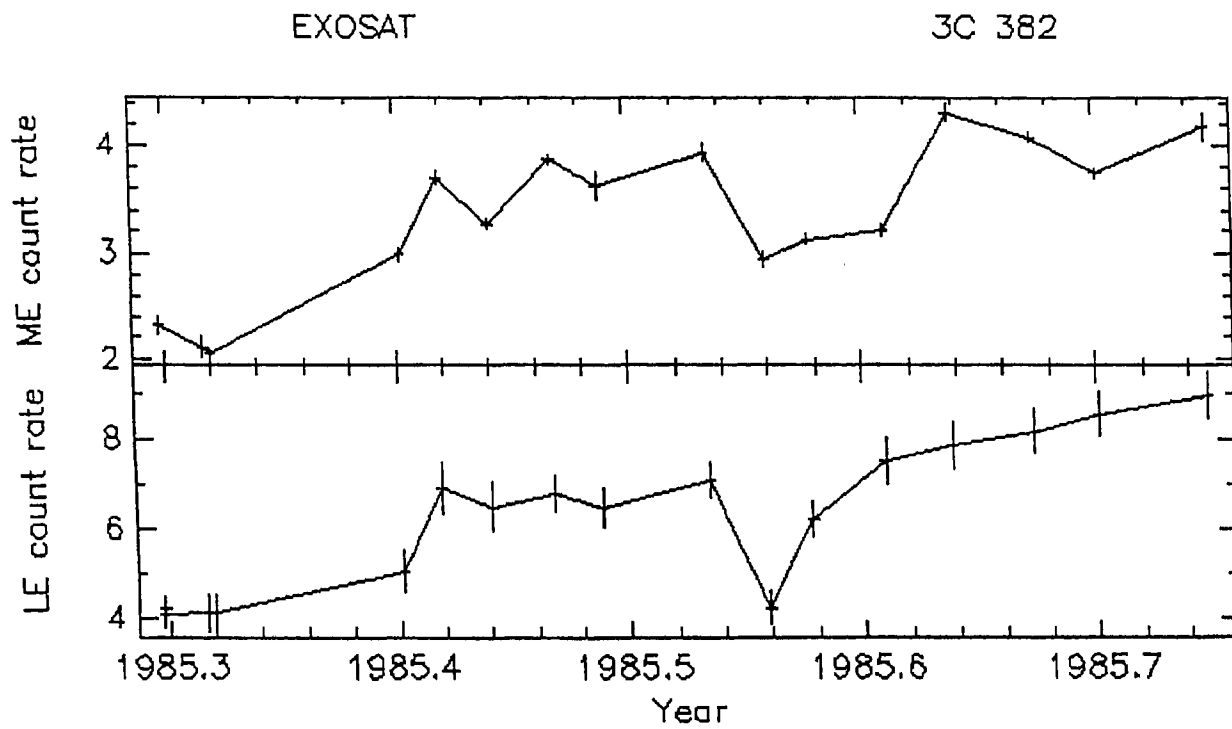


Fig. 3.1.20. Plot of the LE and ME count rates versus the date of observations.



EXOSAT

1985/246

3C 382

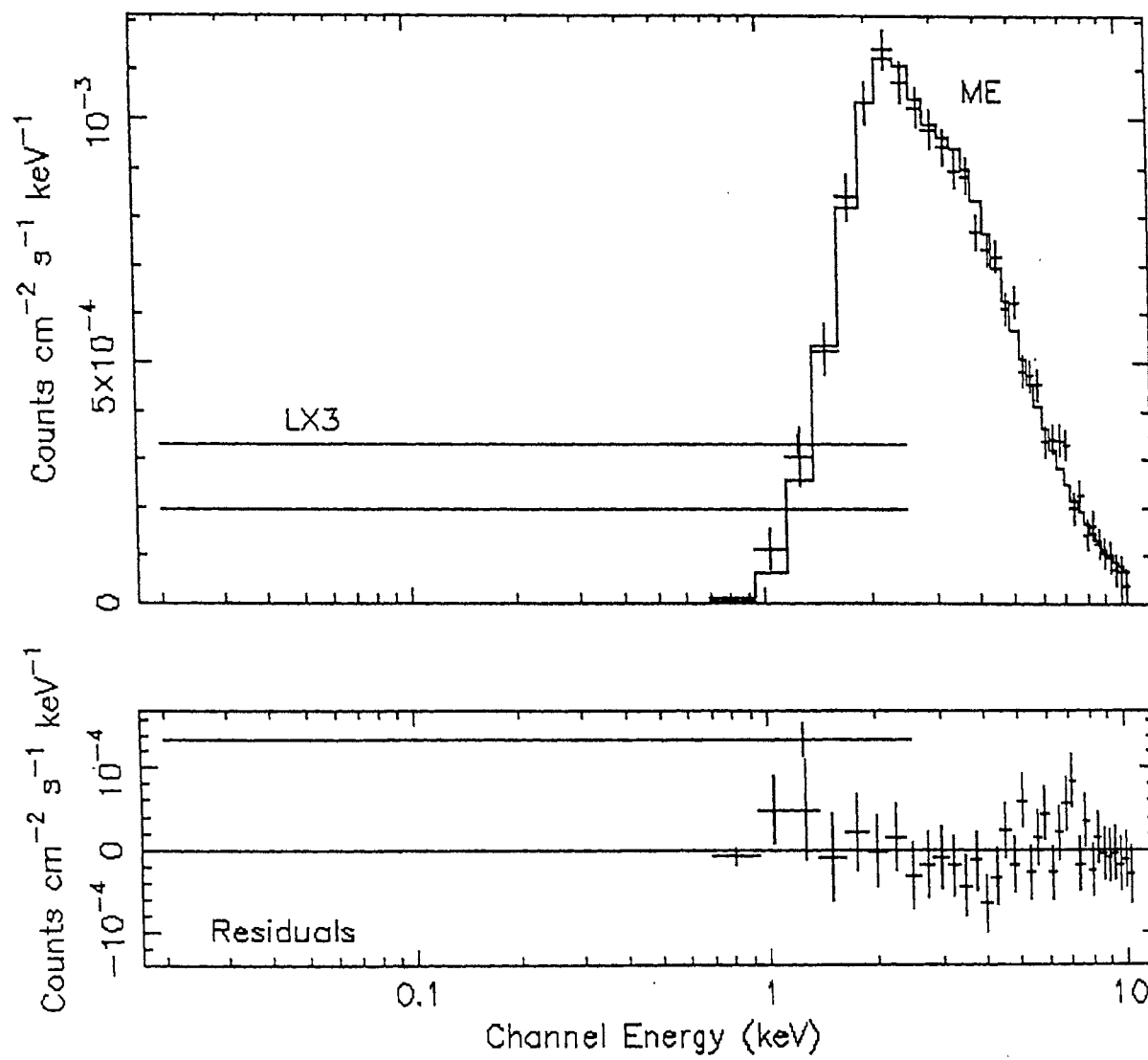


Fig. 3.1.23. Observed spectrum of 3C382 fitted with a simple power-law and fixed absorption model.

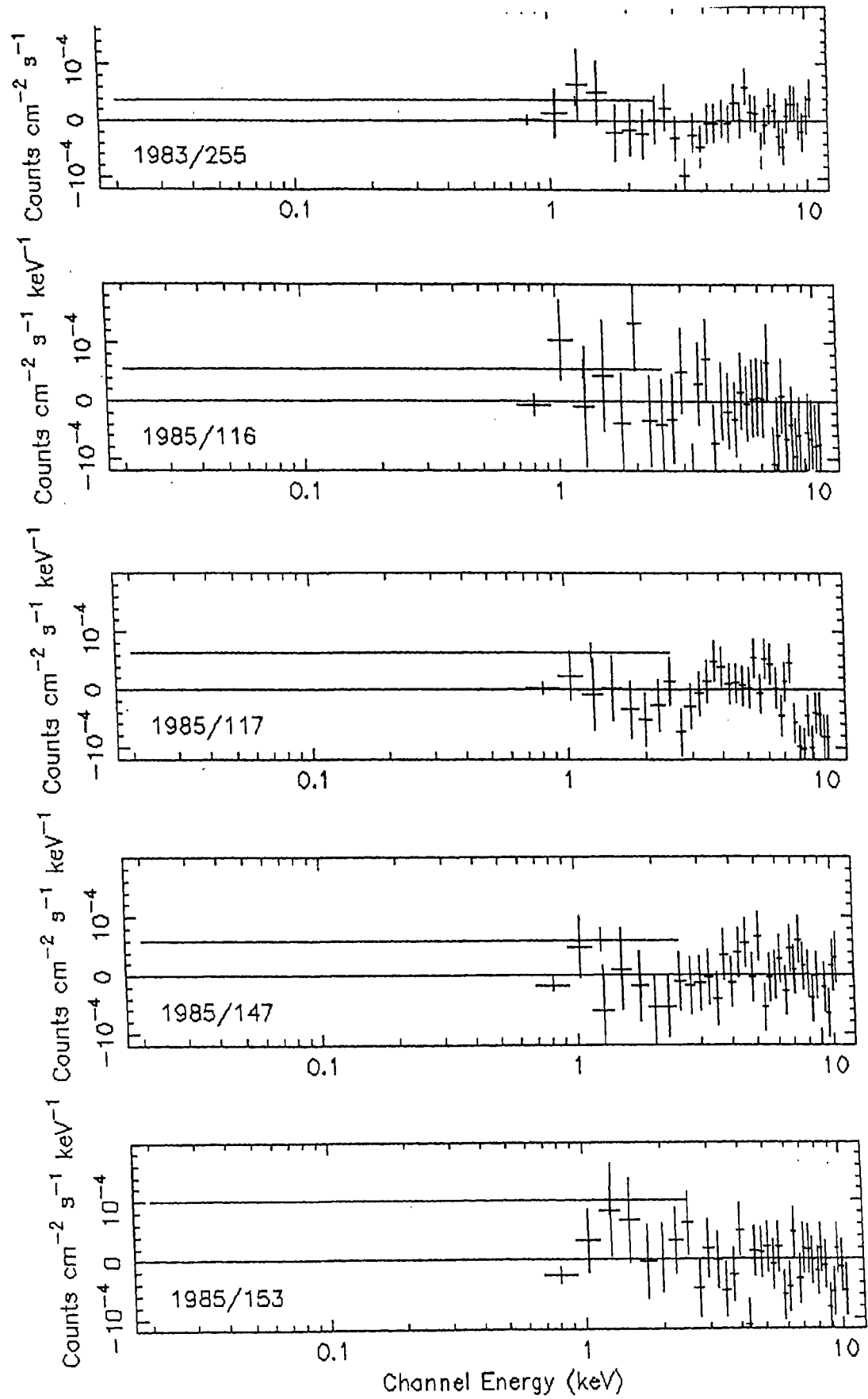


Fig. 3.1.24a. Residuals between the observed spectra and the model (power-law + fixed absorption).

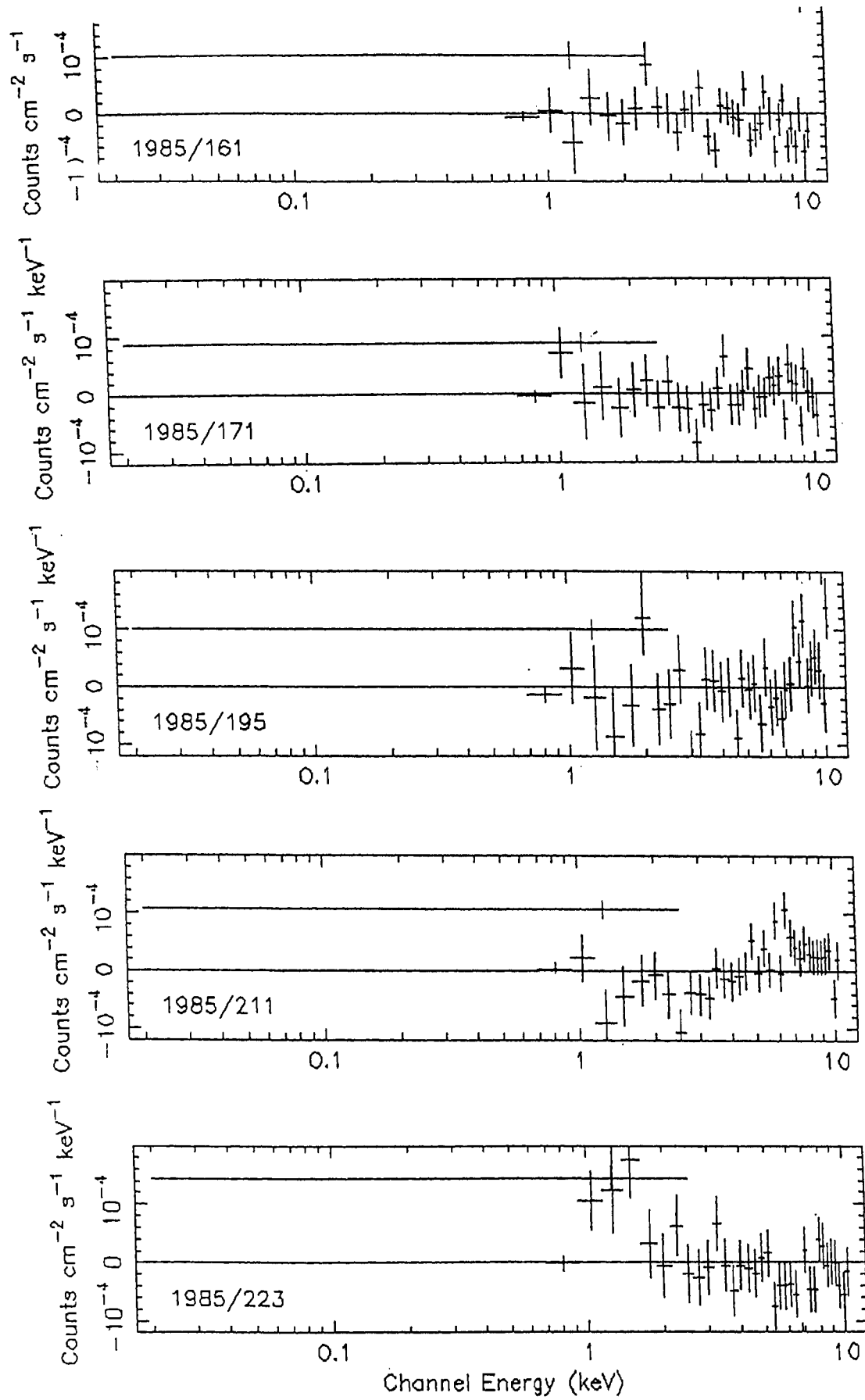


Fig. 3.1.24b. Same as Fig. 3.1.24a but for different dates.



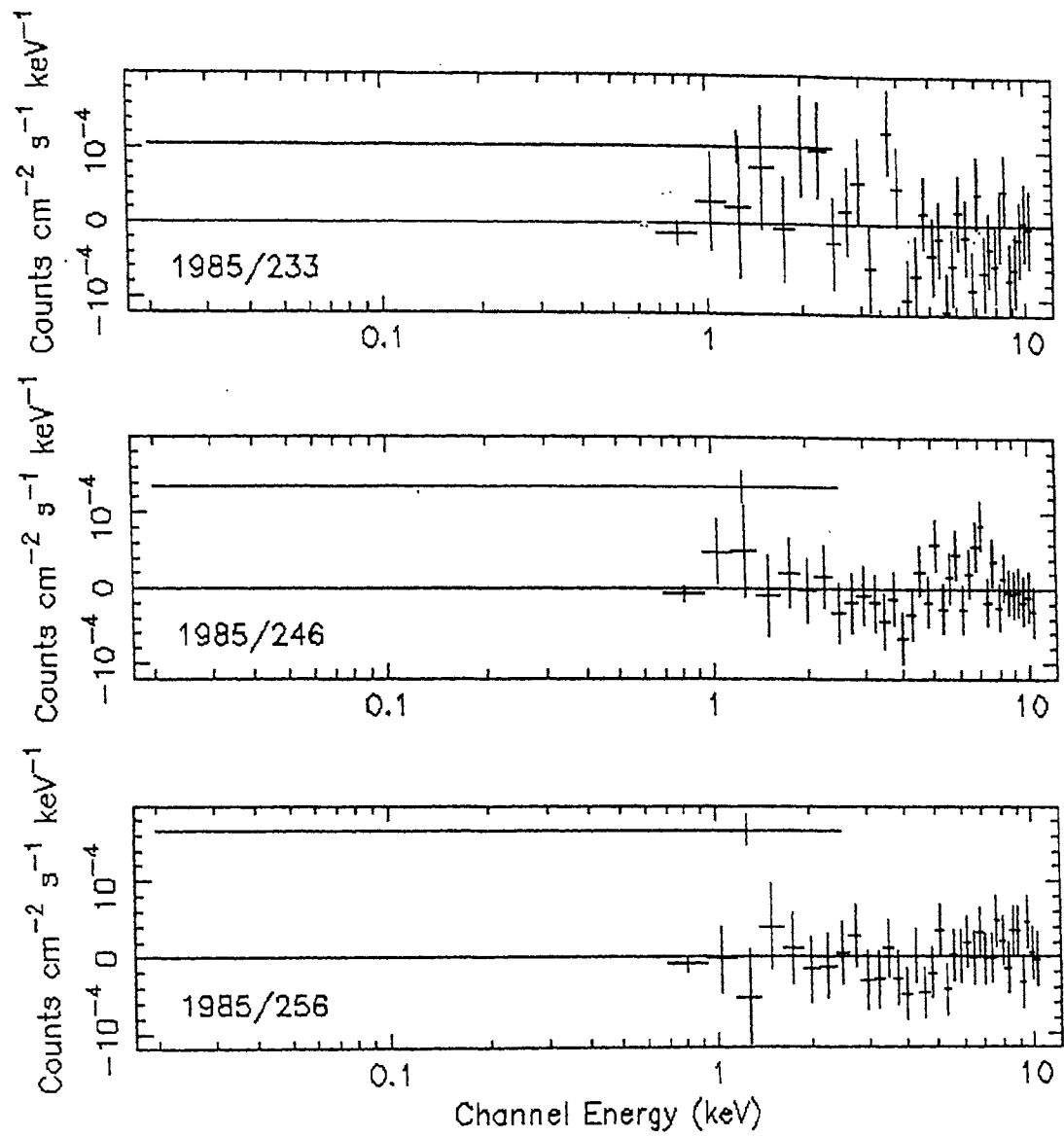


Fig. 3.1.24c. Same as Fig. 3.1.24a but for different dates.

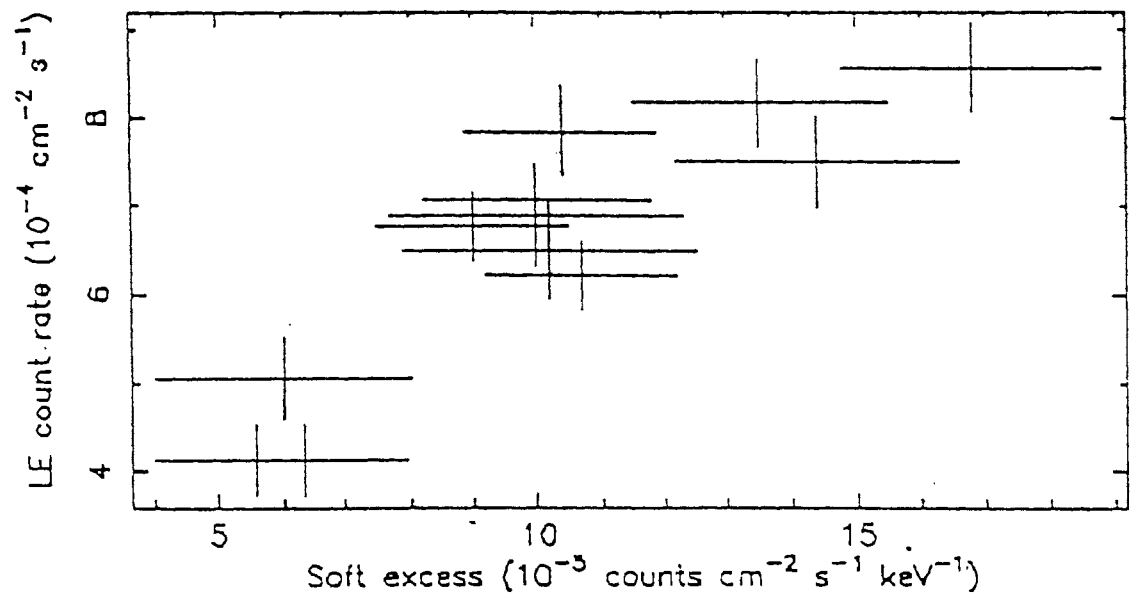


Fig. 3.1.25. Plot of the soft excess versus LE count rate.

EXOSAT

1985/246

3C 382

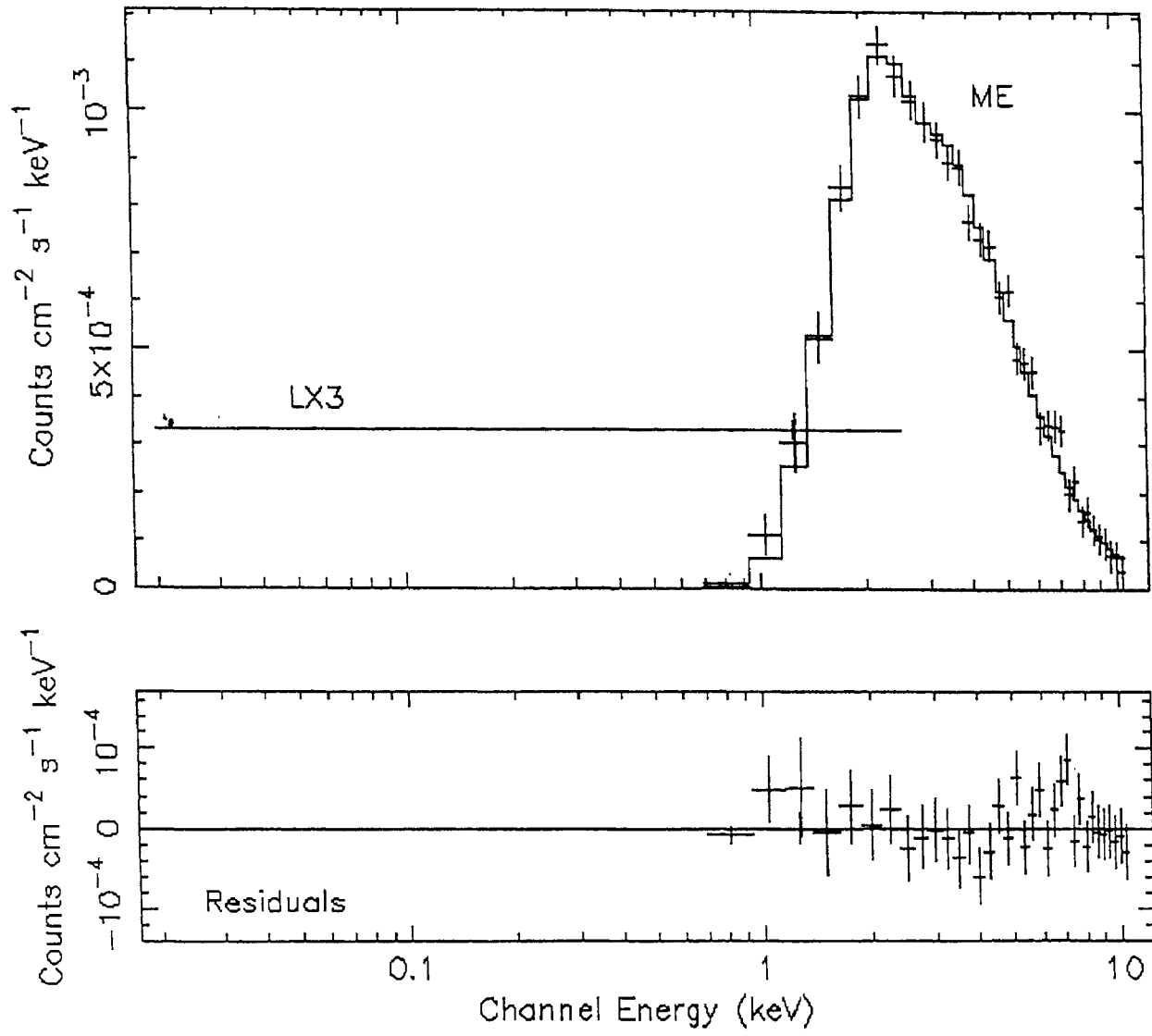


Fig. 3.1.26. Observed spectrum of 3C382 fitted with the broken power-law model.

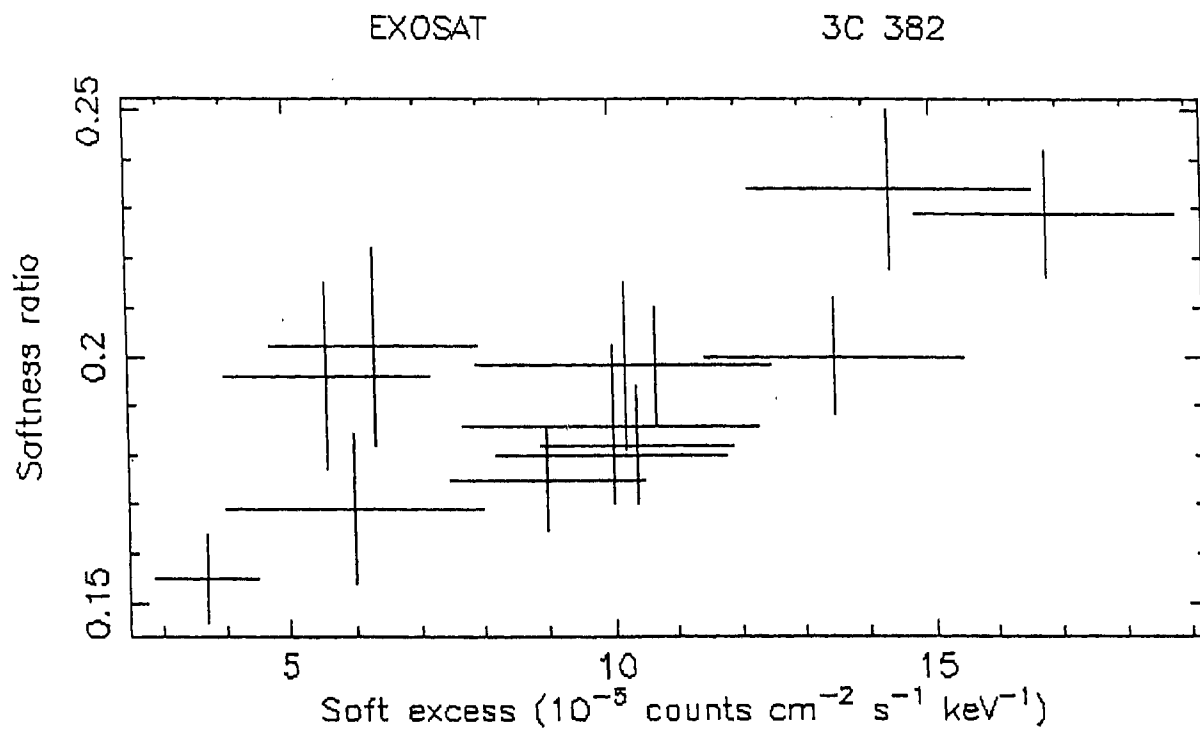


Fig. 3.1.27a Plot of the soft excess versus softness ratio of 3C 382



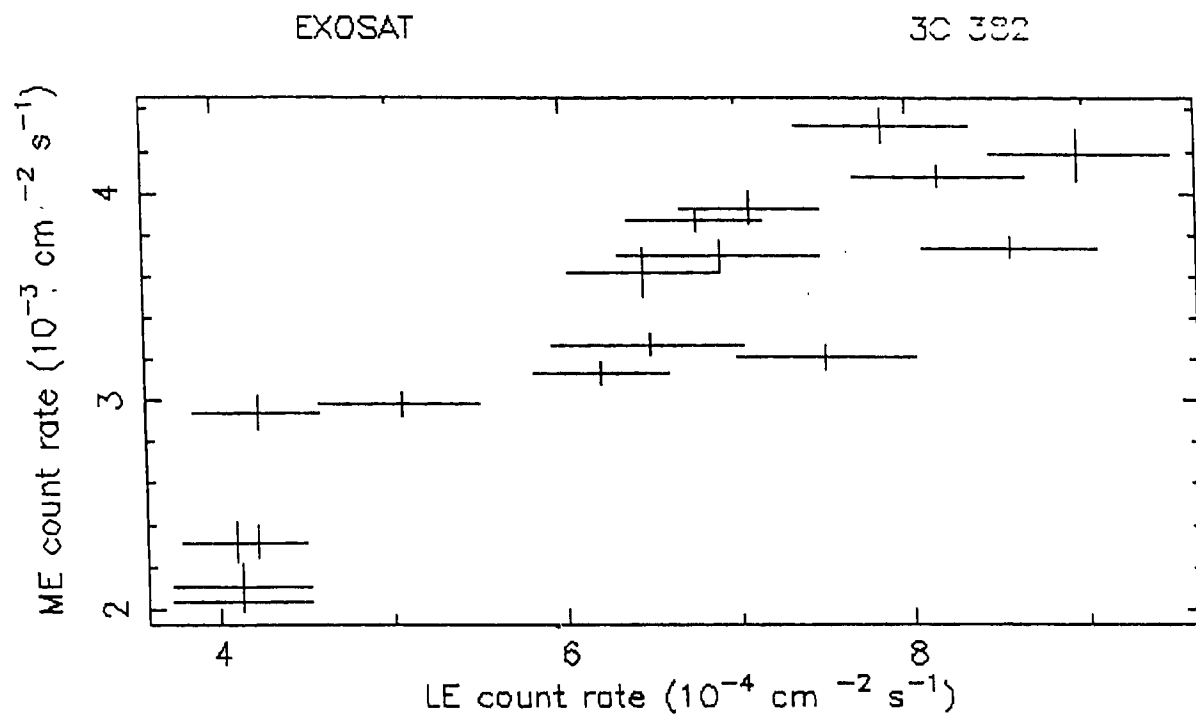


Fig. 3.1.29 Observed count rates of LE versus ME

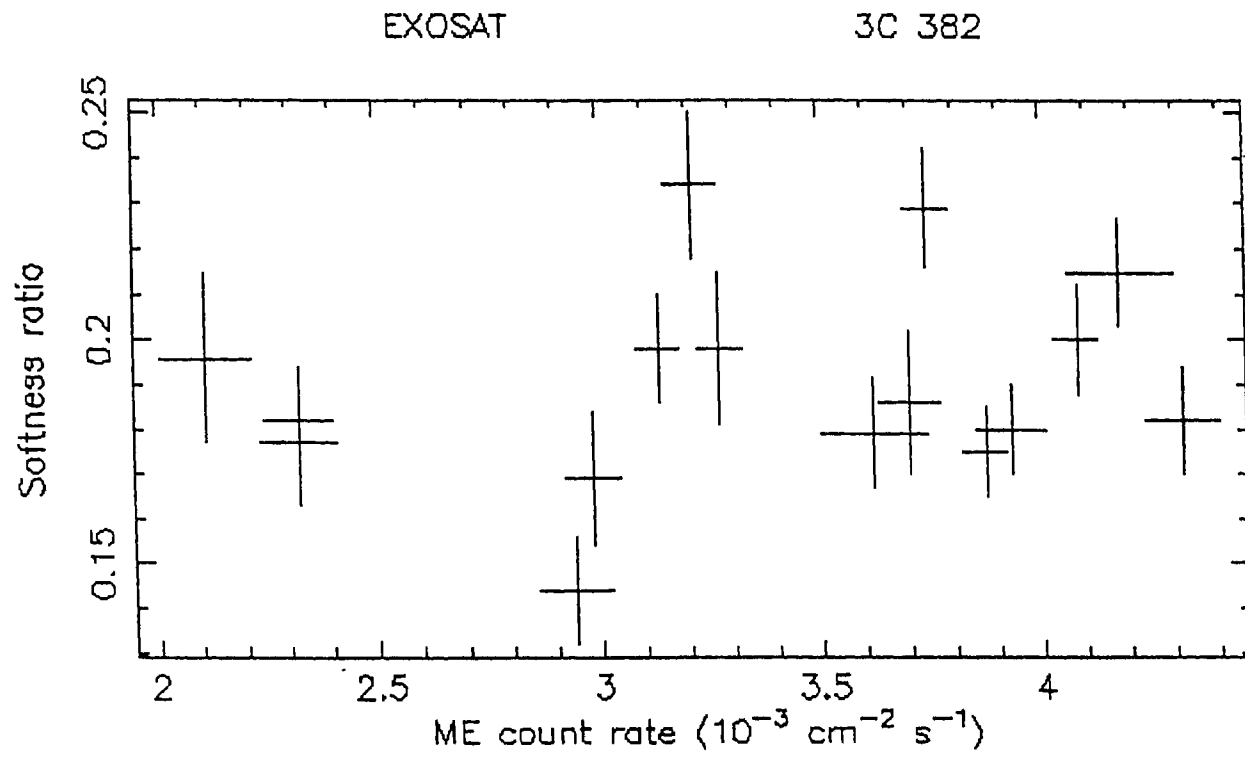


Fig. 3.1.30 Plot of the ME count rate versus the softness ratio

the fit being random to be  $\sim 0.05\%$ ). Two power-law (Table 3.1.2G), broken power-law (Table 3.1.2F) and thermal bremsstrahlung models were used to fit the soft excesses. Since the average value of the ME photon index of this galaxy is  $\sim 1.7$  (Figs 3.1.21 & 3.1.22), we have fixed the value of the hard component slope (for two component models) with 1.7. Two power-law model fits well to the data but this model is insensitive to compute the error bars of the fit parameters. Thermal bremsstrahlung model is not acceptable because the  $\chi^2_r$  values are greater than 2.0. However, broken power-law provided better fit. Fig.3.1.26 shows the observed LE + ME spectrum observed on 1985/246 fitted with broken power-law model convolved through the detector response. Soft spectral indices (obtained from the broken power-law fits) versus the softness ratio of 3C382 are plotted in Fig. 3.1.27b which shows these two parameters are correlated (correlation coefficient is 0.93).

To fit the emission feature around 6.0 keV a Gaussian line feature is added with the power-law model (Table 3.1.2H). F-test results computed between this model and power-law plus fixed absorption model show that the inclusion of the Gaussian line is highly significant ( $>99.9\%$ ). Average line centre energy is best estimated to be  $6.2 \pm 0.6$  keV and the equivalent width of this line ranges between 100 and 1100 eV.

Hard X-ray luminosities of 3C382 which were obtained from Ariel V (Elvis et al. 1978), HEAO 1 (Marshall et al. 1979; Mushotzky 1984), Einstein (Urry et al. 1989), EXOSAT (Table 3.1.2D) and Ginga (Kastrup et al. 1991) data show that there was a strong outburst of this galaxy in 1985 during EXOSAT observations. The soft photon index ( $\Gamma \sim 2.3$ ; Walter & Fink 1993) observed with ROSAT during the all-sky survey is very much flatter than the average soft photon index value of EXOSAT ( $\Gamma_1 > 3.0$ ; Table 3.1.2F).



### 3.1.2m. MCG-2-58-22

Six spectra of MCG-2-58-22 obtained over 10 days in 1984 November were analyzed separately to avoid systematic effects due to background variations and possible source variations. First, a simple power-law model with low energy absorption was used to fit the source. This model provided acceptable fits (Table 3.1.2C). However, the column density values ( $N_H$ ) are smaller than the galactic value. So the power-law plus fixed absorption (fixed with fixed  $N_H$  value) was tried (Table 3.1.2D). Fig.3.1.31 shows the LE+ME spectra of MCG-2-58-22 observed on 1984/321 along with the power-law plus fixed absorption model. Figs 3.1.32a-b shows the residuals between the observed spectra and this model for different dates. The  $\chi^2_r$  values of this model are high (Table 3.1.2D) and hence this model is unacceptable. The residual plots show the presence of variable soft excess and they also show the presence of an emission line around 6.0 keV. Thermal bremsstrahlung and two power-law models were used to fit the spectra. Thermal bremsstrahlung model is not acceptable because of the large  $\chi^2_r$  values ( $>2.0$ ). However, two power-law model provides acceptable fits to the data. Best fit parameters of this model are presented in Table 3.1.2G. From the F-test statistics, computed between power-law plus fixed absorption model and two power-law plus fixed absorption model, it is evident that the inclusion of the soft power-law component is highly significant (Fig. 3.1.33). The derived soft and hard fluxes are plotted in Fig. 3.1.34. This figure shows that MCG 2-58-22 displayed weak variations in both the LE and ME bands during EXOSAT observations. However they are uncorrelated (Fig. 3.1.35). The soft spectral index ( $\Gamma_1$ ) is correlated with the LE count rate (correlation coefficient 0.65 for 6 observations; Fig. 3.1.36a) whereas the hardness ratio (ratio of ME and LE count rates, a measure of hardness nature of the emission) of the source is anti correlated with the LE count rate (correlation coefficient is -0.86 for 6 observations; Fig. 3.1.36b). Hard spectral index ( $\Gamma_2$ ) did not vary, and the ME count rate and hardness ratio of the source are uncorrelated. Mean ME photon index ( $\Gamma_2$ ) obtained from EXOSAT observations ( $\sim 1.48$ ) is in close agreement with that obtained from HEAO 1 ( $\sim 1.55$ ), HEAO 2 ( $\sim 1.53$ ; Mushotzky 1984) and Einstein SSS + MPC ( $\sim 1.45$ ; Holt et al. 1989).

A Gaussian component was added to the two power-law plus fixed absorption model to fit the emission feature detected around 6 keV (Fig. 3.1.33). The best fit parameters are listed in Table

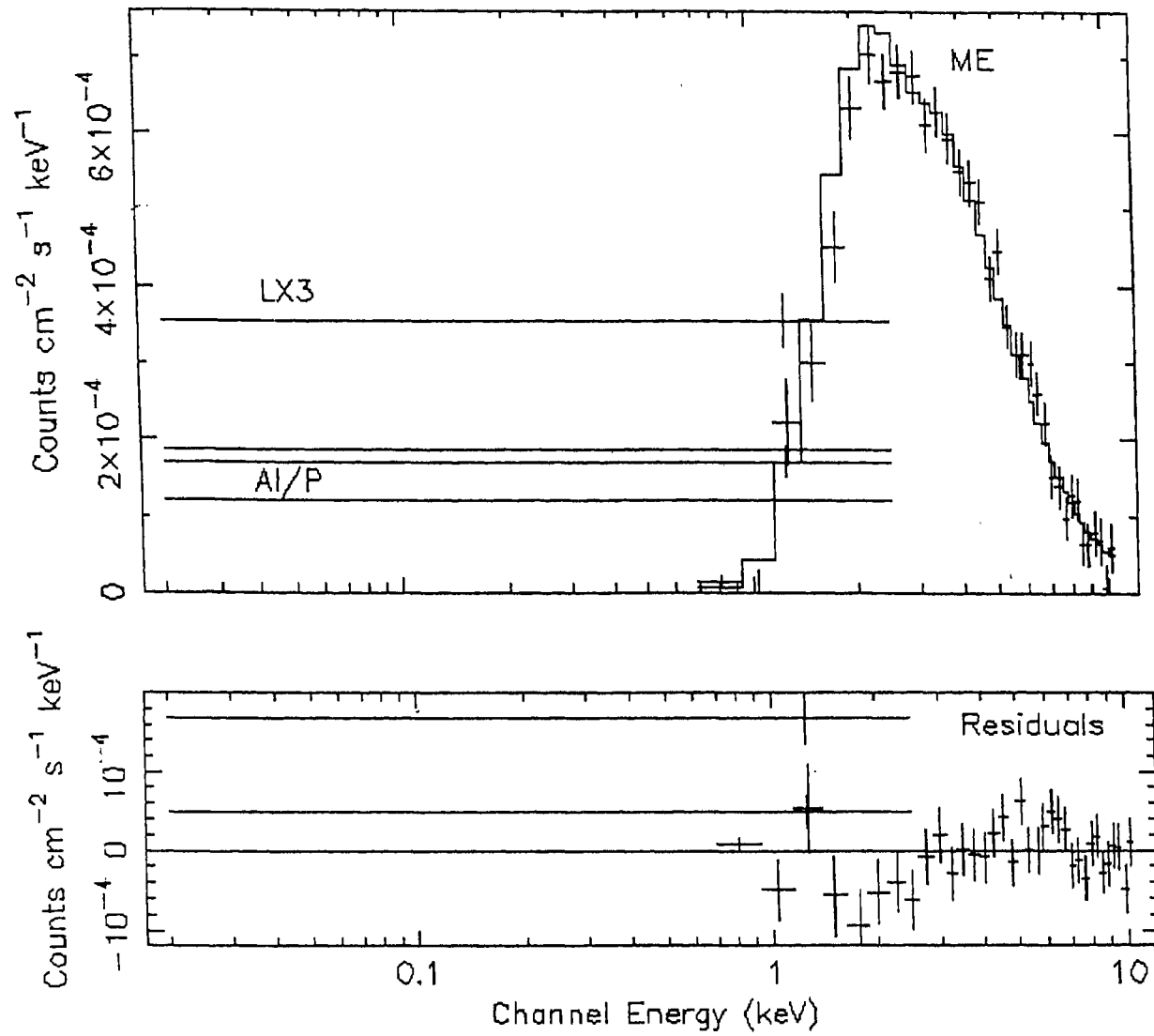


Fig. 3.1.31. Observed spectrum of MCG-2-58-22 fitted with a simple power-law and fixed absorption model.

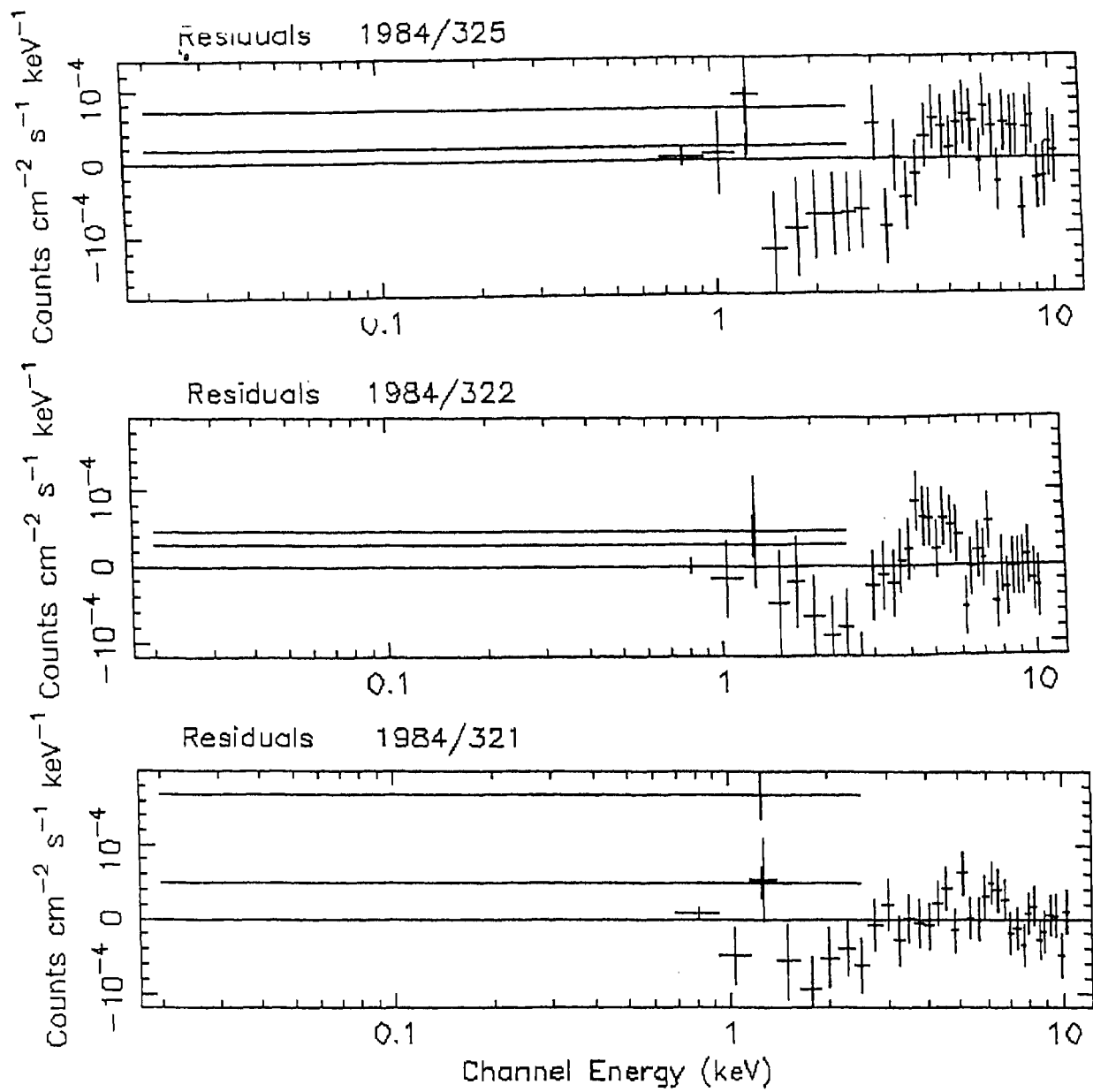


Fig. 3.1.32a. Residuals between the observed spectra and the model (power-law + fixed absorption) for different dates of observations.

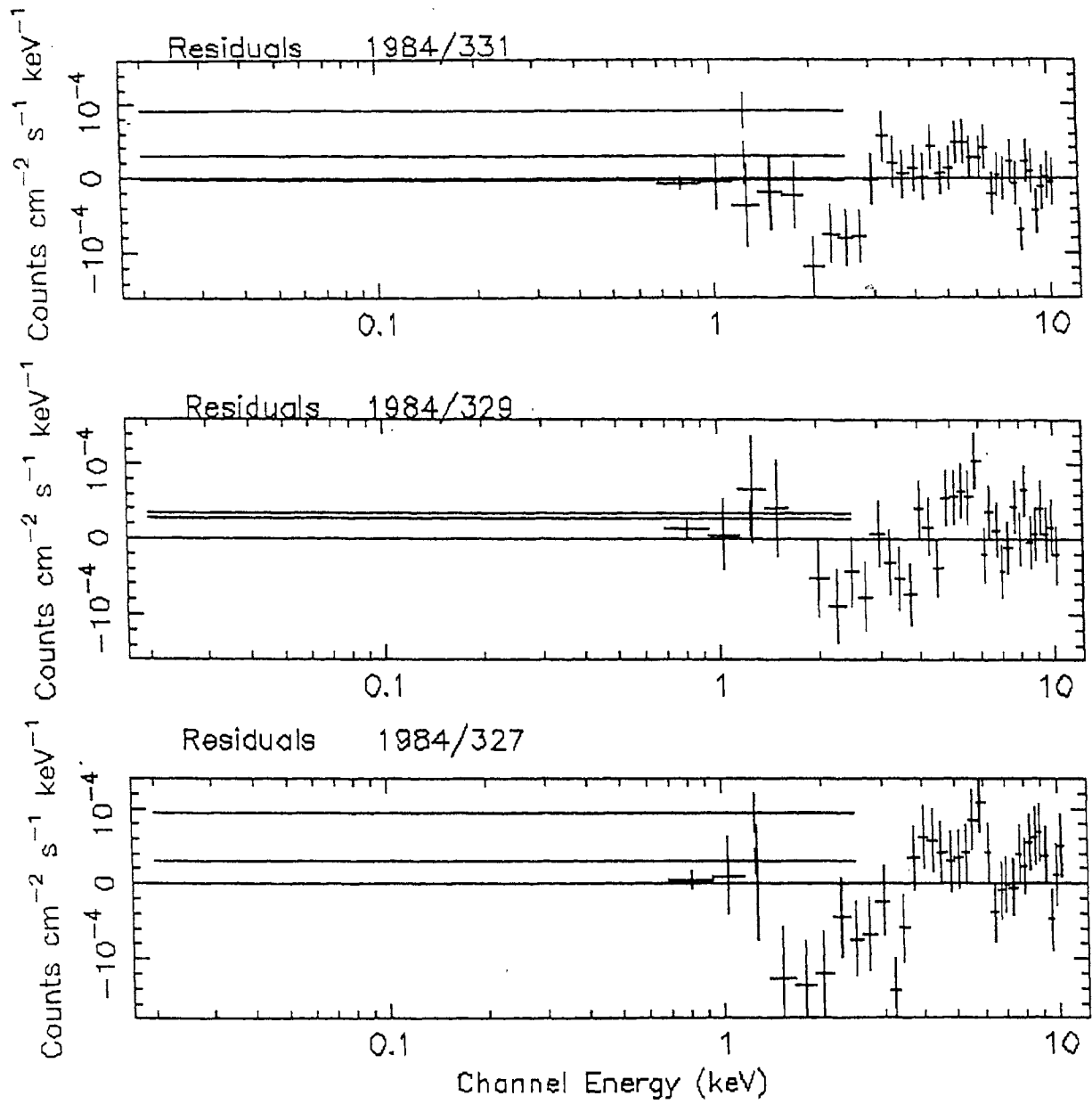


Fig. 3.1.32b. Same as Fig. 3.1.32a but for different dates of observations.

EXOSAT

MCG 2-58-22

1984/321

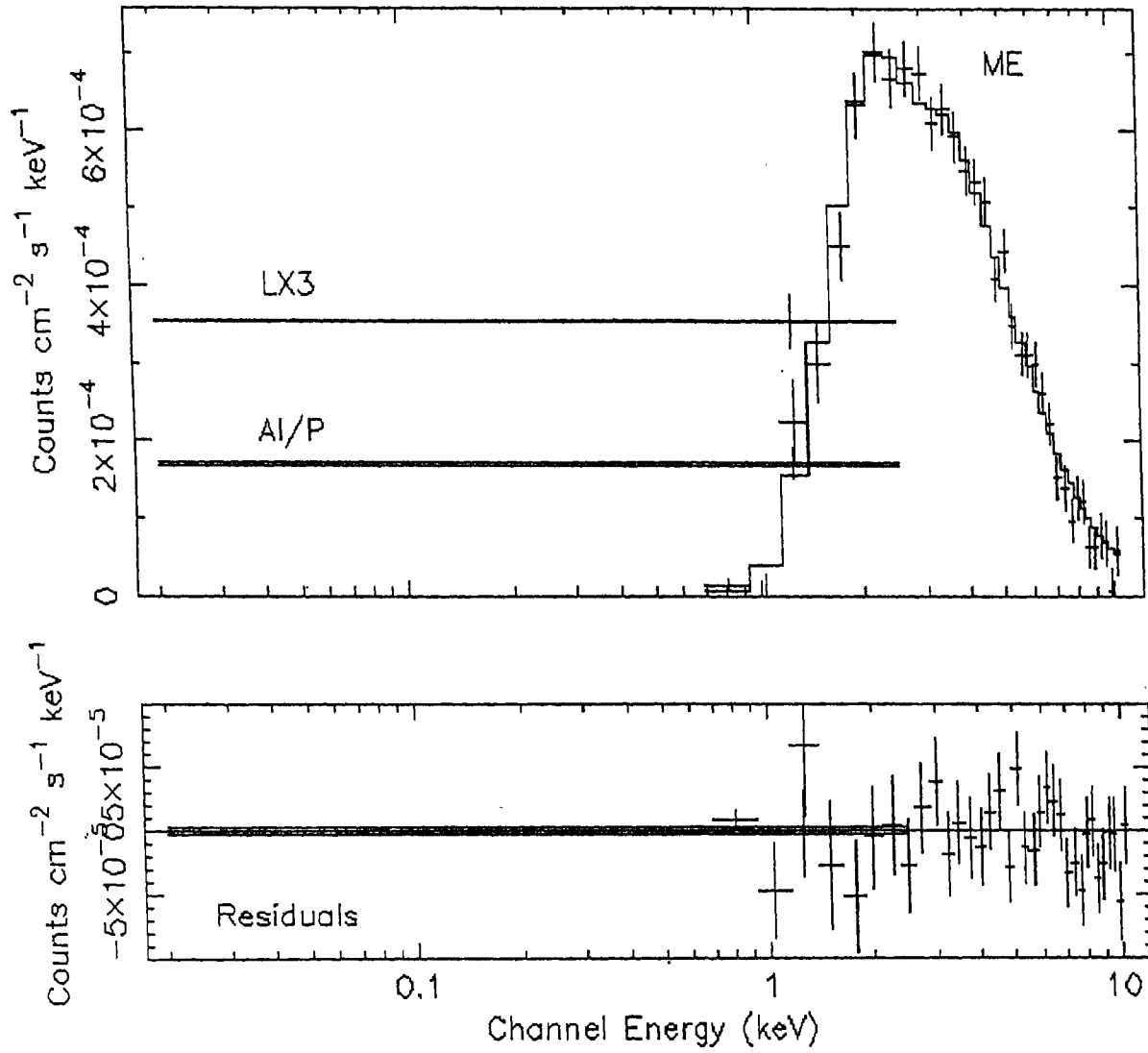


Fig. 3.1.33. Observed spectrum of MCG-2-58-22 fitted with two power-law + fixed absorption model.

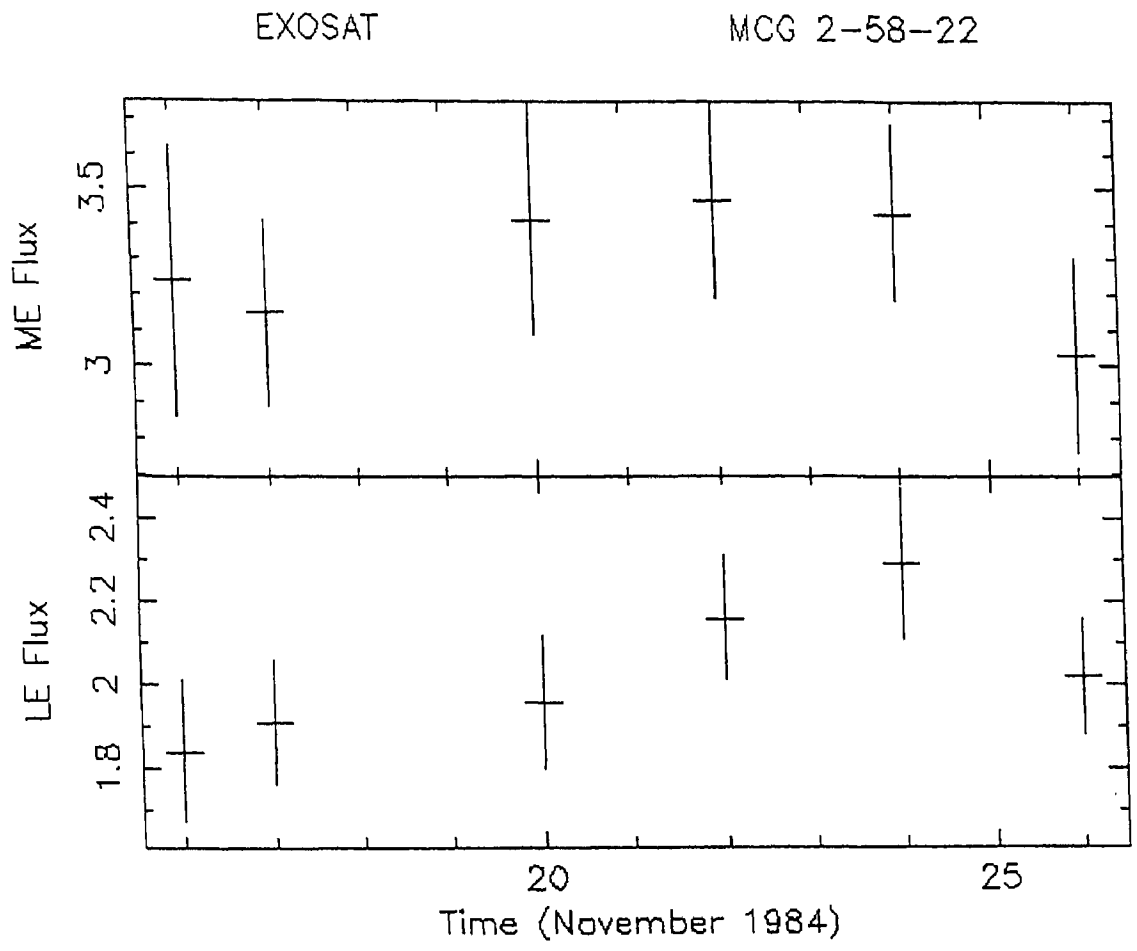


Fig. 3.1.34. Plot of the LE and ME fluxes versus date of observations

EXOSAT

MCG 2-58-22

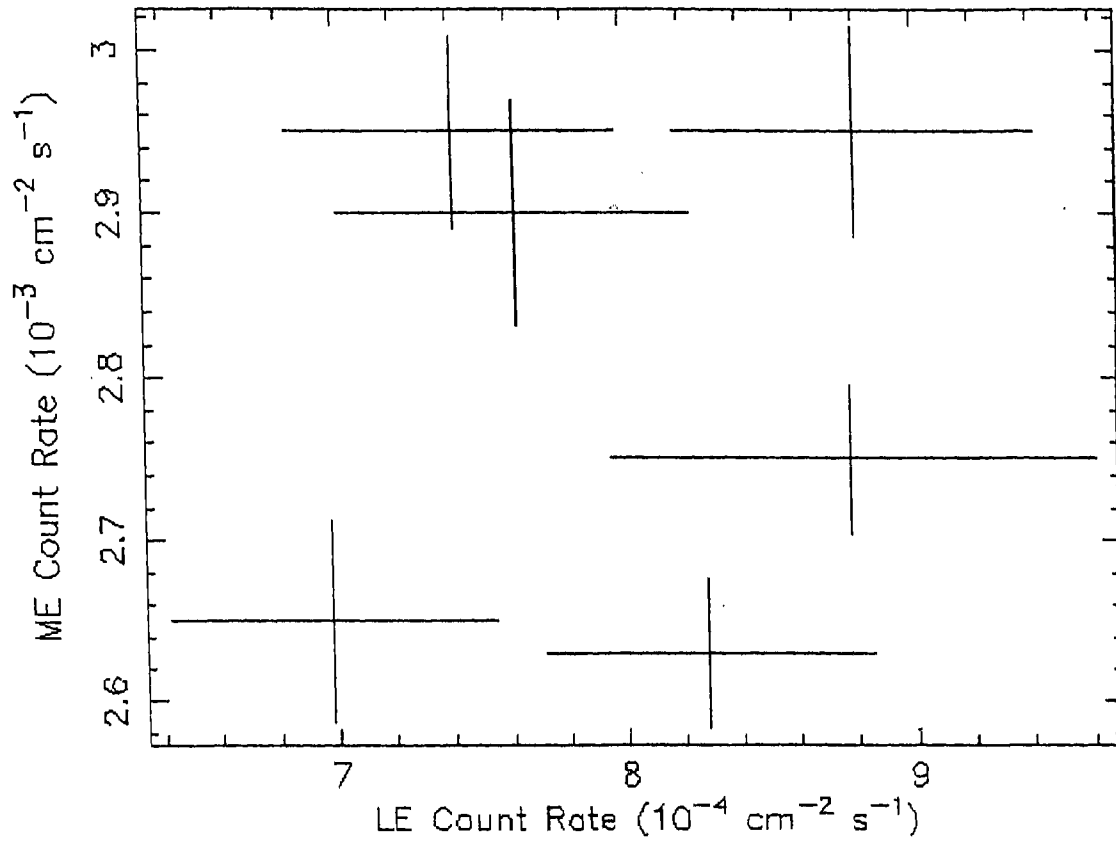


Fig. 3.1.35. Plot of the LE count rate versus and ME count rate





3.1.2I. From the  $\chi^2$  statistics we find that there are definite improvements in the fit with the addition of the Gaussian line around 6.0 keV and the F-statistics show that the inclusion of the Gaussian line is highly significant. The best fit equivalent width of the iron line is around  $160 \pm 110$  eV. This value is consistent with the Ginga value ( $\langle EW \rangle \sim 156 \pm 091$ ; Nandra & Pounds 1994) observed during 1989 and ASCA value ( $EW \sim 150 \pm 075$ ; Nandra et al. 1997) observed on 1993 May 25. The ME spectral slope also remained nearly unchanged during these observations.

### **3.1.3. *International AGN Watch Campaign Results of Fairall -9***

The continuum source and the broad-line region (BLR) in AGNs are far too small to be resolved spatially even with diffraction-limited 10m class telescopes. Consequently, much of what is known about the small-scale (i.e. parsec or less) structure is based on studies of continuum and emission-line variability. Since the late 1980s attempts have been made to make use of continuum emission-line variations to determine the structure and kinematics of BLR (Blandford & McKee). Early spectroscopic monitoring programs on AGNs (Peterson 1988) made it clear that while emission-line and continuum variability afforded a potentially powerful tool to probe the inner structure of AGNs, very massive observational efforts would be required to do this effectively. This led to the formation of large consortia to carry out multiwavelength spectroscopic monitoring programs on AGNs. We describe here the recent work by the largest of these consortia, the International AGN Watch (Alloin et al. 1994), on the high luminosity Seyfert 1 galaxy Fairall 9 ( $-24 < M_V < -23$ ). We participated in this program and monitored this source using the telescopes at VBO with CCDs as detectors (Santos-Lleo et al. 1997). This program was undertaken in support of a concurrent UV monitoring program carried out with the IUE (Rodriguez-Pascual et al. 1997).

Fairall 9 (F9) is a southern hemisphere galaxy, at a redshift  $z = 0.0461$ . It has previously been extensively studied at many wavelengths (Recondo-Gonzalez et al. 1997). It has undergone the most dramatic variations ever observed in nonblazar AGN; between 1978 and 1984, the UV

continuum flux decreased by a factor of 30. Since 1984, it has continued to vary, but with an amplitude more characteristic of mean-luminosity Seyfert 1 galaxies (i.e., over a factor of 2-3).

The specific reasons for carrying out a contemporaneous ground based optical campaign are as follows:

1. To test whether variations on short timescales (days to weeks) are superimposed on the long-term changes already known to occur in F9. This would provide clues about the physical origin of the variations of the continuum.
2. To check whether the UV and optical continua vary simultaneously, as has been found for lower luminosity Seyfert galaxies.
3. To measure time lags between the optical-line and continuum variations, which gives an indication of the size of the line-emitting region.
4. To look for profile variability of the H $\beta$  emission line in order to put constraints on the kinematical models of the BLR.

### **Observations and results**

The CCD imaging observations of F9 were carried out during 1994, November 19 to 1994, December 13 on six nights in the B, V and R photometric passbands, using a GEC P8603 Astromed CCD detector at the prime focus of the 2.34m Vainu Bappu Telescope. A detailed log of observations is given in Table 3.1.3. The data were reduced using the DAOPHOT software package installed on the SUN workstations at the Vainu Bappu Observatory. Details of data processing is described in the Chapter 2. Regular spectroscopic observations of the active nucleus of Fairall 9 were obtained by the various other members of this International AGN Watch program, using the 1.5m telescope of the European Southern Observatory (ESO), the 2.15m telescope of Complejo Astronomico Leoncito (CASLEO) in Argentina, the 1.6m telescope of Observatorio do Pico dos Dias (Brazil) and ESO 3.6m telescope. Details of the various instruments used to obtain the spectroscopic data and the spectroscopic data reduction procedures are described by Santos-Lleo et al. (1997).

**TABLE 3.1.3. LOG OF VISUAL OBSERVATIONS OF FAIRALL-9**

Object	z	Date of observation	Tele-scope (m)	No of obs	UT (start)	Integ. (s)	Filter
Fairall-9	0.046	1994 12 01	2.34	1	14:54	1200	V
		1994 12 02	2.34	1	14:55	1200	V
		1994 12 07	2.34	2	13:49	1200	V
					14:16	1200	V
		1994 12 10	2.34	2	14:57	1200	V
				15:04	1800	V	

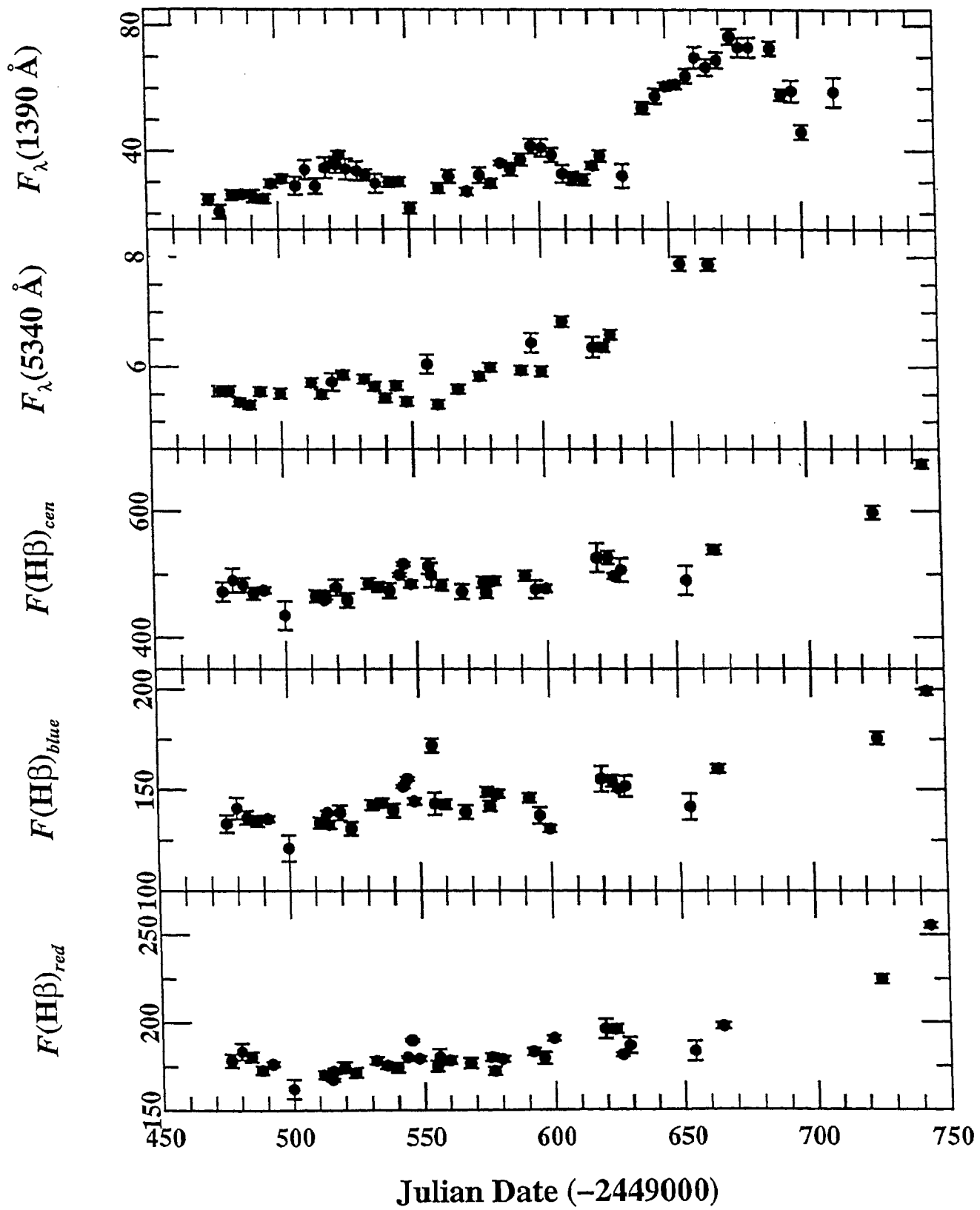


Fig. 3.1.37. From top to bottom we show first the 1390 Å UV continuum light curve next the 5340 Å optical continuum light curve and then Hβ<sub>cen</sub>, Hβ<sub>blue</sub> and Hβ<sub>red</sub> fluxes of Fairall 9

The main results of the campaign on the active nucleus in the Seyfert galaxy Fairall 9 are as follows:

During this monitoring period the optical continuum varied significantly. Continuum variations of amplitude  $\sim 12\%$  are detected on time scales as short as  $\sim 20$  days. Over  $\sim 94$  days, a factor of 2 change in the nuclear continuum was observed. The amplitude of optical continuum variations is about the same as that of the UV continuum. The optical and UV continuum light curves (Fig. 3.1.37) show two events of low-amplitude variations with a duration of  $\sim 70$  days. There is no measurable lag between the UV and optical continuum light curves. The UV data show a third larger amplitude event that occurred after the optical monitoring had terminated.

The H $\beta$  emission-line flux also underwent significant low-amplitude ( $\geq 20\%$ ) variations. It is estimated that (Santos-Lleo et al. 1997) H $\beta$  lags behind the UV continuum by about 23 days, a value much smaller than what was previously suggested by earlier variability studies (Rodríguez-Pascual et al. 1997). However this small lag is consistent with the lags for the UV lines during this campaign in the sense that H $\beta$  lag is nearly 50% larger than that of Ly  $\alpha$  which is similar to the results for lower luminosity AGNs such as NGC 4151, NGC5548 and NGC3783.

#### **3.1.4. Discussion**

In Sections 3.1.2 and 3.1.3, the results of the X-ray spectral analysis of 13 Seyfert galaxies have been presented along with the simultaneous multifrequency observational campaign results of the luminous Seyfert 1 galaxy Fairall 9. In this section the obtained results are summarized, their implications discussed and physical interpretations are derived.

EXOSAT X-ray spectral analysis of the 13 Seyfert galaxies presented in Section 3.1.1 shows that the ME (2-10 keV) spectra can be adequately described by a simple power-law. In the LE region (0.1-2 keV) all the sources in our sample, other than ESO140-G43, show soft excess emissions. No low-energy absorption was found in these soft excess sources, except NGC3516 which displays very weak soft excess. Low energy absorption was detected in ESO140-G43 in which no soft-excess emission was found. Probably ESO140-G43 also has a weak soft excess, which was hidden by its  $N_{\text{H}} \sim 10^{21} \text{ cm}^{-2}$  absorber. Thus we suggest that soft excesses are a

common feature of Seyfert galaxies and the detection of soft excess depends on the low-energy absorption in the line-of-sight to the source. Two power-law, thermal bremsstrahlung and broken power-law models were used to fit the detected soft excesses. Two power-law model provides acceptable fits to the data sets but the model is insensitive to compute the errors. The derived plasma temperatures of the thermal bremsstrahlung model are unacceptably very high in most cases and furthermore, in general, there were no improvements in the  $\chi^2_r$  values of the thermal bremsstrahlung model over the power-law plus fixed absorption model. Broken power-law model provides good fit to the soft excess which indicates that two components (soft and hard) are required to fit the spectrum.

Our results show the presence of variable soft excess in 3C382 which is correlated (Figs 3.1.24a-c, 3.1.25, 3.1.27a-b) with the LE count rate, with the soft spectral slope and with the softness ratio (ratio of LE and ME count rates). Although the variability of LE and ME count rates was correlated (Fig.3.1.29) the ME spectral slope remained roughly constant. There is no relation between the ME count rate and the softness ratio (Fig.3.1.30). The results suggest that soft excess was maximum and soft spectral slope was steepest when this galaxy was in its brightest state.. The hard spectral component was practically unchanged even though there were dramatic variations in the source. The hard spectral index, in the case of MCG 2-58-22 also, remained unchanged during soft excess variations. The above mentioned results indicate that the soft and hard X-rays originate from distinct sources. Most probably, the soft X-rays originate in an optically thin part of an accretion disk and hard X-rays in an optically thick part. Our results do not favour thermal emission from hot plasma (Table 3.1.2E). The successful description of the observed data by the broken power-law model (Table 3.1.2F) indicates non-thermal origin for the soft X-ray emission. Since the signal-to-noise ratio and energy resolution of the EXOSAT detectors are low at the soft X-ray region, it is not possible to draw a definite conclusion about the origin of the soft excess. Recent observations of radio-quiet AGNs with ROSAT PSPC (Fiore et al. 1994) found that the strength of emission line features in the soft X-ray band to be very low. The absence of strong line features argue against emission from an ionized plasma as the main contributor to the soft X-ray component. Also ROSAT PSPC results could not rule out the possibility of non-thermal origin for the soft X-ray emission. To

understand more about the details of soft X-ray emission instruments with better energy resolution than ROSAT PSPC are needed.

Majority (nine out of thirteen) of the sources in our sample show a statistically significant improvement in the goodness of the fit upon the addition of a Gaussian emission line at energies (around 6.0 keV) characteristic of iron  $K_{\alpha}$  line emission. The line is either due to the redshifted 6.4 keV fluorescent iron line from cold material or due to the helium-like 6.7 keV iron line from highly ionized hot plasma (House 1968). But from the spectral analysis, we find that thermal bremsstrahlung model did not provide good fit to the X-ray spectra. Also from the distribution of redshifted Fe line energies of our analysis, plotted in Fig.3.1.38, it can be noted that the data are consistent with 6.4 keV. Moreover, from the studies of a large sample of Seyfert galaxies by others based on Ginga data (Nandra & Pounds 1994; Awaki 1991) it was found that the mean line energy to be  $\sim 6.4$  keV which is consistent with fluorescence from cold material (House 1968). If the line arises from fluorescence from cold material, then its strength indicates that a significant fraction of the solid angle visible to the continuum source must be filled with material of column density  $> 10^{22.5}$  atoms  $\text{cm}^{-2}$  (Makishima 1986; Matt et al. 1991; George & Fabian 1991). However, all the sources in our sample displaying iron  $K_{\alpha}$  line emission have no significant absorbing column densities above the critical value mentioned above. Consequently the line can not arise in material uniformly covering the source. The measured average equivalent widths, of the order of few hundreds of eV, are sufficiently high to indicate that the material may be optically thick to Compton scattering. Given the above arguments it can be stated that the observed iron  $K_{\alpha}$  line emission is consistent with the theoretical concept that the primary X-rays are reprocessed in optically thick material in a putative accretion disk subtending a substantial solid angle to the X-ray source (Lightman & White 1988; George & Fabian 1991; Matt et al. 1991). In such cases Doppler and gravitational broadening will combine to produce a characteristic broad, skewed line profile (Fabian et al. 1989; Laor 1991; Matt et al. 1991), with a Gaussian width of hundreds of eV as has been seen in our results of NGC3516. However, the detailed shape of the line feature could not be obtained with EXOSAT because of the energy resolution limitations. Whereas recent high resolution X-ray observations of AGNs with ASCA have found the iron  $K_{\alpha}$  line at 6.4 keV to be broadened and skewed towards low energies

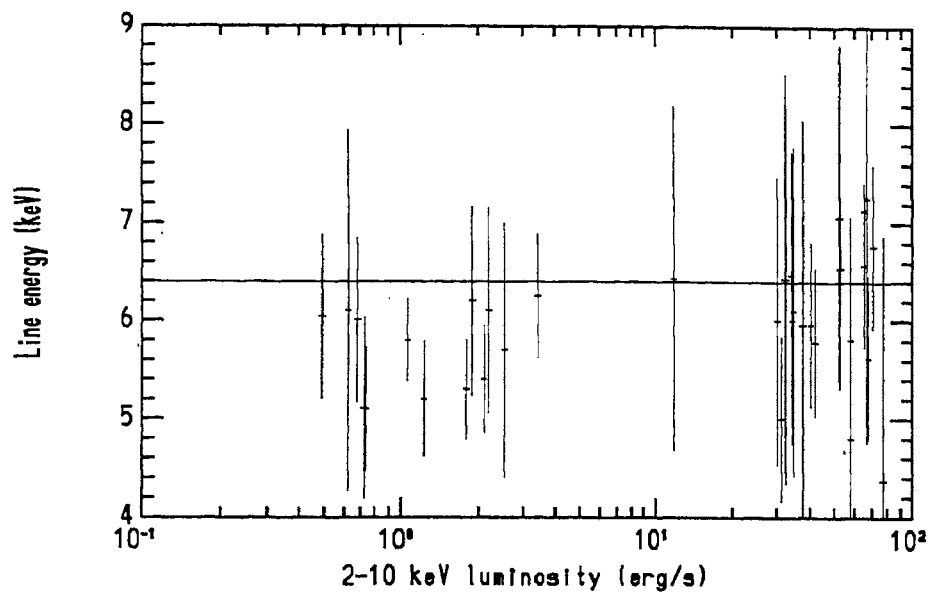


Fig. 3.1.38. Fe K line energy versus X-ray luminosity. The solid line is drawn at 6.4 keV.



(Tanaka et al. 1995; Fabian et al. 1995; Nandra 1997; Reynolds & Fabian 1997). The line profile is found to be in good agreement with that expected if it were to originate from the inner regions of an accretion disk around a black hole. It is believed that the extremely high density of the fluorescing material (Matt et al. 1993) keeps the disk to remain relatively neutral even when exposed to the intense radiation very close to the nuclear region.

The results derived from the multifrequency monitoring campaign of the high-luminosity Seyfert 1 galaxy Fairall 9 show that the source display variability on similar time scales and with comparable amplitudes as other radio-quiet AGNs of 1-2 orders of magnitude lower intrinsic luminosity, such as, NGC5548, NGC3783 and NGC4151.

The absence of detectable lag between the UV and optical continuum variations places severe constraints on current models to explain the origin of the UV-optical continuum emission. In particular, for accretion disk models, where the radiation at any wavelength arises predominantly from a specific distance to the black hole, the lack of detectable UV/optical continuum lag requires the signal connecting the different parts emitting at different wavelengths propagates at speeds close to a significant fraction of the speed of light (e.g., Courvoisier & Clavel 1991).

This campaign also shown that variations of at least a factor of 2 on time scales of 70-90 days are superimposed on the long-term changes already known to occur in F9 (e.g., Clavel, Wamsteker & Glass 1989). Therefore, the emitting region must be smaller than a few light months across.

The delay in H $\beta$  response to continuum fluctuations gives an indication of the length scale of the inner H $\beta$  emitting regions in the BLR of F9. Based on the estimated luminosity and H $\beta$  time delay in the lower luminosity Seyfert NGC5548 (Peterson et al. 1994) the expected H $\beta$  time delay in F9, assuming the  $r \propto L^{1/2}$  dependence, (~50 days) is larger than the value measured during this campaign ( $23 \pm 3$  days), but it is of the same order of magnitude. Also the observed result that the H $\beta$  lag is nearly 50% larger than that of Ly  $\alpha$ , suggests that the physical

properties of photoionised BLR range with the distance to the central source, i.e., the highest ionization lines arising in the regions which are closest to the central source.

### **3.1.5. Conclusions**

We carried out the X-ray spectral analysis of 13 Seyfert galaxies and participated in the International AGN Watch Campaign to obtain multifrequency data on the luminous Seyfert 1 galaxy Fairall-9. The major results obtained are presented here.

The ME (2-10 keV) X-ray spectra of Seyferts can be adequately described by a simple power-law.

In the LE region (0.1-2 keV) all the sources in our sample, other than ESO140-G43, show soft excess emissions. No low-energy absorption was found in these soft excess sources, except NGC3516 which displays very weak soft excess. Low energy absorption was detected in ESO140-G43 in which no soft-excess emission was found. Probably ESO140-G43 also has a weak soft excess, which was hidden by its  $N_{\text{H}} \sim 10^{21} \text{ cm}^{-2}$  absorber. Thus we suggest that soft excesses are a common feature of Seyfert galaxies and the detection of soft excess depends on the low-energy absorption in the line-of-sight to the source.

Two power-law, thermal bremsstrahlung and broken power-law models were used to fit the detected soft excesses. Only broken power-law model provides good fit to the soft excess which indicates that two components (soft and hard) are required to fit the spectrum.

Our results show the presence of variable soft excess in 3C382 which is correlated with the LE count rate, with the soft spectral slope and with the softness ratio. Although the variability of LE and ME count rates was correlated the ME spectral slope remained roughly constant. There is no relation between the ME count rate and the softness ratio. The results suggest that soft excess was maximum and soft spectral slope was steepest when this galaxy was in its brightest state. The hard spectral component was practically unchanged even though there were dramatic variations in the source. The hard spectral index, in the case of MCG 2-58-22 also, remained

unchanged during soft excess variations. The above mentioned results indicate that the soft and hard X-rays originate from distinct sources.

Majority (nine out of thirteen) of the sources in our sample show a statistically significant improvement in the goodness of the fit upon the addition of a Gaussian emission line at energies (around 6.0 keV) characteristic of iron  $K_{\alpha}$  line emission. From the distribution of redshifted Fe line energies of our analysis, it is noted that the data are consistent with 6.4 keV.

The main results of the campaign on the active nucleus in the Seyfert galaxy Fairall 9 are as follows:

During this monitoring period the optical continuum varied significantly. Continuum variations of amplitude  $\sim 12\%$  are detected on time scales as short as  $\sim 20$  days. Over  $\sim 94$  days, a factor of 2 change in the nuclear continuum was observed. The amplitude of optical continuum variations is about the same as that of the UV continuum. The optical and UV continuum light curves show two events of low-amplitude variations with a duration of  $\sim 70$  days. There is no measurable lag between the UV and optical continuum light curves. The UV data show a third larger amplitude event that occurred after the optical monitoring had terminated.

The  $H\beta$  emission-line flux also underwent significant low-amplitude ( $\geq 20\%$ ) variations. It is estimated that  $H\beta$  lags behind the UV continuum by about 23 days, a value much smaller than what was previously suggested by earlier variability studies. However this small lag is consistent with the lags for the UV lines during this campaign in the sense that  $H\beta$  lag is nearly 50% larger than that of  $Ly\ \alpha$  which is similar to the results for lower luminosity AGNs such as NGC 4151, NGC5548 and NGC3783.

## 3.2. Blazars

### 3.2.1. Introduction

The term 'blazar' was coined by E. Speigel in a banquet speech at the Pittsburgh meeting on BL Lacertae objects (Wolfe 1978), which was the topic of the first conference after the discovery of the first example (Schmidt 1968). Around that time the characteristics of BL Lac objects were reviewed by Kinman (1975), Stein, O'Dell & Strittmatter (1976), and Stein (1978), and more than 50 objects were classified as BL Lac objects based on the following characteristics : (1) strong variability at radio, optical, infrared and X-ray frequencies; (2) strong and variable linear polarization in the radio, infrared, and optical bands; and (3) featureless (or weak emission and/or absorption) optical spectrum. The featureless optical continuum may be due to the absence of gas around the BL Lac objects, which was suggested based on the radio (Jones & O'Dell 1977), optical (Strittmatter et al. 1974; Wills & Wills 1976; Miller, French & Hawley 1978), ultraviolet (Boksenberg et al. 1978), and X-ray (Mushotzky et al. 1978) observations. However, several BL Lac objects which are embedded in the nuclei of galaxies were also detected (Ulrich et al. 1975). The above listed characteristics of blazars suggest that the overall electromagnetic spectra are dominated by Doppler-boosted (details of Doppler-boosting can be seen in Chapter 1.4.6) radiation from relativistic jet pointing closely to our line-of-sight.

In 1980 Angel & Stockman (1980) made a list of blazars which were usually variable and highly polarized objects. Later Moore & Stockman (1981, 1984) produced a list of highly polarized quasars (HPQs) and around that time the term 'optically violent variable' (OVV) was also introduced (Angel & Stockman 1980); Ledden & O'Dell 1985). Presently, BL Lac objects, HPQs and OVVs are classed as blazars. They are core dominated sources, displaying rapid variability, and relatively high optical polarization (Stickel et al. 1991; Padovani & Urry 1992; and references therein). Also these objects have displayed variable optical polarization, which often shows various types of frequency dependence on the polarization (Smith et al. 1987; Mead et al. 1990; Valtaoja et al. 1991). Impey (1992) studied a sample of 65 blazars using the VLBI and optical spectroscopic and polarimetric data. He has suggested that BL Lac objects with measured VLBI kinematics have slower apparent superluminal motion ( $v/c < 4$ ) than HPQs/OVVs ( $v/c > 8$ ). Also, it has been suggested by him that BL Lac objects differ

significantly from HPQs/OVVs in terms of luminosity, continuum shape, and apparent superluminal motions.

It can be seen from the literature that the strength of the emission lines ( $5 \text{ \AA}$  equivalent width) was used to classify a sample of flat-spectrum radio sources from the Parkes catalog (Wilkes 1986) and a sample of X-ray-selected BL Lac objects (XBLs) from the *Einstein* Extended Medium Sensitivity Survey (EMSS) (Stocke et al. 1990). It is also evident from the literature that the same object displayed weak and strong emission lines during its brighter and fainter states, respectively (Stein et al 1976; Moore & Stockman 1981, 1984). Thus the classification of blazars based on the line emission strength criteria may be arbitrary. However, they may be classified based on their detection technique, because most of the blazars have been discovered either at radio or at X-ray frequencies, which has led to a subdivision of the blazars into radio-selected blazars (RBLs) and X-ray-selected blazars (XBLs). RBLs and XBLs have common characteristics, but important differences have also been detected in their core dominance, optical polarization, radio-luminosity, and variability properties (Perlman & Stocke 1993; Jannuzi, Smith & Elston 1994). Also, the number counts and cosmological evolution of RBLs appear to be different from those of XBLs (Morris et al. 1991; Wolter et al. 1994).

### **3.2.2. X-ray Properties and Multifrequency Continua of a Sample of Blazars**

In this section we present the results of the X-ray spectral analysis (0.1-10 keV) of 28 blazars (Table 3.2.1) which were observed with EXOSAT. Also, the multifrequency spectra and the luminosities at different frequencies of 28 blazars have been used for the analysis (Ghosh & Soundararajaperumal 1995).

#### **The EXOSAT blazar sample**

We have selected all the BL Lac objects, HPQs, and OVVs from the EXOSAT database system (ESA TM-13[1991]). Our selection led to a total of 49 blazars observed by EXOSAT. All the objects in our sample contained in the list of Burbidge & Hewitt (1992) and in the catalog of Veron-Cetty & Veron (1993). A number of criteria were then imposed on this sample to make sure that the spectra analyzed were good and were uncontaminated. The criteria followed to reject the spectra are as follows: (1) a flux less than 4 times its error and (2) quality factor less than 3 (the data-quality flag takes account of solar contamination, high background, and other

TABLE  
INFORMATION ABOUT THE BLAZARS

Object Name	R.A. (1950)	Decl. (1950)	z	$F_{5\text{GHz}}$ (Jy)	5 GHz Reference	$M_{\text{abs}}$	Selection*
3C 66A .....	02 <sup>h</sup> 19 <sup>m</sup> 30 <sup>s</sup>	42°48'30"	0.444	1.04	1	-27.2	R
AO 0235+164 .....	02 35 53	16 24 05	0.940	2.79	2	-28.7	R
1E 0317+18 .....	03 17 21	18 31 45	0.190	0.01	3	-22.1	X
H0323+022 .....	03 23 38	02 14 47	0.147	0.04	4	-23.1	X
NRAO 140 .....	03 33 22	32 08 36	1.263	2.50	5	-27.6	R
1H 0414+009 .....	04 14 18	00 58 03	0.287	0.08	6	-24.9	X
3C 120 .....	04 30 32	05 14 59	0.033	5.09	5	-21.4	R
PKS 0521-36 .....	05 21 13	-36 30 16	0.061	8.89	7	-23.2	R
PKS 0548-32 .....	05 48 50	-32 16 36	0.069	0.08	3	-22.6	X
PKS 0754+10 .....	07 54 23	10 04 40	...	1.48	1	...	R
OJ 287 .....	08 51 57	20 17 58	0.306	3.60	8	-26.0	R
Mrk 421 .....	11 01 41	38 28 43	0.031	0.53	9	-22.8	X
Mrk 180 .....	11 33 30	70 25 00	0.046	0.25	10	-22.7	X
B2 1147+245 .....	11 47 44	24 34 35	...	1.00	11	...	R
3C 273 .....	12 26 33	02 19 43	0.158	43.41	5	-27.0	R
1E 1402+04 .....	14 02 20	04 16 21	...	0.018	12	...	X
1E 1415+259 .....	14 15 41	25 57 15	0.237	0.05	13	-24.8	X
1H 1427+42 .....	14 26 36	42 53 46	0.129	0.03	14	-22.9	X
PKS 1510-089 .....	15 10 09	-08 54 48	0.361	4.36	5	-25.3	R
Mrk 501 .....	16 52 12	39 50 26	0.034	1.20	15	-22.6	X
4U 1722+119 .....	17 22 44	11 54 52	...	0.08	16	...	X
1 Zw 186 .....	17 27 04	50 15 31	0.055	0.15	1	-21.6	X
3C 371 .....	18 07 18	69 48 58	0.051	1.45	17	-23.2	R
3C 390.3 .....	18 45 37	79 43 06	0.057	4.48	5	-22.3	R
OV 236 .....	19 21 42	-29 20 27	0.352	8.00	18	-24.3	R
1928+73 (4C 73.18) .....	19 28 49	73 51 45	0.302	3.34	10	-25.9	R
PKS 2005-489 .....	20 05 47	-48 58 43	0.071	1.19	19	-24.8	X
PKS 2155-304 .....	21 55 58	-30 27 52	0.341	0.31	20	-26.1	X

\* R = radio-selected BL Lac objects and X = X-ray-selected BL Lac objects.

REFERENCES.—(1) Weiler & Johnston 1980; (2) Pauliny-Toth et al. 1972; (3) Stocke et al. 1985; (4) Feigelson et al. 1986; (5) Pauliny-Toth & Kellermann 1968; (6) Ulmer et al. 1983; (7) Shimmins & Bolton 1972; (8) Laundau et al. 1983; (9) Ulvestad, Johnston, & Weiler 1983; (10) Kuhr et al. 1981b; (11) Pauliny-Toth & Kellermann 1972; (12) Feigelson, Maccacaro, & Zamorani 1982; (13) Halpern et al. 1986; (14) Remillard et al. 1989; (15) Mufson et al. 1984; (16) Griffiths et al. 1989; (17) Perley 1982; (18) Giacani & Colomb 1988; (19) Wall et al. 1975; (20) Shimmins & Bolton 1974.

factors that would affect the quality of the detection [for details see ESA TM-12 (1991)]. Based on the above criteria, we have rejected the spectra (2-10 keV) of 16 blazars (GC 0109+224, 0300+470 [4C47.08], PKS 0537-44, 0855+143 [3C212], 0923+39, MC 1057+100, 1150+812 [S5 1150+812], B2 1156+295, 1E1235+63, 3C279, B2 1308+326, OQ530, AP Lib, 4C14.60, BL Lac, and PHL5200) whose signal-to-noise ratios were too poor to derive any spectral parameters. Also, the spectra of five blazars (PKS 0735+17, 1E1207.9+3945, ON 325, 2A1218+304, and 3C446) were rejected because they were contaminated by other bright sources in the field. Finally, we are left with 28 blazars, and they are listed in Table 3.2.1. These 28 blazars form the complete sample of EXOSAT blazars (for spectroscopic studies), because we have not excluded any object for which good spectrum (at least at the level of  $4\sigma$  signal significance) is available from EXOSAT observations. Most of the objects of this sample (except NRAO140, 3C120, 3C273, PKS 1510-089, OV 236, 3C390.3, and 1928+73) have already been classified into RBLs and XBLs by Giommi et al (1990), and we have followed the same classification. NRAO 140, 3C 273, PKS 1510-089, OV 236, and 1928+73 have been classified as RBLs following the classification of the Revised and Updated Catalog of Quasi-stellar Objects of Hewitt & Burbidge (1993). 3C 120 and 3C390.3 are radio galaxies with superluminal motions (Zensus 1989; Porcas 1987) and also known as blazars (Angel & Stockman 1980; Ledden & O'Dell 1985; Webb et al. 1988). We have classified these two radio-loud blazars as RBLs. It can be seen from Table 3.2.1 that there are 14 XBLs and 14 RBLs in the present sample. Two-point spectral indices between the radio and optical bands ( $\alpha_{RO}$ ) and between the optical and X-ray bands ( $\alpha_{OX}$ ) are plotted in Fig. 3.2.1. The indices  $\alpha_{RO}$  and  $\alpha_{OX}$  are defined as  $\alpha_{RO} = -\log(F_R / F_O) / \log(\nu_R / \nu_O)$  and  $\alpha_{OX} = -\log(F_O / F_X) / \log(\nu_O / \nu_X)$ , where  $F_R$ ,  $F_O$ , and  $F_X$  are the fluxes at 5 GHz ( $\nu_R$ ), 5560 Å ( $\nu_O$ ), and 1 keV ( $\nu_X$ ), respectively. Circles with crosses correspond to RBLs, and circles with dots to XBLs. The solid line shows the correlation between  $\alpha_{RO}$  and  $\alpha_{OX}$ , which is similar to that found by Ledden & O'Dell (1985) in a sample of blazars observed with *Einstein Observatory*. From this figure it can also be seen that the XBLs are located to a region of the plane defined by  $0.2 < \alpha_{RO} < 0.6$  and  $0.7 < \alpha_{OX} < 1.2$ . This clearly shows the bimodal nature of the distribution of blazars in the present sample, which was also noted in other samples observed with *Einstein* (Ledden & O'Dell 1985; Stocke et al. 1985; 1988; Worrall et al. 1987). Note that the same distribution, as found with EXOSAT blazars, is

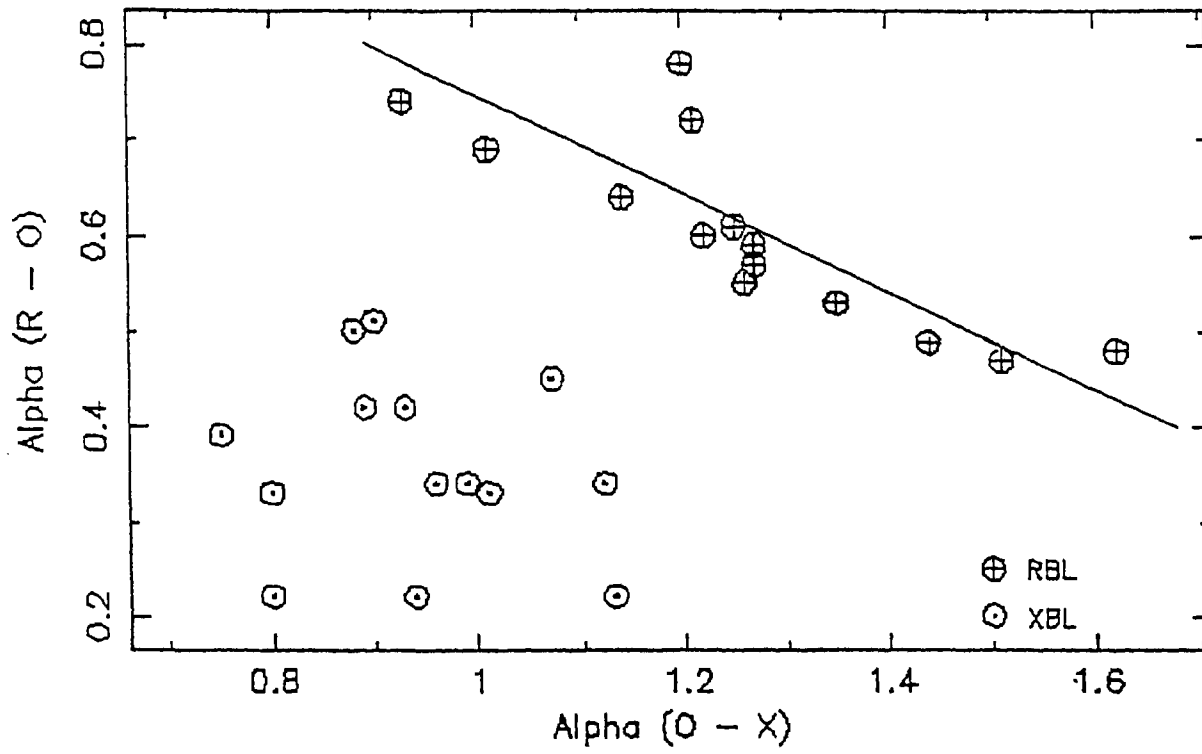


Fig. 3.2.1. Plot of two-point spectral indices of 28 blazars between radio and optical bands ( $\alpha_{RO}$ ) and between the optical and X-ray bands ( $\alpha_{OX}$ )



also present in the two complete samples of radio- and X-ray selected blazars (Stickel et al. 1991; Morris et al. 1991).

### **Observations and Analysis**

EXOSAT observations of these sources were carried out with EXOSAT using low- and medium-energy (LE and ME) detectors. Details of the detectors and data reduction methods are described in Chapter 2.1. The observations flagged 3 or above with flux  $\geq 4 \sigma$  were retrieved from the EXOSAT database. A log of the LE and ME observations and the corresponding count rates are given in Table 3.2.2. The last two columns of this table show the channel range and the signal significance of the blazars. In this table we have included only those observations of EXOSAT which have signal significance above  $4 \sigma$ .

The LE and ME spectra of 28 blazars were analyzed with the X-ray Spectral Fitting (XSPEC) program. A number of trial models, folded with the instrumental response, were used to fit the data, and the best fitting parameters were obtained by minimizing  $\chi^2_r$ . A simple power-law plus uniform absorption model with the effective photoelectric cross sections given by Morrison & McCammon (1983) and with the absorption column density  $N_H$  was used to fit the spectra. This model fits well with the spectra of most of the sources. However, the best-fit parameters of this model for two sources (3C273, PKS2155-304) show that the derived values of  $N_H$  are smaller than the corresponding Galactic  $N_H$  values. In the next model we have fitted the spectra of these two sources by freezing the values of  $N_H$  with the corresponding Galactic  $N_H$  values. The best fitting parameters of the above models are listed in Table 3.2.3 along with the computed fluxes for the 0.1-2 and 2-10 keV ranges. These fluxes were obtained from the spectral fitting using the power-law plus absorption model. The 90% confidence error bars, which were computed for each parameter keeping the rest of the parameters free following the procedure detailed by Lampton, Margon & Bowyer (1976), of the fit parameters are also listed in Table 3.2.3 along with the  $\chi^2_r$  values. It may be noted from Table 3.2.3 that the X-ray spectra of few sources (Mkn 421, 3C273 and PKS 2155-304) can not be well represented by the power-law plus absorption model ( $\chi^2_r > 2$ ). To fit the spectra of these sources, we have added other spectral components, such as blackbody, thermal bremsstrahlung, high-energy cutoff and absorption edge, with the power-law plus fixed absorption model. Also we have used the broken power-law and double

TABLE  
LOG OF OBSERVATIONS OF THE LE AND ME SPECTRA AND COUNT RATES OF BLAZARS

SOURCE	START TIME <sup>a</sup>	END TIME <sup>b</sup>	LE COUNT RATE (10 <sup>-4</sup> cm <sup>-2</sup> s <sup>-1</sup> )		ME <sup>c</sup> COUNT RATE (10 <sup>-3</sup> cm <sup>-2</sup> s <sup>-1</sup> )	ME SIGNAL SIGNIFICANCE	
			LAS	AI/P		Channel Range	Signal
3C 66A	1986, 006, 10:24	006, 15:29	0.51 ± 0.09	...	0.43 ± 0.04	5-13	~4 σ
	1986, 032, 08:12	032, 19:25	0.33 ± 0.06	...	0.47 ± 0.02	5-20	≥4 σ
AO 0235+164	1984, 214, 03:22	214, 07:49	0.08 ± 0.02	...	0.25 ± 0.04	6-30	≥4 σ
1E 0317+18	1985, 013, 18:55	013, 23:14	0.95 ± 0.21	...	1.04 ± 0.09	5-14	≥4 σ
	1985, 039, 22:08	040, 03:05	0.89 ± 0.14	0.97 ± 0.16	0.70 ± 0.04	5-18	≥4 σ
H0323+022	1984, 265, 06:47	265, 12:16	3.58 ± 0.42	...	1.33 ± 0.12	5-15	≥4 σ
	1984, 267, 06:26	267, 12:16	3.07 ± 0.22	...	0.89 ± 0.04	4-16	≥4 σ
NRAO 140	1985, 025, 14:43	025, 22:43	0.31 ± 0.04	...	0.77 ± 0.03	4-23	≥4 σ
	1985, 025, 23:56	026, 08:56	0.31 ± 0.04	...	0.80 ± 0.03	5-25	≥4 σ
1H 0414+009	1984, 253, 09:16	253, 02:45	3.99 ± 0.50	2.68 ± 0.36	2.16 ± 0.05	4-24	≥4 σ
	1984, 258, 07:48	258, 11:20	4.25 ± 0.40	3.00 ± 0.28	2.57 ± 0.05	3-25	≥4 σ
	1984, 266, 10:16	266, 13:16	4.31 ± 0.50	2.45 ± 0.25	1.70 ± 0.05	4-19	≥4 σ
	1984, 274, 09:01	274, 11:49	4.37 ± 0.46	2.81 ± 0.34	1.29 ± 0.05	5-16	≥4 σ
3C 120	1983, 228, 08:47	229, 07:35	4.37 ± 0.23	3.22 ± 0.23	3.34 ± 0.04	3-33	≥4 σ
	1983, 305, 08:20	305, 13:50	4.83 ± 0.34	3.57 ± 0.34	3.16 ± 0.04	3-24	≥4 σ
	1984, 249, 11:53	249, 19:41	4.48 ± 0.48	3.95 ± 0.45	4.25 ± 0.04	3-33	≥4 σ
	1984, 276, 06:36	276, 18:28	3.92 ± 0.23	3.25 ± 0.33	4.44 ± 0.03	3-32	≥4 σ
	1984, 277, 10:24	277, 15:48	3.18 ± 0.19	2.79 ± 0.28	3.83 ± 0.08	4-31	≥4 σ
	1984, 278, 13:02	278, 18:34	3.21 ± 0.39	3.13 ± 0.31	3.40 ± 0.04	4-29	≥4 σ
	1984, 280, 13:48	280, 20:35	3.12 ± 0.17	2.44 ± 0.27	2.87 ± 0.04	4-31	≥4 σ
	1984, 284, 03:27	284, 08:46	3.29 ± 0.23	2.29 ± 0.26	3.27 ± 0.04	3-27	≥4 σ
	1984, 286, 01:26	286, 06:33	3.88 ± 0.30	2.33 ± 0.33	3.61 ± 0.04	3-29	≥4 σ
	1985, 044, 23:35	045, 05:46	3.29 ± 0.22	...	3.07 ± 0.05	4-26	≥4 σ
	1985, 283, 19:59	284, 10:00	4.05 ± 0.27	2.44 ± 0.39	3.87 ± 0.04	3-30	≥4 σ
	1986, 044, 15:02	044, 21:00	2.83 ± 0.44	2.10 ± 0.36	2.43 ± 0.04	4-26	≥4 σ
PKS 0521-36	1983, 306, 10:30	306, 15:00	1.29 ± 0.20	1.27 ± 0.20	0.97 ± 0.04	6-20	≥4 σ
	1983, 334, 10:06	334, 14:59	1.36 ± 0.30	1.08 ± 0.25	0.99 ± 0.07	6-16	≥4 σ
PKS 0548-32	1983, 306, 16:51	306, 19:59	12.30 ± 1.00	6.47 ± 0.70	3.04 ± 0.05	3-22	≥4 σ
	1983, 334, 16:56	334, 19:40	12.30 ± 1.50	6.31 ± 0.77	2.76 ± 0.06	4-20	≥4 σ
	1986, 066, 04:39	066, 11:40	10.40 ± 0.40	...	2.01 ± 0.04	4-23	≥4 σ
	1986, 066, 11:45	066, 18:05	10.40 ± 0.40	...	2.08 ± 0.04	4-21	≥4 σ
	1986, 066, 23:55	067, 04:00	10.40 ± 0.40	...	2.12 ± 0.05	4-21	≥4 σ
PKS 0754+10	1984, 043, 06:07	043, 13:36	0.70 ± 0.10	0.29 ± 0.08	0.51 ± 0.04	5-23	≥4 σ
OJ 287	1983, 281, 14:39	281, 21:05	4.00 ± 0.38	...	0.83 ± 0.07	4-11	≥4 σ
	1984, 040, 07:49	040, 11:00	4.75 ± 0.65	...	0.49 ± 0.05	5-14	≥4 σ
Mrk 421	1984, 035, 12:32	035, 15:36	48.70 ± 2.50	18.10 ± 1.00	1.25 ± 0.10	6-16	≥4 σ
	1984, 337, 17:04	337, 20:18	100.00 ± 4.0	42.20 ± 1.70	11.08 ± 0.06	2-32	≥4 σ
	1984, 338, 19:12	339, 02:08	126.60 ± 2.40	54.70 ± 2.00	13.95 ± 0.06	2-33	≥4 σ
	1984, 340, 19:12	340, 22:30	128.60 ± 5.00	57.50 ± 2.00	14.10 ± 0.10	3-27	≥4 σ
	1985, 004, 14:26	004, 18:03	56.30 ± 3.00	20.50 ± 4.00	1.76 ± 0.06	4-18	≥4 σ
	1985, 112, 05:19	112, 10:35	63.60 ± 2.20	26.90 ± 1.20	3.05 ± 0.04	3-24	≥4 σ
	1985, 118, 19:18	119, 01:04	49.00 ± 1.70	20.10 ± 0.90	2.99 ± 0.04	3-26	≥4 σ
	1985, 126, 22:24	127, 04:56	48.60 ± 1.70	19.90 ± 0.80	1.84 ± 0.04	4-23	≥4 σ
	1985, 131, 20:51	132, 03:16	56.50 ± 2.00	21.60 ± 1.00	2.66 ± 0.04	3-24	≥4 σ
	1985, 132, 15:34	132, 16:59	54.10 ± 2.00	...	1.92 ± 0.08	4-18	≥4 σ
	1985, 141, 13:00	141, 19:00	44.40 ± 1.60	17.70 ± 0.90	2.09 ± 0.05	4-21	≥4 σ
Mrk 180	1984, 333, 04:43	333, 09:20	11.30 ± 0.80	5.04 ± 0.52	0.44 ± 0.04	5-10	≥4 σ
	1985, 093, 16:35	093, 19:30	21.30 ± 1.60	...	1.01 ± 0.07	5-16	≥4 σ
B2 1147+245	1984, 016, 06:44	016, 15:35	0.41 ± 0.06	...	0.30 ± 0.04	6-11	≥4 σ
3C 273	1984, 005, 23:00	006, 13:17	21.80 ± 0.10	...	7.49 ± 0.07	4-30	≥4 σ
	1985, 032, 13:34	032, 19:00	21.17 ± 0.12	...	6.46 ± 0.06	2-34	≥4 σ
	1985, 138, 11:49	138, 17:37	29.90 ± 0.10	...	6.79 ± 0.04	3-35	≥4 σ
	1986, 017, 18:19	017, 05:51	35.40 ± 0.11	...	9.36 ± 0.03	2-41	≥4 σ
	1986, 018, 06:07	019, 06:08	36.10 ± 0.10	...	9.06 ± 0.03	2-41	≥4 σ
1E 1402+04	1985, 031, 16:05	032, 10:19	1.26 ± 0.11	...	0.21 ± 0.02	7-11	≥4 σ
1E 1415+259	1986, 063, 19:24	064, 06:02	6.94 ± 0.20	...	0.49 ± 0.03	4-16	≥4 σ
1H 1427+42	1985, 012, 21:14	012, 23:25	37.60 ± 0.90	...	4.78 ± 0.07	3-26	≥4 σ
PKS 1510-089	1984, 216, 12:56	218, 00:20	0.47 ± 0.07	0.41 ± 0.06	0.59 ± 0.03	6-19	≥4 σ
	1985, 212, 23:59	213, 11:11	0.52 ± 0.08	...	0.46 ± 0.03	6-19	≥4 σ
Mrk 501	1984, 034, 12:02	034, 14:26	48.30 ± 2.00	22.90 ± 2.00	4.62 ± 0.05	3-24	≥4 σ
	1984, 086, 12:00	086, 14:30	42.50 ± 2.00	18.50 ± 2.00	4.14 ± 0.07	4-24	≥4 σ
	1984, 183, 20:25	183, 23:47	46.50 ± 2.00	19.00 ± 1.00	2.47 ± 0.05	3-20	≥4 σ
	1984, 191, 06:09	191, 08:44	42.00 ± 2.00	18.20 ± 1.00	2.69 ± 0.07	3-19	≥4 σ
	1984, 201, 06:44	201, 09:45	41.00 ± 2.00	16.80 ± 1.00	2.78 ± 0.05	3-24	≥4 σ
	1984, 207, 00:24	207, 03:37	44.50 ± 2.00	21.50 ± 1.00	3.05 ± 0.06	3-22	≥4 σ

TABLE

SOURCE	START TIME <sup>a</sup>	END TIME <sup>b</sup>	LE COUNT RATE ( $10^{-4} \text{ cm}^{-2} \text{ s}^{-1}$ )		ME <sup>c</sup> COUNT RATE ( $10^{-3} \text{ cm}^{-2} \text{ s}^{-1}$ )	ME SIGNAL SIGNIFICANCE	
			LX3	Al/P		Channel Range	Signal
	1984, 209, 20:14	209, 23:50	41.70 ± 2.00	19.20 ± 1.00	3.36 ± 0.05	3-25	≥4 σ
	1985, 099, 09:43	099, 14:26	41.20 ± 2.00	18.90 ± 0.90	2.54 ± 0.06	4-21	≥4 σ
	1986, 074, 13:44	075, 14:28	44.50 ± 1.00	...	4.29 ± 0.03	4-21	≥4 σ
4U 1722+119 .....	1985, 246, 11:45	246, 16:59	2.89 ± 0.30	2.00 ± 0.30	0.84 ± 0.04	5-16	≥4 σ
1 Zw 186 .....	1984, 181, 15:20	181, 23:09	9.16 ± 0.60	4.71 ± 0.50	0.85 ± 0.04	5-17	≥4 σ
3C 371 .....	1984, 255, 20:14	256, 08:25	5.18 ± 0.23	...	0.42 ± 0.04	7-17	≥4 σ
3C 390.3 .....	1985, 033, 06:39	033, 09:14	...	1.51 ± 0.17	2.48 ± 0.07	4-24	≥4 σ
	1985, 033, 09:31	033, 22:09	1.84 ± 0.34	1.51 ± 0.17	2.60 ± 0.06	4-26	≥4 σ
	1986, 076, 12:00	076, 22:59	2.30 ± 0.23	1.44 ± 0.17	1.84 ± 0.04	4-25	≥4 σ
OV 236 .....	1984, 287, 06:49	287, 14:01	0.54 ± 0.11	...	0.36 ± 0.04	6-14	≥4 σ
1928+73 (4C 73.18) .....	1983, 283, 03:52	283, 11:59	1.00 ± 0.39	...	0.37 ± 0.06	6-13	≥4 σ
	1983, 344, 04:07	344, 11:29	0.68 ± 0.08	...	0.45 ± 0.05	6-12	≥4 σ
PKS 2005-489 .....	1984, 254, 07:30	254, 13:05	50.10 ± 2.00	28.60 ± 1.00	3.16 ± 0.04	3-23	≥4 σ
	1984, 287, 16:09	287, 21:49	68.60 ± 3.00	36.70 ± 1.70	6.96 ± 0.06	2-24	≥4 σ
	1985, 289, 07:30	289, 13:20	17.30 ± 0.90	9.54 ± 0.50	0.65 ± 0.04	4-10	≥4 σ
PKS 2155-304 .....	1983, 304, 00:44	304, 16:11	90.70 ± 3.00	...	2.16 ± 0.03	3-24	≥4 σ
	1984, 311, 13:42	311, 17:47	230.00 ± 8.00	...	9.37 ± 0.06	2-29	≥4 σ
	1984, 312, 09:47	312, 13:47	280.00 ± 9.00	...	12.80 ± 0.06	2-31	≥4 σ
	1984, 316, 11:24	316, 14:43	274.00 ± 9.00	...	8.34 ± 0.06	2-27	≥4 σ
	1985, 297, 10:59	298, 00:56	438.00 ± 13.0	...	17.80 ± 0.06	2-32	≥4 σ
	1985, 305, 20:45	305, 22:40	218.00 ± 6.00	...	5.80 ± 0.15	3-21	≥4 σ
	1985, 306, 07:57	307, 00:56	211.00 ± 8.00	...	6.22 ± 0.03	4-29	≥4 σ
	1985, 316, 12:05	317, 06:10	274.00 ± 9.00	...	8.34 ± 0.06	2-22	≥4 σ

<sup>a</sup> Format: year, day, hour:minutes.

<sup>b</sup> Format: day, hour:minutes.

<sup>c</sup> ME count rates are for PHA channels 4-23 corresponding to the energy range 1.3-7 keV with the best signal-to-noise ratio.

TABLE  
POWER LAW PLUS ABSORPTION

SOURCE	DATE (year, day)	$\Gamma^a$	$N^b$	$N_H^c$	$N_H^d$	FLUX <sup>e</sup> (keV)		$\chi^2/\text{dof}$
						0.1-2	2-10	
3C 66A .....	1986, 006	$1.90^{+0.60}_{-0.30}$	$1.85^{+1.80}_{-0.80}$	$14^{+20}_{-11}$	7.5	$0.34 \pm 0.06$	$0.40 \pm 0.04$	0.55/17
	1986, 032	$1.96^{+0.33}_{-0.30}$	$2.80^{+2.00}_{-1.27}$	$30^{+18}_{-16}$		$0.28 \pm 0.05$	$0.45 \pm 0.02$	0.58/18
AO 0235+164 .....	1984, 214	$1.75^{+0.80}_{-0.55}$	$2.17^{+2.00}_{-2.00}$	$80^{+90}_{-70}$	9.1	$0.09 \pm 0.02$	$0.24 \pm 0.04$	0.48/14
0317+18 .....	1985, 013	$2.41^{+0.75}_{-0.60}$	$6.97^{+3.90}_{-3.90}$	$32^{+33}_{-30}$		9.8	$0.62 \pm 0.13$	$1.08 \pm 0.09$
H0323+022 .....	1985, 039	$2.11^{+0.30}_{-0.30}$	$3.62^{+1.80}_{-1.19}$	$15^{+11}_{-11}$	8.4		$0.42 \pm 0.07$	$0.82 \pm 0.05$
	1984, 265	$2.84^{+0.33}_{-0.30}$	$10.45^{+4.30}_{-4.30}$	$12^{+12}_{-10}$		$1.72 \pm 0.20$	$0.79 \pm 0.03$	0.62/17
NRAO 140	1984, 267	$2.50^{+0.23}_{-0.24}$	$7.60^{+1.90}_{-1.90}$	$10^{+11}_{-11}$	14.2	$1.36 \pm 0.10$	$1.13 \pm 0.10$	0.79/17
	1985, 025	$1.36^{+0.26}_{-0.22}$	$1.54^{+0.67}_{-0.44}$	$19^{+11}_{-10}$		$0.22 \pm 0.03$	$1.08 \pm 0.04$	0.89/12
1H 0414+009 .....	1985, 025	$1.54^{+0.20}_{-0.20}$	$2.09^{+0.68}_{-0.50}$	$29^{+11}_{-11}$	8.6	$0.26 \pm 0.03$	$0.99 \pm 0.04$	0.65/18
	1984, 253	$1.91^{+0.19}_{-0.19}$	$8.40^{+0.77}_{-0.74}$	$7.90^{+4.10}_{-2.30}$		$1.71 \pm 0.21$	$2.41 \pm 0.05$	0.66/21
3C 120 .....	1984, 258	$1.88^{+0.08}_{-0.08}$	$9.70^{+0.63}_{-0.63}$	$8.10^{+3.20}_{-2.83}$	10.0	$1.91 \pm 0.18$	$2.86 \pm 0.06$	0.43/25
	1984, 266	$2.38^{+0.25}_{-0.27}$	$8.32^{+0.66}_{-0.60}$	$13.0^{+1.0}_{-1.0}$		$1.66 \pm 0.19$	$1.74 \pm 0.05$	0.95/20
	1984, 274	$2.44^{+0.09}_{-0.10}$	$8.48^{+0.80}_{-0.80}$	$10.8^{+1.1}_{-1.1}$		$1.79 \pm 0.19$	$1.24 \pm 0.05$	0.72/18
	1983, 228	$1.60^{+0.06}_{-0.05}$	$8.51^{+0.79}_{-0.63}$	$4.82^{+1.15}_{-0.96}$		$1.95 \pm 0.10$	$4.02 \pm 0.05$	1.12/22
PKS 0521-36 .....	1983, 305	$1.94^{+0.08}_{-0.08}$	$14.85^{+1.79}_{-1.79}$	$13.30^{+3.07}_{-2.83}$	3.5	$2.54 \pm 0.18$	$3.41 \pm 0.04$	1.34/16
	1984, 249	$1.81^{+0.06}_{-0.06}$	$14.02^{+1.27}_{-1.11}$	$11.54^{+1.40}_{-1.47}$		$2.48 \pm 0.26$	$4.79 \pm 0.04$	0.67/19
	1984, 276	$1.72^{+0.03}_{-0.03}$	$13.20^{+0.87}_{-0.90}$	$12.32^{+2.40}_{-2.08}$		$2.29 \pm 0.13$	$5.19 \pm 0.03$	0.33/19
	1984, 277	$1.76^{+0.07}_{-0.07}$	$12.15^{+1.12}_{-1.08}$	$14.25^{+2.30}_{-2.30}$		$1.98 \pm 0.12$	$4.44 \pm 0.09$	1.32/20
	1984, 278	$1.67^{+0.06}_{-0.06}$	$11.31^{+1.03}_{-1.03}$	$10.81^{+1.12}_{-1.12}$		$2.06 \pm 0.25$	$4.81 \pm 0.06$	0.44/21
	1984, 280	$1.65^{+0.08}_{-0.07}$	$9.39^{+1.04}_{-0.93}$	$10.33^{+1.70}_{-2.19}$		$1.74 \pm 0.09$	$4.09 \pm 0.06$	0.71/18
	1984, 284	$1.90^{+0.08}_{-0.08}$	$12.45^{+1.31}_{-1.18}$	$16.30^{+3.40}_{-3.10}$		$1.89 \pm 0.13$	$3.67 \pm 0.04$	0.58/22
	1984, 286	$1.74^{+0.06}_{-0.06}$	$11.19^{+1.02}_{-1.02}$	$10.97^{+2.29}_{-2.29}$		$2.02 \pm 0.15$	$4.28 \pm 0.05$	0.37/19
	1985, 044	$1.72^{+0.10}_{-0.10}$	$9.11^{+1.73}_{-1.73}$	$9.41^{+2.31}_{-2.31}$		$1.73 \pm 0.11$	$3.57 \pm 0.06$	0.57/18
	1985, 283	$1.80^{+0.08}_{-0.08}$	$13.01^{+1.36}_{-1.36}$	$12.74^{+2.33}_{-2.33}$		$2.22 \pm 0.15$	$4.50 \pm 0.05$	1.02/15
	1986, 044	$1.86^{+0.10}_{-0.10}$	$8.88^{+1.07}_{-1.07}$	$13.21^{+4.09}_{-4.09}$		$1.48 \pm 0.23$	$2.77 \pm 0.04$	0.57/19
	1983, 306	$1.70^{+0.20}_{-0.20}$	$2.88^{+0.80}_{-0.80}$	$5.76^{+1.90}_{-1.90}$		$0.64 \pm 0.10$	$1.15 \pm 0.04$	0.70/19
	1983, 334	$1.81^{+0.30}_{-0.30}$	$3.50^{+1.80}_{-1.80}$	$8.60^{+1.60}_{-1.60}$		$0.69 \pm 0.15$	$1.17 \pm 0.08$	0.53/19
	PKS 0548-32 .....	1983, 306	$2.33^{+0.09}_{-0.09}$	$18.93^{+2.00}_{-2.00}$		$7.20^{+2.10}_{-1.70}$	2.49	$4.10 \pm 0.33$
1983, 334		$2.14^{+0.12}_{-0.12}$	$13.90^{+2.10}_{-2.10}$	$4.40^{+2.10}_{-1.48}$	$3.48 \pm 0.42$	$2.90 \pm 0.06$		0.61/19
1986, 066		$2.15^{+0.08}_{-0.08}$	$10.47^{+1.10}_{-1.10}$	$3.40^{+0.70}_{-0.70}$	$2.80 \pm 0.11$	$2.20 \pm 0.04$		0.98/21
1986, 066		$2.24^{+0.11}_{-0.11}$	$11.27^{+1.33}_{-1.33}$	$4.01^{+1.15}_{-1.00}$	$2.97 \pm 0.11$	$2.04 \pm 0.04$		0.96/17
PKS 0754+10 .....	1986, 066	$2.11^{+0.12}_{-0.12}$	$10.23^{+1.47}_{-1.47}$	$3.20^{+1.00}_{-1.00}$	2.7	$2.80 \pm 0.11$	$2.23 \pm 0.05$	0.65/18
	1984, 043	$1.70^{+0.20}_{-0.20}$	$8.87^{+0.10}_{-0.10}$	$3.40^{+2.00}_{-1.00}$		$0.23 \pm 0.03$	$0.54 \pm 0.05$	0.55/09
OJ 287 .....	1983, 281	$3.15^{+1.02}_{-1.02}$	$9.97^{+17.80}_{-17.80}$	$15.73^{+21.30}_{-21.30}$	3.0	$1.60 \pm 0.15$	$0.52 \pm 0.01$	0.28/8
	1984, 040	$2.94^{+0.54}_{-0.54}$	$6.85^{+3.42}_{-3.08}$	$8.82^{+11.00}_{-11.00}$		$1.55 \pm 0.21$	$0.47 \pm 0.01$	0.30/10
Mrk 421 .....	1984, 035	$-2.70^{+0.12}_{-0.12}$	$11.48^{+1.90}_{-1.49}$	$1.80^{+0.73}_{-0.50}$	1.8	$5.57 \pm 0.28$	$0.98 \pm 0.08$	0.47/13
	1984, 337	$2.16^{+0.06}_{-0.05}$	$53.50^{+0.25}_{-0.20}$	$2.30^{+0.55}_{-0.40}$		$17.80 \pm 0.71$	$11.20 \pm 0.06$	1.62/20
	1984, 338	$2.17^{+0.03}_{-0.03}$	$67.00^{+0.90}_{-0.84}$	$2.25^{+0.47}_{-0.15}$		$22.60 \pm 0.43$	$14.20 \pm 0.06$	2.68/25
	1984, 340	$2.31^{+0.04}_{-0.04}$	$82.40^{+1.80}_{-1.81}$	$2.61^{+0.31}_{-0.33}$		$23.90 \pm 0.93$	$13.80 \pm 0.10$	1.89/23
	1985, 004	$2.73^{+0.20}_{-0.07}$	$15.80^{+1.10}_{-0.80}$	$1.88^{+0.70}_{-0.50}$		$6.77 \pm 0.36$	$1.49 \pm 0.05$	0.48/15
	1985, 112	$2.55^{+0.02}_{-0.02}$	$23.49^{+0.67}_{-0.54}$	$2.20^{+0.33}_{-0.33}$		$9.10 \pm 0.31$	$2.75 \pm 0.04$	0.71/20
	1985, 118	$2.42^{+0.09}_{-0.09}$	$19.93^{+0.67}_{-0.50}$	$1.85^{+0.33}_{-0.33}$		$7.21 \pm 0.25$	$2.80 \pm 0.04$	0.67/24
	1985, 126	$2.64^{+0.09}_{-0.08}$	$15.80^{+0.47}_{-0.47}$	$1.95^{+0.37}_{-0.37}$		$6.45 \pm 0.22$	$1.63 \pm 0.03$	0.71/20
	1985, 131	$2.34^{+0.08}_{-0.08}$	$20.00^{+0.66}_{-0.55}$	$1.55^{+0.51}_{-0.51}$		$7.08 \pm 0.25$	$2.51 \pm 0.04$	0.80/24
	1985, 132	$2.66^{+0.60}_{-0.50}$	$17.10^{+2.15}_{-1.15}$	$2.38^{+2.80}_{-1.90}$		$7.14 \pm 0.26$	$1.70 \pm 0.07$	0.64/15
	1985, 141	$2.44^{+0.12}_{-0.08}$	$15.87^{+0.88}_{-0.50}$	$1.94^{+0.88}_{-1.15}$		$6.12 \pm 0.22$	$1.86 \pm 0.04$	0.58/19
Mrk 180 .....	1984, 333	$2.49^{+0.42}_{-0.40}$	$3.19^{+0.35}_{-0.31}$	$2.25^{+2.15}_{-1.45}$	1.4	$1.39 \pm 0.09$	$0.38 \pm 0.03$	0.65/15
	1985, 093	$2.53^{+0.16}_{-0.16}$	$8.50^{+3.70}_{-2.70}$	$1.92^{+2.00}_{-1.50}$		$3.18 \pm 0.24$	$1.02 \pm 0.07$	0.35/16
B2 1147+245 .....	1984, 016	$1.96^{+0.84}_{-0.40}$	$1.07^{+1.23}_{-0.50}$	$8.76^{+16.90}_{-4.60}$	1.8	$0.21 \pm 0.03$	$0.56 \pm 0.07$	0.57/12
3C 273 .....	1984, 005	$1.58^{+0.03}_{-0.03}$	$19.55^{+0.79}_{-0.79}$	1.8		$5.34 \pm 0.02$	$9.66 \pm 0.09$	1.98/16
3C 273 .....	1985, 032	$1.71^{+0.02}_{-0.02}$	$18.97^{+0.21}_{-0.22}$	1.8	$5.31 \pm 0.02$	$7.65 \pm 0.08$	11.84/16	
	1985, 138	$1.85^{+0.01}_{-0.01}$	$23.68^{+0.23}_{-0.23}$	1.8	$6.88 \pm 0.02$	$7.58 \pm 0.05$	13.22/18	
	1986, 017 -	1.61	24.72	1.8	$6.79 \pm 0.02$	$11.62 \pm 0.04$	7.56/20	
	1986, 018	1.63	24.69	1.8	$6.81 \pm 0.02$	$11.16 \pm 0.04$	7.94/19	

TABLE

SOURCE	DATE (year, day)	$\Gamma^a$	$N^b$	$N_H^c$	$N_H^d$	FLUX <sup>e</sup> (keV)		$\chi^2/\text{dof}$
						0.1-2	2-10	
1E 1402+04 .....	1985, 031	$2.42^{+0.10}_{-0.10}$	$1.66^{+0.18}_{-0.18}$	2.2	2.2	$0.50 \pm 0.05$	$0.19 \pm 0.04$	1.40/18
1E 1415+259 .....	1986, 063	$2.91^{+0.30}_{-0.30}$	$6.06^{+2.20}_{-2.20}$	$5.60^{+2.30}_{-2.30}$	1.6	$1.92 \pm 0.05$	$0.39 \pm 0.02$	0.19/13
1H 1427+42 .....	1985, 012	$2.06^{+0.07}_{-0.07}$	$21.30^{+1.90}_{-1.90}$	$1.55^{+0.38}_{-0.38}$	1.4	$6.81 \pm 0.16$	$5.00 \pm 0.07$	0.61/18
PKS 1510-089 .....	1984, 216	$1.46^{+0.27}_{-0.27}$	$1.33^{+0.42}_{-0.42}$	$5.30^{+1.1}_{-1.1}$	7.6	$0.27 \pm 0.04$	$0.79 \pm 0.04$	0.82/16
	1985, 212	$1.60^{+0.29}_{-0.29}$	$1.32^{+0.37}_{-0.37}$	$8.70^{+1.5}_{-1.5}$		$0.27 \pm 0.04$	$0.61 \pm 0.04$	0.44/12
Mrk 501 .....	1984, 034	$2.44^{+0.08}_{-0.08}$	$32.33^{+2.90}_{-2.90}$	$3.00^{+0.40}_{-0.40}$	...	$10.00 \pm 0.41$	$4.41 \pm 0.05$	1.01/19
	1984, 086	$2.29^{+0.09}_{-0.09}$	$24.30^{+2.30}_{-2.30}$	$2.14^{+0.48}_{-0.48}$		$7.64 \pm 0.36$	$4.17 \pm 0.07$	0.79/16
	1984, 183	$2.58^{+0.09}_{-0.09}$	$20.02^{+1.80}_{-1.80}$	$2.31^{+0.48}_{-0.48}$		$7.23 \pm 0.31$	$2.24 \pm 0.04$	1.15/18
	1984, 191	$2.39^{+0.12}_{-0.12}$	$17.60^{+2.10}_{-2.10}$	$1.75^{+0.30}_{-0.30}$		$6.36 \pm 0.30$	$2.53 \pm 0.06$	0.55/17
	1984, 201	$2.43^{+0.08}_{-0.08}$	$18.64^{+1.40}_{-1.40}$	$2.00^{+0.40}_{-0.40}$		$6.50 \pm 0.32$	$2.59 \pm 0.05$	0.92/16
	1984, 207	$2.63^{+0.09}_{-0.09}$	$25.70^{+2.50}_{-2.50}$	$3.11^{+0.43}_{-0.43}$		$8.57 \pm 0.38$	$2.68 \pm 0.05$	0.72/18
	1984, 209	$2.38^{+0.07}_{-0.07}$	$21.90^{+1.70}_{-1.70}$	$2.20^{+0.40}_{-0.40}$		$7.55 \pm 0.36$	$3.14 \pm 0.05$	0.63/17
	1985, 099	$2.58^{+0.10}_{-0.10}$	$20.15^{+1.75}_{-1.75}$	$2.47^{+0.40}_{-0.40}$		$6.35 \pm 0.31$	$2.35 \pm 0.06$	0.99/15
	1986, 074	$2.39^{+0.08}_{-0.08}$	$28.59^{+1.85}_{-1.85}$	$2.65^{+0.35}_{-0.35}$		$9.01 \pm 0.20$	$4.15 \pm 0.03$	1.40/16
4U 1722+119 .....	1985, 245	$2.66^{+0.30}_{-0.30}$	$8.00^{+2.20}_{-2.20}$	$15^{+2}_{-2}$	8.6	$1.26 \pm 0.13$	$0.76 \pm 0.04$	0.63/16
1Zw 186 .....	1984, 181	$2.52^{+0.13}_{-0.13}$	$4.90^{+0.45}_{-0.45}$	$3.90^{+0.30}_{-0.30}$	2.7	$1.88 \pm 0.12$	$0.79 \pm 0.37$	0.96/16
3C 371 .....	1984, 255	$2.80^{+0.09}_{-0.09}$	$4.28^{+0.32}_{-0.32}$	4.90	4.9	$1.25 \pm 0.06$	$0.35 \pm 0.03$	1.10/15
3C 390.3 .....	1985, 033	$1.42^{+0.14}_{-0.14}$	$4.39^{+0.84}_{-0.79}$	$1.04^{+0.18}_{-0.17}$	4.1	$1.25 \pm 0.20$	$2.78 \pm 0.08$	1.18/26
	1985, 033	$1.60^{+0.11}_{-0.11}$	$6.03^{+0.96}_{-0.84}$	$2.34^{+1.23}_{-1.19}$		$1.18 \pm 0.22$	$2.90 \pm 0.07$	0.71/26
	1986, 076	$1.53^{+0.10}_{-0.10}$	$4.09^{+0.42}_{-0.42}$	$1.13^{+0.40}_{-0.40}$		$1.60 \pm 0.16$	$2.15 \pm 0.05$	1.04/29
OV 236 .....	1984, 287	$1.67^{+0.35}_{-0.35}$	$1.03^{+0.31}_{-0.31}$	4.00	...	$0.22 \pm 0.04$	$0.46 \pm 0.05$	1.31/11
1928+73 (4C 73.18) ...	1983, 283	$2.25^{+0.50}_{-0.45}$	$2.84^{+2.30}_{-1.34}$	$13.00^{+7.0}_{-7.0}$	...	$0.47 \pm 0.18$	$0.50 \pm 0.08$	0.97/29
	1983, 344	$2.11^{+0.40}_{-0.41}$	$2.38^{+1.70}_{-1.60}$	$15.00^{+1.0}_{-1.0}$		$0.37 \pm 0.04$	$0.15 \pm 0.02$	0.53/31
PKS 2005-489 .....	1984, 254	$3.04^{+0.07}_{-0.07}$	$42.00^{+3.00}_{-3.00}$	$6.15^{+0.30}_{-0.30}$	4.6	$12.10 \pm 0.48$	$2.50 \pm 0.03$	1.00/18
	1984, 287	$2.70^{+0.06}_{-0.05}$	$64.22^{+2.88}_{-2.77}$	$5.06^{+0.41}_{-0.39}$		$16.70 \pm 0.73$	$6.07 \pm 0.05$	0.52/11
	1985, 289	$3.18^{+0.06}_{-0.06}$	$9.30^{+0.39}_{-0.41}$	$6.12^{+0.46}_{-0.50}$		$3.38 \pm 0.17$	$0.49 \pm 0.03$	0.68/15
PKS 2155-304 .....	1983, 304	$2.77^{+0.02}_{-0.02}$	$21.37^{+0.45}_{-0.45}$	1.8	1.8	$9.44 \pm 0.34$	$1.85 \pm 0.02$	2.81/16
	1984, 311	$2.60^{+0.02}_{-0.02}$	$78.32^{+0.52}_{-0.52}$	1.8		$27.00 \pm 0.93$	$8.58 \pm 0.05$	4.6/19
	1984, 312	$2.52^{+0.03}_{-0.03}$	$96.48^{+2.45}_{-2.50}$	1.8		$36.80 \pm 1.18$	$11.70 \pm 0.05$	2.7/19
	1984, 316	$2.73^{+0.03}_{-0.03}$	$79.10^{+0.20}_{-0.18}$	1.8		$34.10 \pm 1.12$	$7.22 \pm 0.05$	1.26/19
	1985, 297	$2.65^{+0.02}_{-0.02}$	$155.00^{+2.70}_{-2.70}$	1.8		$63.50 \pm 1.88$	$15.80 \pm 0.05$	3.6/19
	1985, 305	$2.81^{+0.03}_{-0.03}$	$56.80^{+1.20}_{-1.20}$	1.8		$25.80 \pm 0.71$	$4.63 \pm 0.12$	0.60/19
	1985, 306	$2.74^{+0.03}_{-0.03}$	$60.50^{+1.21}_{-1.18}$	1.8		$26.30 \pm 0.99$	$5.42 \pm 0.03$	3.35/19
	1985, 316	$2.90^{+0.02}_{-0.02}$	$36.50^{+2.88}_{-2.72}$	1.8		$17.60 \pm 0.58$	$2.67 \pm 0.02$	2.20/19

<sup>a</sup> Photon index.

<sup>b</sup> Normalization in  $10^{-3}$  photons  $\text{cm}^{-2} \text{s}^{-1} \text{keV}^{-1}$  at 1 keV.

<sup>c</sup> Observed hydrogen column density in  $10^{20} \text{cm}^{-2}$ .

<sup>d</sup> Galactic column density in  $10^{20} \text{cm}^{-2}$ .

<sup>e</sup> Flux in  $10^{-11}$  ergs  $\text{cm}^{-2} \text{s}^{-1}$ .

<sup>f</sup> Fixed with corresponding Galactic column density value.

TABLE  
PARAMETERS OF BROKEN POWER-LAW MODEL FOR PKS 0548-322

Date (year, day)	$\Gamma_1^a$	$\Gamma_2^a$	$N_H^b$	$E_b^c$	$\chi^2/\text{dof}$
1983, 306 .....	$1.66^{+0.42}_{-0.61}$	$2.33^{+0.40}_{-0.21}$	$2.60^{+2.10}_{-1.50}$	$2.20^{+0.96}_{-0.58}$	0.67/16
1986, 066 .....	$1.61^{+0.41}_{-0.48}$	$2.41^{+0.34}_{-0.35}$	$2.10^{+2.00}_{-1.50}$	$2.00^{+0.97}_{-0.61}$	0.71/19

<sup>a</sup> Photon index.

<sup>b</sup> Hydrogen column density in  $10^{20} \text{cm}^{-2}$ .

<sup>c</sup> Break energy in keV.

TABLE 4B  
PARAMETERS OF HIGH-ENERGY CUTOFF MODEL FOR MARKARIAN 421

Date (year, day)	$\Gamma^a$	$N_H^b$	$E_c^c$	$E_r^d$	$\chi^2/\text{dof}$
1984, 337 .....	$2.10^{+0.10}_{-0.22}$	$1.73^{+0.74}_{-0.58}$	$2.98^{+1.88}_{-2.41}$	$24.90^{+39.20}_{-16.40}$	1.29/18
1984, 338 .....	$1.94^{+0.18}_{-0.20}$	$1.41^{+0.81}_{-0.64}$	$2.58^{+0.90}_{-1.21}$	$17.40^{+4.80}_{-}$	1.27/23
1984, 340 .....	$2.04^{+0.23}_{-0.13}$	$1.33^{+0.96}_{-0.91}$	$2.81^{+0.91}_{-1.08}$	$7.90^{+2.80}_{-2.94}$	1.27/18

- <sup>a</sup> Photon index.  
<sup>b</sup> Hydrogen column density in  $10^{20} \text{ cm}^{-2}$ .  
<sup>c</sup> Cutoff energy in keV.  
<sup>d</sup> Rate in keV.

TABLE 4C  
PARAMETERS OF POWER-LAW PLUS ABSORPTION-EDGE MODEL FOR MARKARIAN 421

Date (year, day)	$\Gamma^a$	$N^b$	$N_H^c$	$E^d$	$\tau^e$	$\chi^2/\text{dof}$
1984, 337 .....	$2.27^{+0.06}_{-0.06}$	$65.60^{+6.90}_{-6.20}$	$2.01^{+0.36}_{-0.32}$	$0.52^{+0.10}_{-0.07}$	$4.62^{+5.11}_{-3.02}$	1.06/22
1984, 338 .....	$2.29^{+0.03}_{-0.04}$	$86.20^{+6.00}_{-6.00}$	$2.14^{+0.24}_{-0.22}$	$0.55^{+0.08}_{-0.06}$	$5.98^{+4.80}_{-3.80}$	0.85/21
1984, 340 .....	$2.38^{+0.03}_{-0.04}$	$91.97^{+4.10}_{-4.80}$	$2.57^{+0.30}_{-0.41}$	$0.51^{+0.11}_{-0.10}$	$2.90^{+2.11}_{-1.39}$	1.34/21

- <sup>a</sup> Photon index.  
<sup>b</sup> Normalization in  $10^{-3} \text{ photons cm}^{-2} \text{ s}^{-1} \text{ keV}^{-1}$  at 1 keV.  
<sup>c</sup> Hydrogen column density in  $10^{20} \text{ cm}^{-2}$ .  
<sup>d</sup> Edge energy in keV.  
<sup>e</sup> Optical depth.

TABLE 4D  
POWER-LAW PLUS THERMAL BREMSSTRAHLUNG PLUS FIXED ABSORPTION FITS TO THE SPECTRA OF 3C 273

Date (year, day)	$\Gamma^a$	$N^b$	$kT^c$	$N_B^d$	$\chi^2/\text{dof}$
1984, 005 .....	$1.48^{+0.03}_{-0.03}$	$17.30^{+1.13}_{-1.07}$	$0.10^{+0.33}_{-0.00}$	$218.6^{+82.0}_{-83.1}$	0.88/17
1985, 032 .....	$1.39^{+0.08}_{-0.09}$	$12.72^{+1.45}_{-1.37}$	$0.13^{+0.13}_{-0.03}$	$187.4^{+82.6}_{-86.1}$	0.62/15
1985, 138 .....	$1.52^{+0.05}_{-0.04}$	$15.57^{+0.83}_{-0.83}$	$0.40^{+0.04}_{-0.04}$	$54.69^{+3.60}_{-3.11}$	0.65/17
1986, 017 .....	$1.53^{+0.02}_{-0.02}$	$22.44^{+0.59}_{-0.37}$	$0.10^{+0.03}_{-0.03}$	$482.1^{+65.0}_{-63.0}$	0.65/19
1986, 018 .....	$1.56^{+0.02}_{-0.03}$	$22.40^{+0.58}_{-0.53}$	$0.12^{+0.04}_{-0.03}$	$491.8^{+68.0}_{-64.2}$	0.79/19

- <sup>a</sup> Photon index.  
<sup>b</sup> Normalization in  $10^{-3} \text{ photons cm}^{-2} \text{ s}^{-1} \text{ keV}^{-1}$  at 1 keV.  
<sup>c</sup> Plasma temperature in keV.  
<sup>d</sup> Bremsstrahlung normalization in  $10^{-3} \text{ photons cm}^{-2} \text{ s}^{-1} \text{ keV}^{-1}$  at 1 keV.

TABLE 4E  
POWER-LAW PLUS BLACKBODY PLUS FIXED ABSORPTION FITS TO THE SPECTRA OF 3C 273

Date (year, day)	$\Gamma^a$	$N^b$	$kT^c$	$N_{\text{BB}}^d$	$\chi^2/\text{dof}$
1984, 005 .....	$1.48^{+0.03}_{-0.03}$	$17.29^{+1.17}_{-1.10}$	$0.05^{+0.03}_{-0.04}$	$0.23^{+0.20}_{-0.12}$	0.88/17
1985, 032 .....	$1.39^{+0.08}_{-0.09}$	$12.69^{+1.46}_{-1.34}$	$0.06^{+0.03}_{-0.04}$	$0.29^{+0.12}_{-0.06}$	0.60/15
1985, 138 .....	$1.55^{+0.04}_{-0.04}$	$16.28^{+0.71}_{-0.69}$	$0.08^{+0.03}_{-0.03}$	$0.39^{+0.03}_{-0.03}$	0.69/17
1986, 017 .....	$1.54^{+0.02}_{-0.02}$	$22.45^{+0.59}_{-0.37}$	$0.04^{+0.02}_{-0.02}$	$0.57^{+0.21}_{-0.22}$	0.64/19
1986, 018 .....	$1.56^{+0.02}_{-0.03}$	$22.41^{+0.58}_{-0.52}$	$0.04^{+0.02}_{-0.02}$	$0.56^{+0.20}_{-0.21}$	0.79/19

- <sup>a</sup> Photon index.  
<sup>b</sup> Normalization in  $10^{-3} \text{ photons cm}^{-2} \text{ s}^{-1} \text{ keV}^{-1}$  at 1 keV.  
<sup>c</sup> Plasma temperature in keV.  
<sup>d</sup> Blackbody normalization in  $10^{-3} \text{ photons cm}^{-2} \text{ s}^{-1} \text{ keV}^{-1}$  at 1 keV.

Tables 3.2.4B - 3.2.4E

TABLE 4F  
POWER-LAW PLUS ABSORPTION-EDGE FIT TO THE SPECTRA OF PKS 2155-304

Date (year, day)	$\Gamma^a$	$N_H^b$	$E^c$	$\tau^d$	$\chi^2/\text{dof}$
1983, 304 .....	$2.81^{+0.10}_{-0.07}$	$1.92^{+0.20}_{-0.18}$	$0.65^{+0.07}_{-0.08}$	$3.20^{+1.30}_{-1.30}$	1.41/14
1984, 311 .....	$2.61^{+0.08}_{-0.05}$	$1.63^{+0.14}_{-0.12}$	$0.88^{+0.13}_{-0.11}$	$1.30^{+0.44}_{-0.39}$	1.10/16
1984, 312 .....	$2.59^{+0.07}_{-0.06}$	$1.69^{+0.11}_{-0.10}$	$0.60^{+0.07}_{-0.06}$	$1.85^{+0.46}_{-0.41}$	1.33/16
1984, 316 .....	$2.89^{+0.07}_{-0.05}$	$3.41^{+0.47}_{-0.40}$	$0.70^{+0.08}_{-0.08}$	$2.96^{+0.56}_{-0.47}$	1.24/16
1985, 297 .....	$2.71^{+0.05}_{-0.03}$	$2.85^{+0.17}_{-0.14}$	$0.57^{+0.23}_{-0.21}$	$1.88^{+0.47}_{-0.41}$	1.20/16
1985, 306 .....	$2.81^{+0.08}_{-0.07}$	$2.41^{+0.24}_{-0.19}$	$0.59^{+0.23}_{-0.21}$	$1.94^{+0.32}_{-0.28}$	1.10/16
1985, 316 .....	$2.94^{+0.09}_{-0.07}$	$2.32^{+0.27}_{-0.22}$	$0.62^{+0.23}_{-0.21}$	$1.39^{+0.31}_{-0.27}$	1.40/16

<sup>a</sup> Photon index.

<sup>b</sup> Hydrogen column density in  $10^{20} \text{ cm}^{-2}$ .

<sup>c</sup> Edge energy in keV.

<sup>d</sup> Optical depth.

TABLE 4G  
BROKEN POWER-LAW FIT TO THE SPECTRA OF PKS 2155-304

Date (year, day)	$\Gamma_1^a$	$\Gamma_2^a$	$E_B^b$	$N_H^c$	$\chi^2/\text{dof}$
1983, 304 .....	$5.31^{+1.71}_{-1.39}$	$2.60^{+0.11}_{-0.09}$	$0.47^{+0.09}_{-0.08}$	$3.62^{+1.67}_{-1.32}$	1.43/14
1984, 311 .....	$3.42^{+0.37}_{-0.35}$	$2.37^{+0.08}_{-0.08}$	$0.59^{+0.21}_{-0.28}$	$2.10^{+0.36}_{-1.30}$	2.77/16
1984, 312 .....	$7.90^{+1.31}_{-1.44}$	$2.31^{+0.08}_{-0.06}$	$0.39^{+0.03}_{-0.05}$	$6.90^{+1.62}_{-1.50}$	1.90/16
1984, 316 .....	$5.69^{+1.33}_{-1.10}$	$2.80^{+0.08}_{-0.07}$	$0.51^{+0.11}_{-0.09}$	$6.71^{+1.53}_{-1.27}$	1.21/16
1985, 297 .....	$6.11^{+1.80}_{-1.30}$	$2.40^{+0.18}_{-0.14}$	$0.49^{+0.15}_{-0.11}$	$4.30^{+1.61}_{-1.22}$	2.81/16
1985, 306 .....	$5.90^{+1.52}_{-1.33}$	$2.49^{+0.21}_{-0.17}$	$0.42^{+0.19}_{-0.14}$	$3.51^{+1.94}_{-1.69}$	2.69/16
1985, 316 .....	$7.43^{+1.94}_{-1.81}$	$2.64^{+0.88}_{-0.21}$	$0.51^{+0.20}_{-0.15}$	$4.60^{+1.32}_{-1.22}$	1.80/16

<sup>a</sup> Photon index.

<sup>b</sup> Break energy in keV.

<sup>c</sup> Hydrogen column density in  $10^{20} \text{ cm}^{-2}$ .

Tables 3.2.4F - 3.2.4G

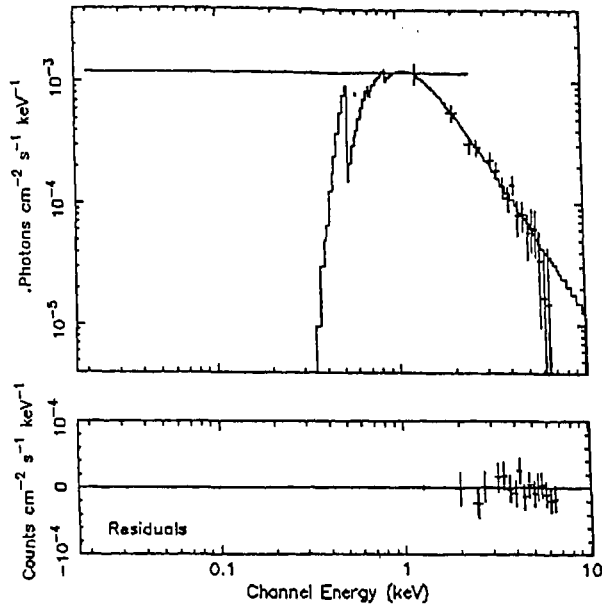


FIG. 2a

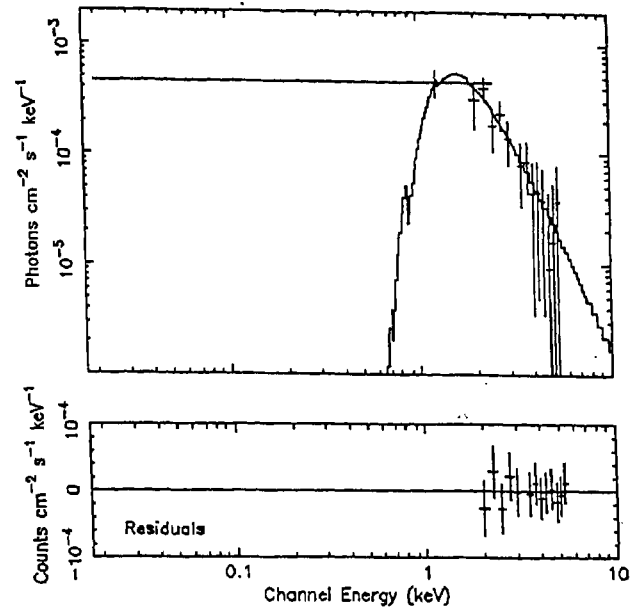


FIG. 2b

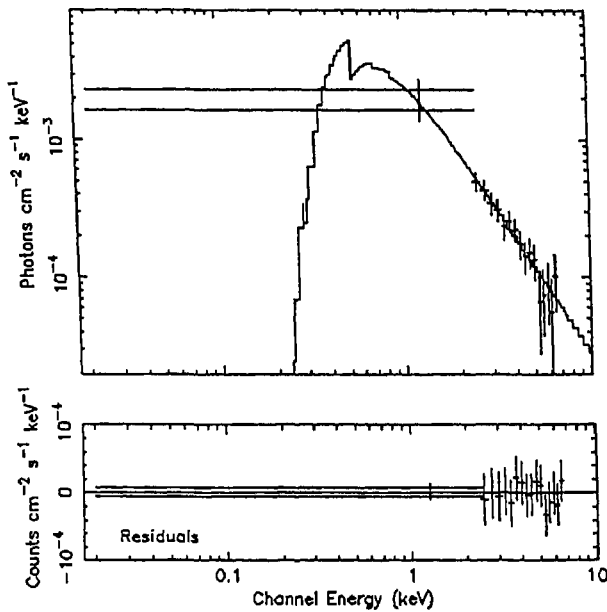


FIG. 2c

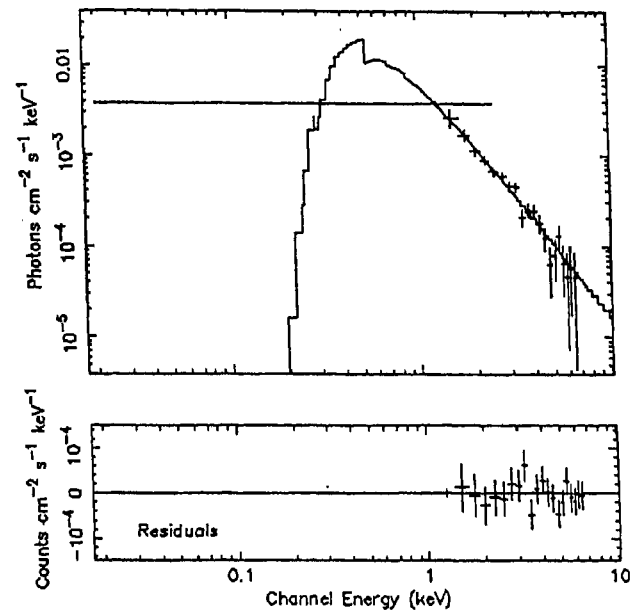


FIG. 2d

(a) Incident spectrum of the blazar 3C 66A. Solid line shows the fitted power-law model convolved through the detector response. The lower panel of the figure shows the residuals between the model and the spectrum, which was observed on 1986, day 032. (b) Same as (a), but for the blazar AO 0235+164, observed on 1984, day 214. (c) Same as (a), but for the blazar 0317+18, observed on 1985, day 039. (d) Same as (a), but for the blazar H0323+022, observed on 1984, day 267. (e) Same as (a), but for the blazar NRAO 140, observed on 1985, day 025. (f) Same as (a), but for the blazar 1H 0414+009, observed on 1984, day 258. (g) Same as (a), but for the blazar 3C 120, observed on 1984, day 278. (h) Same as (a), but for the blazar PKS 0521-365; observed on 1983, day 334. (i) Same as (a), but for the blazar PKS 0548-32, observed on 1983, day 306. (j) Same as (a), but for the blazar PKS 0754+100, observed on 1984, day 043. (k) Same as (a), but for the blazar OJ 287, observed on 1984, day 040. (l) Same as (a), but for the blazar Mrk 421, observed on 1985, day 112. (m) Same as (a), but for the blazar Mrk 180, observed on 1985, day 093. (n) Same as (a), but for the blazar B2 1147+245, observed on 1984, day 016. (o) Same as (a), but for the blazar 3C 273, observed on 1986, day 018. (p) Same as (a), but for the blazar 1E 1402+04, observed on 1985, day 187. (q) Same as (a), but for the blazar 1E 1415+259, observed on 1986, day 063. (r) Same as (a), but for the blazar 1H 1427+42, observed on 1985, day 012. (s) Same as (a), but for the blazar PKS 1510-089, observed on 1984, day 216. (t) Same as (a), but for the blazar Mrk 501, observed on 1984, day 207. (u) Same as (a), but for the blazar 4U 1722+119, observed on 1985, day 246. (v) Same as (a), but for the blazar I Zw 186, observed on 1984, day 181. (w) Same as (a), but for the blazar 3C 371, observed on 1984, day 273. (x) Same as (a), but for the blazar 3C 390.3, observed on 1986, day 076. (y) Same as (a), but for the blazar OV 236, observed on 1984, day 287. (z) Same as (a), but for the blazar 1928+73, observed on 1983, day 344. (aa) Same as (a), but for the blazar PKS 2005-489, observed on 1984, day 287. (ab) Same as (a), but for the blazar PKS 2155-304, observed on 1984, day 316.

### Figs. 3.2.2



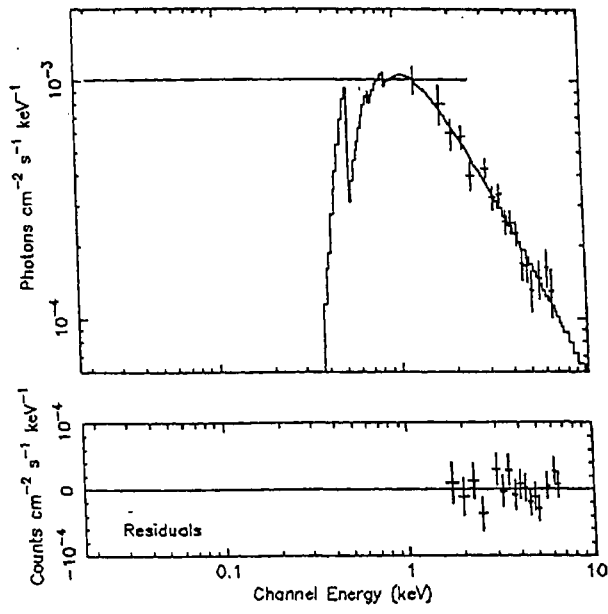


FIG. 2e

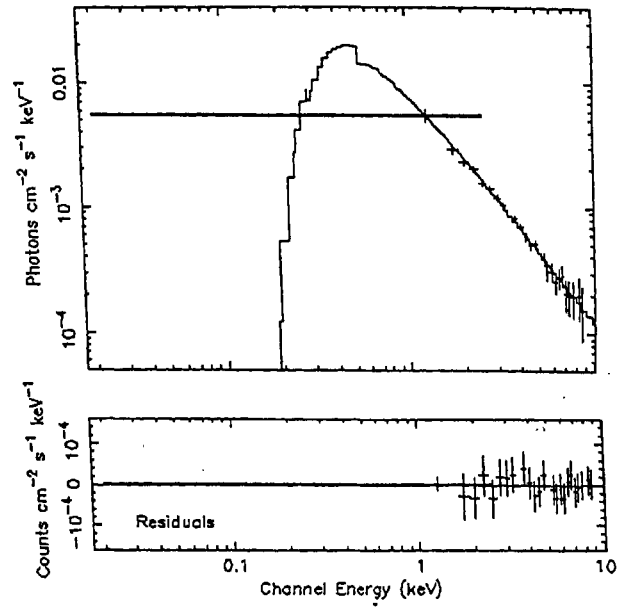


FIG. 2f

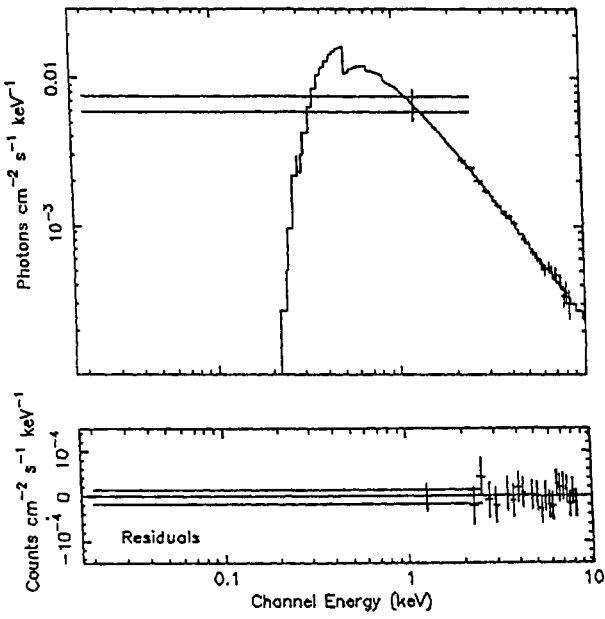


FIG. 2g

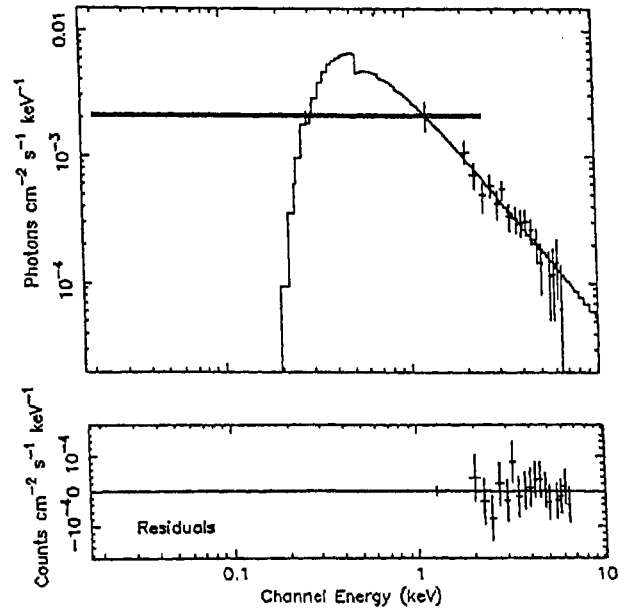


FIG. 2h

Figs. 3.2.2 (continued)

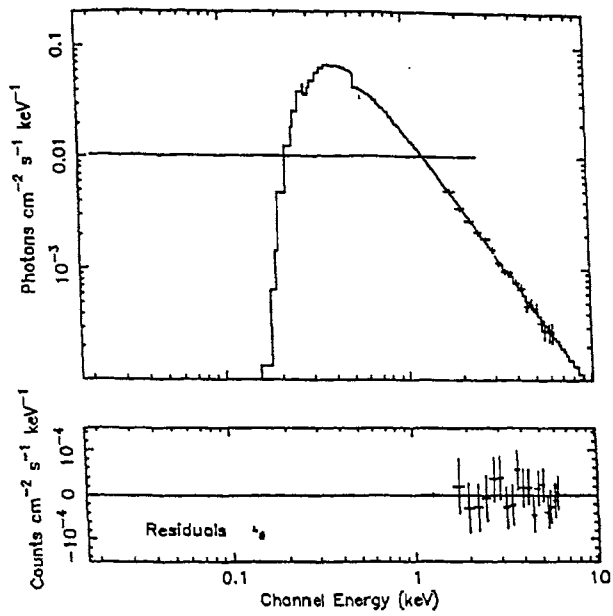


FIG. 2i

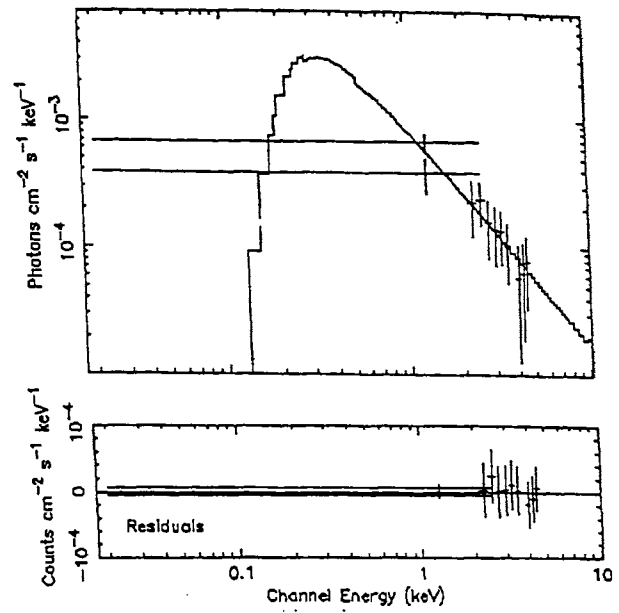


FIG. 2j

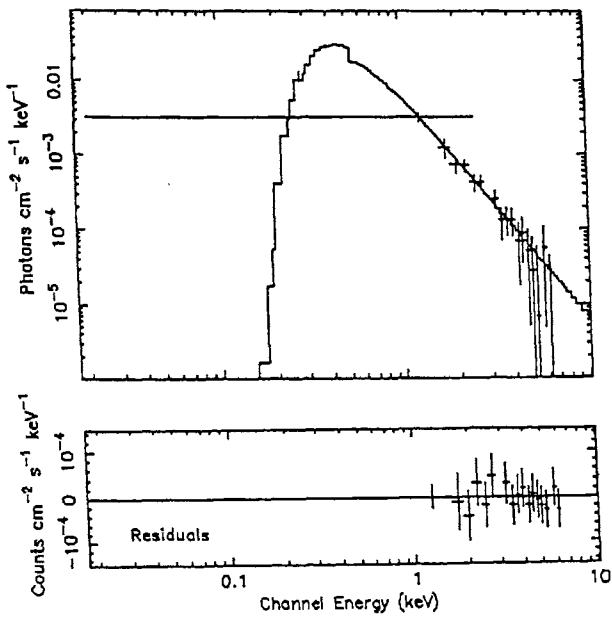


FIG. 2k

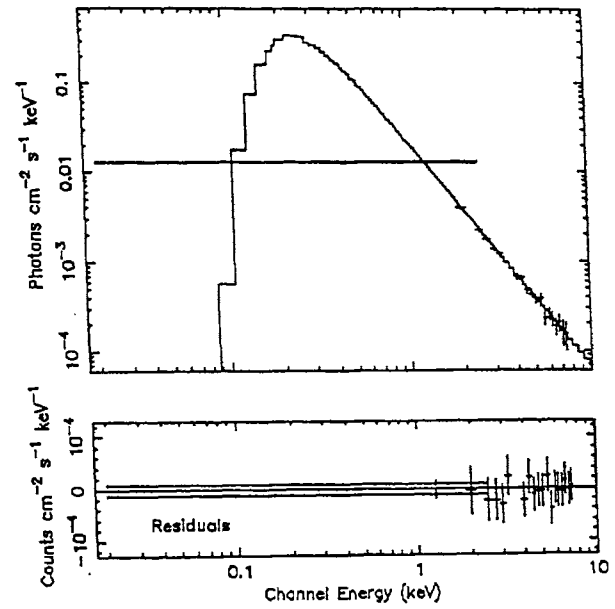


FIG. 2l

Figs. 3.2.2 (continued)

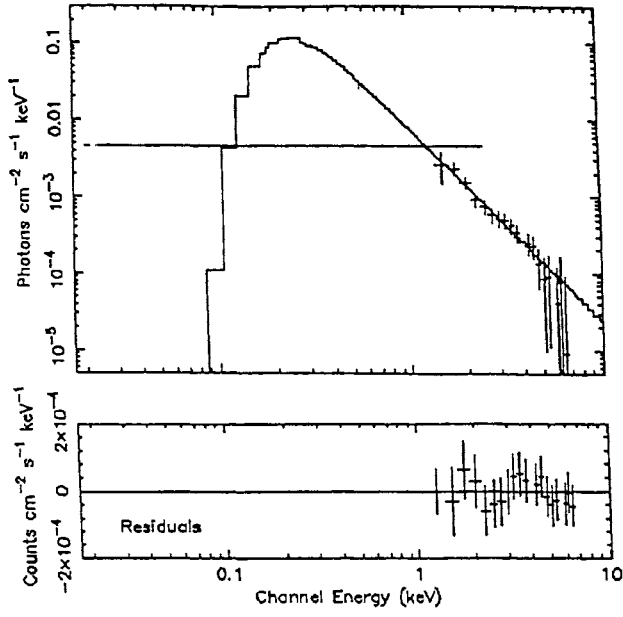


FIG. 2m

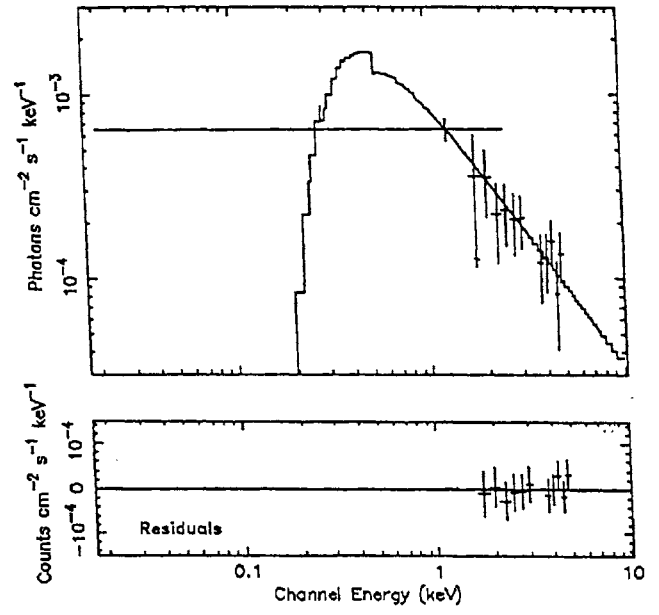


FIG. 2n

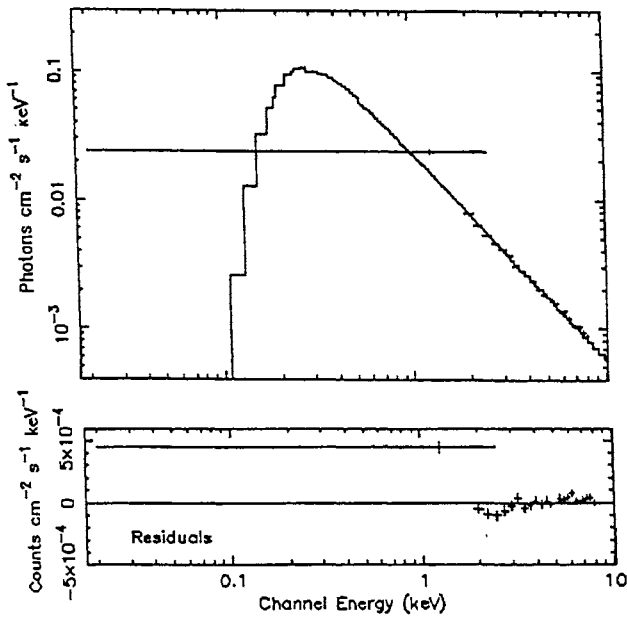


FIG. 2o

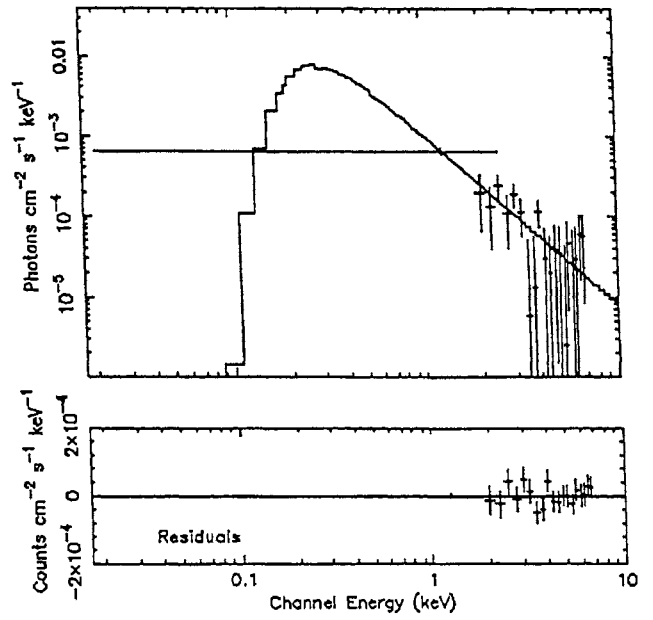


FIG. 2p

Figs. 3.2.2 (continued)

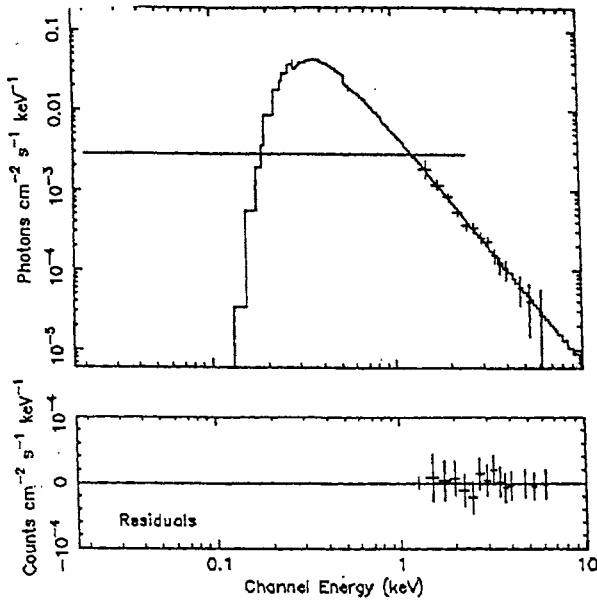


FIG. 2q

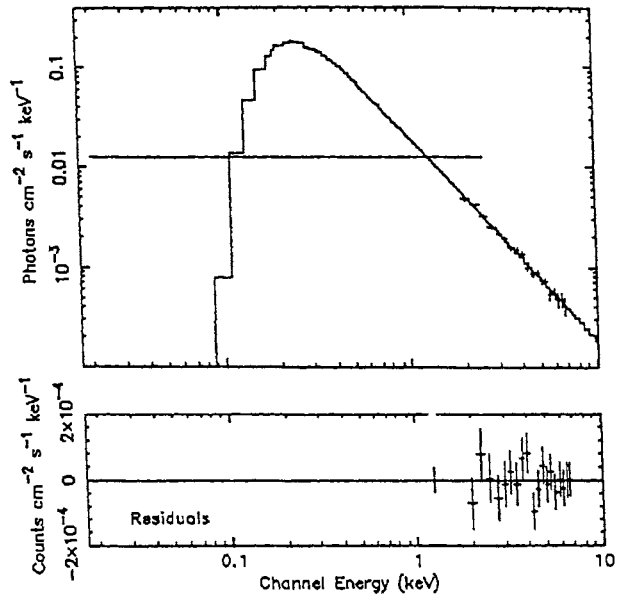


FIG. 2r

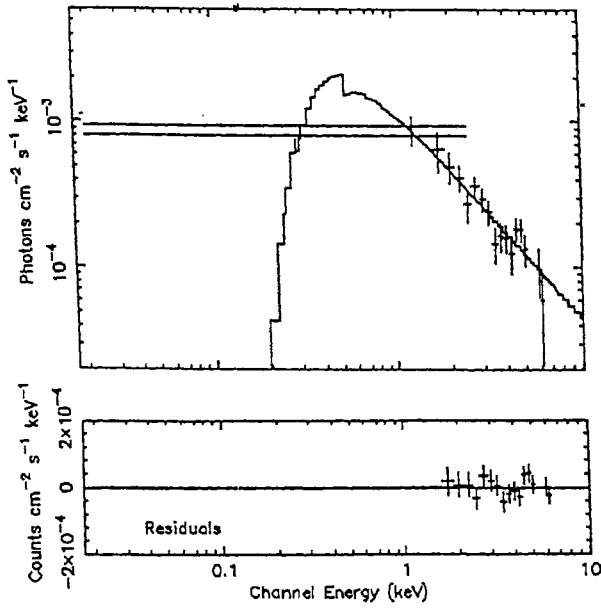


FIG. 2s

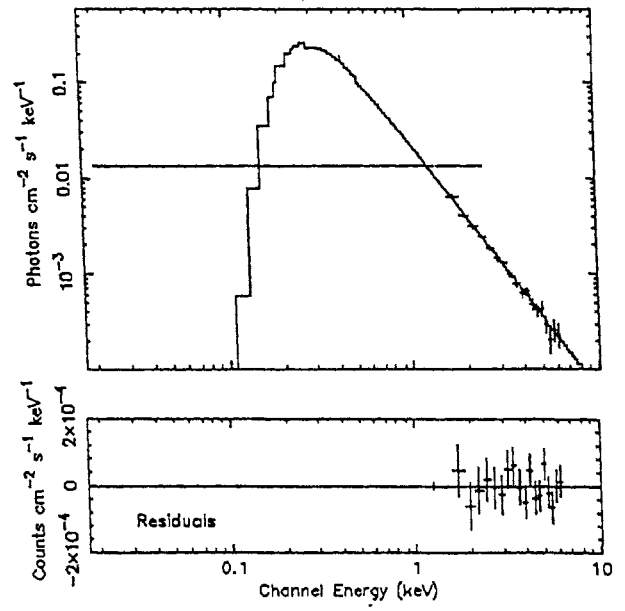


FIG. 2t

Figs. 3.2.2 (continued)

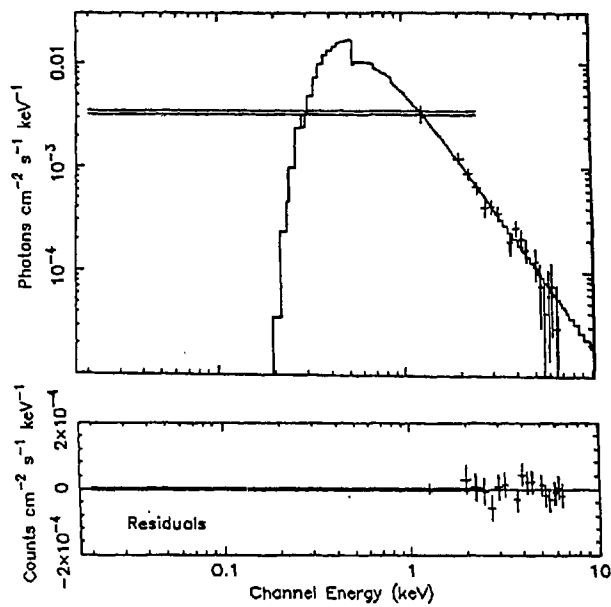


FIG. 2ii

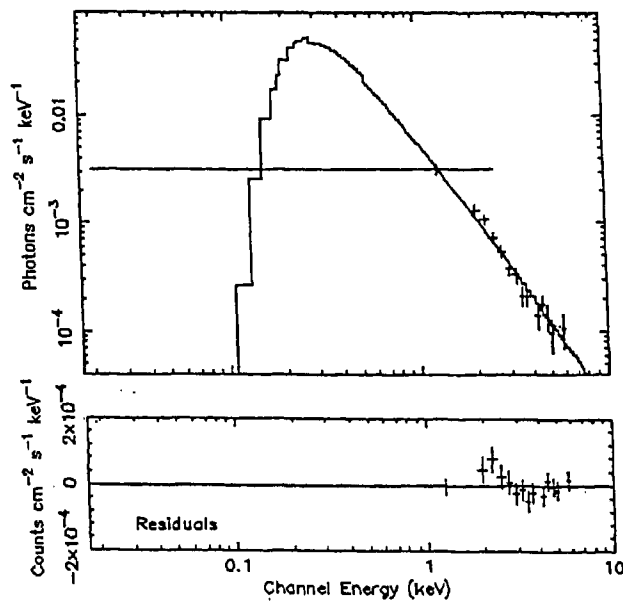


FIG. 2j

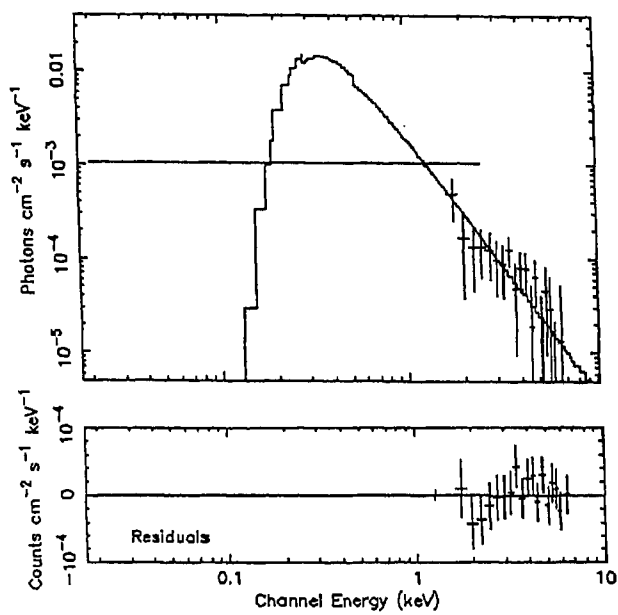


FIG. 2w

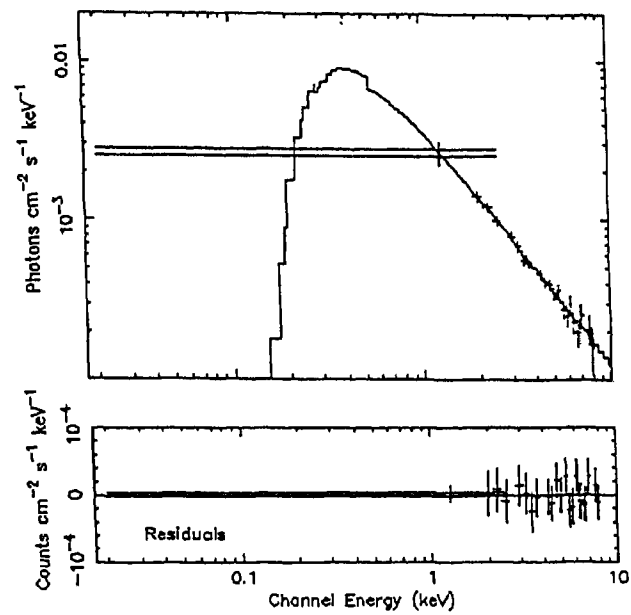


FIG. 2x

Figs. 3.2.2.(continued)

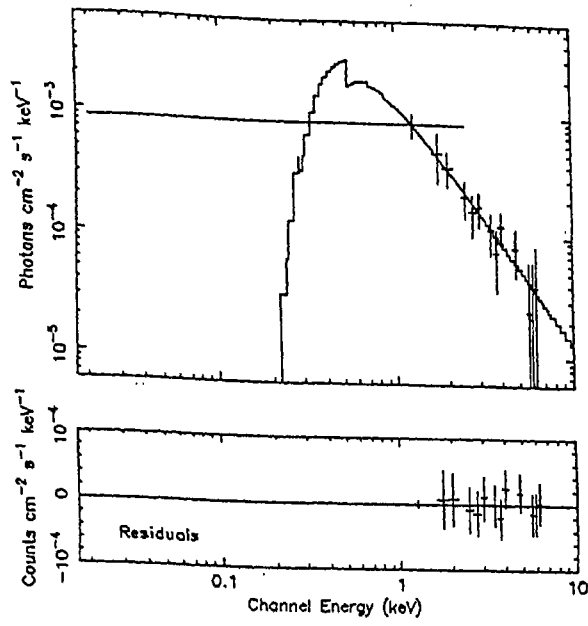


FIG. 2y

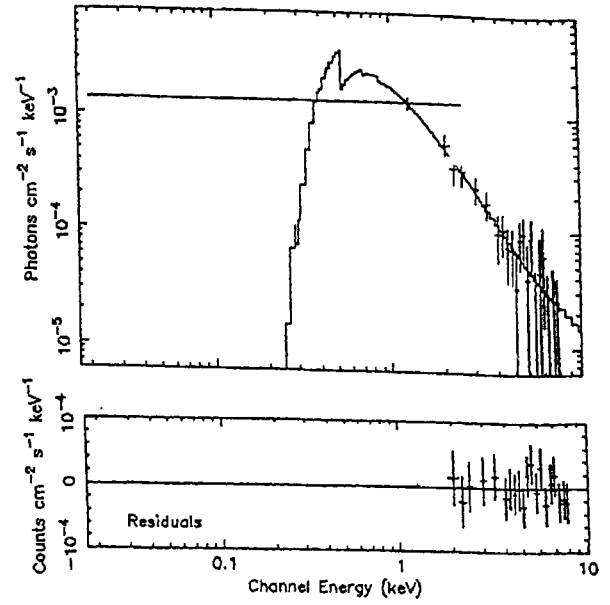


FIG. 2z

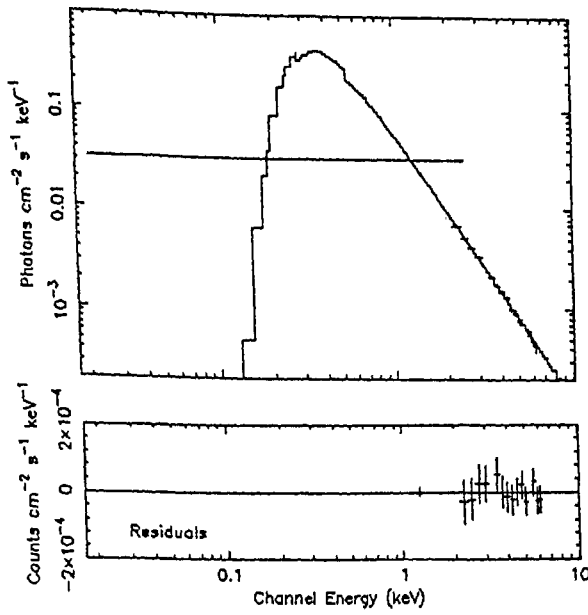


FIG. 2aa

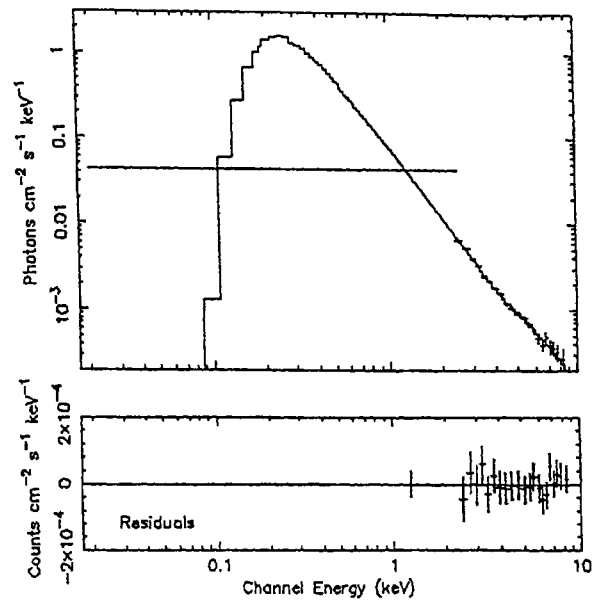


FIG. 2ab

Figs. 3.2.2 (continued)

power-law models to fit the spectra of Mkn 421, 3C273, and PKS 2155-304, The power-law plus fixed absorption plus absorption edge model (or high energy cut off model) fits the spectra of Mkn421 better than the power-law plus fixed absorption model, the power-law plus fixed absorption plus blackbody model, the power-law plus fixed absorption plus thermal bremsstrahlung model, the broken power-law plus fixed absorption model, or the double power-law plus fixed absorption model ( $\Delta\chi^2 > 10$  ; for details see 3.2.4C and 3.2.4D). Similarly, we find that the best fits to the spectra of 3C273 were obtained with the power-law plus fixed absorption plus blackbody model or the power-law plus fixed absorption plus thermal bremsstrahlung model, and these two models resulted in significant improvements ( $\Delta\chi^2 > 10$ ) over other models (for comparison see Tables 3.2.3, 3.2.4D, and 3.2.4E). Spectra of PKS 2155-304 can be best described by the power-law plus fixed absorption plus absorption-edge model or by the broken power-law with fixed absorption model (Tables 3.2.4F and 3.2.4G). The photon spectra of 28 blazars are presented in Figs. 3.2.2a-2ab along with the power-law model. The residuals between the model and spectra are shown in the lower panel of each figure.

### **Multifrequency spectra**

All the objects in the EXOSAT blazar sample are included in the list of Burbidge & Hewitt (1992) and in the catalog of Veron-Cetty & Veron (1993), where many references to radio, optical and X-ray data are listed. We have also surveyed the literature, and from the published results we have selected the average flux value at each energy band (radio, millimetre, infrared and optical), except for far-infrared, ultraviolet and X-rays, for each blazar. Far-infrared, ultraviolet and X-ray fluxes were obtained from the IRAS survey, the IUE Uniform Low Dispersion Archive (ULDA) database (installed on our computer) and the present analysis, respectively. To derive the average fluxes at each frequency, we have imposed a number of criteria to select the data and they are as follows: (1) we have excluded the data during the flare states of the blazars (when the source brightness increased by a factor of 3 or more on timescales of weeks to months, we considered that the source was in flare state); (2) observations of certain objects were simultaneous with the EXOSAT data, and we have selected data only from those observations; (3) for objects for which simultaneous observations are not available, we have selected data from the literature for near-simultaneity observations (when the

observations were made within a week from the EXOSAT observations, those observations were considered as near-simultaneity observations); (4) for objects with multiple EXOSAT observations, we have selected flattest and steepest X-ray spectra for multifrequency continuum energy distribution. Radio through X-ray continuum emission spectra of 28 blazars are plotted in Figs 3.2.3a-n and 3.2.4a-n for RBLs and XBLs respectively. To compute the errors for fluxes plotted in Figs 3.2.3 and 3.2.4, we have followed the following steps. First, for simultaneous observations we have plotted the observational errors with the fluxes at different frequencies. Then we found that the error bars are smaller than the sizes of different symbols used in the multifrequency plots (plotted on logarithmic scale). Next we computed rms deviation errors for nonsimultaneous observations (fluxes were collected from near simultaneity observations). The values of the rms deviation errors were different at different frequencies for different blazars, and in many cases the error bars were smaller than the sizes of different symbols used in the plots. From the computed values of the rms deviation errors, for all the 28 blazars at different frequencies, we have found that the highest value of the error was around 36% of the average flux value of 1928+73 which was observed nonsimultaneously and only on few epochs. Then we decided to plot 40% error bars for all the objects at all frequencies along with the flux values (see Figs. 3.2.3 and 3.2.4). Precise references for the multifrequency plots are given in the figure captions.

We have computed the two point spectral indices, between the two adjacent energy bands,  $\alpha_{12}$  defined by  $\alpha_{12} = -[\log(F_1 / F_2) / \log(\nu_1 / \nu_2)]$ , where  $F_1$  and  $F_2$  are the observed fluxes at the frequencies  $\nu_1$  and  $\nu_2$ , respectively. Computed values of  $\alpha_{12}$  between different energy bands are quoted on each multifrequency plot. It can be seen from the values of  $\alpha_{12}$  that the multifrequency spectra can be fitted with different values of spectral indices which gradually increase from radio to ultraviolet for RBLs and from radio to X-rays for XBLs. Multifrequency spectra of RBLs display spectral discontinuity between the UV and the X-ray region, and it is not present in XBLs. This result has been confirmed using the simultaneous observations at UV and X-rays of 12 blazars (6 RBLs and 6 XBLs) of the present sample (see Figs. 3.2.3d-g, i, k and 3.2.4b,e, f, j,m,n). The multifrequency spectra of 28 blazars presented in this paper are well represented by functions with continuous curvature such as parabolae. Two such parabolae are required to represent the multifrequency spectra of RBLs, and a single parabola is needed for XBLs. Rapid



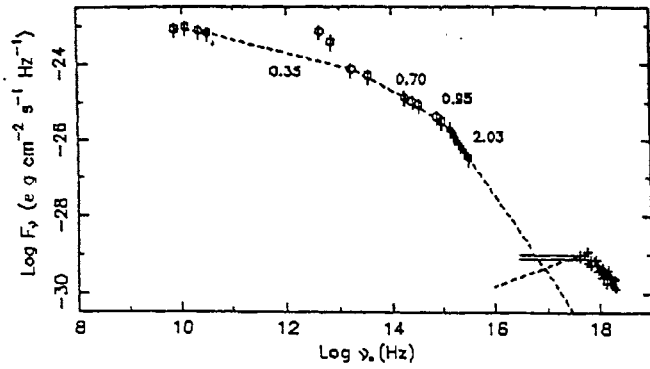


FIG. 3a

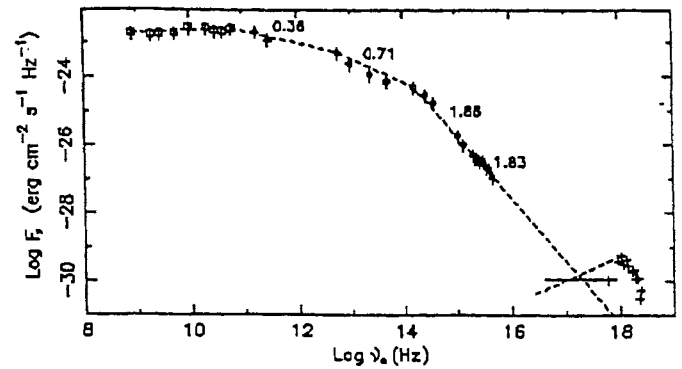


FIG. 3b

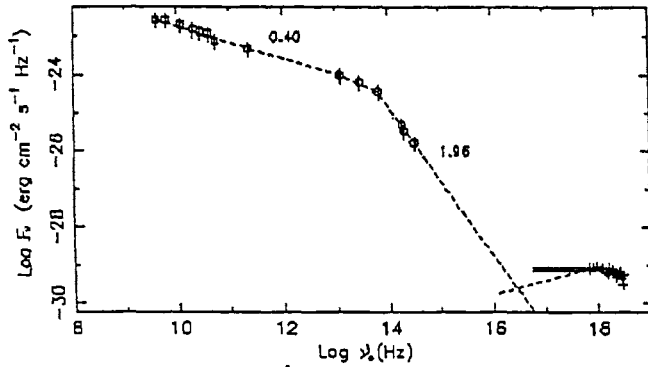


FIG. 3c

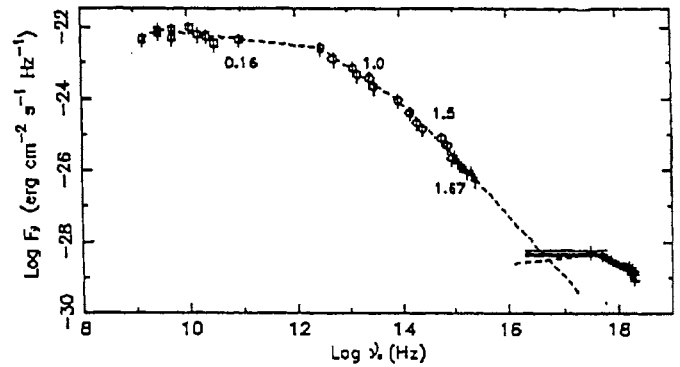


FIG. 3d

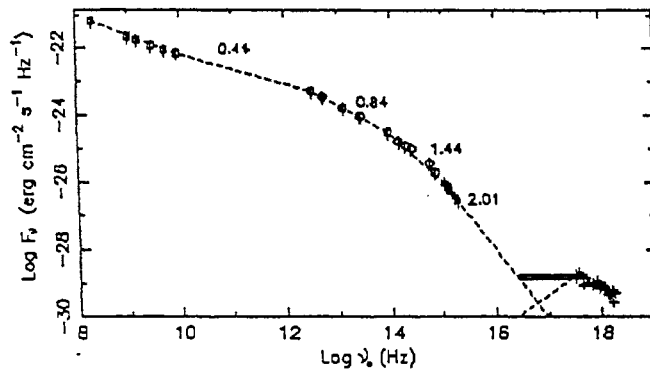


FIG. 3e

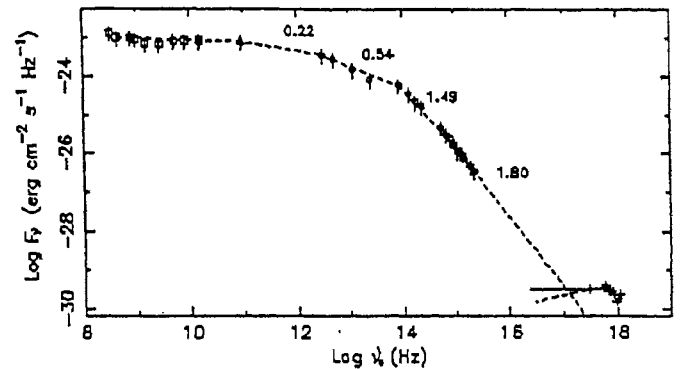


FIG. 3f

(a) Multifrequency spectrum of 3C 66A with two X-ray spectra. Error bars are 40% of the local fluxes. *Open squares*: Worrall et al. (1984b). *Circles*: Impey & Neugebauer (1988); Worrall et al. (1984b). *Filled squares*: IUE-ULDA database. *Plus signs*: present paper. (b) Same as (a), but for the blazar AO 0235+164 with one X-ray spectrum. *Open squares*: Kuhr et al. (1981b); Landau, Epstein, & Rather (1980); Brown et al. (1989). *Triangles*: Brown et al. (1989). *Circles*: Impey & Neugebauer (1988); Brown et al. (1989); Cruz-Gonzalez & Huchra (1984). *Filled squares*: IUE-ULDA database. *Plus signs*: present paper. (c) Same as (a), but for the blazar NRAO 140. *Squares*: Marscher (1988). *Circles*: Neugebauer et al. (1986); Courvoisier, Bell-Burnell, & Blecha (1986). *Plus signs*: present paper. (d) Same as (a), but for the blazar 3C 120. *Open squares*: Kuhr et al. (1981b). *Circles*: Ward et al. (1987); Maraschi et al. (1991). *Filled squares*: IUE-ULDA database. *Plus signs*: present paper. (e) Same as (a), but for the blazar PKS 0521-365. *Open squares*: Kuhr et al. (1981b). *Circles*: Impey & Neugebauer (1988); Cruz-Gonzalez & Huchra (1984). *Filled squares*: IUE-ULDA database. *Plus signs*: present paper. (f) Same as (a), but for the blazar PKS 0754+100 with one X-ray spectrum. *Open squares*: Worrall et al. (1984b); Owen, Spangler, & Cotton (1980). *Triangles*: Owen et al. (1980). *Circles*: Impey & Neugebauer (1988); Worrall et al. (1984b). *Filled squares*: IUE-ULDA database. *Plus signs*: present paper. (g) Same as (a), but for the blazar OJ 287. *Open squares*: Brown et al. (1989); Landau et al. (1980). *Triangles*: Brown et al. (1989). *Circles*: Impey & Neugebauer (1988); Brown et al. (1989); Landau et al. (1986). *Filled squares*: IUE-ULDA database. *Plus signs*: present paper. (h) Same as (a), but for the blazar B2 1147+245 with one X-ray spectrum. *Squares*: Owen et al. (1980). *Circles*: Impey & Neugebauer (1988); Impey et al. (1984); Ledden & O'Dell (1985). *Plus signs*: present paper. (i) Same as (a), but for the blazar 3C 273. *Open squares*: Kuhr et al. (1981b); Landau et al. (1986). *Circles*: Ward et al. (1987); Landau et al. (1986). *Filled squares*: IUE-ULDA database. *Plus signs*: present paper. (j) Same as (a), but for the blazar PKS 1510-089. *Open squares*: Steppe et al. (1988); O'Dea, Barvainis, & Challis (1988). *Circles*: Impey & Neugebauer (1988); Landau et al. (1986). *Filled squares*: IUE-ULDA database. *Plus signs*: present paper. (k) Same as (a), but for the blazar 3C 371 with one X-ray spectrum. *Open squares*: Landau et al. (1986); Kuhr et al. (1981b); Worrall et al. (1984a). *Circles*: Impey & Neugebauer (1988); Worrall et al. (1984a). *Filled squares*: IUE-ULDA database. *Plus signs*: present paper. (l) Same as (a), but for the blazar 3C 390.3. *Open squares*: Kuhr et al. (1981b). *Circles*: Impey & Neugebauer (1988); McAlary et al. (1983). *Filled squares*: IUE-ULDA database. *Plus signs*: present paper. (m) Same as (a), but for the blazar OV 236 with one X-ray spectrum. *Open squares*: Brown et al. (1989); Giacani & Colomb (1988). *Triangles*: Brown et al. (1989); Gear et al. (1986); Roelling et al. (1986). *Circles*: Brown et al. (1989); Impey & Neugebauer (1988); Gear et al. (1986). *Filled squares*: IUE-ULDA database. *Plus signs*: present paper. (n) Same as (a), but for the blazar 1928+73 with one X-ray spectrum. *Open squares*: Kuhr et al. (1981b); Edelson (1987). *Filled squares*: IUE-ULDA database. *Plus signs*: present paper.

### Figs. 3.2.3.

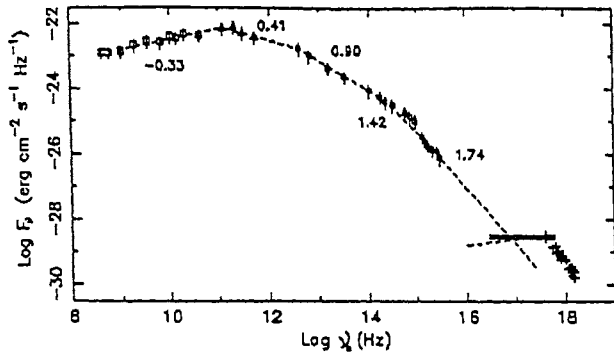


FIG. 3g

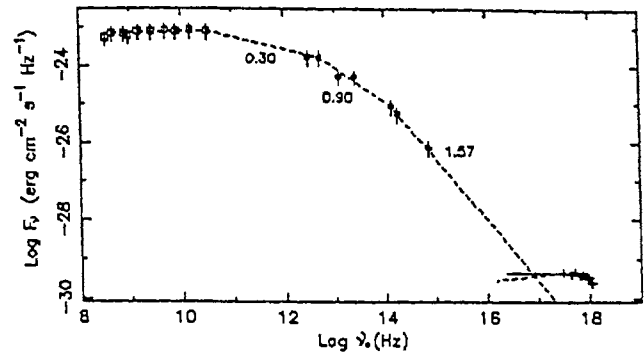


FIG. 3h

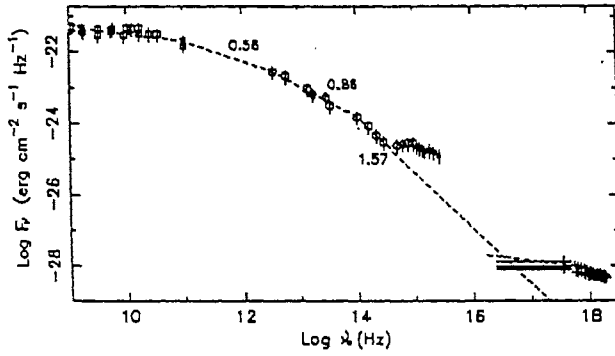


FIG. 3i

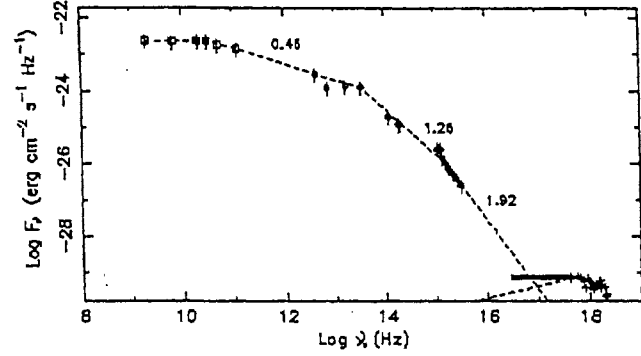


FIG. 3j

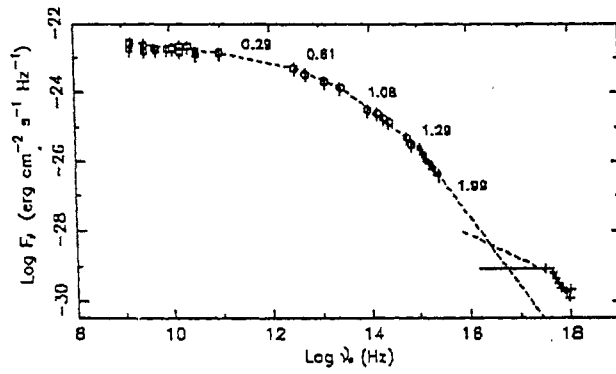


FIG. 3k

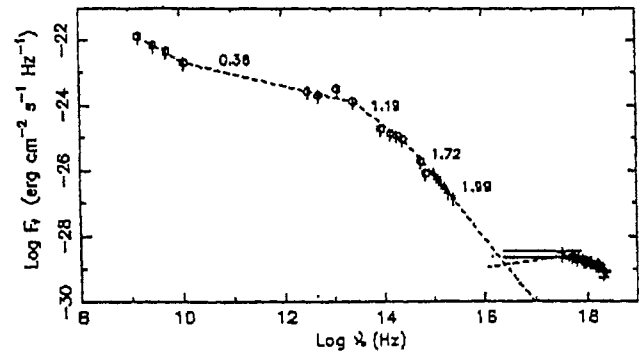


FIG. 3l

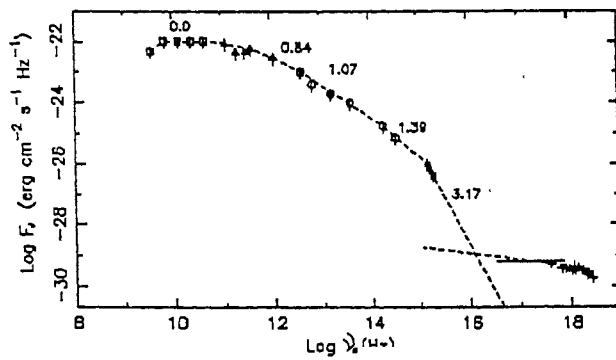


FIG. 3m

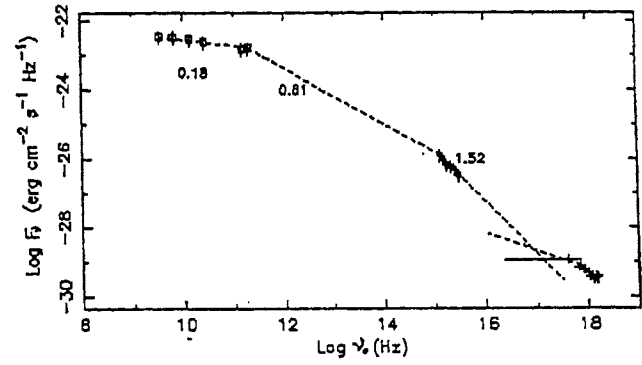


FIG. 3n

Figs. 3.2.3. (continued)

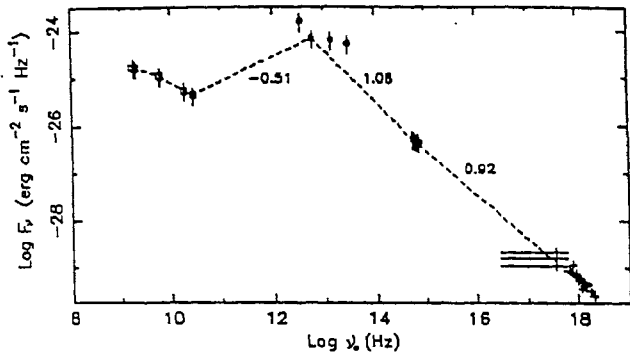


FIG. 4a

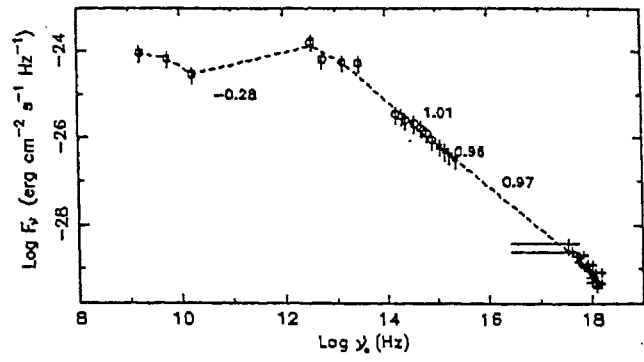


FIG. 4b

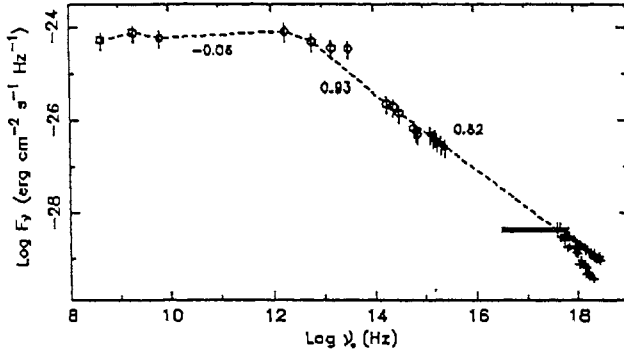


FIG. 4c

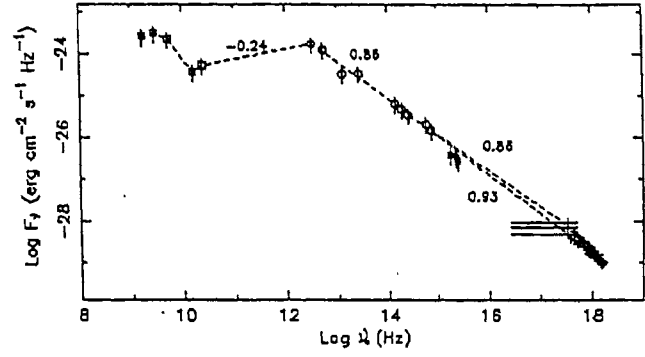


FIG. 4d

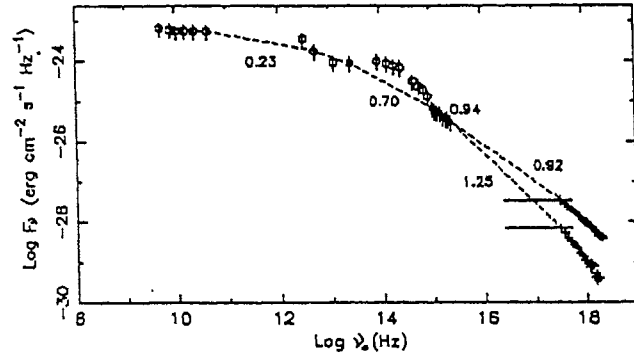


FIG. 4e

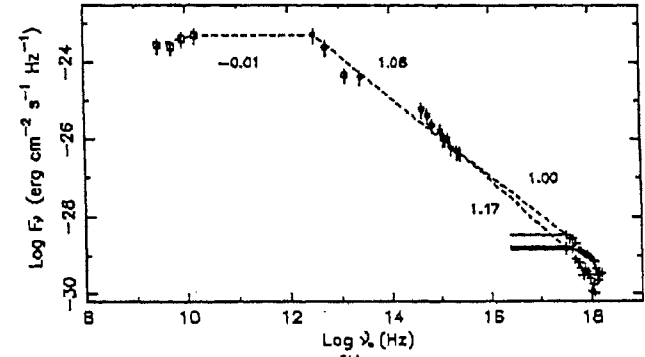


FIG. 4f

—(a) Multifrequency spectrum of 1E 0317+18 with two X-ray spectra. *Squares*: Stocke et al. (1985). *Circles*: Impey & Neugebauer (1988); Stocke et al. (1985). *Plus signs*: present paper. (b) Same as (a), but for the blazar HO323+022. *Open squares*: Feigelson et al. (1986). *Circles*: Impey & Neugebauer (1988); Feigelson et al. (1986). *Filled squares*: IUE-ULDA database. *Plus signs*: present paper. (c) Same as (a), but for the blazar 1H 0414+009. *Open squares*: Ulmer et al. (1983). *Circles*: Impey & Neugebauer (1988); Halpern et al. (1991); Bersanelli et al. (1992). *Filled squares*: IUE-ULDA database. *Plus signs*: present paper. (d) Same as (a), but for the blazar PKS 0548-32. *Open squares*: Cruz-Gonzalez & Huchra (1984). *Circles*: Impey & Neugebauer (1988); Cruz-Gonzalez & Huchra (1984). *Filled squares*: IUE-ULDA database. *Plus signs*: present paper. (e) Same as (a), but for the blazar Mrk 421. *Open squares*: Makino et al. (1987). *Circles*: Impey & Neugebauer (1988); Makino et al. (1987). *Filled squares*: IUE-ULDA database. *Plus signs*: present paper. (f) Same as (a), but for the blazar Mrk 180. *Open squares*: Kuhr et al. (1981a); Mufson et al. (1984). *Circles*: Impey & Neugebauer (1988); Mufson et al. (1984). *Filled squares*: IUE-ULDA database. *Plus signs*: present paper. (g) Same as (a), but for the blazar 1E 1402+04 with one X-ray spectrum. *Squares*: Feigelson et al. (1982). *Circles*: Impey & Neugebauer (1988). *Plus signs*: present paper. (h) Same as (a), but for the blazar 1E 1415+259 with one X-ray spectrum. *Open squares*: Halpern et al. (1986). *Circles*: Impey & Neugebauer (1988); Halpern et al. (1986). *Filled squares*: IUE-ULDA database. *Plus signs*: present paper. (i) Same as (a), but for the blazar 1H 1427+42 with one X-ray spectrum. *Squares*: Remillard et al. (1989). *Circles*: Remillard et al. (1989). *Plus signs*: present paper. (j) Same as (a), but for the blazar Mrk 501. *Open squares*: Angel & Stockman (1980); Kuhr et al. (1981b); Landau et al. (1980); Sembay et al. (1985); Mufson et al. (1984). *Circles*: Sembay et al. (1985); Mufson et al. (1984); Cruz-Gonzalez & Huchra (1984). *Filled squares*: IUE-ULDA database. *Plus signs*: present paper. (k) Same as (a), but for the blazar 4U 1722+119 with one X-ray spectrum. *Squares*: Griffiths et al. (1989). *Circles*: Impey & Neugebauer (1988); Brissenden et al. (1990); Bersanelli et al. (1992). *Plus signs*: present paper. (l) Same as (a), but for the blazar I Zw 186 with one X-ray spectrum. *Open squares*: Bregman et al. (1982). *Circles*: Impey & Neugebauer (1988); Bregman et al. (1982). *Filled squares*: IUE-ULDA database. *Plus signs*: present paper. (m) Same as (a), but for the blazar PKS 2005-489. *Open squares*: Large et al. (1981); Wall et al. (1975); *Circles*: Impey & Neugebauer (1988); Wall et al. (1986); Bersanelli et al. (1992). *Filled squares*: IUE-ULDA database; Wall et al. (1986). *Plus signs*: present paper. (n) Same as (a), but for the blazar PKS 2155-304. *Open squares*: Angel & Stockman (1980); Hjellming, Schnopper, & Moran (1978). *Circles*: Impey & Neugebauer (1988); Treves et al. (1989). *Filled squares*: IUE-ULDA database. *Plus signs*: present paper.

Figs. 3.2.4.

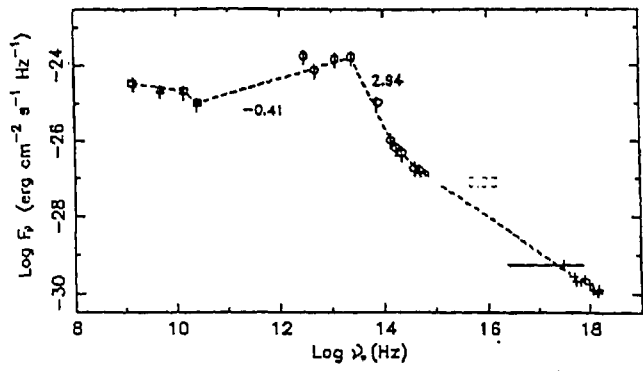


FIG. 4g

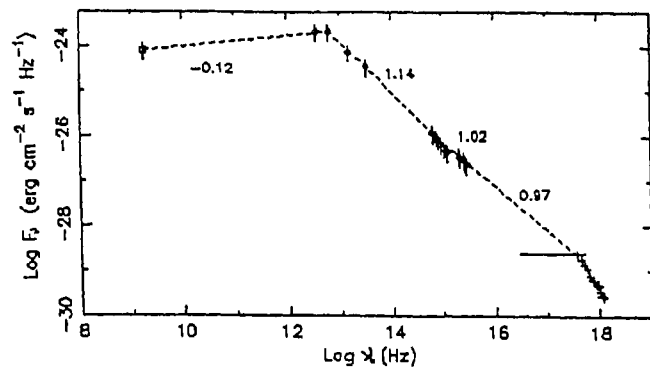


FIG. 4h

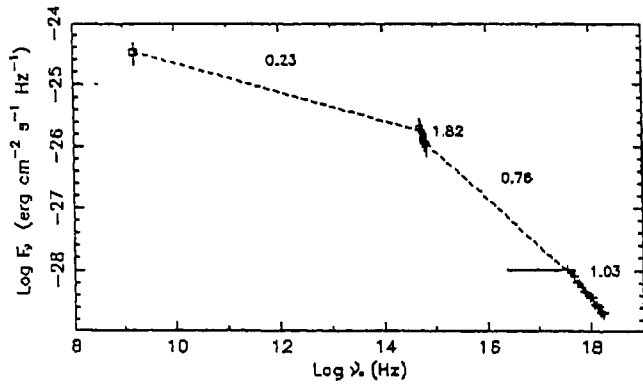


FIG. 4i

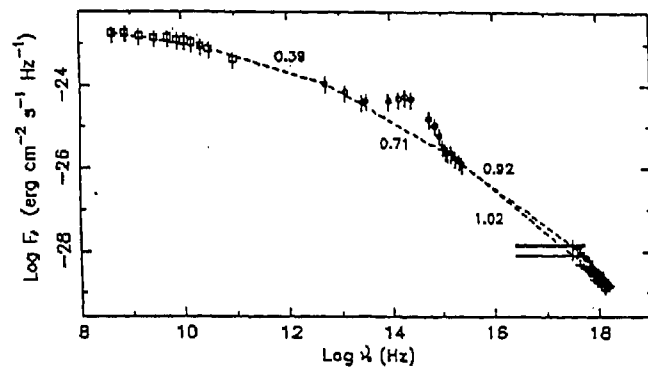


FIG. 4j

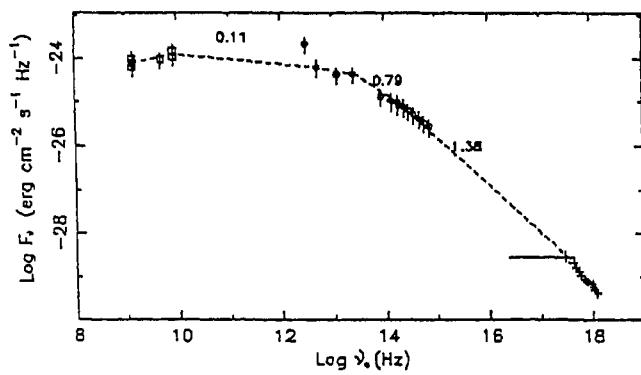


FIG. 4k

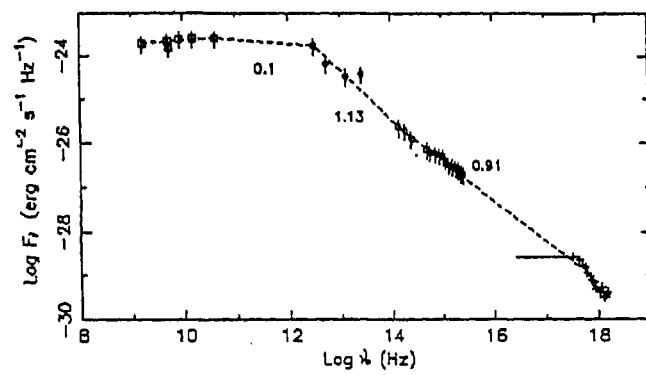


FIG. 4l

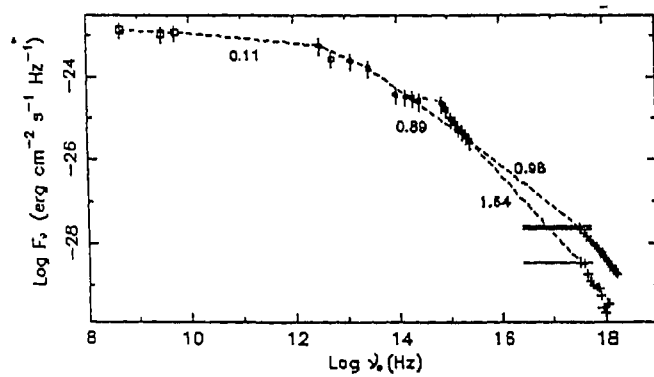


FIG. 4m

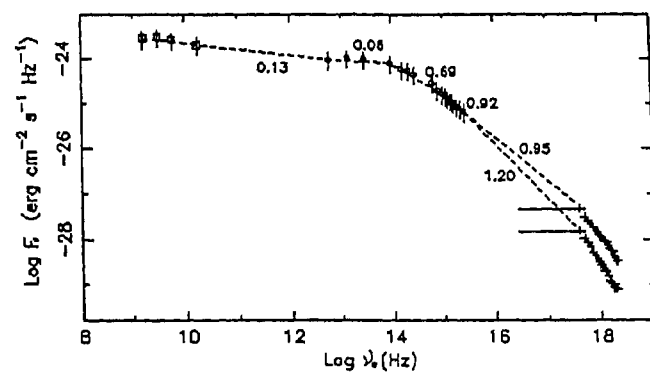


FIG. 4n

Figs. 3.2.4. (continued)

variability of blazars demands that any multifrequency studies need simultaneous or quasi-simultaneous observations. The average continuum energy distribution of blazars presented in this work is based on observations which are partly simultaneous/quasi-simultaneous and partly nonsimultaneous. However, from simultaneous observations, correlated flux variations from infrared to X-ray has been detected in blazars (Brown et al. 1989; Kawai, Bregman & Matsuoka 1989; Makino et al. 1989, 1991 and references therein), and such parallel variations of fluxes at different bands of these objects suggest that the shape of the multifrequency spectrum will not be affected by the variability (Kawai et al. 1989). Additional reasons for the above suggestion are as follows: (1) It may be noted from Figs. 3.2.3 and 3.2.4 that the multifrequency spectra of RBLs and XBLs can be represented by two parabolic components and by a single parabolic component respectively. These two types of multifrequency spectra for RBLs and XBLs have already been noted by other researchers from simultaneous/quasi-simultaneous observations of blazars (Landau et al. 1986; Bregman et al. 1982; Brown et al. 1989; Kawai et al. 1989; Makino 1989; Mufson et al. 1984). (2) Blazars emit radio to X-ray continuum radiation over nearly 8-9 decades in flux ( $\text{erg cm}^{-2} \text{s}^{-1} \text{Hz}^{-1}$ ), and the variability of blazars even by factors 2-3 (except the flares), will not substantially affect the overall shape of the average multifrequency spectra of these objects, which have been plotted on a logarithmic scale (Impey & Neugebauer 1988).

## Results

The X-ray photon index  $\Gamma$  and the radio (5GHz), far-infrared (FIR:60 $\mu\text{m}$ ), near-infrared (NIR:2.2  $\mu\text{m}$ ), optical (5560  $\text{\AA}$ ) UV (2000  $\text{\AA}$ ), and X-ray (2-10 keV) luminosities of 28 blazars are listed in Tables 3.2.5A (for RBLs) and 3.2.5B (for XBLs). Each luminosity was computed using  $H_0 = 50 \text{ km s}^{-1} \text{ Mpc}$ , and  $q_0 = 0$  and assuming isotropic emission. No correction for Galactic extinction was made to the computed luminosities. Measured fluxes at each frequency (except for FIR, UV, and X-ray fluxes) were taken from the literature. Brief results for these objects are given below:

### 3.2.2a. 3C 66A

3C 66A is a well-known blazar (Angel & Stockman 1980), and its optical images appears to be a stellar-like object ( $\theta_{\text{VLA}} \sim 11''$ ). A broad emission line of Mg present in the optical spectrum of this object. It has displayed high optical polarization ( $\sim 16\%$ ; Mead et al. 1990) and large-

TABLE 5A  
HARDNESS RATIO, PHOTON INDEX, AND LUMINOSITIES OF RBLs

Object Name	$\Gamma^a$	$L_3^b$	$L_{60}^c$	$L_{2.2}^d$	$L_O^e$	$L_{UV}^f$	$L_{2-10}^g$
3C 66A .....	1.39	0.66	6.53	28.80	33.50	21.80	7.21
AO 0235+164 .....	1.80	11.40	225.80	648.00	250.40	93.40	27.90
NRAO 140 .....	1.62	22.80	121.50	164.10	45.90	16.80	199.00
3C 120 .....	1.75	0.02	0.33	0.28	0.22	0.09	0.21
PKS 0521-36 .....	1.56	0.06	0.25	0.32	0.17	0.10	0.17
PKS 0754+10 .....	1.70	...	...	...	...	...	...
OJ 287 .....	2.94	0.96	38.40	54.10	33.80	20.10	2.62
B2 1147+245 .....	1.90	...	...	...	...	...	...
3C 273 .....	1.71	2.73	12.55	14.80	6.78	4.02	14.27
PKS 1510-089 .....	1.46	1.69	9.56	16.99	14.90	12.80	6.13
3C 371 .....	2.80	0.01	0.20	0.33	0.30	0.21	0.02
3C 390.3 .....	1.42	0.03	0.17	0.37	0.20	0.07	0.41
OV 236 .....	1.41	3.68	29.40	23.90	1.59	1.85	4.35
1928+73 (4C 73.18) ..	2.25	1.09	52.80	23.10	11.10	7.50	1.40

- <sup>a</sup> X-ray (0.1–10 keV) photon index.
- <sup>b</sup> 5 GHz radio luminosity in  $10^{44}$  ergs  $s^{-1}$ .
- <sup>c</sup> Far-IR (60  $\mu$ m) luminosity in  $10^{45}$  ergs  $s^{-1}$ .
- <sup>d</sup> Near-IR (2.2  $\mu$ m) luminosity in  $10^{45}$  ergs  $s^{-1}$ .
- <sup>e</sup> Optical (5560 Å) luminosity in  $10^{45}$  ergs  $s^{-1}$ .
- <sup>f</sup> UV (2000 Å) luminosity in  $10^{45}$  ergs  $s^{-1}$ .
- <sup>g</sup> X-ray (2–10 keV) luminosity in  $10^{45}$  ergs  $s^{-1}$ .

TABLE 5B  
HARDNESS RATIO, PHOTON INDEX, AND LUMINOSITIES OF XBLs

Object Name	$\Gamma^a$	$L_3^b$	$L_{60}^c$	$L_{2.2}^d$	$L_O^e$	$L_{UV}^f$	$L_{2-10}^g$
0317+18 .....	1.92	1.02	0.11	1.10	2.60	3.13	1.49
H0323+022 .....	2.41	2.10	0.45	5.32	7.32	7.79	1.33
1H 0414+009 .....	2.40	19.20	10.10	17.80	19.20	27.80	8.06
PKS 0548-32 .....	2.02	2.52	1.29	2.06	2.28	2.44	0.67
Mrk 421 .....	2.87	1.48	0.40	1.60	2.41	3.05	0.47
Mrk 180 .....	2.59	1.40	1.48	1.22	1.13	1.06	0.11
1E 1402+04 .....	2.30	...	...	...	...	...	...
1E 1415+259 .....	2.13	8.16	36.50	26.60	22.70	21.50	1.48
1H 1427+42 .....	2.03	1.54	0.23	2.76	8.16	9.81	4.46
Mrk 501 .....	2.47	3.37	0.28	0.73	1.09	1.39	0.17
4U 1722+119 .....	2.38	...	...	...	...	...	...
1Zw 186 .....	2.42	1.17	0.43	0.46	0.55	0.51	0.11
PKS 2005-489 .....	3.21	13.80	5.08	12.00	14.10	15.60	0.61
PKS 2155-304 .....	2.82	11.20	3.30	56.10	85.80	105.00	3.57

- <sup>a</sup> X-ray (0.1–10 keV) photon index.
- <sup>b</sup> 5 GHz radio luminosity in  $10^{41}$  ergs  $s^{-1}$ .
- <sup>c</sup> Far-IR (60  $\mu$ m) luminosity in  $10^{44}$  ergs  $s^{-1}$ .
- <sup>d</sup> Near-IR (2.2  $\mu$ m) luminosity in  $10^{44}$  ergs  $s^{-1}$ .
- <sup>e</sup> Optical (5560 Å) luminosity in  $10^{44}$  ergs  $s^{-1}$ .
- <sup>f</sup> UV (2000 Å) luminosity in  $10^{44}$  ergs  $s^{-1}$ .
- <sup>g</sup> X-ray (2–10 keV) luminosity in  $10^{45}$  ergs  $s^{-1}$ .

Tables 3.2.5A and 3.2.5B

amplitude ( $\Delta B \sim 1.4$  mag) optical variations during the flare states (Cruz-Gonzalez & Huchra 1984). Also, from Fig. 3.2.1, which plots  $\alpha_{\text{ro}}$  against  $\alpha_{\text{ox}}$ , we find that 3C 66A occupies the position in the upper part of the plot where all other RBLs are present. Also, this source has been classified as an RBL (Giommi et al. 1990; Hewitt & Burbidge 1993).

3C 66A was observed with EXOSAT on three occasions between 1986 January 6 and a February 1. On one occasion (1986 January 15) the LE observation was contaminated by the other object in the field, and we have excluded this observation from our analysis. During EXOSAT observations, the LE count rate of this object did not vary, but the ME count rates varied on a timescale of weeks (see Table 3.2.2). Neither the LE nor the ME observations displayed any rapid variability (on timescales of hours) within each single observation. Spectral fits with  $N_{\text{H}}$  free to vary show that the  $\Gamma$  values of the LE+ME spectra are in the range 1.4-2.5, and the lower limit value of  $N_{\text{H}}$  (4 times higher than the Galactic  $N_{\text{H}}$  value) suggests that no significant absorption is present in the X-ray spectra of this source (Table 3.2.3). Our results are in agreement with the results of Maccagni et al. (1987). We have also used other models (power-law plus absorption plus blackbody, power-law plus absorption plus thermal bremsstrahlung, power-law plus absorption plus high-energy cutoff, power-law plus absorption plus absorption-edge, broken power-law plus absorption, and double power-law plus absorption) to fit the X-ray spectra of this RBL. However, we could not find any significant improvement over the power-law plus absorption model ( $\Delta\chi^2 < 2$ ). Measured fluxes from simultaneous observations at radio, NIR, optical, and UV (Worrall et al. 1984b) and nonsimultaneous observations at FIR and X-ray frequencies have been used to construct the multifrequency spectrum of this blazar, which can be well represented by two parabolic components (see Fig. 3.2.3a)

### **3.2.2b. AO 0235+164**

AO 0235+164 is a strong emission-line object (Cohen et al 1987). It is highly variable ( $\Delta V \sim 5$  mag during the flare states) and highly polarized ( $\sim 25\%$ ; Rieke et al 1976; Macleod, Andrew, & Harvey 1976; Ledden, Aller, & Dent 1976; Angel & Stockman 1980; Stickel et al. 1991; Webb et al. 1988; Mead et al 1990) superluminal source (Impey 1987). It is also known as an OVV blazar (Burbidge & Hewitt 1992), and it has been classified as an RBL (Giommi et al 1990; Hewitt & Burbidge 1993). The X-ray spectrum of this source, which was observed on 1984

August 1 by I.McHardy can be well represented by the power-law plus absorption model. Best fit parameters of the spectrum (Table 3.2.3) suggest that no intrinsic absorption is present in this source. We have also used other models, mentioned in Chapter 2.1.3 to fit the spectrum, but other models do not yield significant improvement over the power-law model. The multifrequency spectrum of this blazar was constructed using the measured fluxes from simultaneous observations at radio, millimeter, NIR, and optical wavelength. (Brown et al. 1989) and nonsimultaneous observations at FIR, UV, and X-ray frequencies (Fig.3.2.3b)

### **3.2.2c. IE 0317+18**

IE0317+18 is a BL Lac object (Stocke et al 1989,1990; Burbidge & Hewitt 1992) which has also been classified as an XBL (Giommi et al. 1990; Hewitt & Burbidge 1993). X-ray spectra of this source can be best fitted with the power-law plus absorption model. It is a steep X-ray spectrum source ( $\Gamma \sim 2.4 \pm 0.60$ ; Table 3.2.3 and Giommi et al. 1987), and it did not vary during EXOSAT observations (1985 January 14 and February 9 ). Derived values of  $N_H$  are consistent with the galactic  $N_H$  value. No rapid X-ray variability on the timescales of hours was detected in this source. The radio to X-ray spectrum of this blazar can be represented by a single parabolic curve (Fig. 3.2.4a ).

### **3.2.2d. IH0323+022**

This Blazar is an XBL (Giommi et al 1990; Mead et al. 1990). EXOSAT spectra of this source have been described by the power-law plus absorption model (Sambruna et al. 1993). Results of our spectral analysis are consistent with the results of Sambruna et al. (1993). We have also tried to improve the fit statistics by using other models as mentioned in Chapter 2.1.3 but no significant improvement was found. During the EXOSAT observations the LE flux did not vary but the ME flux varied with the spectral slope. The spectrum hardness when the source brightens, and the measured  $N_H$  is in agreement with the Galactic value. Neither the LE nor the ME fluxes varied on hourly timescales. Measured fluxes from simultaneous observations between radio and optical frequencies have been plotted in Fig.3.2.4b which can be represented by single parabolic curve.



### **3.2.2e. NRAO 140**

NRAO 140 is a broad and strong emission-line quasar (Kristian & Sandage 1970; Burbidge & Strittmatter 1972) with superluminal motion in it (Zensus 1989). It has been classified as an RBL (Hewitt & Burbidge 1993). Details of X-ray observations of this source using HEAO 1, the Einstein Observatory, and EXOSAT are given in Marscher (1988). NRAO 140 was observed with EXOSAT on 1985 January 25 and 26, and no rapid or long term flux (LE and ME) and spectral index variations were noted in this source. The power-law plus absorption model results in the best fit with the spectra of this source. It is a flat spectrum ( $\Gamma \sim 1.5 \pm 0.2$ ) source and it displayed correlated variability of compact radio and X-ray fluxes between 1979 and 1985 (Marscher 1988). Using the simultaneously measured radio and X-ray fluxes and nonsimultaneously measured FIR and optical fluxes, we have constructed the multifrequency spectrum (Fig. 3.2.3c) of this RBL, which can be fitted with two parabolic components.

### **3.2.2f. 1H0414+009**

1H0414+009 is a BL Lac object (Impey & Tapia 1988; Mead et al 1990; Massing et al. 1989; Halpern et al. 1991) and has been classified as an XBL (Giommi et al 1990; Hewitt & Burbidge 1993). It was observed with EXOSAT on four occasions during 1984 September 9-30 (Sambruna et al. 1993). No variations of the LE flux were noticed in this source, but the ME flux varied by a factor of 2 within 16 days (1984 days 258-274). Rapid (on the timescales of hours) variability of the ME flux of this blazar was found on 1984 September 9, which was also noted by Giommi et al.(1990). We have used the power-law plus absorption model and other models mentioned in 2.1.3 to fit the spectra of this XBL. We find that the power law plus absorption model fits the spectra best, and the other models do not differ significantly (i.e., with significance at less than the 5% level) from the power-law model. The best-fit parameters of the spectral analysis are given in Table 3.2.3. From the results of the spectral analysis of 1H 0414+009, we find that the spectral slope steepened when the source intensity (2-10 keV) decreased (Table 3.2.3). The multifrequency spectrum of this source can be represented by a single parabolic component, except for the infrared fluxes, which are much stronger than the radio and optical fluxes (Fig.3.2.4c).

### **3.2.2g. 3C120**

3C120 is a superluminal source (Zensus 1989), and the optical continuum is highly variable (Wierick, Westerlund & Garnier 1979; French & Miller 1980 ; Oke , Redhead & Sargent 1980). It is an OVV-type blazar (Webb et al. 1988; Burbidge & Hewitt 1992). This source was observed on 14 occasions with EXOSAT between 1983 August and 1986 February. Results of simultaneous/quasi-simultaneous observations of this blazar in the optical, ultraviolet, and X-ray bands have been described by Maraschi et al. (1991).

Best-fit parameters of the LE and ME spectra with the power-law plus absorption model are listed in Table. 3.2.3. results of our analysis are consistent with the result of Turner & Pounds (1989) and Maraschi et al. (1991). it may be noted from Table 3.2.3 that the spectral slope ( $\Gamma \sim 1.6-1.94$ ) is correlated with the LE flux and anticorrelated with the ME flux. This result suggests a pivoting of the spectrum around 2 keV. Derived values of  $N_H$  from the power-law fits suggest that no intrinsic absorption is present in this source. Variability in the LE and ME bands with timescales shorter than a day is not found. Using the simultaneous observations of optical, ultraviolet and X-ray bands (Maraschi et al. 1991) and nonsimultaneous observations between radio and IR bands, we have constructed the multifrequency spectrum of this blazar (Fig. 3.2.3d), which shows the spectral discontinuity between UV and X-ray region, and two parabolic components can represent the multifrequency spectrum.

### **3.2.2h. PKS 0521-36**

The optical spectrum of this blazar (Angel & Stockman 1980) is dominated by the permitted and forbidden emission lines (Danziger et al. 1979), very similar to the optical spectrum of the OVV object, 3C 371 (Angel & Stockman 1980). PKS 0521-36 is an optical variable ( $\Delta V > 1$  mag during the flare states) and highly polarized quasar (Angel & Stockman 1980). Angel & Stockman (1980) have classified PKS 0521-36 and 3C 371 (an OVV object ) as the same type of blazar. Also, this source has been classified as an RBL (Giommi et al. 1990; Hewitt & Burbidge 1993).

This RBL was observed on 1983 November 2 and 30 with EXOSAT (Garilli & Maccagni 1990). No rapid or long-term variations of the LE and ME count rates of PKS0521-36 were found during EXOSAT observations. The Power-law plus absorption model and other models,

which were mentioned in Chapter 2.1.3 were used to fit the spectra of this source. F-test analysis shows that the power-law plus absorption model fits best with the spectra of PKS 0521-36. Best fitting parameters of the spectra are given in Table 3.2.3, and it can be seen from this table that PKS 0521-36 is a flat-spectrum ( $\Gamma = 1.7 \pm 0.2$ ) source with no intrinsic absorption. Results of our spectral analysis are in agreement with the results of Garilli & Maccagni (1990). Fluxes from simultaneous observations of radio to optical frequencies were used to draw the multifrequency spectrum of this blazar (Fig. 3.2.3e). Two spectral components are required to represent this spectrum.

### *3.2.2i. PKS 0548-32*

PKS 0548-32 is a BL Lac object (Angel & Stockman 1980; Maccagni et al. 1989; Burbidge & Hewitt 1992), and it is also an XBL blazar (Giommi et al. 1990; Hewitt & Burbidge 1993). It was observed at five epochs with EXOSAT between 1983 and 1986 (Barr, Giommi, & Maccagni 1988; Garilli & Maccagni 1990). This source did not display long-term variability of the ME count rates, but significant rapid variability of the ME count rate was found on 1983 November 2 and 1986 March 7 and 8, which was also noted by Giommi et al. (1990). The parameters of the power-law fit are listed in Table 3.2.3, and they are consistent with the results of Barr et al. (1988) and Garilli & Maccagni (1990). No intrinsic absorption is present in this source. Also we have used different models described in Chapter 2.1.3 and found that the broken power-law model also fits the spectra well but not significantly better than the power-law model (Table 3.2.4A). However, there is a trend of spectral steeping around 2-3 keV (Table 3.2.4A). A single parabola can represent the multifrequency spectrum of this blazar (Fig. 3.2.4d)

### *3.2.2j. PKS 0754+10*

The optical image of this source appears to be a stellar-like object, and it is a compact radio source of  $\theta_{\text{VLA}} \sim 1''.8$ . Optically it is a highly variable ( $\Delta B > 2$  mag during the flare states) and highly polarized ( $P \sim 26\%$ ) object (Angel & Stockman 1980; Mead et al. 1990). It has been classified as an RBL (Giommi et al. 1990; Hewitt & Burbidge 1993). This blazar was observed on 1984 February 12 with EXOSAT, and the spectrum has not been published. The power-law plus absorption model fits the spectrum of this blazar best, it is a flat-spectrum ( $\Gamma = 1.7 \pm 0.2$ ) source (Table 3.2.3). The derived value of  $N_{\text{H}}$  is consistent with the Galactic value. No rapid

variability was found within the single observation of this source. Using the fluxes from simultaneous/quasi-simultaneous multifrequency observations (Worrall et al. 1984b), we have constructed the multifrequency spectrum (Fig. 3.2.3f) of this blazar. Two spectral components are required to represent this multifrequency spectrum.

### 3.2.2k. OJ287

OJ287, which is a superluminal source (Porcas 1987), has displayed both sharp and broad emission lines in its optical spectrum (Miller, French & Hawley 1978; Sitko & Junkkarinen 1985; Stickel et al. 1991). It is an optical variable ( $\Delta V > 3$  mag during the flare states) and highly polarized (32%) blazar (Angel & Stockman 1980; Mead et al. 1990). It has been classified as an RBL (Giommi et al. 1990; Hewitt & Burbidge 1993). This blazar was observed on many occasions with EXOSAT, but only two spectra have single significance above  $4\sigma$  (Table 3.2.2). The power-law plus absorption model and other models that were mentioned in Chapter 2.1.3. were used to fit the spectra of this RBL. From F-test analysis we find that the power-law model fits the spectra best. Result of the spectral analysis are given in Table 3.2.3. Photon index values of the two spectra in the 0.1-5 keV range, are slightly steeper than those usually found in RBLs. However, from *Ginga* observations it has been inferred that this RBL is a flat X-ray spectrum source (Makino 1989). Values of  $N_H$  are very close to the Galactic value. Fluxes from simultaneous radio through X-ray observation (Brown et al. 1989) were used to construct the multifrequency spectrum of this RBL, and it has been plotted in Fig. 3.2.3g.

### 3.2.2l. Mkn 421

This blazar (Angel & Stockman 1980; Maccagni et al. 1989; Burbidge & Hewitt 1992) has been classified as an XBL object. It was observed on many epochs with EXOSAT and IUE between 1984 and 1985 (George, Warwick & Bromage 1988a; Edelson et al. 1992). X-ray spectra of this blazar were fitted using a power-law plus absorption model, and the fitting parameters are listed in Table 3.2.3. This model fitted all the spectra well, except for three spectra of this source when it was in a brighter state (1984: days 337, 338 and 340). Next we have used other models, mentioned in Chapter 2.1.3, to fit the three spectra. From F test analysis we find that, among all these models, the power-law plus absorption plus high-energy cutoff and the power-law plus absorption plus absorption-edge models, fit best with the three spectra and these two models are

highly significant compared with the simple power-law model ( $\Delta\chi^2 > 15$ , which is significant at better than 99.9% level). Results of the fit parameters are listed in Tables 3.2.4B and 4C suggest that no intrinsic absorption is present in Mkn 421. It has displayed rapid and correlated variability of the ME count rate with the hardness ratio, which was also noted by Giommi et al. (1990). Derived values of  $\Gamma$  and ME fluxes (Table 3.2.3) are also correlated (George et al. 1988a). Simultaneous observations of radio through X-rays were used to construct the multifrequency spectrum of Mkn 421 (Makino et al 1987), and it can be fitted by a single parabolic curve (Fig. 3.2.4e). The presence of the blue emission bump can also be seen in this figure.

### **3.2.2m. Mkn180**

Mkn180 is a BL Lac object (Angel & Stockman 1980; Maccagni et al. 1989; Burbidge & Hewitt 1992). It has been classified as an XBL (Giommi et al 1990; Hewitt & Burbidge 1993). X-ray spectra of this source were obtained with EXOSAT on 1984 November 28 and 1985 April 3 (George, Warwick & McHardy 1988b). Both the LE and ME fluxes increased by a factor of 2 between the EXOSAT observations. Correlated variability of the ME count rate and the hardness ratio of the source was also noted in this blazar (Giommi et al. 1990). X-ray spectra of Mkn180 (Fig. 3.2.2m) are best fitted with the power-law plus absorption model (Table 3.2.3), and our results are in good agreement with that of George et al. (1988b). Mkn180 is a steep-spectrum source with no intrinsic absorption. Radio to X-ray fluxes were obtained from simultaneous and quasi-simultaneous (Mufson et al. 1984) observations of Mkn180 and were used to construct the multifrequency spectrum (Fig.3.2.4f), which can be fitted with a single parabola.

### **3.2.2n. B2 1147+245**

This blazar (Angel & Stockman 1980; Ledden & O'Dell 1985; Stickel et al. 1991; Burbidge & Hewitt 1992) has been classified as an RBL (Giommi et al 1990; Hewitt & Burbidge 1993). It was observed with EXOSAT on 1984 January by A.P. Willmore, but the results have not been published. We have carried out detailed spectral analysis and have found that the power-law plus absorption model fits best with the spectrum of this source. Results of the analysis are listed in

Table 3.2.3. The value of  $N_H$  is consistent with the Galactic value. Radio through X-ray continuum emission fluxes can be well represented by two parabolic curves (Fig.3.2.3h)

### **3.2.2o. 3C 273**

3C 273 is a superluminal source (Zensus 1989), and it has been classified as an RBL object (Giommi et al. 1990; Hewitt & Burbidge 1993). This blazar was observed with EXOSAT on six occasions between 1984 and 1986. Both EXOSAT and Ginga observations of this source have been described by Turner et al. (1990; and references therein). We used the power-law plus absorption model to fit the EXOSAT spectra of 3C 273, but the derived values of  $N_H$  are smaller than galactic value. Next we fitted the spectra using the power-law plus fixed absorption model, and the results are listed in Table 3.2.3. It can be seen from this table that the reduced  $\chi^2$  values are very large, which suggests that the fits to the fits to the spectra are not acceptable. then we tried to fit the spectra using all the models mentioned in 2.1.3. From the F-test analysis (using Tables 3.2.3, 3.2.4D, and 3.2.4E) we find that the power-law plus blackbody and thermal bremsstrahlung plus fixed absorption models fit the spectra best, and also these two models are highly significant (>99.99%) over the power-law model. Simultaneous multifrequency observations of this source were carried out at different epochs (Landau et al. 1986; Courvoisier et al. 1990 and references therein), and the results of such observations were used to construct the multifrequency spectrum of this RBL (Fig. 3.2.3i) which can be represented by two parabolic curves.

### **3.2.2p. IE 1402+04**

IE 1402+04 is a BL Lac object (Ledden & O'Dell 1985; Stock et al. 1990; Burbidge & Hewitt 1992) and is also known as an XBL (Giommi et al.1990; Hewitt & Burbidge 1993). It was observed at three epochs with EXOSAT (Giommi et 1986, 1987), but only one spectrum has signal significance above  $4\sigma$  . This spectrum can be best modeled by a power-law plus fixed absorption model (see Table 3.2.3). Rapid X-ray variability, on time scales of hours, was detected in this blazar, which was also noted by Giommi et al. (1990). Radio, far-infrared, infrared, optical, and X-ray fluxes of this XBL are plotted in Fig.3.2.4g. Optical to X-ray fluxes can be fitted by a smooth curve. However, because of the steep radio spectrum and

nonavailability of measured millimeter fluxes, we are not sure about the nature of the multifrequency spectrum between radio and infrared frequencies.

### **3.2.2q. IE 1415+259**

IE 1415+259 is an XBL (Impey & Tapia 1988; Maccagni et al. 1989; Burbidge & Hewitt 1992; Hewitt & Burbidge 1993), and it was observed on 1986 March 7 with EXOSAT (Giommi et al. 1987). The X-ray spectrum of this blazar can be best described by a power-law plus absorption model (Fig.3.2.2u). No rapid variability of this source was noted within the single observation. The multifrequency spectrum of this source, which was constructed using nonsimultaneous observations, can be represented by a single parabolic curve (Fig.3.2.4h).

### **3.2.2r. IH 1427+42**

IH 1427+42 is an XBL (Maccagni et al. 1980; Remillard et al 1989; Burbidge & Hewitt 1992; Giommi et al. 1990; Hewitt & Burbidge 1993). It was observed with EXOSAT on 1985 January 12 . The power-law plus absorption model fits this spectrum best (Table 3.2.3). This blazar is a steep-spectrum ( $\Gamma = 2.10 \pm 0.07$ ) source with no intrinsic absorption (Remillard et al. 1989). The radio through X-ray spectrum of this blazar is shown in Fig.3.2.4i, and it can be represented by a single parabolic spectral component.

### **3.2.2s. PKS 1510-089**

PKS 1510-089 was confirmed as a blazar by Moore & Stockman (1984) and Smith et al. (1987). It is one of the most violently variable ( $\Delta V \sim 5.4$  during the flare states) and highly polarized quasar (Moore & Stockman 1981; Ledden & O'Dell 1985; Mead et al. 1990; Burbidge & Hewitt 1992). This blazar has been classified as an RBL (Hewitt & Burbidge). Two spectra of this source, obtained with EXOSAT, have signal significances above  $4\sigma$ , and these two spectra can be best fitted with power-law plus absorption model; the parameters are listed in Table 3.2.3. Variations of the LE and ME fluxes, on time-scales of hours, are absent in this source. There is no detection of any significant low-energy absorption within this flat spectrum. Results of our spectral analysis are consistent with the results of Singh, Rao & Vahia (1990). Radio through X-ray continuum fluxes of this object are shown in Fig.3.2.3j, and the spectrum can be well represented by two parabolic components.

### **3.2.2t. Mkn501**

Mkn 501 is a well-known BL Lac object (Angel & Stockman 1980; Maccagni et al. 1989; Stickel et al. 1991; Burbidge & Hewitt 1992). It has been classified as an XBL (Giommi et al. 1990; Hewitt & Burbidge 1993). Mkn 501 was observed on many occasions with EXOSAT. In Table 3.2.2 we have listed only those observations which have signal significance above  $4\sigma$ . Details of X-ray observations of this source with *Uhuru*, *Ariel V*, *HEAO 1* and *2*, and EXOSAT are given in Staubert et al. (1986a), and EXOSAT and IUE observations are given in George et al. (1988b) and Edelson et al. (1992). Correlated variability of the ME count rates with the hardness ratio of this source was detected from EXOSAT observations (Giommi et al.). This blazar also displayed rapid variability of the ME flux on timescale hours. To fit the spectra of Mkn 501, we have used different models, mentioned in 4.1. we have found that the power-law plus absorption model fits these spectra best. Results of the fit parameters show that Mkn 501 is a steep-spectrum (Fig.3.2.2x) source with no intrinsic absorption (Table 3.2.3). The multifrequency spectrum of this XBL was constructed using simultaneous/quasi-simultaneous multifrequency observations (Mufson et al. 1984; Sembay et al 1985). This spectrum (Fig.3.2.4j) can be represented by a single spectral component.

### **3.2.2u. 4U 1722+119**

4U 1722+119 is an X-ray- selected BL Lac object ( Griffiths et al. 1989; Brissenden et al. 1990; Burbidge & Hewitt 1992; Hewitt & Burbidge 1993; Giommi et al. 1990). The X-ray spectrum of this blazar, observed with EXOSAT, can be best fitted with the power-law plus absorption model. The fit parameters are listed in Table 3.2.3, and it can be seen from this table that 4U 1722+119 is a steep-spectrum source with no intrinsic absorption. Using the fluxes from nonsimultaneous observations, we have constructed the multifrequency spectrum of this blazar, which can be fitted with a single parabolic curve (Fig.3.2.4k).

### **3.2.2v. I Zw 186**

I zw 186 is a BL Lac object ( Angel & Stockman 1980; Maccagni et al. 1989 ; Burbidge & tt1992), and it has been classified as an XBL ( Giommi et al. 1990; Hewitt & Burbidge ). The EXOSAT spectrum of this blazar can be best described by power-law plus absorption model. The best-fitting spectral parameters are listed in Table 3.2.3, and our results are in agreement



with the results of Garilli & Maccagni (1990). Simultaneous observations at radio, NIR, and optical frequencies (Bregman et al. 1982) and nonsimultaneous observations at FIR, UV, and X-rays were used to construct the multifrequency continuum energy distribution of this blazar, which can be fitted with a single parabolic spectral component (Fig. 3.2.4)

### 3.2.2w. 3C 371

3C 371 is an optically violent variable object (Angel & Stockman 1980; Webb et al. 1988; Stickel et al. 1991; Burbidge & Hewitt 1992) and is also a superluminal source (Mutel 1989). Which has been classified as a RBL (Giommi et al. 1990; Hewitt & Burbidge 1993). EXOSAT observations of this blazar were carried out on 1984 September 11 and 29 (Staubert, Brunner, & Worrall 1986b), but only the spectrum of September 11 has signal significance above  $4\sigma$ . In the present analysis we have used only this spectrum, which can be best fitted with a power-law plus fixed absorption model. Best-fitting parameters are listed in Table 3.2.3. Results of our analysis are in agreement with that of Staubert et al. (1986b). Using the simultaneous observations at radio, NIR, Optical and UV wavelengths during 1981 May (Worrall et al. 1984a), radio and millimeter wavelengths during 1983 March-April (Landau et al. 1986), and UV and X-rays during September 29 and 30, 1984, we have constructed the multifrequency spectrum of this blazar (Fig.3.2.3k), and it can be well represented by two parabolic spectral components.

### 3.2.2x. 3C390.3

3C 390.3 is a radio galaxy and is also called a highly polarized quasar (Angel & Stockman 1980; Ledden & O'Dell 1985; Burbidge & Hewitt 1992). It is also known as a superluminal source (Porcas 1987), and we have classified this blazar as an RBL. This source was observed with EXOSAT on many occasions between 1984 and 1986, but only three spectra have signal significances above  $4\sigma$ . Detailed results of the X-ray spectral analysis of this blazar, based on EXOSAT observations, have been described by Ghosh & S.Soundararajaperumal (1991). We have used different models to fit the spectra and have found that only the broken power-law plus fixed absorption and the power-law plus fixed absorption plus emission line models fit slightly better than the power-law plus fixed absorption model, but these two models are not statistically

significant ( $\Delta\chi^2 \sim 2 - 4$ ) over the power-law plus absorption model. Radio through X-ray continuum fluxes of this RBL can be fitted with two parabolic components (Fig. 3.2.3l).

### **3.2.2y. OV 236**

OV 236 is a highly polarized quasar as well as an optically violent variable blazar (Ledden & O'Dell 1985; Pica et al. 1988; Mead et al. 1990; Burbidge & Hewitt 1992). It is also known as an RBL object (Hewitt & Burbidge 1993). The X-ray spectrum of this blazar can be best described by a power-law plus absorption model (Table 3.2.3). The multifrequency spectrum (Fig. 3.2.3m) of this luminous source has been constructed using the fluxes from simultaneous observations at radio, millimeter, NIR, and optical wavelengths (Brown et al. 1989) and nonsimultaneous observations at UV and X-rays.

### **3.2.2z. 1928+73**

The object 1928+73 is a superluminal source (Zensus 1989), and it is known as a HPQ/OVV-type blazar (Burbidge & Hewitt 1992; Ghosh & S.Soundararajaperumal 1992), and it has also been classified as an RBL (Hewitt & Burbidge 1993). It was observed with EXOSAT at four epochs between 1983 and 1984, but only two spectra have signal significances above  $4\sigma$ . Detailed spectral analysis of this source has been described by Ghosh & S.Soundararajaperumal (1992). Best fitting parameters of the power-law plus absorption model are listed in Table 3.2.3. This source displayed uncorrelated variability of the LE and ME fluxes. Variations of this type indicate that the LE and ME fluxes have different origins (Ghosh & S.Soundararajaperumal 1992; Turner et al. 1990). A soft excess for such sources may not be significant above the extrapolation of the ME power-law, but the distribution of their fluxes indicate a separate component. The multifrequency spectrum of this blazar is shown in Fig. 3.2.3n, and it can be represented by two parabolic curves.

### **3.2.2aa. PKS 2005-489**

Pks 2005-489 is an X-ray-selected BL Lac object (Stickel et al. 1991; Burbidge & Hewitt 1992; Giommi et al. 1990). It was observed on five occasions with EXOSAT in 1984 and 1985. Out of five observations, only three have signal significance above  $4\sigma$ . These three spectra were best fitted with the power-law plus absorption model (Table 3.2.3). It can be seen from Tables

3.2.2 and 3.2.3 that the spectral slope flattened as the ME count rate of the source increased. Also, rapid variability of the ME count rate was observed in this source (Giommi et al. 1990). Using the simultaneous observations at UV and X-rays and nonsimultaneous observations at radio, FIR, NIR, and optical frequencies, we have constructed the multifrequency spectrum of this source, which can be fitted with a single parabolic curve. A weak emission bump around the near-infrared and optical bands is present, and there is no discontinuity in the UV-X-ray region (Fig. 3.2.4m).

### **3.2.2ab. PKS 2155-304**

PKS 2155-304 is a well studied XBL (Angel & Stockman 1980; Mead et al. 1990; Maccagni et al. 1989; Burbidge & Hewitt 1992; Giommi et al. 1990; Hewitt & Burbidge 1993). Simultaneous multifrequency observations of this blazar were carried out during EXOSAT observations, and correlated flux variability at different frequencies was observed in this source (Treves et al. 1989). The power-law plus absorption model was used to fit the LE and ME spectra, but this model did not fit well with the spectra of this blazar ( $\chi^2_r > 2$ ). Next we have used several other models and from the F-test analysis we find that the spectra of PKS 2155-304 can be best described by the power-law plus fixed absorption plus absorption-edge model (Table 3.2.4F) or by the broken power-law with fixed absorption model (Table 3.2.4G). The derived values of  $N_H$  are consistent with the Galactic value. Results of our spectral analysis are consistent with the results of Treves et al. (1989). PKS 2155-304 has displayed the same type of spectral variability in X-rays as was seen in PKS2005-489 (Morini et al. 1986; Giommi et al. 1990; also see Tables 3.2.2 and 3.2.3). The multifrequency spectrum of this source, which has been constructed using fluxes at different frequencies from simultaneous observations, is also similar to that of the XBL PKS 2005-489 (Fig. 3.2.4n).

### **3.2.3. International Multifrequency Monitoring Campaign Results of Blazars**

Variability is one of the salient properties of AGNs and a powerful constraint on models for these sources. Observations show that blazars are characterized by rapid and large amplitude continuum variations over the entire electromagnetic spectrum. Beaming and relativistic boosting are considered to cause the rapid large amplitude variations in these objects.

Relativistic shock propagating down a jet and its interaction with irregularities in the flow can cause the observed variations (e.g., Maraschi et al. 1989; Qian et al. 1991; Marscher, Gear & Travis 1992). In this picture electrons diffuse from high to low energies so the amplitude of variability is expected to be larger at higher energies and the higher energy variations are expected to precede the lower energy variations. It is believed that radio through UV continuum in radio-selected blazars (RBLs) and radio-through X-ray continuum in X-ray selected blazars (XBLs) originate in a beamed jet of plasma motion through synchrotron process (Ghosh & Soundararajaperumal 1995). Synchrotron Self-Compton (SSC) process is made responsible for the higher energy emission in these sources (Jones, O'Dell & Stein 1974; Konigl 1981; Ghisellini et al. 1992; Marscher, Gear & Travis 1992). The observed correlation between lower energy synchrotron components and high energy SSC components in certain objects (e.g. BL Lac, 3C446; Bregman et al. 1988, 1990) proves this suggestion. The size of emitting regions are inferred by the variability studies. Casualty arguments limit the radius of the emitting region to,  $r < c\Delta t/(1+z)$ , with the light travel time  $\Delta t$  corresponding to timescale of variations (Wagner & Witzel, 1995; and references therein). The typical timescales of variability in blazars is months to years in the radio region, days in optical and hours in the X-ray region (Bregman 1990). Radio-quiet AGNs mostly show smaller amplitude variations in the IR, optical and UV bands which may be of completely different origin, e.g., instabilities in accretion disks.

Although single waveband variability studies can provide details on the source sizes, energy densities, etc., for a better understanding of the continuum and line emission process as well as the geometry of the innermost unresolvable regions in these objects, variability monitoring in multiwavebands will be more effective. Now it has become possible to combine simultaneous observations taken at different wavebands and with different ground-based and space-bound telescopes through large international collaborative efforts. We participated in such collaborative programs to monitor six blazars (PKS0528+13, Mkn501, 3C390.3, BL Lac, 3C446, CTA102) and a Seyfert (Fairall 9). Results of our simultaneous multifrequency monitoring program on the luminous Seyfert 1 galaxy (Fairall 9) are presented in Chapter 3.1.2. In this Chapter we present the results of a ground-based optical monitoring campaign by the International AGN Watch consortium (Alloin et al. 1994; Dietrich et al. 1998) on 3C390.3 in 1994-1995. We present the

TABLE 3.2.6A SOURCE LOG OF CAMPAIGN BLAZARS

Source	Position (1950)		Redshift $z$	$m_V$	$M_{abs}$
	R.A.	Dec.			
PKS0528+13	05 28 07	+13 29 42	2.07	20.00	-26.0
Mkn501	16 52 12	+39 50 25	0.033	13.78	-22.4
3C390.3	18 45 37	+79 43 06	0.057	15.38	-21.6
BL Lac	22 00 39	+42 02 09	0.069	14.72	-22.4
3C446	22 23 11	-05 12 17	1.404	18.39	-26.2
CTA102	22 30 08	+11 28 23	1.037	17.33	-26.6

**TABLE 3.2.6B. LOG OF VISUAL OBSERVATIONS OF BLAZARS**

Object	z	Date of observation	Telescope (m)	No of obs	UT (start)	Integ. (s)	Filter	
PKS0528+13	2.07	1997 02 02	2.34	1	13:57	1800	V	
		1997 02 04	2.34	1	14:05	1800	V	
		1997 02 06	2.34	1	16:05	1800	V	
		1997 02 11	2.34	1	13:56	2400	V	
		1997 02 12	2.34	1	13:39	1800	V	
		1997 02 13	2.34	1	15:10	1800	V	
		1997 02 14	2.34	2	14:15	1800	V	
						14:51	1800	V
		1997 03 05	2.34	2	14:20	1800	V	
						15:10	1800	V
		1997 03 07	2.34	1	15:09	1800	V	
Mkn501	0.33	1997 03 16	2.34	10	21:47	600	V	
					22:00	600	V	
					22:12	600	V	
					22:24	600	V	
					22:38	600	V	
					22:50	600	V	
					23:02	600	V	
					23:14	600	V	
					23:26	600	V	
					23:39	600	V	
		23:50	600	V				
		1997 04 29	2.34	8	20:59	900	V	
					21:28	600	V	
					21:43	600	V	
					21:55	600	V	
					22:07	600	V	
					22:22	600	V	
					22:36	600	V	
					22:48	600	V	
		1997 04 30	2.34	7	19:13	600	V	
					19:26	600	V	
					19:42	600	V	
					19:54	600	V	
			20:06	600	V			
			20:18	600	V			
			20:30	600	V			

**TABLE 3.2.6B. - continued**

Object	z	Date of observation	Tele-scope (m)	No of obs	UT (start)	Integ. (s)	Filter
Mkn501 (contd.)	0.33	1997 05 02	2.34	13	19:00	600	V
					19:14	600	V
					19:25	600	V
					19:38	600	V
					19:51	600	V
					20:04	600	V
					20:17	600	V
					20:30	600	V
					20:54	600	V
					21:08	600	V
					21:21	600	V
					21:34	600	V
					21:46	600	V
	1997 06 01	2.34	10	16:41	600	V	
				16:54	600	V	
				17:08	600	V	
				17:21	600	V	
				17:32	600	V	
				17:44	600	V	
				17:56	600	V	
				18:33	600	V	
				18:45	600	V	
				18:57	600	V	
				1997 06 06	1.02	3	20:21
	20:57	1200	V				
	21:19	1200	V				
	1997 06 07	1.02	2	21:27	1800	V	
21:44				1800	V		
1997 06 08	1.02	8	16:22	1200	V		
			16:44	1200	V		
			17:12	1200	V		
			18:15	1800	V		
			18:44	1200	V		
			19:05	1200	V		
19:29	1200	V					
			19:52	1200	V		

TABLE 3.2.6B. - continued

Object	z	Date of observation	Telescope (m)	No of obs	UT (start)	Integ. (s)	Filter
Mkn501 (contd.)	0.33	1997 06 09	1.02	6	16:01	1800	V
					16:51	1800	V
					17:21	1800	V
					18:07	1800	V
					18:48	1800	V
					19:27	1800	V
		1997 06 15	2.34	5	18:50	900	V
					19:08	900	V
					19:26	900	V
					19:44	900	V
					20:01	900	V
3C390.3	0.057	1995 03 07	2.34	2	23:39	600	V
					23:57	420	V
		1995 03 08	2.34	2	23:16	900	V
					23:35	900	V
		1995 03 11	2.34	2	23:20	900	V
					23:37	900	V
		1995 04 08	1.02	1	23:26	1200	V
		1995 05 22	1.02	1	22:41	1800	V
		1995 05 23	2.34	1	23:03	1200	V
		1995 05 29	1.02	1	21:13	1800	V
		1995 05 25	2.34	3	22:20	900	V
					22:39	900	V
					22:56	900	V
		1995 06 07	2.34	1	21:23	1200	V
		1995 06 08	1.02	2	21:01	1800	V
					21:35	1800	V
					1995 06 09	1.02	3
					21:00	2700	V
					22:50	2700	V
					1995 06 29	2.34	2
			20:38	900	V		
			1995 07 03	2.34	2	18:56	1200
			21:23	1200	V		
			1995 09 24	2.34	1	16:46	900
1995 10 13	2.34	2	14:05	600	V		
			14:19	600	V		



TABLE 3.2.6B. - continued

Object	z	Date of observation	Telescope (m)	No of obs	UT (start)	Integ. (s)	Filter			
BL Lac	0.069	1997 08 02	2.34	9	16:44	300	I			
					16:53	300	I			
					17:53	300	I			
					17:01	300	I			
					18:09	300	I			
					18:18	300	I			
					18:49	300	I			
					18:35	300	I			
					18:43	300	I			
		1997 08 23	1.02	7	20:02	600	B			
					20:13	600	B			
					20:26	600	B			
					20:39	600	B			
					20:51	600	B			
					21:06	600	B			
					21:20	600	B			
					1997 08 29	1.02	6	18:41	1800	B
								19:14	1800	B
		19:47	1800	B						
		20:20	1800	B						
		20:53	1800	B						
		21:26	1800	B						
		1997 08 31	1.02	6	18:06	1800	B			
					19:30	1800	B			
					20:04	1800	B			
					20:36	1800	B			
					21:09	1800	B			
21:42	1800				B					
1997 09 01	1.02	5	20:22	1800	B					
			20:57	1800	B					
			21:32	1800	B					
			22:06	1800	B					
			22:39	1800	B					
1997 09 13	1.02	2	17:00	1800	B					
			17:55	1800	B					

TABLE 3.2.6B. - continued

Object	z	Date of observation	Tele-scope (m)	No of obs	UT (start)	Integ. (s)	Filter
BL Lac (contd.)	0.069	1997 09 14	1.02	2	20:58	1800	B
					21:29	1800	B
		1997 09 19	1.02	2	16:46	1800	B
					17:52	1800	B
		1997 09 26	1.02	1	17:58	1800	B
		1997 09 28	1.02	2	16:51	1800	B
					17:29	2700	B
		1997 09 28	2.34	1	18:16	600	V
		1997 10 08	2.34	4	16:14	1800	V
					16:47	1800	V
17:19	1800				V		
17:51	1800				V		
3C446	1.404	1997 06 07	2.34	2	21:59	2400	V
					22:44	2400	V
		1997 06 08	2.34	3	21:40	2400	V
					22:28	2400	V
					23:11	1800	V
		1997 06 15	2.34	3	20:34	2400	V
					21:21	2400	V
					22:05	2400	V
					22:17	1800	V
					22:53	1800	V
CTA102	1.037	1997 05 30	2.34	2	22:17	1800	V
					22:53	1800	V
		1997 06 05	2.34	3	21:30	1500	V
					22:01	1800	V
					22:36	1800	V
		1997 06 08	1.02	4	21:29	1800	V
					22:01	1800	V
					22:33	1800	V
					23:05	1800	V

optical photometric and spectroscopic observations of 3C390.3 that were obtained as a part of this campaign that covered over eight decades in frequency. For the remaining sources (PKS0528+13, Mkn501, BL Lac, 3C446 and CTA102) the massive works of data coordination, reduction and combined spectral and photometric analysis are in progress. Consequently, the results of our optical CCD imaging photometry alone are presented in this chapter for these five blazars in which four (PKS0528+13, Mkn501, BL Lac, and CTA102) were monitored in simultaneity with CGRO. Celestial coordinate, redshift, apparent visual magnitude and absolute magnitude for our sample of six blazars are listed in Table 3.2.6A. Log of observations is presented in Table 3.2.6B.

The CCD observations were carried out in the B, V, R and I photometric passbands using the 2.34m VBT and the 1m telescope of Vainu Bappu Observatory. Details of optical instrumentation, detector characteristics and image reduction procedures are presented in Chapter 2.2.

## Results

### 3.2.3a. PKS0528+13

$\gamma$ -ray blazars have been identified as a distinct class of objects through observations of the *Energetic Gamma Ray Experiment Telescope* (EGRET) on the *Compton Gamma Ray Observatory* satellite (von Montigny et al. 1995a). So far EGRET has detected 51 AGNs, and all of them are blazars (Mukherjee et al. 1996). Their properties include intense and variable emission at energies exceeding 100 MeV, a variable flat radio spectrum, apparent superluminal motion and optical polarization.  $\gamma$ -ray emission has not been detected from a substantial fraction of blazars not otherwise differentiable from  $\gamma$ -ray blazars (von Montigny et al. 1995b). A thorough multiband and polarization studies of these  $\gamma$ -ray loud sources, will be helpful to understand the properties that separate them from the rest. PKS0528+13 is one of the brightest AGNs ( $M_V \sim -26.0$ ) detected by the EGRET (Mukherjee et al. 1996). This is a compact flat spectrum radio source displaying superluminal motion (Pohl et al. 1995). Although this source is identified as a radio-loud quasar in certain catalogues, it displays all the characters of a blazar, namely, a nonthermal continuum spectrum (Mukherjee et al. 1996), a flat radio spectrum (Kühr

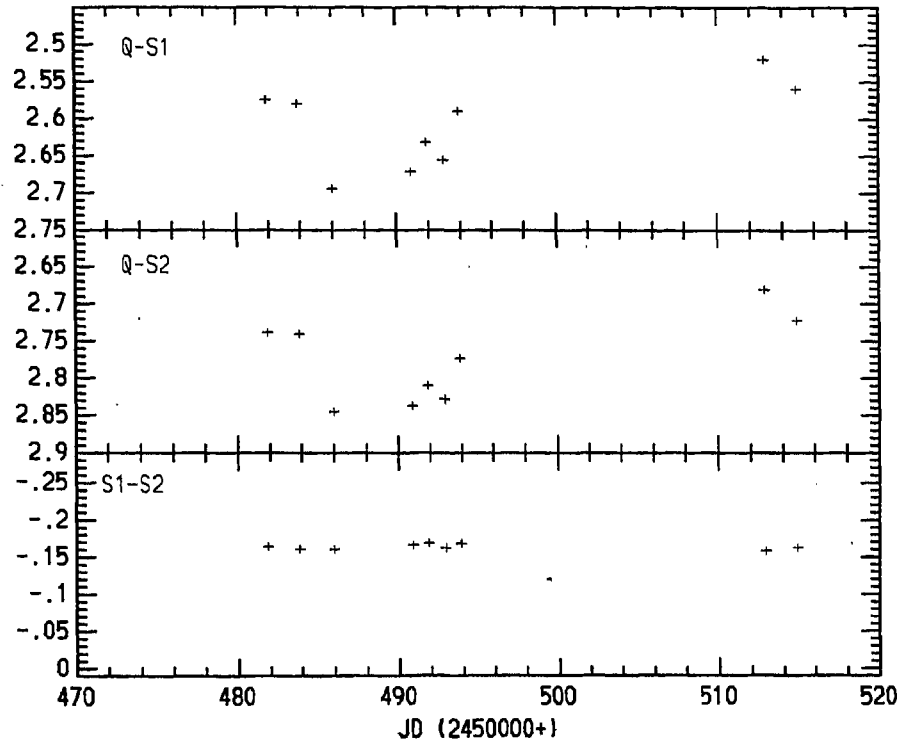


Fig.3.2.7 Differential photometric light curve of PKS0528+15 in V band

et al. 1981), strong variability (Aller et al. 1985; Zhang et al. 1994; Mukherjee et al. 1996), and optical polarization (Fugmann & Meisenheimer 1988). PKS0528+13 displayed a high amplitude variations in  $\gamma$ -ray flux in 1993 March (Mukherjee et al. 1996). During the flare the  $\gamma$ -ray flux displayed correlated variations with the radio flux. No simultaneous optical data are available during the flare. However, we monitored this source on nine nights during February, March 1997 in V band with the VBT (Table 3.2.6B), when another  $\gamma$ -ray flare was detected in this source (Hartman 1997). Although the  $\gamma$ -ray results are not available immediately for comparison, the optical data clearly shows gradual night to night variations during this period (Fig 3.2.7). The V band flux was found to drop by  $\sim 0.15$  magnitude within two days, remained steady for  $\sim 4$  days and recovered  $\sim 0.15$  magnitude again in about 3 days time during February observations. In March it was found to be in high state again. Telescope time restrictions prevented us to monitor this source beyond the first week of March 1997.

### 3.2.3.b. *Mkn501*

Markarian 501 (Mkn501) is one of the nearest ( $z=0.034$ ) and brightest blazar. Based on the spectral energy distribution the source is classified as an XBL (Ghosh & S.Soundararajaperumal 1995; also see Chapter 3.2.1). Mkn501 is one of the only three extragalactic sources (Mkn501, Mkn421, 1ES2344+514) so far detected at TeV energies (Pian et al. 1998; Quin et al. 1996). The correlated variability from soft X-rays to the TeV band, found in this blazar (Pian et al. 1998) points to models in which the same population of relativistic electrons produces the X-ray continuum via synchrotron radiation and the TeV emission by SSC process. For the first time in any blazar the synchrotron power is observed to peak at hard X-ray energies, during the flaring of this source in 1997 April (Pian et al. 1998). Usually blazars are found to peak at UV/soft X-ray regime (e.g., Kubo et al. 1997). Assuming the SSC model for the origin for this large shift of the synchrotron peak frequency during the flare implies that intrinsic changes in the relativistic electron spectrum caused the increase in the emitted power.

When the source was in high state, we observed the blazar Mkn501 in V band using the VBT and the 1m telescope of VBO, Kavalur, in March - June 1996 as a part of a multiwavelength campaign involving ground based TeV Cerenkov telescopes (Whipple, HEGRA and CAT), plus

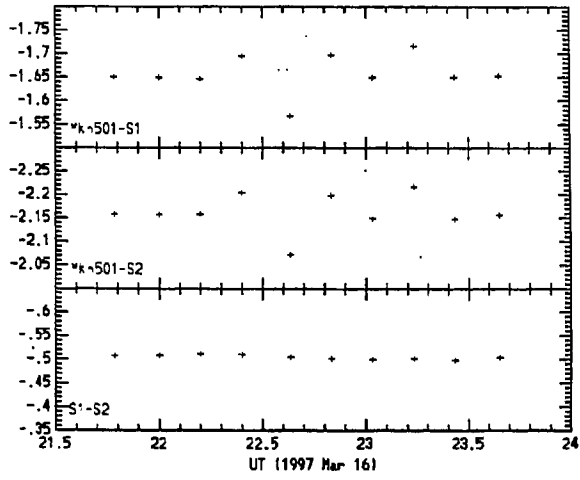


Fig.3.2.8a Differential intranight light curve of Mkn501 in V band

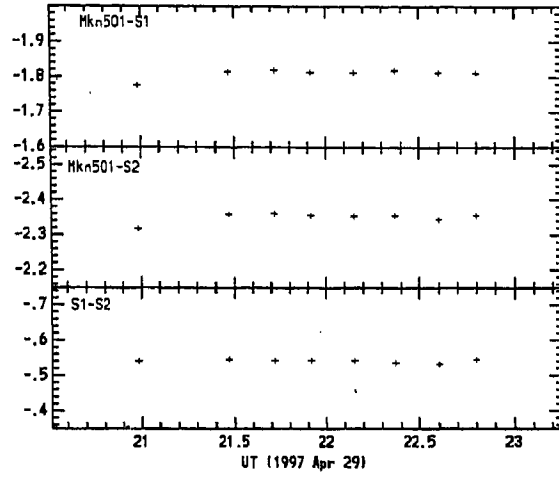


Fig.3.2.8b Same as Fig.3.2.8a but for different date

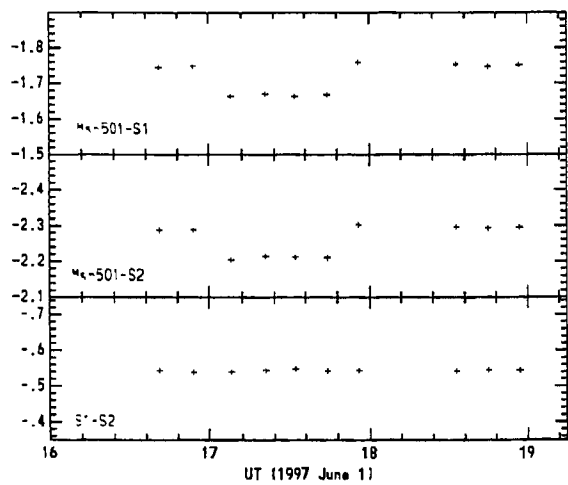


Fig.3.2.8c Same as Fig.3.2.8a but for different date

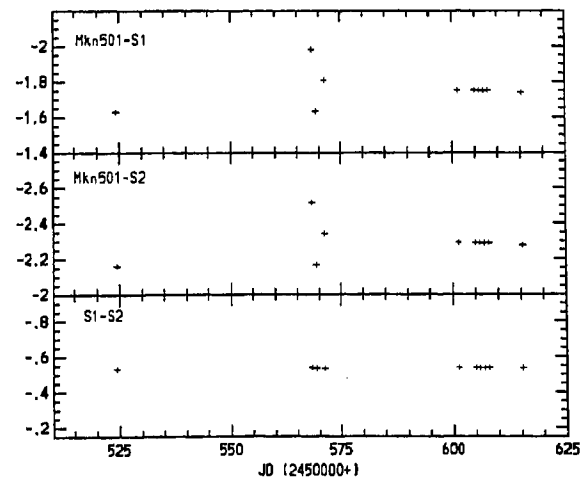


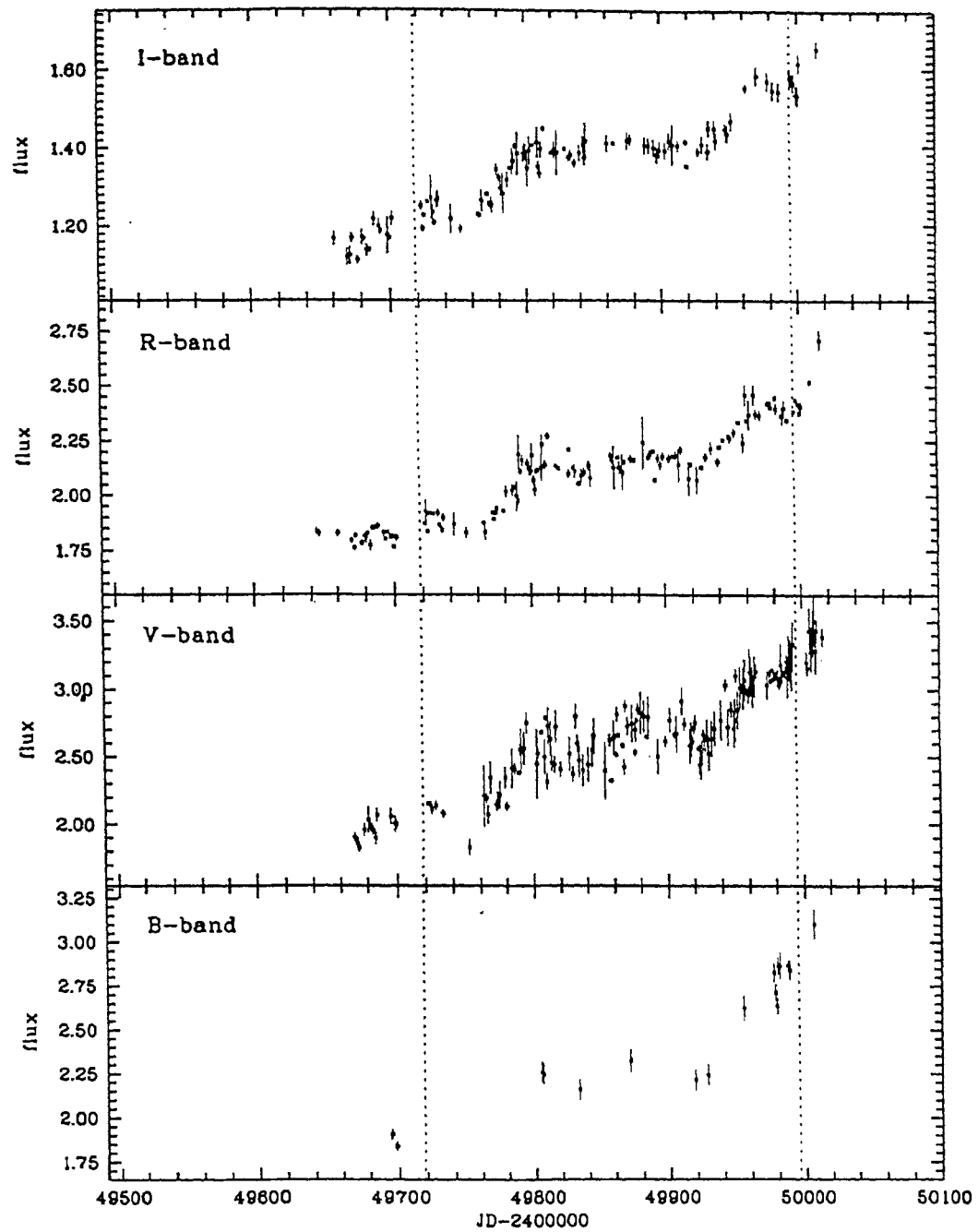
Fig.3.2.8d Differential photometric light curve of MKN501 in V band

other satellites like *CGRO*, *Infrared Space Observatory* and *SAX* (Italian and Dutch 0.1-200 keV X-ray satellite). Preliminary X-ray results are presented by Pian et al. (1998). A log of our optical CCD observations is presented in Table 3.2.6B. Rapid and large amplitude variations were found in this blazar during our observations. In April 29, 30, the source had displayed a dramatic 0.5 magnitude variation within a day (Fig. 3.2.8d). On three nights of March 16, April 29 and June 1 (Figs. 3.2.8a-c) the source was found to display intranight microvariabilities. Preliminary analysis show correlated variations of optical and hard X-ray to  $\gamma$ -ray continua (Pian et al. 1998). However, the amplitude of variations in the optical band are very small compared to the hard X-ray and  $\gamma$ -ray variations. An increase of the bolometric luminosity by a factor of  $\geq 20$  with respect to previous epochs was detected in hard X-ray and  $\gamma$ -ray bands of Mkn501 during April 1996 (Pian et al. 1998; Catanese et al. 1997). Optical observations taken during April 7 - 15 with the 1.2m Ritchey-Chretien telescope of the Whipple Observatory also show similar variations like our results in the UBVRI bands (Catanese et al. 1997; and references therein).

### 3.2.3.c. 3C390.3

In late 1994, the International AGN Watch group (Alloin et al. 1994; Dietrich et al. 1998) began a multiwavelength monitoring campaign on the blazar 3C390.3, a prominent nearby ( $z=0.056$ ) AGN. 3C390.3 has a well-known variability history (e.g., Selmes & Perez 1984; Veilleux & Zheng 1991; Zheng 1996; Wamsteker et al. 1997). Zheng (1996) and Wamsteker et al. (1997) analyzed the IUE spectra of 3C390.3 that have been taken from 1978 until 1992. The variable broad Ly  $\alpha$  and C IV emission are delayed by  $\sim 60$  days with respect to the UV continuum variations. 3C390.3 is an extended double lobed FR II radio source (Leahy & Perley 1995) with a 60" one-sided narrow jet. This is a highly polarized quasar (Angel & Stockman 1980; Ledden & O'dell 1985; Burbidge & Hewlett 1992) that shows superluminal motions, with  $v/c \sim 4.0$  (Alef et al. 1996). Based on the multifrequency behaviour, this source has been classified as a RBL by Ghosh & S.Soundararajaperumal (1995; also see Chapter 3.2.1).

The photometric observations were made through different combinations of broadband filters. We monitored this blazar using the 1m and 2.34m (VBT) telescopes of Vainu Bappu Observatory, Kavalur between 1995 May 7 and 1995 October 13 on 15 nights. A log of



—Optical broadband light curves of 3C 390.3 from 1994 October to 1995 October. Fluxes are in units of  $10^{-15}$  ergs  $s^{-1}$   $cm^{-2}$   $\text{\AA}^{-1}$ . The larger uncertainties of the *V*-band measurements might be due to a lower signal than in the *R*-band measurements that contain the broad  $H\alpha$  emission. The dashed vertical lines mark the temporal range of the X-ray observations.

Fig. 3.2.9a



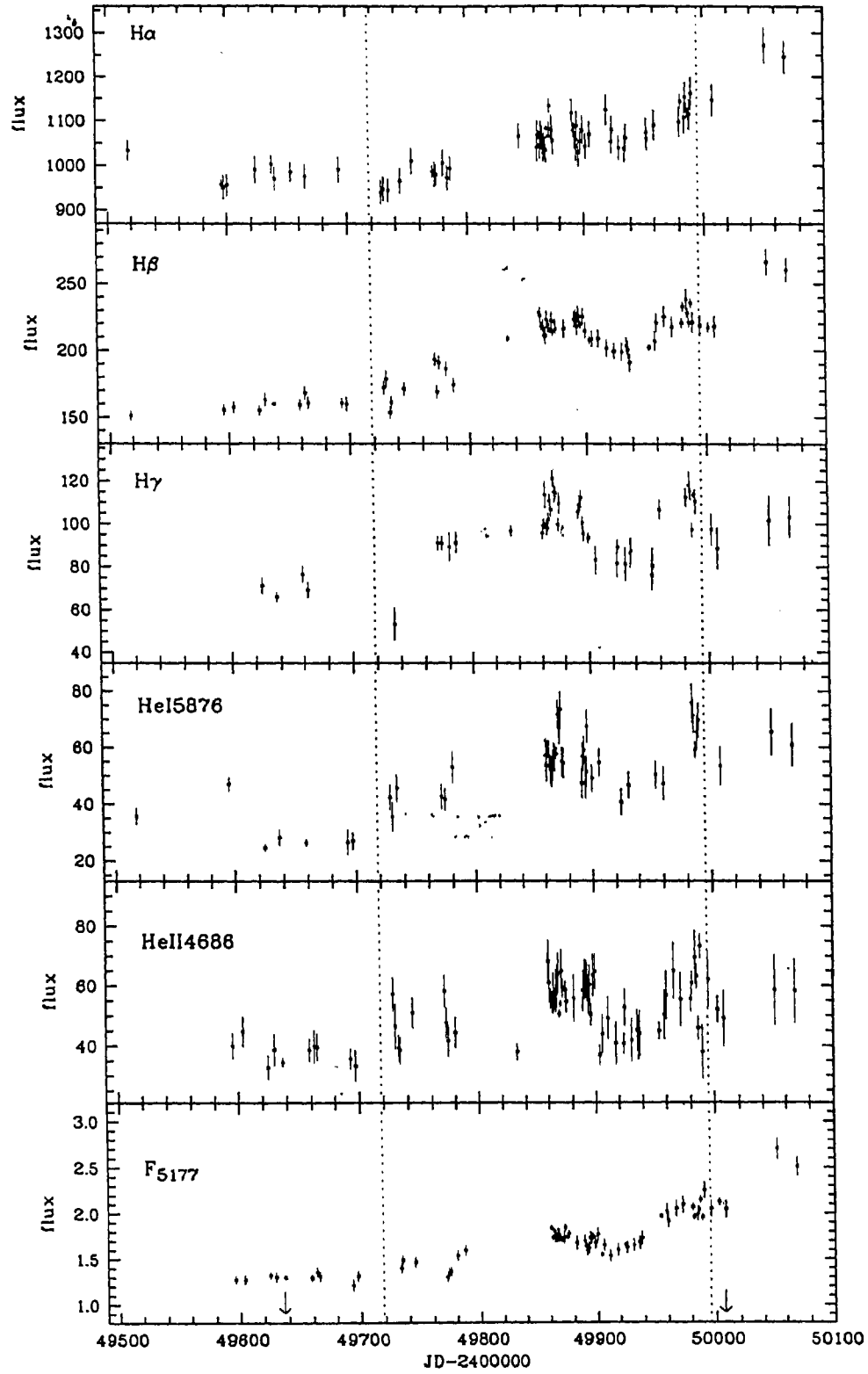


Fig. 3.2.9b  
 Light curves for the emission lines and the optical continuum flux at 5177 Å. The vertical scale is in units of  $10^{-15}$  erg s $^{-1}$  cm $^{-2}$  for the lines and  $10^{-15}$  erg s $^{-1}$  cm $^{-2}$  Å $^{-1}$  for the continuum.

photometric observations is given in Table 3.2.6B. Generally, the brightness of 3C390.3 was scaled with respect to standard stars in the photometric sequence defined by Penston, Penston & Sandage (1971), plus a *Hubble Space Telescope* (HST) guide star located close to 3C390.3. Since the stars and the AGN are within the same field of view of the CCD images, effects of different spectral energy distributions and airmasses on the internal calibration can be neglected. Dietrich et al. (1998) have given a detailed description on the photometric and spectroscopic data reduction procedures, time-series analysis. Major results of this campaign are presented below.

The broadband fluxes (B, V, R and I), the spectrophotometric optical continuum flux  $F_{\lambda}$  (5177 Å), and the integrated emission-line fluxes of H $\alpha$ , H $\beta$ , H $\gamma$ , He I ( $\lambda$ 5876) and He II  $\lambda$ 4686 all show a nearly monotonic increase with episodes of milder short-term variations superposed (Figs. 3.2.9a & 3.2.9b). The amplitude of the continuum variations increases with decreasing wavelength (4400-9000 Å) (Fig. 3.2.9a). The optical continuum variations follow the variations in the ultraviolet and X-ray with time delays, measured from the centroids of the cross-correlation functions, typically around 5 days, but with uncertainties also typically around 5 days; zero time delay between the high energy and low-energy continuum variations can not be ruled out. The strong optical emission lines H $\alpha$ , H $\beta$ , H $\gamma$  and He I ( $\lambda$ 5876) respond to the high-energy continuum variations with time delays typically about  $20 \pm 08$  days. There is some evidence that He II ( $\lambda$ 4686) responds somewhat more rapidly with a time delay of  $\sim 10$  days, but the uncertainties are large ( $\sim 8$  days).

#### 3.2.3.d. *BL Lacertae*

BL Lacertae (BL Lac) is the prototype object for the class of BL Lac objects. BL Lac lies in a giant elliptical galaxy at a redshift of 0.068 (Stickel, Fried and Kuhr, 1993). Superluminal components are seen frequently on the milliarcsec scale (Baath et al. 1981; Wardle & Roberts 1988). BL Lac is one of the very few AGNs detected by the EGRET. The optical and infrared emissions of BL Lac is variable and polarized (Sitko, Schmidt & Stein 1985). Radio and optical polarizations displayed correlated variations. Earlier simultaneous multifrequency study (Bregman et al. 1990) found no time delay between optical and infrared bands. However, it was

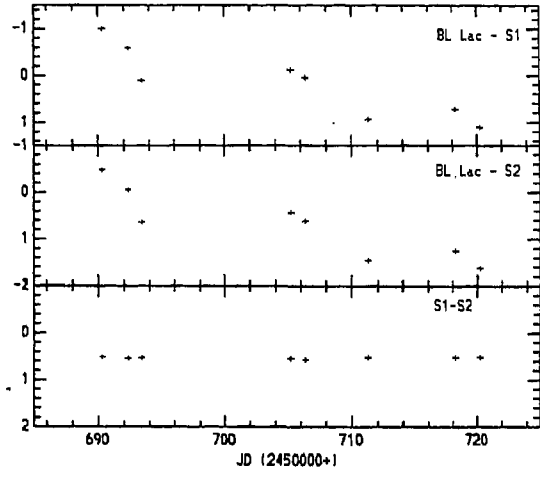


Fig.3.2.10a Same as Fig.3.2.7 but for BL Lac in B band

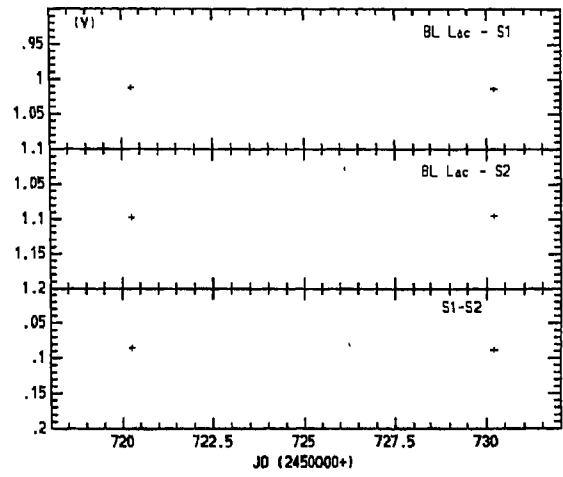


Fig.3.2.10b Same as Fig.3.2.10a but in V band

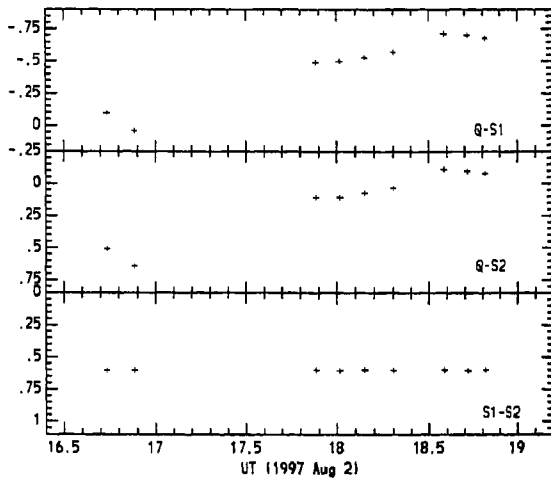


Fig.3.2.10c Differential intranight light curve of BL Lac in I band

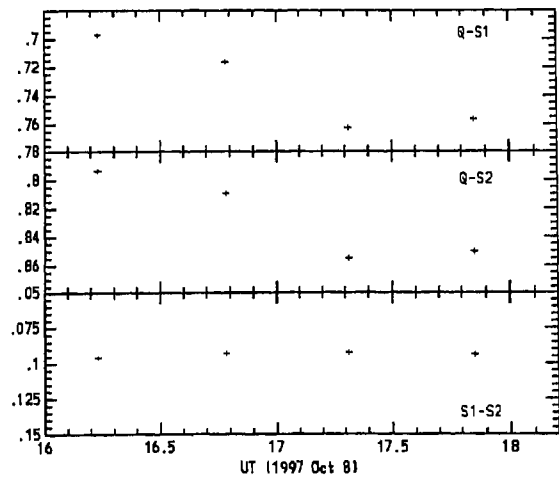


Fig.3.2.10d Same as Fig.3.2.10c but in V band

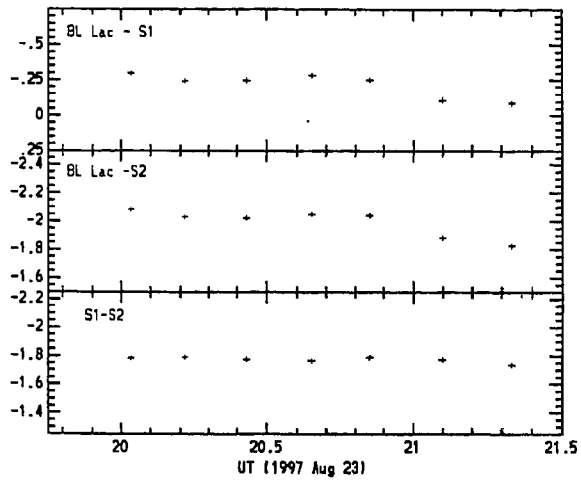


Fig.3.2.10e Same as Fig.3.2.10c but in B band

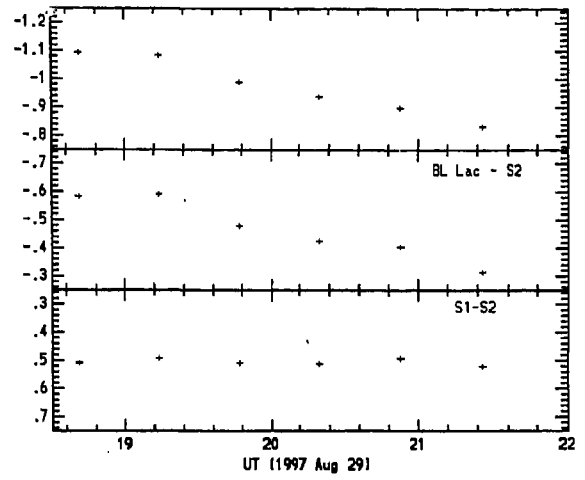


Fig.3.2.10f Same as Fig.3.2.10e but for different date

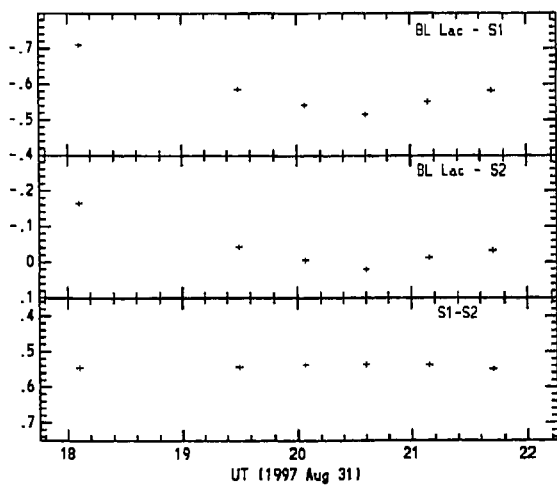


Fig.3.2.10g Same as Fig.3.2.10e but for different date

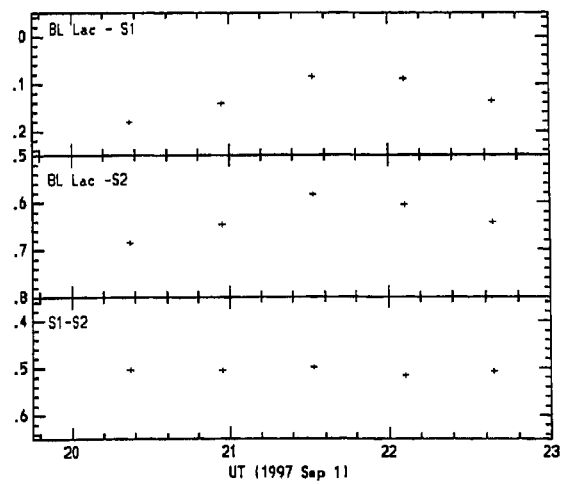


Fig.3.2.10h Same as Fig.3.2.10e but for different date

found that, the optical variations precede that of radio variations by a few years. Also, high frequency radio variability perched low frequency variations by weeks. In the multifrequency continuum the X-ray continuum is not connected smoothly to optical-UV continuum. This indicates that two different processes are involved in the production of multifrequency continuum, perhaps, synchrotron for radio through UV continuum and SSC for the higher energy continuum (Ghosh & Soundararajaperumal 1995). Correlated X-ray flux variations with the sub-millimetre band, and not with the other bands also suggest X-ray emission may be closely related to radio-infrared band which also suggest SSC origin for the X-ray emission.

This source showed signs of flaring during 1997 July. When ASCA observed this source on 1997, July 18, the 2-10 keV average X-ray flux was found to be  $2.6 \times 10^{-11} \text{ erg cm}^{-2} \text{ s}^{-1}$ , which is about 4 times higher than that observed in its low states with *Ginga* (Makino et al. 1997). We started monitoring this source, contemporaneously with ASCA and EGRET; during August-October 1997 using the 2.34m VBT and the 1m telescope of VBO, Kavalur, when it continued to be in high state. High amplitude ( $\sim 2$  magnitude in B band) was observed during this period (Fig. 3.2.10a). The source showed rapid variation of  $\sim 1.5$  magnitudes within 8 days between August 23 and August 31 observations. A large amplitude, rapid ( $\sim 0.75$  magnitude in I band, within  $\sim 2$  hrs) intranight variation was detected on 1997 August 7, when we monitored this source with the 2.34m VBT (Fig. 3.2.10c). Also, noticeable intranight variations (in B band) occurred on August 23, 29 and 31, and September 1 (Figs. 3.2.10e-h). We could not find any measurable variations on the nights of 13, 14 and 19 September, when we have only each two observations taken within maximum one hour time interval.

#### 3.2.3.e. 3C446

3C446 is a OVV quasar, a sub-class of blazar, with a steep, polarized optical continuum, polarized radio emission and variability in all wavebands (Moore & Stockman 1981). During an earlier outburst in 1983, this source was found to show a correlation between optical and radio outbursts with optical flare preceding radio activity by 400-600 days (Bregman et al. 1988). High frequency radio activity also found to precede low frequency radio variations. The earlier multifrequency observations as presented by Bregman et al. (1988) suggest SSC origin for the

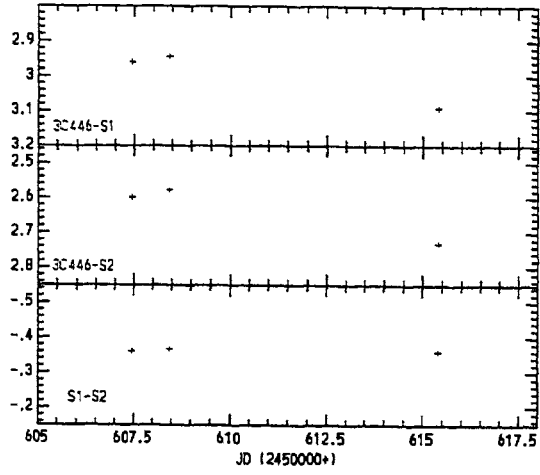


Fig.3.2.11 Same as Fig.3.2.7 but for 3C446

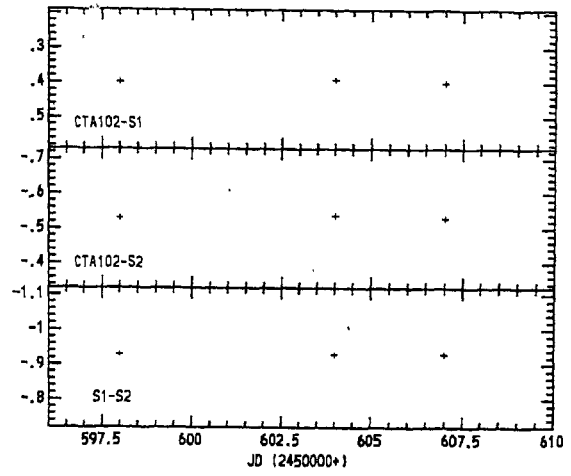


Fig.3.2.1:

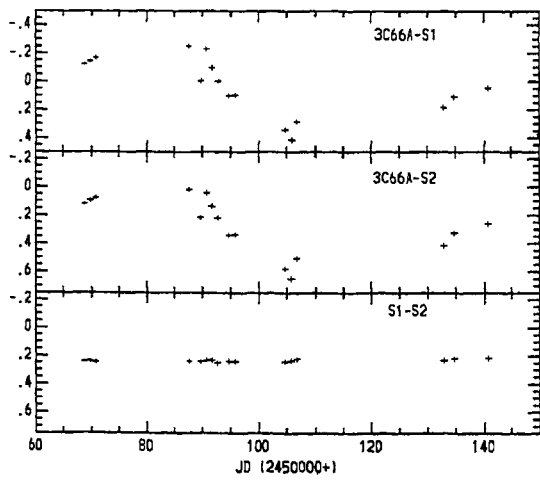


Fig.3.2.13 Differential photometric light curve of 3C66A

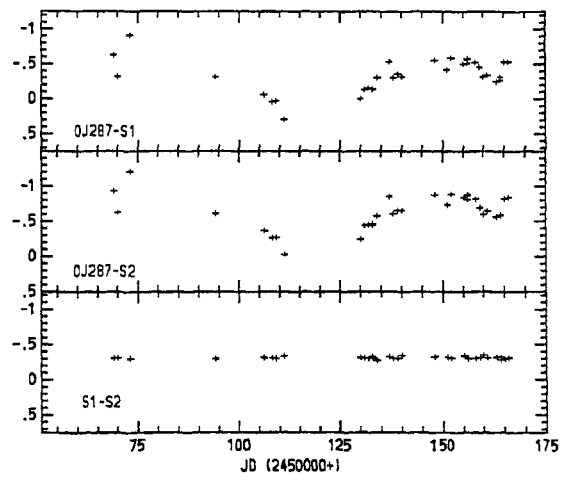


Fig.3.2.14. Same as Fig.3.2.13 but for OJ287

observed X-ray emission in this source. Barbieri et al. (1990) found a 1540 day periodicity for the observed flares in 3C446 in the optical band, which is matching with the observed flares. During the recent outburst in 1997 June, we monitored 3C446 on 3 epochs on 6, 8 and 15 June 1997 in V band using the VBT (Table 3.2.6B). Although we could not measure any intranight variations, a mild variation of  $\sim 0.15$  magnitude was measured within 7 days between 8 and 15 June 1997 (Fig. 3.2.11).

### **3.2.3.f. CTA 102**

CTA 102 is one of the EGRET  $\gamma$ -ray blazars. Baath (1987) observed superluminal motion in this object. Flaring activity was reported (Hartman 1997) in this source during the EGRET observations in May 1997. We monitored this source using VBT and the 1m telescope of VBO, Kavalur, in V band, in simultaneity with the EGRET on three nights on 30 May and 5 and 8 June 1997. However, we could not detect any measurable variations in this source during this period (Fig. 3.2.12).

### **3.2.4. CCD Imaging Photometry of the Blazars 3C66A and OJ287**

To study the variations of the two blazars 3C66A and OJ287 in flare states we undertook a program to monitor these sources using the 75 cm telescope of the Vainu Bappu Observatory, Kavalur. The white-light CCD observations of these sources were obtained during 1995 December to 1996 March, when these two sources were in high states. To overcome the tracking imperfection in the telescope we obtained several short (30 sec), exposures of these two bright sources on each night. The exposures were then co-aligned and added to get the master frame for the night. Details of CCD image aligning, processing and data reduction procedures can be seen in Chapter 2.2. Details of the number of frames added, the total effective exposure time for each frame, and time of observation are presented for the two blazars in Tables 3.2.7B and 3.2.7C. A source log, giving information of celestial co-ordinate, redshift, apparent visual magnitude and absolute magnitude of these two sources, is given in Table 3.2.7A.

**TABLE 3.2.7A SOURCE LOG OF 3C66A AND OJ287**

Source	Position (1950)		Redshift $z$	$m_v$	$M_{\text{abs}}$
	R.A.	Dec.			
3C66A	02 19 30	+42 48 30	0.444	15.21	-26.5
OJ287	08 51 57	+20 17 58	0.306	15.43	-25.5

**TABLE 3.2.7B LOG OF OBSERVATIONS OF 3C 66A**

Date	No. of frames	Mid UT	Total Integ (s)
1995:12:17	19	14:30	570
1995:12:18	11	14:32	330
1995:12:19	07	14:15	210
1996:01:05	03	15:03	090
1996:01:07	10	14:37	300
1996:01:08	12	14:09	360
1996:01:09	11	14:29	330
1996:01:10	23	15:00	690
1996:01:12	29	14:10	870
1996:01:13	25	14:33	750
1996:01:22	10	14:25	300
1996:01:23	15	14:35	450
1996:01:24	19	14:32	570
1996:02:19	08	14:40	240
1996:02:27	03	14:01	150



**TABLE 3.2.7C LOG OF OBSERVATIONS  
OF OJ287**

Date	No. of frames	Mid UT	Total Integ (s)
1995:12:18	06	21:08	180
1995:12:19	11	20:05	330
1995:12:22	12	20:23	360
1996:01:12	04	19:42	120
1996:01:24	10	18:20	300
1996:01:26	11	19:12	330
1996:01:27	10	19:07	300
1996:01:29	28	18:36	840
1996:02:17	06	19:10	180
1996:02:18	07	19:06	210
1996:02:19	10	20:43	300
1996:02:20	05	19:37	150
1996:02:20	13	19:58	390
1996:02:21	03	19:05	090
1996:02:24	40	17:31	1200
1996:02:25	16	18:10	480
1996:02:26	21	18:10	630
1996:02:27	15	17:28	450
1996:03:06	16	17:34	480
1996:03:09	07	16:33	210
1996:03:10	15	14:38	450
1996:03:13	19	17:16	570
1996:03:14	11	15:01	330
1996:03:14	08	16:01	240
1996:03:14	09	16:56	270
1996:03:15	42	15:49	1260
1996:03:16	33	15:47	990
1996:03:17	11	15:30	330
1996:03:18	05	15:40	150
1996:03:19	13	16:57	390
1996:03:21	05	14:44	150
1996:03:22	14	14:41	420
1996:03:22	06	15:00	180
1996:03:23	14	15:04	420
1996:03:24	15	14:44	450

## Results

### 3.2.4a. 3C66A

3C66A is a well known blazar and its optical image appears to be a stellar-like object. It has displayed high optical polarization and large-amplitude optical variations during flare states (Cruz-Gonzalez & Huchra 1984). We observed 3C 66A over a period of 72 days (17 December 1995 to 27 February 1996). The white-light CCD photometric light curve presented in Fig.3.2.13 clearly shows a major flare during this period. A high-amplitude variation of  $\sim 0.5$  magnitude decline within 15 days time has been noticed during 1996 January. After this dip around the end of January 1996 the source has brightened up by  $\sim 0.4$  magnitude in 25 days. This source is being observed since 1969 from the Rosemary Hill Observatory (RHO), Florida (Pica et al. 1980, 1988). It was found from RHO observations that flickering more than 0.4 magnitude is common in this BL Lacertid during flares. It showed earlier peak activity during 1979-1980.

### 3.2.4b. OJ287

The blazar OJ287 is being studied in all wavelength regions for a very long period and is known to exhibit periodic outbursts with an interval of about 11.6 years (Sillnpaa et al. 1988). The source was exhibiting flaring activity during 1994-1996. Earlier outbursts were recorded during 1913, 1937, 1947, 1959, 1972 and 1984 (Takalo 1994). We monitored this superluminal RBL OJ287 continuously between 1995 December 18 to 1996 March 24. The results of the CCI photometric analysis are plotted in Fig.3.2.14. During the period of observations this source has shown two major long term flaring activity. In the first case it displayed nearly 1.2 magnitude decline in about 38 days during 1995 December to 1996 January. The source again brightened up about 1 magnitude in 39 days. The light curve presented in Fig.3.2.14 also shows at least two major short time variabilities. It displayed a dramatic 0.7 magnitude variation within 3 days between 19 and 22 December 1995. Another gradual variation of  $\sim 0.4$  magnitude decline occurred during 14 to 20 March 1996 and again it recovered about 0.4 magnitude within two days. Our observations of flaring activity in this blazar support the proposed periodicity of 11 years. OJ287 is the only blazar in which this kind of periodicity is well established.

### **3.2.5. Discussion**

In the previous sections (sections 3.2.1-3.2.4) results of the X-ray spectral analysis of 28 EXOSAT blazars are presented and their X-ray spectra are compared with the corresponding radio-through UV multifrequency spectra. The optical CCD photometry results of 6 blazars, which were monitored as part of multifrequency monitoring campaigns in simultaneity with other wavelengths, are presented. All these blazars were observed when they were in flare state. We have also presented the results of the optical CCD photometry results of the blazars 3C66A and OJ 287. In this section we present a summary of our results, discuss their implications and derive physical interpretations.

In Tables 3.2.5A and 3.2.5B we have listed the values of X-ray photon indices and luminosities at different frequencies between radio and X-rays for RBLs and XBLs, respectively. It may be noted from these tables that the X-ray spectral indices of RBLs are in general flatter than those of XBLs. Also, it can be seen from these tables that the RBLs are much more luminous in radio than the XBLs (by two or three orders of magnitude). However, the RBLs, which are in general higher redshift objects than the XBLs, are slightly more luminous in X-rays (by factors of 4-7) than the XBLs. Luminosities in different bands (radio, FIR, IR, optical, UV and X-ray) for RBLs and XBLs are given in Tables 3.2.5A and 3.2.5B, respectively. Radio luminosity versus FIR (60  $\mu\text{m}$ ), IR (2.2  $\mu\text{m}$ ), optical (5560  $\text{\AA}$ ), UV (2000  $\text{\AA}$ ) and X-ray (2-10 keV) luminosities of RBLs and XBLs are plotted in Figs. 3.2.5a-e. These figures clearly show the bimodal nature of the distribution of blazars. Also it may be noted from the comparison of the above figures that the separation between RBLs and XBLs gradually increases as we move from Fig. 3.2.5a to 3.2.5e, and the largest separation and the best correlations are present in the X-ray versus radio luminosity plot (Fig. 3.2.5e).

Most of the objects of our sample have not been observed in the millimeter-wavelength region and the lack of such observations did not allow us to plot radio luminosity versus millimeter-wave luminosity and millimeter-wave luminosity versus FIR luminosity. FIR luminosity versus IR, optical, UV and X-ray luminosities are plotted in Figs. 3.2.5f-i. Similarly, IR luminosity versus optical, UV and X-ray luminosities; optical luminosity versus UV and X-ray luminosities; and UV versus X-ray luminosities are plotted in Figs. 3.2.5j-l. Figs. 3.2.5m-n and Fig 5o respectively. It can be seen from these luminosity luminosity plots that the best correlations are

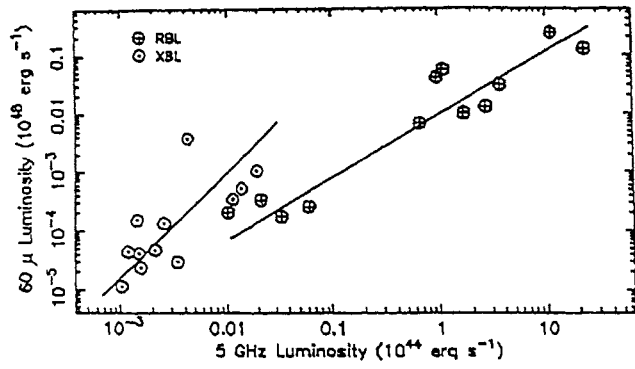


FIG. 5a

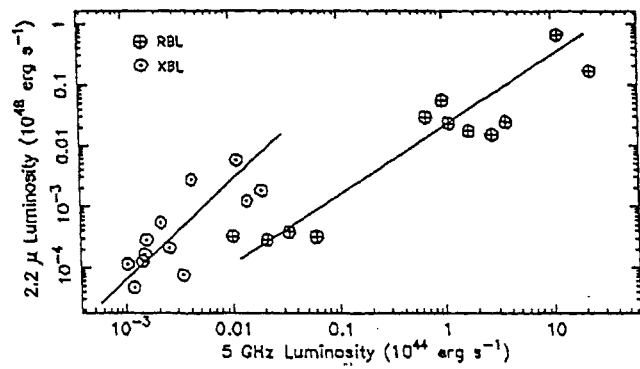


FIG. 5b

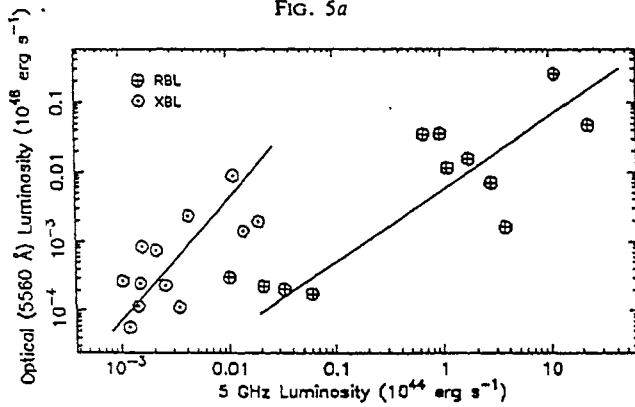


FIG. 5c

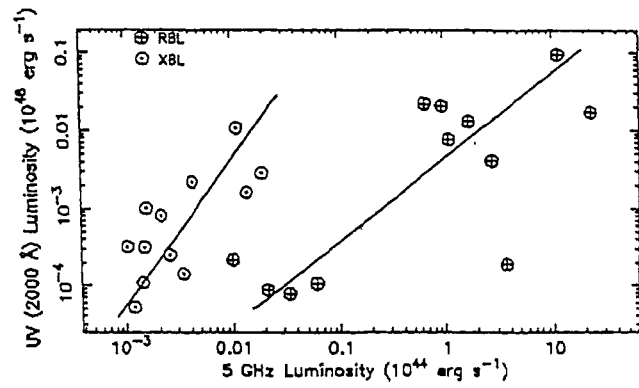


FIG. 5d

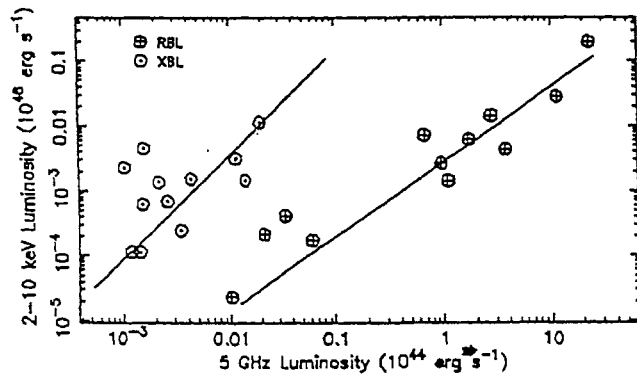


FIG. 5e

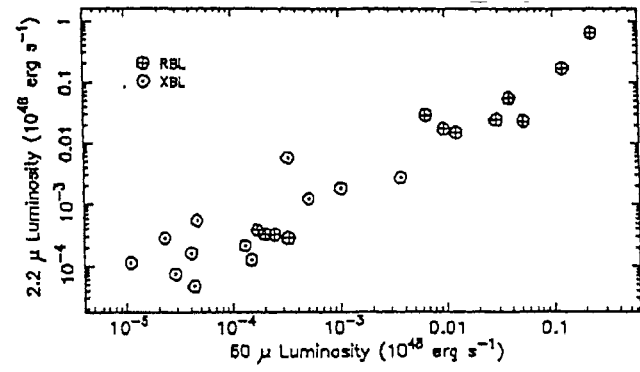


FIG. 5f

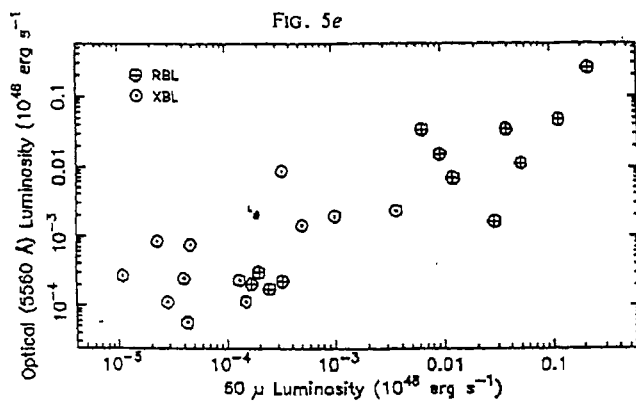


FIG. 5g

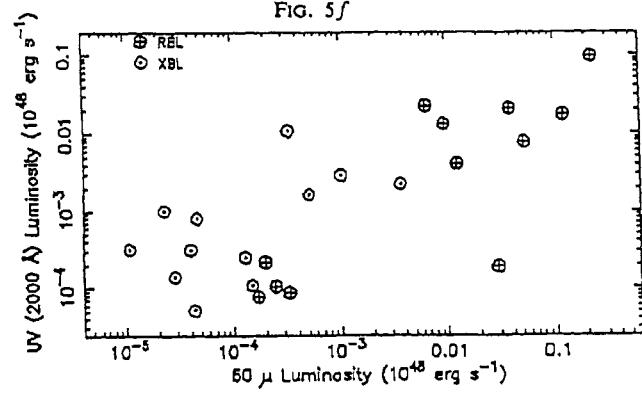


FIG. 5h

(a) Radio (5 GHz) luminosity vs. FIR (60  $\mu\text{m}$ ) luminosity of blazars. (b) Same as (a), but for radio vs. NIR (2.2  $\mu\text{m}$ ). (c) Same as (a), but for radio vs. optical (5560  $\text{\AA}$ ). (d) Same as (a), but for radio vs. X-ray (2-10 keV). (e) Same as (a), but for FIR vs. NIR. (f) Same as (a), but for FIR vs. optical. (g) Same as (a), but for FIR vs. optical. (h) Same as (a), but for FIR vs. UV. (i) Same as (a), but for FIR vs. X-ray. (j) Same as (a), but for NIR vs. optical. (k) Same as (a), but for NIR vs. UV. (l) Same as (a), but for NIR vs. X-ray. (m) Same as (a), but for optical vs. UV. (n) Same as (a), but for optical vs. X-ray. (o) Same as (a), but for UV vs. X-ray.

Figs. 3.2.5.

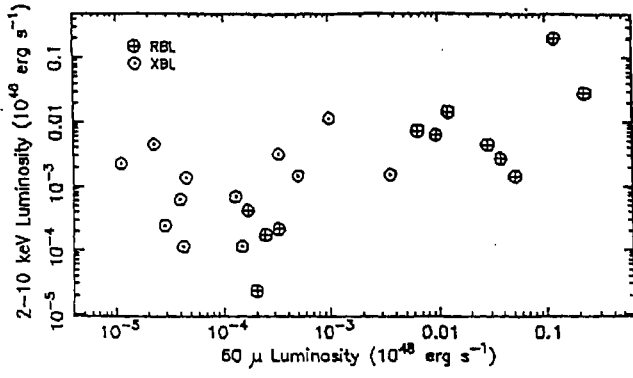


FIG. 5i

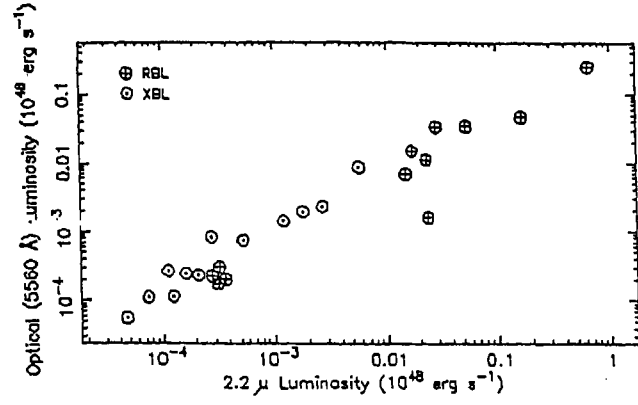


FIG. 5j

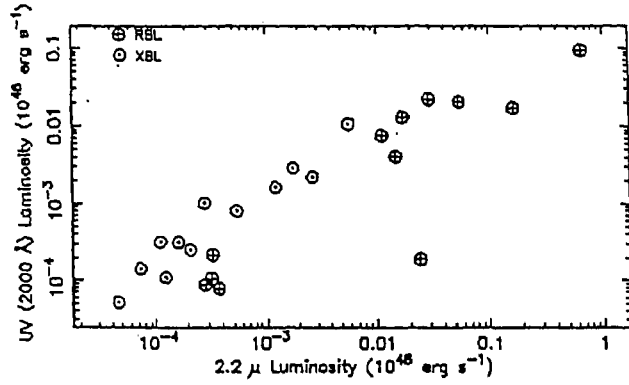


FIG. 5k

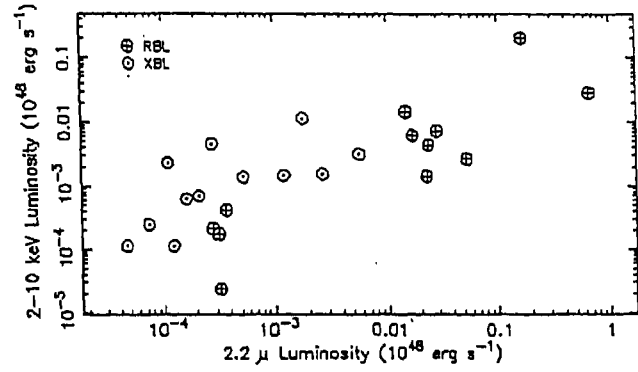


FIG. 5l

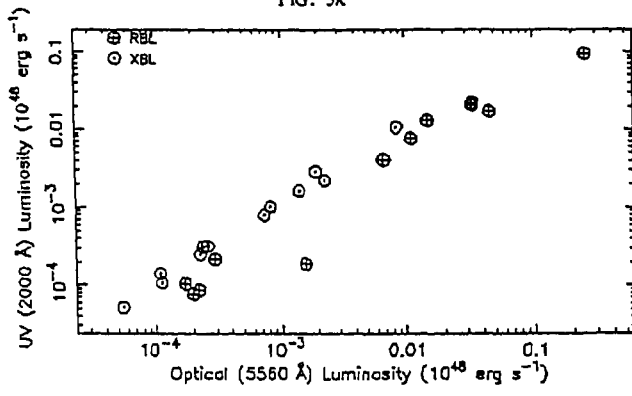


FIG. 5m

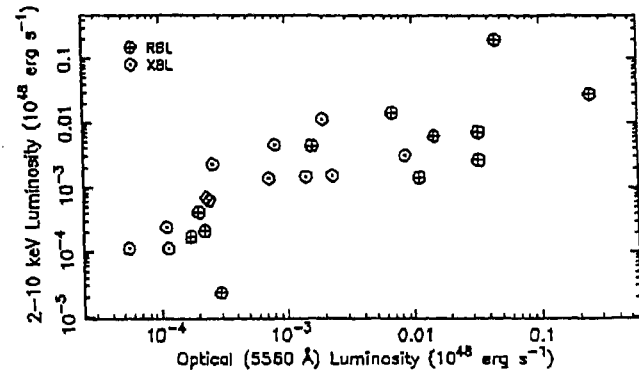


FIG. 5n

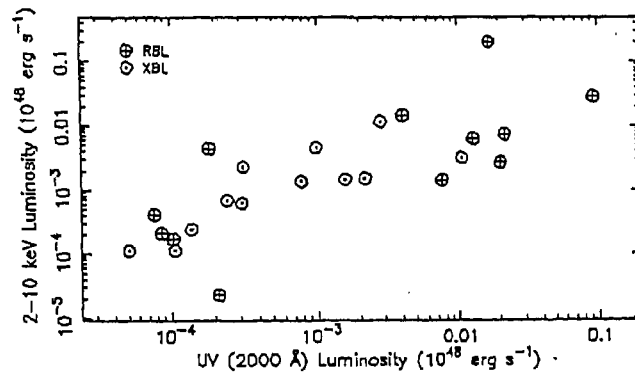


FIG. 5o

Figs. 3.2.5. (continued)

present between FIR versus IR (Fig. 3.2.5f), IR versus optical (Fig. 3.2.5j) and optical versus UV (Fig. 3.2.5m) luminosities. A weak correlation is also present in Fig. 3.2.5o, which displays UV versus X-ray luminosities of blazars. Careful inspection of this figure shows that the UV and X-ray luminosities are better correlated if we consider only the XBLs rather than all the blazars (XBLs plus RBLs). This can be clearly seen from Figures 3.2.6a and 3.2.6b, which show the plots of two-point spectral indices between UV and X-ray ( $\alpha_{UV-X}$ ) versus the UV spectral index ( $\alpha_{UV}$ ) for XBLs and RBLs respectively. It may be noted from these figures (Figs. 3.2.5o and 3.2.6a) that the UV and X-ray fluxes from XBLs are correlated and that those from RBLs are not correlated, and because of these results we find the spectral continuity and discontinuity in the UV-X-ray region for XBLs and RBLs respectively. Also we have obtained the same results using only simultaneous UV and X-ray observations of 12 blazars of our sample which were carried out with IUE and EXOSAT (six RBLs: 3C120, PKS0521-36, PKS0754+10, OJ287, 3C273 and 3C371; six XBLs: H0323+022, Mkn421, Mkn180, Mkn501, PKS2005-489 and PKS2155-304).

Multifrequency spectra of 28 blazars are plotted in Figs 3.2.3 and 3.2.4. These spectra have been constructed using simultaneous/nonsimultaneous observations. Almost 50% of the sources of our sample were observed simultaneously at UV and X-rays. Such simultaneous observations are very important for multifrequency studies, because these observations will display how the X-ray spectrum gets connected with the continuum at the lower frequencies. In general, the radio through X-ray continuum emission spectra of XBLs can be represented by a single parabola. Such a smooth change of the continuum spectra of XBLs from radio to X-ray (from flat to steep spectral indices) indicates that they are produced via synchrotron radiation (Konigl 1981; Ghisellini, Maraschi & Treves 1985; Urry, Mushotzky & Holt 1986 ; and references therein). However two parabolae (one for radio through UV and other one for X-rays) are required to represent the multifrequency spectra of RBLs with spectral discontinuity in the UV-X-ray region (Fig. 3.2.3). Also the detected X-ray fluxes from RBLs are much higher than expected from IR through UV extrapolation. Such excess of X-ray indicates that IR through UV and X-rays are produced from different physical processes. It has been suggested that the radio through UV emissions are from the inverse Compton mechanism (Ghisellini et al. 1985 and references therein).

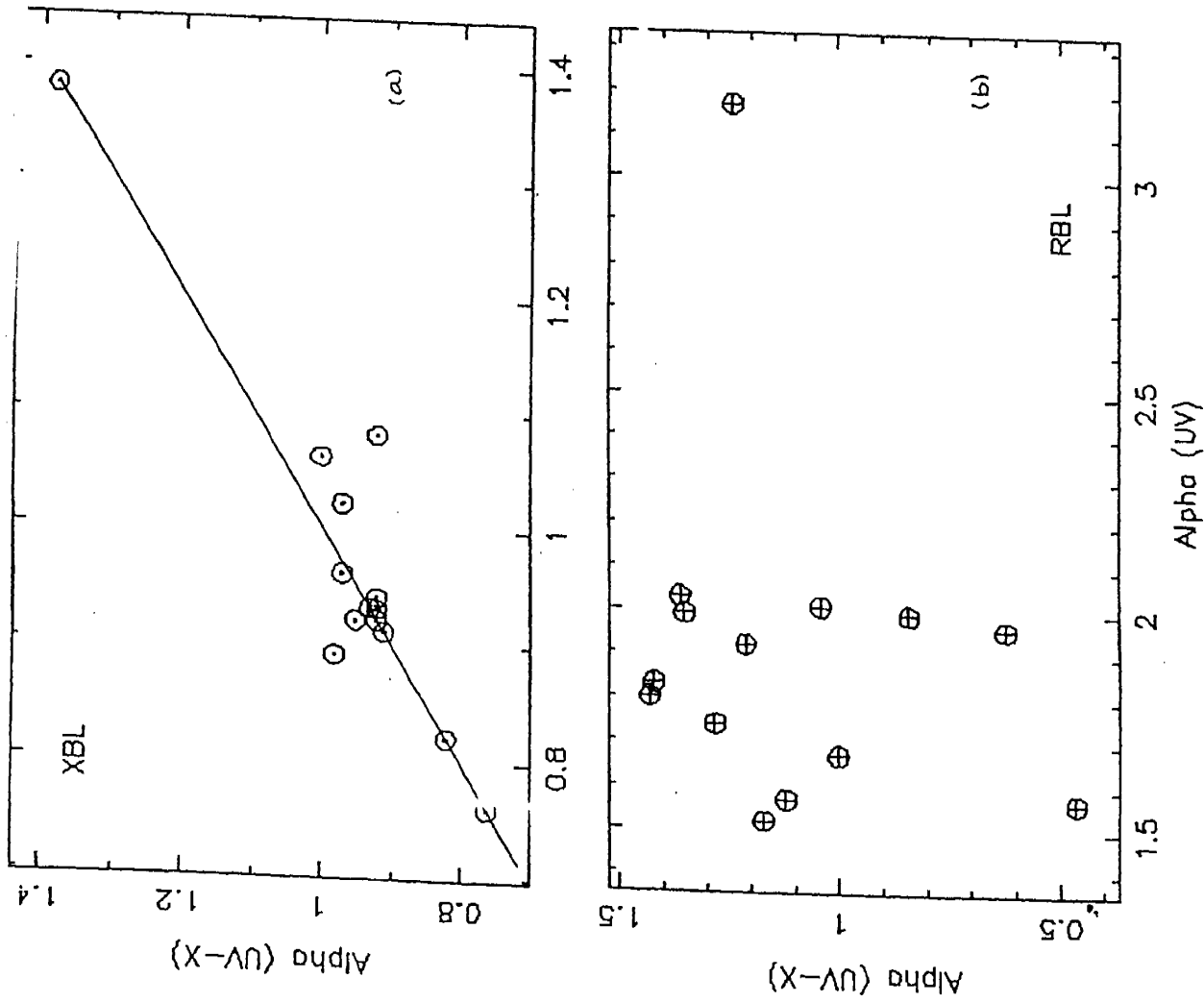


Fig. 3.2.6 (a) Plot of  $\alpha_{UV-X}$  Vs.  $\alpha_{UV}$  for XBLs. (b) Same as (a) but for RBLs

A large number of observational results such as superluminal motion (Zensus 1989), high brightness temperature, rapid variability, paucity of X-ray self-Compton radiation (Blandford 1987) and radio jets (Liang 1988; Garington et al. 1988) have been interpreted in the framework of relativistic beaming models, which was first suggested by Blandford & Rees (1978). At present there are two such beaming models: (1) the ‘accelerating jet’ model (Ghisellini & Maraschi 1989 and references therein) and (2) the ‘wide-jet’ model (Celotti et al. 1993 and references therein). In the accelerating jet model it has been suggested that the flow velocity of the relativistic beam increases with radial distance so that relativistic beaming is weak in the inner, X-ray-emitting region of the jet (Ghisellini & Maraschi 1989). This model explains most of the observed results of blazars including the observed energy distributions, but it is difficult in this model to explain the rapid and large-amplitude X-ray variability (Treves et al. 1989). In the ‘wide jet’ model (Celotti et al. 1993) it is assumed that the flow velocity is constant but the degree of beaming increases with decreasing frequency, that is, the opening angle of the X-ray emitting region at the inner part of the jet is much wider than that of the radio emitting region at the outer part. We will discuss the results for the 28 EXOSAT blazars, presented here, using the wide-jet model with the assumption that the XBLs are observed at intermediate angles and the RBLs are observed at small angles with the jet axis (Urry, Maraschi & Phinney 1991a). If the beaming cone at the inner region of the jet is wider than at the outer region, an observer at intermediate angles will receive, relatively, more X-rays than radio emission. The X-rays produced via synchrotron radiation will have a steep spectrum because of high-energy cutoffs in the particle spectra. The X-ray emission of XBLs (observed at intermediate angles) could thus be interpreted as synchrotron emission from the inner part of the jet and the X-ray luminosity of these objects will be greater than the radio luminosity of the RBLs (see Table 3.2.5B) because the degree of beaming increases with decreasing frequency. Farther out of the X-ray emitting region, the jet becomes more collimated and emits synchrotron radiation from the UV to the radio band.

An observer at small angles with the jet axis will receive dominant fluxes from the outer part rather than the inner part. If the X-rays are produced from the inverse Compton mechanism in the outer region of the jet in a narrower cone, the emitted X-rays will have a flat spectrum and a large excess with respect to the UV emission. In RBLs, the X-rays could thus be interpreted as



due to the inverse Compton mechanism from the outer region of the jet with spectral discontinuity between the UV and X-ray bands.

The bimodal distribution of blazars in the luminosity-luminosity plane (Figs. 3.2.5a-e) and the increase in separation between XBLs and RBLs may be due to the increasing collimation of the jet with distance and the effect of the viewing angles of the two groups of blazars. Also, the bimodal spectral and spatial distribution of XBLs and RBLs (Fig. 3.2.1) may be interpreted if the X-rays are beamed in a wider cone than the radio emissions (Celotti et al. 1993). Even though the wide-jet model can explain the observed properties of blazars, including the rapid and large-amplitude X-ray variability, it will be interesting to test this model with a larger and unbiased complete sample of blazars.

We participated in the international multifrequency monitoring campaigns to monitor six blazars (PKS0528+13, Mkn501, 3C390.3, BL Lac, 3C446 and CTA102) in the optical band simultaneously with multifrequency observations. Four of them (PKS0528+13, Mkn501, BL Lac, and CTA102) were monitored in simultaneity with CGRO. The blazars were observed during their flare states. Our results indicate night to night variations in all the sources, except CTA 102. We have detected intranight variations in two of them (Mkn501, BL Lac). BL Lac showed a large amplitude ( $\sim 0.75$  magnitude) variation within 2 hours in I band on 1997 August 2. It has also showed large amplitude ( $\sim 2$  magnitude) night to night variations in B band.

Beaming and relativistic boosting are considered to cause the rapid large amplitude variations in blazars. Relativistic shock propagating down a jet and its interaction with irregularities in the flow can cause the observed variations (e.g., Maraschi et al. 1989; Qian et al. 1991; Marscher, Gear & Travis 1992). In this picture electrons diffuse from high to low energies so the amplitude of variability is expected to be larger at higher energies and the higher energy variations are expected to precede the lower energy variations. Earlier multifrequency studies of certain blazars (e.g., Bregman et al. 1990) found that, the optical variations precede that of radio variations by a few years. Also, high frequency radio variability precede low frequency variations by weeks, which confirms the theoretical prediction. It is suggested that radio through UV emission in RBLs and radio through X-ray emission XBLs are caused by the synchrotron

emission from the relativistic plasma motion in a jet. The higher energy continuum in both these classes of blazars are believed to be caused by the SSC process. The observed correlation between lower energy synchrotron components and high energy SSC components in certain objects (e.g. BL Lac, 3C446; Bregman et al. 1988, 1990) proves this suggestion. Simultaneous observational data, for these six blazars, in the other wavebands are not available immediately for comparison. The massive works of data coordination, reduction and combined spectral and photometric analysis are in progress. The results of the combined multifrequency studies can yield important results for these sources.

### **3.2.6. Conclusions**

Results of the X-ray spectral analysis of 28 blazars which were observed with EXOSAT are presented in this Chapter. The blazars have been divided into two groups: radio-selected blazars (RBLs) and X-ray selected blazars (XBLs). X-ray results suggest that XBLs are steep spectrum sources and RBLs are relatively flat spectrum sources. Even though RBLs are, in general, higher redshift objects than XBLs, they are slightly more luminous (by a factor of 4-7) in X-rays than XBLs. However, RBLs are much more luminous (by two or three orders of magnitude) in radio than the XBLs. Using simultaneous/quasi-simultaneous and nonsimultaneous observations, we have constructed the multifrequency spectra (radio through X-ray continuum fluxes) of 28 blazars, and they can be well represented with a single parabolic curve for XBLs and with two parabolic curves for RBLs. One of the important differences between the multifrequency spectra of RBLs and XBLs is the spectral discontinuity in the UV-X-ray region of RBLs. This result has been confirmed by only using simultaneous UV and X-ray observations of 50% of the sources of the present sample. Luminosities at different bands have also been computed for all the blazars in the present sample and bimodal character of distribution of these objects has been found in the radio and X-ray luminosity plane. All these results are discussed in the framework of a 'wide-jet' model.

We participated in the international multifrequency monitoring campaigns to monitor six blazars (PKS0528+13, Mkn501, 3C390.3, BL Lac, 3C446 and CTA102) in the visual band simultaneously with multifrequency observations. Four of them (PKS0528+13, Mkn501, BL Lac, and CTA102) were monitored in simultaneity with CGRO. The blazars were observed

during their flare states. Our results indicate night to night variations in all the sources, except CTA 102. We have detected intranight variations in two of them (Mkn501, BL Lac).

To study the variations of the two blazars 3C66A and OJ287 in flare states we undertook a program to monitor these sources using the 75 cm telescope of the Vainu Bappu Observatory, Kavalur. The white-light CCD observations of these sources were obtained during 1995 December to 1996 March, when these two sources were in high states. Large amplitude night to night variations were found in 3C66A and OJ287. Our observations of flaring activity in the blazar OJ287 support the proposed periodicity of 11.6 years.

The optical photometric and spectroscopic observations of 3C390.3 shows that the broad band fluxes (B, V, R and I), the spectrophotometric optical continuum flux  $F_{\lambda}$  (5177 Å), and the integrated emission-line fluxes of H $\alpha$ , H $\beta$ , H $\gamma$ , He I ( $\lambda$ 5876) and He II  $\lambda$ 4686 all show a nearly monotonic increase with episodes of milder short-term variations superposed. The amplitude of the continuum variations increases with decreasing wavelength (4400-9000 Å). The optical continuum variations follow the variations in the ultraviolet and X-ray with time delays, measured from the centroids of the cross-correlation functions, typically around 5 days, but with uncertainties also typically around 5 days; zero time delay between the high energy and low-energy continuum variations can not be ruled out. The strong optical emission lines H $\alpha$ , H $\beta$ , H $\gamma$  and He I ( $\lambda$ 5876) respond to the high-energy continuum variations with time delays typically about  $20 \pm 08$  days. There is some evidence that He II ( $\lambda$ 4686) responds somewhat more rapidly with a time delay of  $\sim 10$  days, but the uncertainties are large ( $\sim 8$  days).

### **3.3. Radio-Quiet Quasars**

#### ***3.3.1. Introduction***

Among quasars, radio-loud sources (RLQs) are found to be highly variable (Penston & Cannon 1970; Pica & Smith 1983). A possible explanation is that there is some contribution to the observed flux at all energies from the relativistic plasma jet motion. Relativistic shock propagating down a jet and its interaction with irregularities in the flow can cause large amplitude and rapid variabilities in RLQs (Maraschi et al. 1989; Qian et al. 1991; Marscher, Gear & Travis 1992). Whereas, radio-quiet quasars (RQQs), mostly show smaller amplitude variations which may be of completely different origin, like, instabilities in accretion disks, (Rees 1984) because, unlike RLQs, RQQs do not show powerful radio jets or extended radio lobes (Siemiginowska 1993). RQQs have only weak radio structures. However, the continuum shape and emission line characteristics from FIR to X-ray are similar for RQQs and RLQs (Elvis et al. 1994). About 90% of all quasars are radio-quiet. It is thought that non-periodic short term and periodic long term variabilities may be present in the case of RQQs. Long term variability is the small and steady variations of the base level or quiescent state from which shorter and high/low amplitude events or flares apparently erupt (Smith & Nair 1995). Occurrence of intranight variability is not yet confirmed in RQQs and positive detection of such variability may provide important clues on the physical emission processes occurring in the innermost regions of these quasars.

#### ***3.3.2. CCD Imaging Photometry of Radio-Quiet Quasars***

In order to detect short and long term variabilities of RQQs, we had selected several such sources for optical monitoring. The radio-quiet quasar sample were selected randomly from the AGN catalog of Veron Cetty and Veron (1993), covering the entire range of right ascension. We monitored these sources using the 2.34m VBT and the 1m telescope of VBO, since 1995 until the beginning of 1998. The telescope time availability restrained the number of objects in our sample to 20. Moreover, the same constraint of telescope time availability, apart from sky conditions prevented us from monitoring all the sources during all the three year's period. Each object was observed minimum twice each night for, at least, twice during this three year's time, in order to detect any likely variations. The CCD observations were carried out in the B, V and I

photometric passbands. Details of reduction procedures and instrument and detector particulars are given in Chapter 2.2. Celestial coordinate, redshift, apparent visual magnitude and absolute magnitude for our sample of RQs are listed in Table 3.3.2A. Log of observations is presented in Table 3.3.2B

### **3.3.3. Discussions**

Our results of differential photometric data reduction are presented in the Figs 3.3.1a-x and 3.3.2a-d. We could not detect any long term variations in our sample within the period of three years, which is evident from the figures presented. However, we could detect indications of microvariability in the RQs - Q0101-304, PC0751+56 and Q1317-05 (Figs 3.3.2a-d). Only on few nights we could observe this intranight microvariability in these sources in our limited set of data. However, even established microvariable blazars also do not show this behaviour during every observing run (e.g., Carini 1990). Since RQs are not believed to have powerful relativistic jets (Siemiginowska 1993), the observed indications of microvariability can be expected to come from the instabilities in accretion disks (Ress 1984; detail references about other theoretical models are given in Sagar et al 1996). Such theoretical considerations suggest that in radio-quiet quasars a self-gravitating thin accretion disk can thermally produce the UV through optical emission (Malkan 1983). The UV to optical continuum of certain RQs show a flat power-law, suggesting a non-thermal origin (Barvainis 1990). So it may be possible that contributions of both thermal and non-thermal emissions are present in the optical continua of these sources. In this picture the size of the emitting region increases with wavelength. Since the variability properties of each of the emitting regions should reflect their sizes, variability studies can provide more information about the emitting regions. Perhaps the reason for the non detection of long-term variability is that the variability time scales are longer than the duration of our program. Hence optical monitoring of these sources for a continued, longer period of time will be helpful in arriving at a clear conclusion. Also more number of RQs have to be observed intensely in order to detect and understand the intranight microvariability.

### **3.3.4. Conclusions**

A sample of 20 radio-quiet quasars were observed at VBO, in B, V and I photometric passbands, during 1995 to 1998. No long term variability could be detected in our sample of

**TABLE 3.3.2A SOURCE LOG OF RQQS OBSERVED AT VBO**

Source	Position (1950)		Redshift <i>z</i>	<i>m<sub>v</sub></i>	<i>M<sub>abs</sub></i>
	R.A.	Dec.			
Q0101-304	01 01 14	-30 25 04	4.07	20.1	-27.5
Q0222-415	02 22 05	-41 31 29	2.00	17.6	-28.1
Q0353-383	03 53 01	-38 18 40	1.959	17.2	-28.4
Q0530-379	05 30 48	-37 55 26	0.29	16.7	-24.6
Q0540-389	05 40 12	-38 57 43	0.83	17.2	-26.6
S40636+68	06 36 47	+68 01 28	3.17	16.6	-30.4
PC0751+56	07 51 41	+56 23 06	4.28	21.8	-27.8
0822+27W1	08 22 46	+27 14 11	2.06	17.7	-28.3
Q0913+07	09 13 35	+07 14 58	2.78	18.1	-28.5
Q1003-026	10 03 38	-02 37 07	2.871	17.6	-29.1
CSO38	10 09 05	+29 56 48	2.62	16.0	-30.9
Q1317-05	13 17 54	-05 07 52	3.7	18.1	-29.3
Q1330+01	13 30 21	+01 08 14	3.51	18.2	-29.4
Q1410+09	14 10 53	+09 36 05	3.24	17.8	-29.2
Q1415+45	14 15 04	+45 09 57	0.114	15.7	-23.5
Q1548+09	15 48 39	+09 17 49	2.749	18.0	-28.6
KP1633+63	16 33 01	+63 04 25	2.15	18.0	-28.1
1E1711+712	17 11 47	+71 16 01	1.60	17.5	-27.6
Q2040-40	20 40 11	-40 01 33	2.07	17.7	-28.1
Q2304-42	23 04 29	-42 19 33	2.63	17.5	-28.9

**TABLE 3.3.2B. LOG OF VISUAL OBSERVATIONS OF RQQs**

Object	z	Date of observation	Tele-scope (m)	No of obs	UT (start)	Integ. (s)	Filter		
Q0101-304	4.07	1995 12 20	2.34	6	14:12	600	V		
					14:40	1800	V		
					15:14	1800	V		
					15:50	1800	V		
					16:28	1800	V		
					17:05	1800	V		
		1995 12 24	2.34	8	14:04	600	I		
					14:23	900	I		
					14:39	1200	I		
					14:59	900	I		
					15:23	900	I		
					15:42	900	I		
					16:03	900	I		
					16:26	900	I		
		1995 12 25	2.34	9	13:51	600	V		
					14:11	1800	V		
					14:46	1800	V		
					15:46	1800	V		
					16:23	300	I		
					16:33	300	I		
Q0222-415	2.00	1996 10 03	1.02	3	18:24	1800	V		
					19:00	1800	V		
					19:30	1800	V		
		1996 10 04	1.02	2	18:08	1800	V		
					18:45	1800	V		
		1997 10 04	2.34	2	18:13	1800	V		
					19:09	1800	V		
		1998 02 06	2.34	2	14:12	1800	V		
					15:02	1800	V		
		Q0353-383	1.959	1996 10 03	2.34	3	20:21	1800	V
							21:01	1800	V
							21:33	1800	V
1998 02 04	2.34			2	14:02	1200	V		
					14:30	1800	V		

TABLE 3.3.2B - Continued

Object	z	Date of observation	Tele- scope (m)	No of obs	UT (start)	Integ. (s)	Filter
Q0530-379	0.290	1996 02 14	1.02	2	15:48	1800	V
					16:47	1800	V
		1996 02 15	1.02	2	15:00	1800	V
					16:17	1800	V
					1997 02 16	2.34	6
					15:15	900	V
					15:35	900	V
					15:51	900	V
					16:08	900	V
					16:24	900	V
Q0540-389	0.830	1996 10 03	2.34	2	22:41	1800	V
					23:50	1800	V
		1998 02 04	2.34	3	15:51	900	V
					16:09	900	V
					16:27	900	V
		1998 02 05	2.34	3	15:23	900	V
					15:40	900	V
					16:02	900	V
S40636+68	3.17	1997 02 13	2.34	2	17:13	1800	V
					17:47	1800	V
		1997 02 16	2.34	4	17:34	900	V
					17:53	900	V
					18:10	900	V
					18:27	900	V
					1997 03 16	2.34	3
					14:48	900	V
					15:06	900	V
		1998 02 04	2.34	3	17:09	900	V
					17:30	900	V
					17:46	900	V
1998 02 05	2.34	2	16:34	900	V		
			16:52	900	V		



TABLE 3.3.2B - Continued

Object	z	Date of observation	Telescope (m)	No of obs	UT (start)	Integ. (s)	Filter
PC0751+56	4.28	1995 12 20	2.34	5	18:45	1800	V
					19:23	1800	V
					20:00	1800	V
					20:52	1800	V
					21:26	1800	V
					22:14	1800	V
		1995 12 24	2.34	5	17:56	600	I
					18:19	900	I
					18:53	1200	I
					19:38	1800	I
					20:35	1800	I
					1995 12 25	2.34	14
		17:45	300	I			
		18:05	900	I			
		18:24	900	I			
		18:43	900	I			
		19:00	900	I			
		19:22	900	I			
		19:39	900	I			
		20:04	1800	V			
		20:36	1800	V			
		21:10	1800	V			
		21:43	1800	V			
		1996 03 20	2.34	9	14:18	1200	I
					14:44	1200	I
					15:13	1200	I
					15:35	1200	I
					16:00	1200	I
					16:24	1200	I
					17:02	1200	I
					17:28	1800	I
					18:09	1200	I

TABLE 3.3.2B - Continued

Object	z	Date of observation	Tele-scope (m)	No of obs	UT (start)	Integ. (s)	Filter
PC0751+56 (contd.)	4.28	1996 03 21	2.34	4	14:42	1800	V
					15:44	1800	V
					16:17	1800	V
					16:50	1800	V
	1996 03 22	2.34	8	14:05	1800	I	
				14:44	1800	I	
				15:16	1800	I	
				15:48	1800	I	
				16:20	1800	I	
				16:54	1800	I	
				17:26	1800	I	
				17:59	1800	I	
	1996 03 23	2.34	8	14:03	1800	V	
				14:35	1800	V	
				15:09	1800	V	
				15:50	1800	V	
16:23				1800	V		
16:56				1800	V		
17:29				1800	V		
18:02				1800	V		
0822+27W1	2.06	1997 02 13	2.34	2	18:30	1800	V
					19:06	1800	V
	1997 03 14	2.34	2	15:02	1800	V	
				15:35	1800	V	
	1998 02 04	2.34	2	18:59	1800	V	
				19:44	1800	V	
	1998 02 06	2.34	2	16:00	1800	V	
				16:35	1800	V	

TABLE 3.3.2B - Continued

Object	z	Date of observation	Telescope (m)	No of obs	UT (start)	Integ. (s)	Filter
Q0913+07	2.78	1996 02 08	1.02	2	17:41	1800	V
					18:20	2700	V
		1996 02 15	1.02	2	17:10	2700	V
					18:03	2700	V
		1997 02 13	2.34	2	19:51	1800	V
					20:26	1800	V
		1997 03 14	2.34	3	16:23	1800	V
					16:55	1800	V
					17:28	1800	V
		1997 03 05	2.34	2	16:19	1800	V
Q1003-026	2.871	1997 02 14	2.34	3	18:15	1800	V
					18:52	1200	V
					19:14	1200	V
		1997 03 14	2.34	3	18:22	1800	V
					18:54	1800	V
					19:26	1800	V
		1998 02 04	2.34	1	21:27	1800	V
		1998 02 06	2.34	2	17:22	1800	V
					18:00	1800	V
		CSO38	2.62	1997 02 14	2.34	2	16:59
17:31	1200						V
1997 03 16	2.34			3	15:36	900	V
					15:54	900	V
					16:12	900	V
1998 02 05	2.34			2	18:51	1800	V
Q1317-05	3.7	1996 01 28	2.34	2	22:17	1800	B
					22:56	1800	B
		1996 01 29	2.34	4	21:15	1800	B
					21:50	1800	B
					22:23	1800	B
					22:58	1800	B
		1996 01 30	2.34	1	22:44	1800	B

TABLE 3.3.2B - Continued

Object	z	Date of observation	Tele-scope (m)	No of obs	UT (start)	Integ. (s)	Filter			
Q1317-05 (contd.)	3.7	1996 01 31	2.34	5	20:30	1800	B			
					21:13	1800	B			
					21:49	1800	B			
					22:28	1800	B			
					23:39	1800	B			
		1996 02 01	2.34	1	20:52	1800	B			
		1996 03 20	2.34	7	20:42	1200	I			
					21:07	1200	I			
					21:29	1200	I			
					21:52	1200	I			
					22:16	1200	I			
					22:38	1200	I			
					23:03	1200	I			
					1996 03 21	2.34	2	22:01	1800	V
					23:13	1800	V			
					1996 03 22	2.34	9	19:58	1200	I
								20:24	1200	I
		20:49	1200	I						
		21:10	1200	I						
		21:32	1200	I						
		21:54	1200	I						
		22:19	1200	I						
		23:09	1200	I						
		23:31	1200	I						
		1996 03 23	2.34	5				20:12	1800	V
								20:44	1800	V
					21:50	1800	V			
22:26	1800				V					
23:01	1800				V					
1997 05 30	2.34	3	14:47	1800	V					
			15:26	1800	V					
			16:12	1800	V					

TABLE 3.3.2B - Continued

Object	z	Date of observation	Telescope (m)	No of obs	UT (start)	Integ. (s)	Filter
Q1330+01	3.51	1995 07 03	1.02	2	15:17	1200	V
					15:51	1200	V
		1997 02 15	1.02	2	19:55	1800	V
					20:29	1800	V
		1997 02 16	2.34	5	20:48	900	V
					21:06	900	V
					21:24	900	V
					21:41	900	V
					21:58	900	V
					21:58	900	V
		1997 03 14	2.34	3	20:20	1800	V
					20:55	1800	V
					21:26	1800	V
		1997 03 16	2.34	2	17:35	1800	V
18:09	1800				V		
Q1410+09	3.24	1995 05 22	1.02	2	18:39	1800	V
					19:13	1800	V
		1995 06 08	1.02	2	14:51	2400	V
					15:40	2700	V
		1997 02 13	2.34	2	22:04	1800	V
					22:38	1800	V
		1997 02 16	2.34	1	23:02	1800	V
		1997 03 16	2.34	2	19:09	1800	V
19:44	1800				V		
Q1415+45	0.114	1997 02 14	2.34	2	21:58	900	V
					22:16	600	V
		1997 06 01	2.34	5	14:50	900	V
					15:21	900	V
					15:40	900	V
					15:58	900	V
					16:15	900	V
		1997 06 02	2.34	2	15:19	900	V
					15:52	900	V

TABLE 3.3.2B - Continued

Object	z	Date of observation	Telescope (m)	No of obs	UT (start)	Integ. (s)	Filter	
Q1548+09	2.749	1995 05 22	1.02	2	20:25	2400	V	
					21:06	2400	V	
		1996 04 27	2.34	6		17:09	900	V
						17:43	900	V
						18:02	900	V
						18:18	900	V
						18:34	900	V
						18:50	900	V
		1997 03 14	2.34	2		22:35	1800	V
						23:07	1800	V
KP1633+63	2.15	1995 07 03	1.02	3	16:49	1200	V	
					17:12	1200	V	
					17:36	1200	V	
		1997 06 01	2.34	2		19:25	900	V
						19:44	900	V
1E1711+712	1.60	1997 06 01	2.34	2	20:23	1200	V	
					20:45	1200	V	
		1997 06 08	1.02	2		19:46	2400	V
						20:34	2400	V
Q2040-40	2.07	1996 10 03	2.34	3	14:32	1800	V	
					15:10	1800	V	
					17:30	1800	V	
		1996 10 04	2.34	3		13:38	1800	V
						14:11	1800	V
						14:44	1800	V
Q2304-42	2.63	1996 10 04	2.34	3	15:45	1800	V	
					16:13	1800	V	
					17:25	1800	V	
		1997 09 28	2.34	1		18:40	1800	V

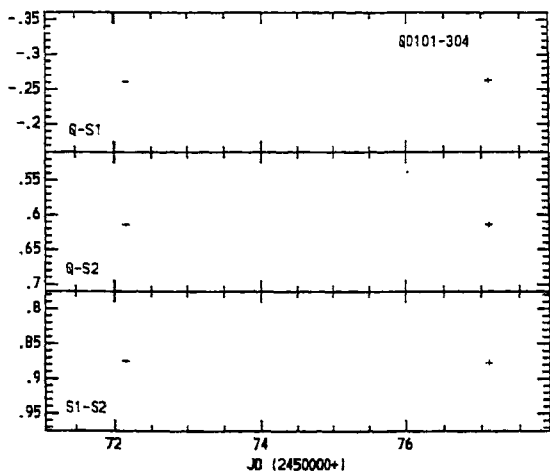


Fig.3.3.1a Differential photometric light curve of Q0101-304 in V band

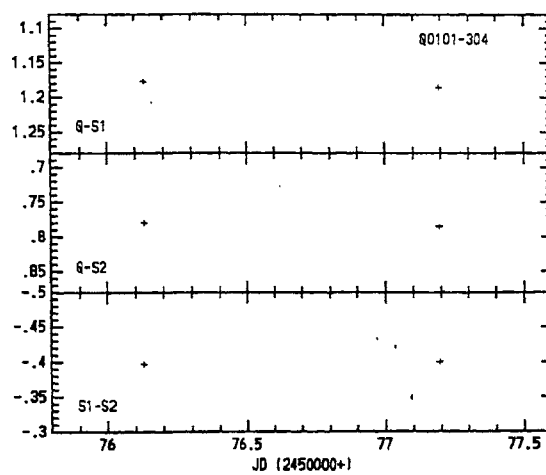


Fig.3.3.1b Same as Fig.3.3.1a but for Q0101-304 in I band

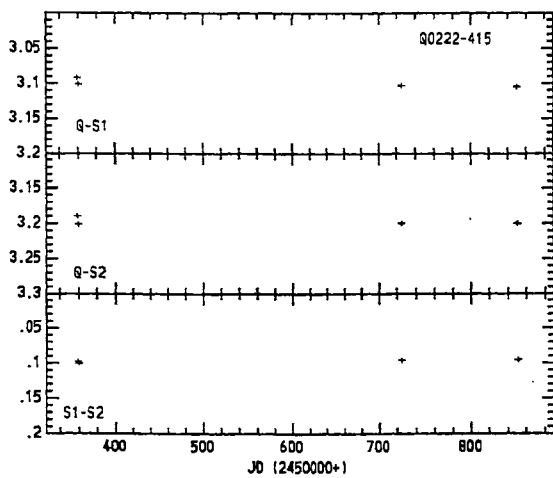


Fig.3.3.1c Same as Fig.3.3.1a but for Q0222-415

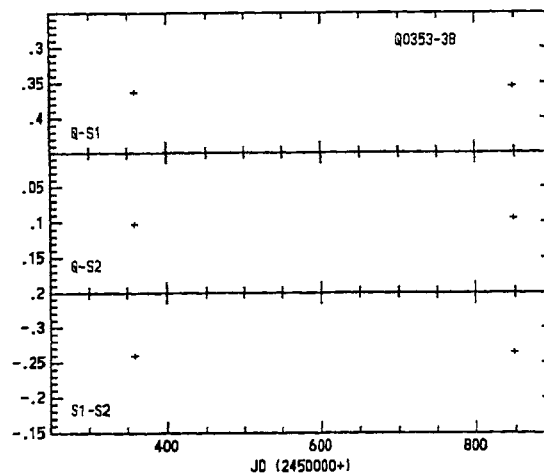


Fig.3.3.1d Same as Fig.3.3.1a but for Q0353-38

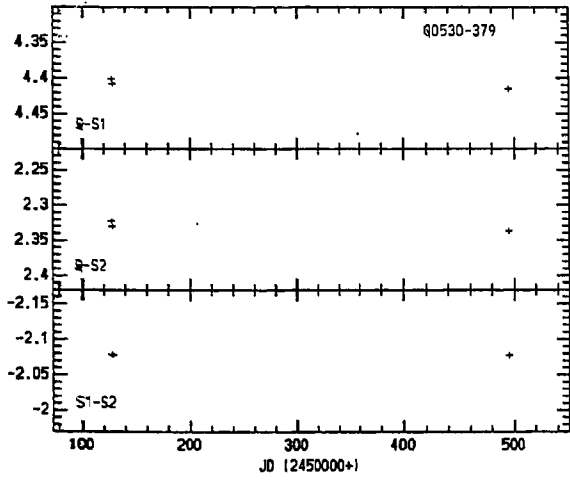


Fig.3.3.1e Same as Fig.3.3.1a but for Q0530-379

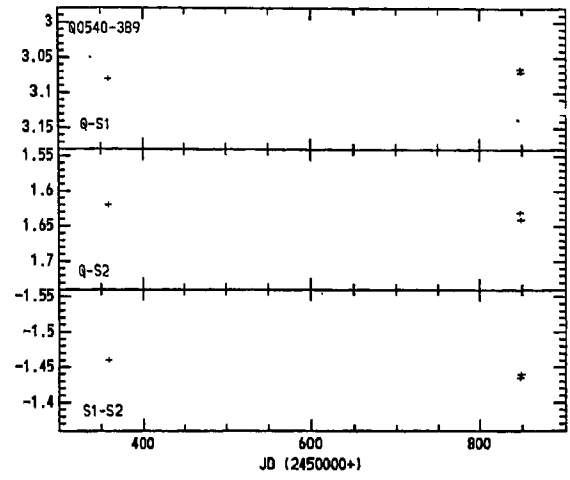


Fig.3.3.1f Same as Fig.3.3.1a but for Q0540-389

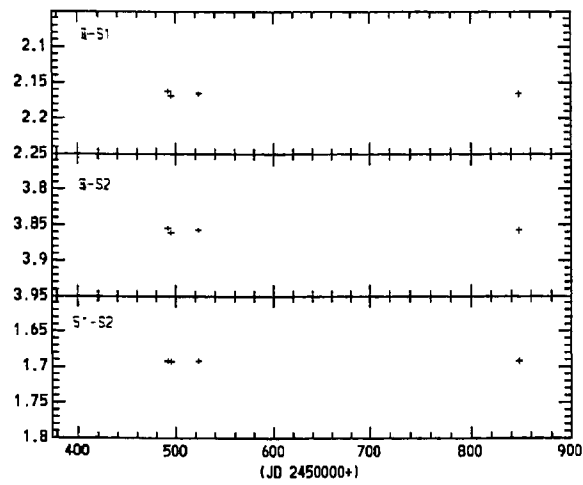


Fig.3.3.1g Same as Fig.3.3.1a but for S4 0636+68

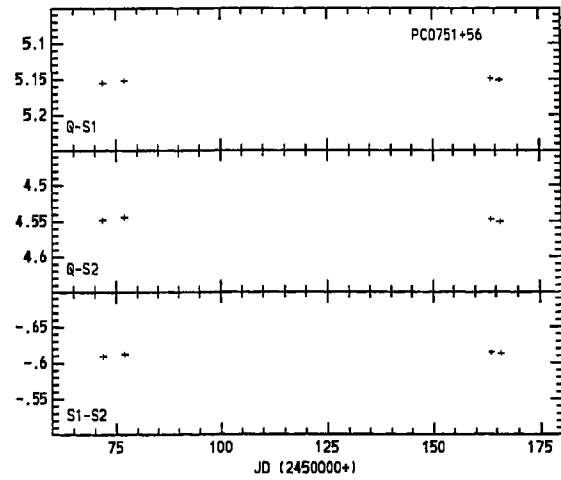


Fig.3.3.1h Same as Fig.3.3.1a but for PC0751+56



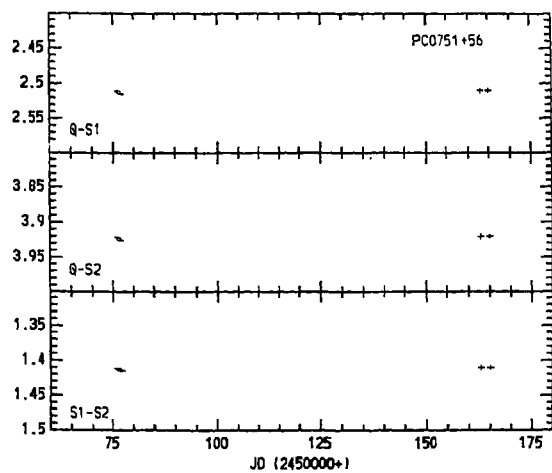


Fig.3.3.1i Same as Fig.3.3.1a but for PC0751+56 in I band

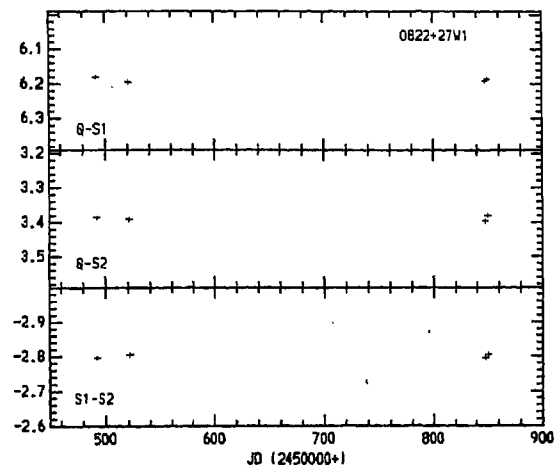


Fig.3.3.1j same as Fig.3.3.1a but for 0822+27W1

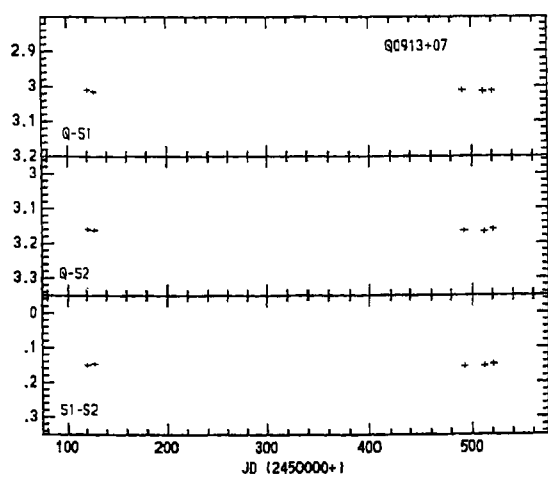


Fig.3.3.1k Same as Fig.3.3.1a but for Q0913+07

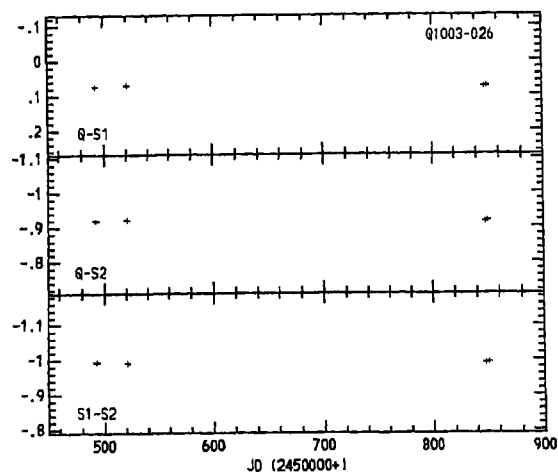


Fig.3.3.1l Same as Fig.3.3.1a but for Q1003-026

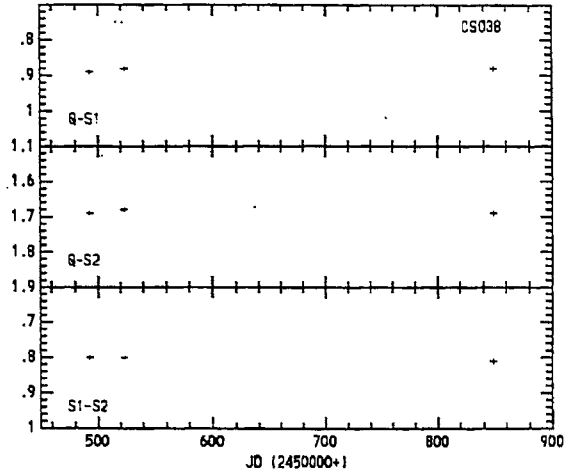


Fig.3.3.1m Same as Fig.3.3.1a but for CS038

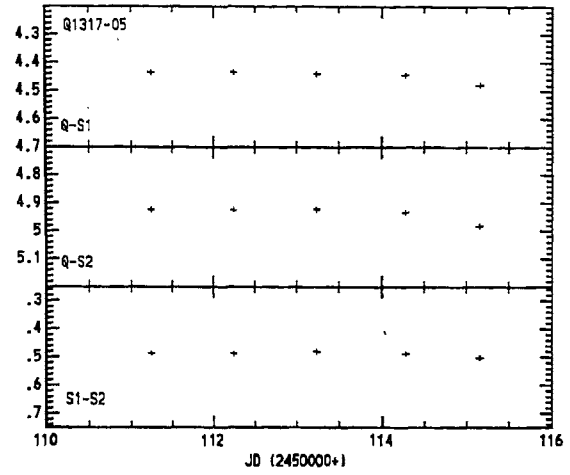


Fig.3.3.1n Same as Fig.3.3.1a but for Q1317-05 in B band

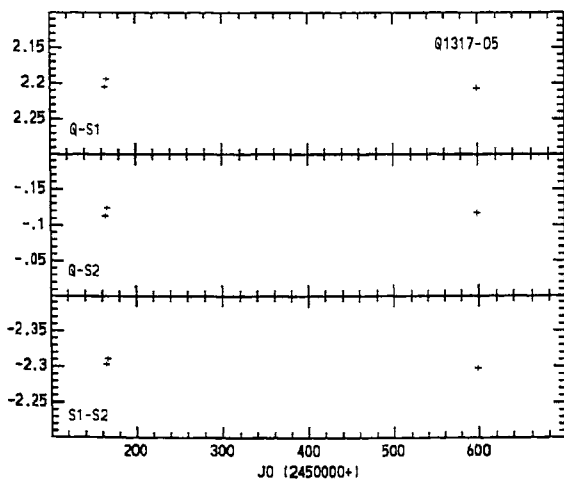


Fig.3.3.1o Same as Fig.3.3.1a but for Q1317-05 in V band

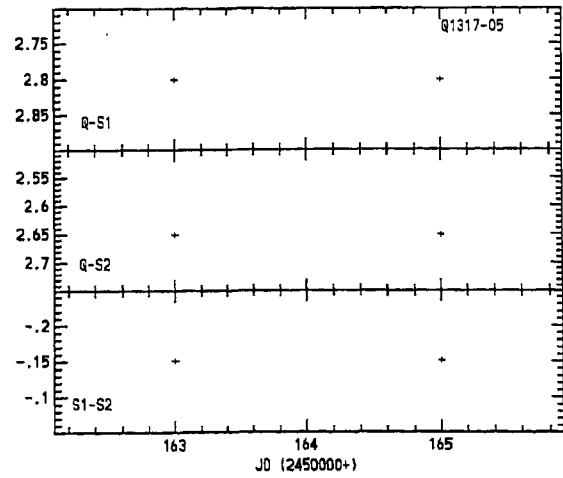


Fig.3.3.1p Same as Fig.3.3.1a but for Q1317-05 in I band

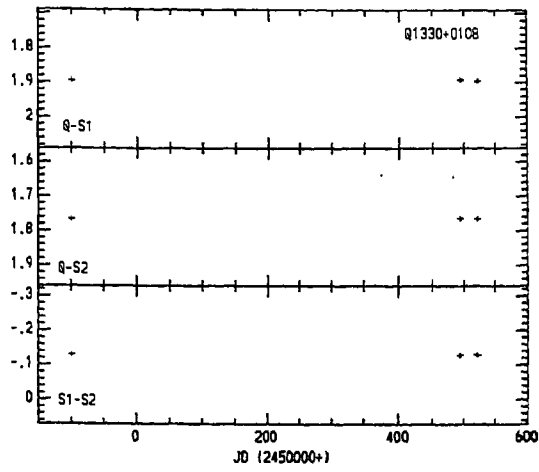


Fig.3.3.1q Same as Fig.3.3.1a but for Q1330+01

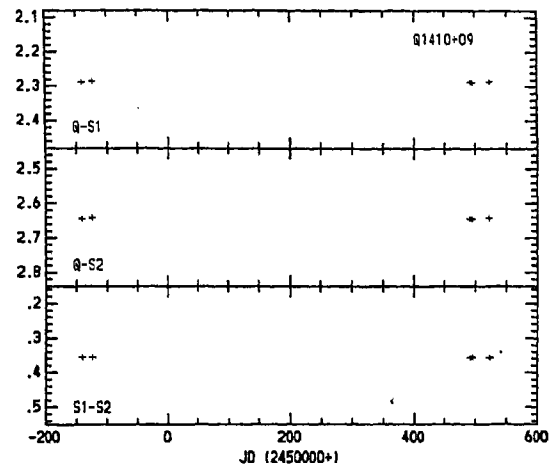


Fig.3.3.1r Same as Fig.3.3.1a but for Q1410+09

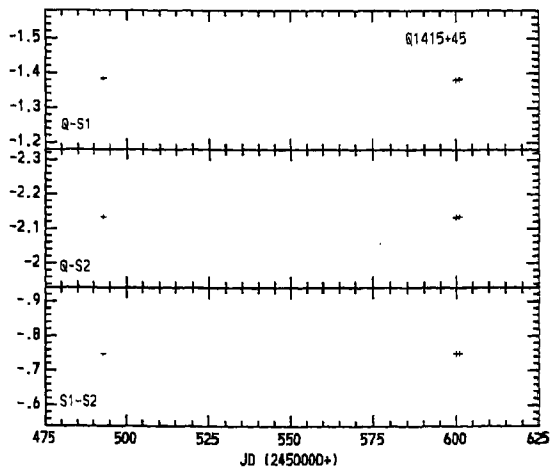


Fig.3.3.1s Same as Fig.3.3.1a but for Q1415+45

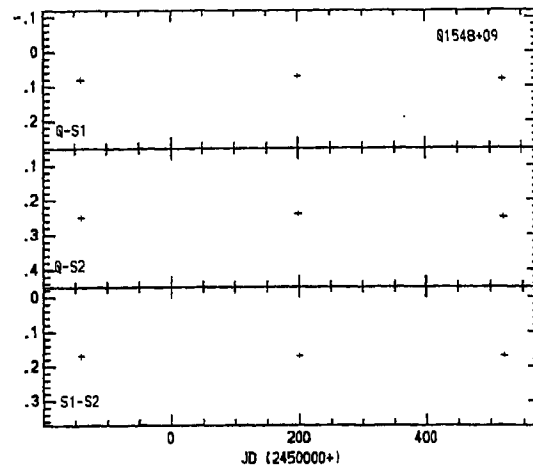


Fig.3.3.1t Same as Fig.3.3.1a but for Q1548+09

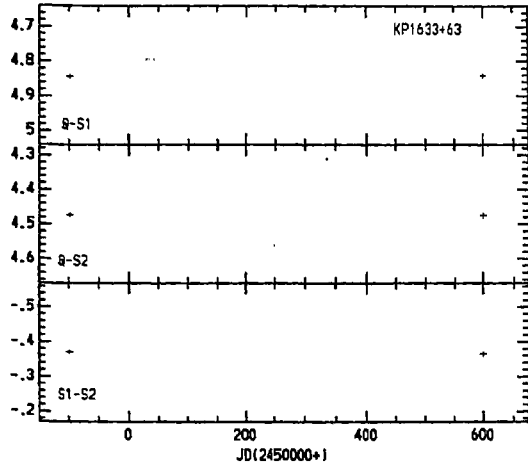


Fig.3.3.1u Same as Fig.3.3.1a but for KP1633+63

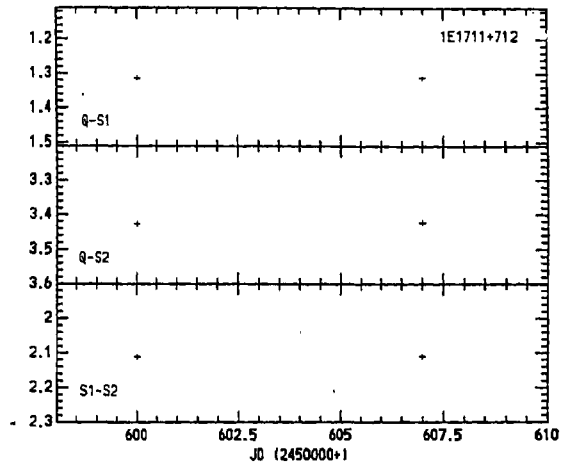


Fig.3.3.1v Same as Fig.3.3.1a but for 1E1711+712

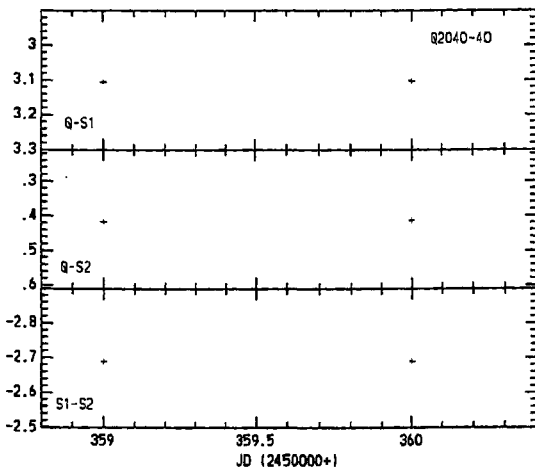


Fig.3.3.1w Same as Fig.3.3.1a but for Q2040-40

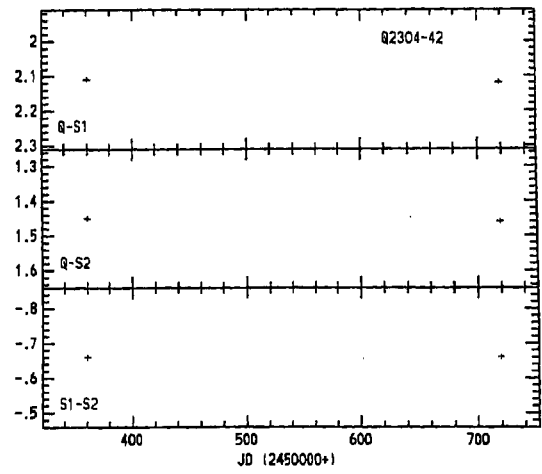


Fig.3.3.1x Same as Fig.3.3.1a but for Q2304-42

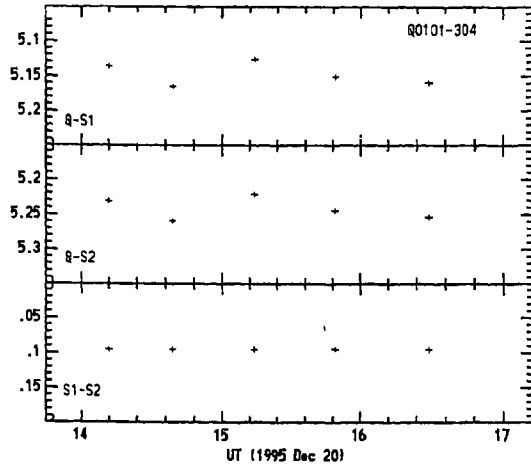


Fig.3.3.2a Intranight differential photometric light curve of Q0101-304

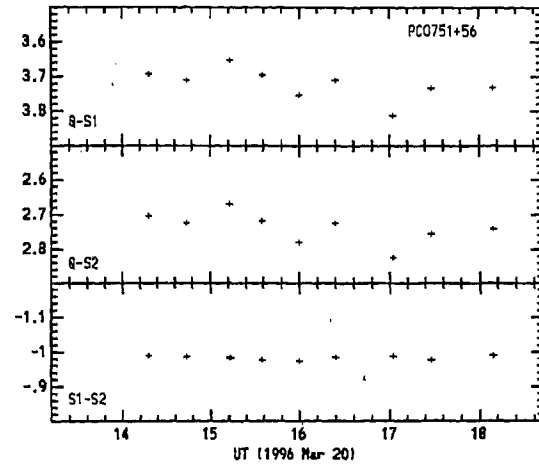


Fig.3.3.2b Same as Fig.3.3.2a but for PC0751+56 in I band

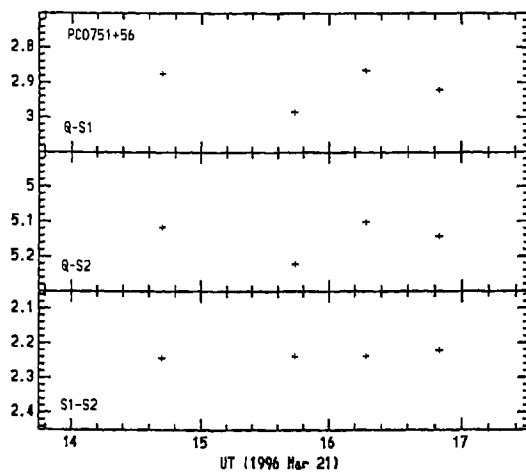


Fig.3.3.2c Same as Fig.3.3.2a but for PC0751+56

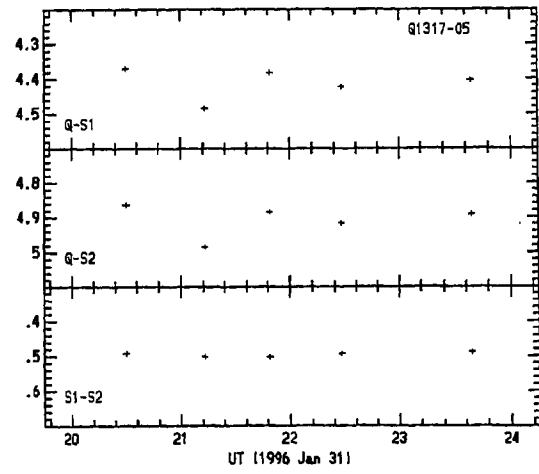


Fig.3.3.2d Same as Fig.3.3.2a but for Q1317-05 in B band

radio-quiet quasars, during our observations. The radio-quiet quasars Q0101-304, PC0751+56 and Q1317-05 displayed intranight microvariations on a few nights. It is suggested that observing more number of radio-quiet sources for a longer duration may be useful as it may be possible that variability periods of the sample sources are longer than the duration of our observations.

## 4. CONCLUSIONS AND FUTURE PROSPECTS

We carried out the EXOSAT X-ray (0.1-10 keV) spectral analysis of a sample of thirteen Seyfert galaxies and a complete sample of twenty eight EXOSAT blazars. The radio through X-ray multifrequency spectra of all these twenty eight blazars were studied. We participated in the International AGN Watch Campaign to obtain multifrequency data on the luminous Seyfert 1 galaxy Fairall-9. We have also participated in the international multifrequency monitoring campaigns to monitor six blazars in the visual band simultaneously with the multifrequency observations. Four of them were monitored in simultaneity with *Compton Gamma Ray Observatory* observations. To study the variations of the two blazars 3C66A and OJ287 in flare state, we undertook a program to monitor these sources during 1995 December to 1996 March, when these two sources were in high state. In order to estimate the long and short term variabilities of radio-quiet quasars, a sample of 20 radio-quiet quasars were observed at VBO, in B, V and I photometric passbands, during 1995 to 1998. Conclusions drawn in Chapter 3, based on the above studies, are summarized here.

### 4.1. Seyfert Galaxies

The results of the EXOSAT X-ray spectral analysis of a sample of thirteen Seyfert galaxies are outlined below:

The ME (2-10 keV) X-ray spectra of Seyferts can be adequately described by a simple power-law. In the LE region (0.1-2 keV) all the sources in our sample, other than ESO140-G43, show soft excess emissions. No low-energy absorption was found in these soft excess sources, except NGC3516 which displays very weak soft excess. Low energy absorption was detected in ESO140-G43 in which no soft-excess emission was found. Probably ESO140-G43 also has a weak soft excess, which was hidden by its  $N_{\text{H}} \sim 10^{21} \text{ cm}^{-2}$  absorber. Thus we suggest that soft excesses are a common feature of Seyfert galaxies and the detection of soft excess depends on the low-energy absorption in the line-of-sight to the source.

Two power-law, thermal bremsstrahlung and broken power-law models were used to fit the detected soft excesses. Only broken power-law model provides good fit to the soft excess which indicates that two components (soft and hard) are required to fit the spectrum.

Our results show the presence of variable soft excess in 3C382 which is correlated with the LE count rate, with the soft spectral slope and with the softness ratio. Although the variability of LE and ME count rates was correlated, the ME spectral slope remained roughly constant. There is no relation between the ME count rate and the softness ratio. These results suggest that soft excess was maximum and soft spectral slope was steepest when this galaxy was in its brightest state.. The hard spectral component was practically unchanged even though there were dramatic variations in the source. The hard spectral index, in the case of MCG 2-58-22 also, remained unchanged during soft excess variations. The above mentioned results indicate that the soft and hard X-rays originate from distinct sources (probably from different nuclear regions of these galaxies).

Majority (nine out of thirteen) of the sources in our sample show a statistically significant improvement in the goodness of the fit upon the addition of a Gaussian emission line at energies (around 6.0 keV) characteristic of iron  $K_{\alpha}$  line emission. From the distribution of redshifted Fe line energies of our analysis, it is noted that the data are consistent with 6.4 keV.

The main results of the campaign on the active nucleus in the Seyfert galaxy Fairall 9 are as follows:

During this monitoring period the optical continuum varied significantly. Continuum variations of amplitude  $\sim 12\%$  are detected on time scales as short as  $\sim 20$  days. Over  $\sim 94$  days, a factor of 2 change in the nuclear continuum was observed. The amplitude of optical continuum variations is about the same as that of the UV continuum. The optical and UV continuum light curves show two events of low-amplitude variations with a duration of  $\sim 70$  days. There is no measurable lag between the UV and the optical continuum light curves. The UV data show a third larger amplitude event that occurred after the optical monitoring had terminated.



The H $\beta$  emission-line flux also underwent significant low-amplitude ( $\geq 20\%$ ) variations. It is estimated that H $\beta$  lags behind the UV continuum by about 23 days, a value much smaller than what was previously suggested by earlier variability studies. However this small lag is consistent with the lags for the UV lines during this campaign in the sense that H $\beta$  lag is nearly 50% larger than that of Ly  $\alpha$  which is similar to the results for lower luminosity AGNs such as NGC 4151, NGC5548 and NGC3783.

## 4.2. Blazars

The blazars have been divided into two groups: radio-selected blazars (RBLs) and X-ray selected blazars (XBLs). Our X-ray results of a complete sample of twenty eight EXOSAT blazars suggest that XBLs are steep spectrum sources and RBLs are relatively flat spectrum sources. Even though RBLs are, in general, higher redshift objects than XBLs, they are only slightly more luminous (by a factor of 4-7) in X-rays than XBLs. However, RBLs are much more luminous (by two or three orders of magnitude) in radio than the XBLs. Using simultaneous/quasi-simultaneous and nonsimultaneous observations, we have constructed the multifrequency spectra (radio through X-ray continuum fluxes) of 28 blazars, and they can be well represented with a single parabolic curve for XBLs and with two parabolic curves for RBLs. One of the important differences between the multifrequency spectra of RBLs and XBLs is the spectral discontinuity in the UV-X-ray region of RBLs. This result has been confirmed by only using simultaneous UV and X-ray observations of 50% of the sources of the present sample. Luminosities at different bands have also been computed for all the blazars in the present sample and bimodal character of distribution of these objects has been found in the radio and X-ray luminosity plane. All these results are discussed in the framework of a 'wide-jet' model.

We participated in the international multifrequency monitoring campaigns to monitor six blazars (PKS0528+13, Mkn501, 3C390.3, BL Lac, 3C446 and CTA102) in the visual band. Four of them (PKS0528+13, Mkn501, BL Lac, and CTA102) were monitored in simultaneity with *Compton Gamma Ray Observatory* observations. The blazars were observed during their flare

states. Our results indicate night to night variations in all the sources, except CTA 102. We have detected intranight variations in two of them (Mkn501, BL Lac).

To study the variations of the two blazars 3C66A and OJ287 in flare states we undertook a program to monitor these sources using the 75 cm telescope of the Vainu Bappu Observatory, Kavalur. The white-light CCD observations of these sources were obtained during 1995 December to 1996 March, when these two sources were in high state. Large amplitude night to night variations were found in 3C66A and OJ287. Our observations of flaring activity in the blazar OJ287 support the proposed periodicity of 11.6 years.

The optical photometric and spectroscopic observations of 3C390.3 show that the broad band fluxes (B, V, R and I), the spectrophotometric optical continuum flux  $F_{\lambda}$  (5177 Å), and the integrated emission-line fluxes of H $\alpha$ , H $\beta$ , H $\gamma$ , He I ( $\lambda$ 5876) and He II  $\lambda$ 4686 show a nearly monotonic increase with episodes of milder short-term variations superposed. The amplitude of the continuum variations increases with decreasing wavelength (4400-9000 Å). The optical continuum variations follow the variations in the ultraviolet and X-ray with time delays, measured from the centroids of the cross-correlation functions, typically around 5 days, but with uncertainties also typically around 5 days. Zero time delay between the high energy and low-energy continuum variations also can not be ruled out. The strong optical emission lines H $\alpha$ , H $\beta$ , H $\gamma$  and He I ( $\lambda$ 5876) respond to the high-energy continuum variations with time delays typically about  $20 \pm 08$  days. There is some evidence that He II ( $\lambda$ 4686) responds somewhat more rapidly with a time delay of  $\sim 10$  days, but the uncertainties are large ( $\sim 8$  days).

### 4.3. Radio-Quiet Quasars

Among quasars, radio-loud sources (RLQs) are found to be highly variable. A possible explanation is that there is some contribution to the observed flux at all energies from the relativistic plasma jet motion. Relativistic shock propagating down a jet and its interaction with irregularities in the flow can cause large amplitude and rapid variabilities in RLQs. Whereas, radio-quiet quasars (RQQs), mostly show smaller amplitude variations which may be of

completely different origin, like, instabilities in accretion disks, because, unlike RLQs, RQQs do not show powerful radio jets or extended radio lobes (Siemiginowska 1993). RQQs have only weak radio structures. However, the continuum shape and the emission line characteristics from FIR to X-ray are similar for RQQs and RLQs (Elvis et al. 1994). About 90% of all quasars are radio-quiet. It is thought that non-periodic short term and periodic long term variabilities may be present in the case of RQQs. Long term variability is the small and steady variations of the base level or quiescent state from which shorter and high/low amplitude events or flares apparently erupt. In order to estimate the long and short term variabilities of RQQs, a sample of 20 radio-quiet quasars were observed at VBO, in B, V and I photometric passbands, during 1995 to 1998. No long term variability have been detected in our sample of radio-quiet quasars, during our observations. However, the radio-quiet quasars Q0101-304, PC0751+56 and Q1317-05 displayed intranight microvariations on a few nights. It is suggested that observing more number of radio-quiet sources for a longer duration may be useful, as it may be possible that the variability periods of the sample sources are longer than the duration of our observations.

#### **4.4. Future Prospects**

The X-ray spectral studies of AGNs is a powerful tool for understanding the nature of AGNs. The origin of the X-ray emission and its power-law shape are still not well understood. Also the origin of the detected emission feature around 6 keV in the X-ray spectra of several AGNs is still under debate. Accurate measurement of the exact line centre energy and the estimation of the shape of the emission feature can yield a better understanding about the emitting region. With the limited energy resolution of EXOSAT it was not possible to estimate the spectral shape and accurate line centre energy of the emission feature around 6 keV detected in our sample of AGNs. However, the recent ASCA observations of the Seyfert 1 galaxy MCG-6-30-15 (Tanaka et al. 1995) has suggested an asymmetry in the iron  $K\alpha$  line profile confirming theoretical models which attribute the iron line emission to an accretion disc orbiting around a blackhole. Probably the results to be obtained from the future X-ray missions will be able to address these questions.

Another important unresolved question is about the origin of the detected soft X-ray excesses. Since the signal-to-noise ratio and energy resolution of the EXOSAT detectors are low at the soft X-ray region, it is not possible to draw a definite conclusion about the origin of the soft excess. Recent observations of radio-quiet AGNs with ROSAT PSPC (Fiore et al. 1994) found that the strength of emission line features in the soft X-ray band to be very low. The absence of strong line features argue against emission from an ionized plasma as the main contributor to the soft X-ray component. Also ROSAT PSPC results could not rule out the possibility of non-thermal origin for the soft X-ray emission. To understand more about the details of soft X-ray emission, detectors with better energy resolution than the ROSAT and the ASCA detectors are needed. Thus the future high energy resolution spectroscopic studies of a more number of AGNs are very much needed to understand further the nature of AGNs.

In AGNs a large variety of physical processes occur and as a result they emit radiation from radio to  $\gamma$ -rays. Therefore simultaneous multifrequency observations are essential in order to understand the AGN paradigm.

## List of Publications

1. Ghosh, K. K. and Soundararajaperumal, S. 1993, *Astron. Astrophys.*, **273**, 397.  
"X-ray spectral variability of the Seyfert galaxy NGC 4593".
2. Ghosh, K. K. & Soundararajaperumal, S. 1993, *Proc. IAU Symp.* **159**, .505.  
"Multifrequency Spectra of blazars".
3. Ghosh, K.K. and Soundararajaperumal, S. 1994,  
in 'Frontiers of Space & Ground-based Astronomy - The Astrophys. of the 21st Century',  
(Eds. W. Wamsteker, M. S. Longair, & Y. Kondo : Dordrecht: Kluwer Academic  
Publishers) *Astrophys. & Space Sci. Lib.*, **187**, .687.  
" Multifrequency Spectra of Blazars",
4. Ghosh, K. K. & Soundararajaperumal, S. 1995, *J. Astrophys. & Astron. Suppl.*, **16**, 189.  
"Anisotropic emissions from AGNs".
5. Ghosh, K. K. & Soundararajaperumal, S. 1995, *Astrophys. J. Suppl.* **100**, 37.  
"Multifrequency spectra of EXOSAT blazars".
6. Santos-Lleo, M., Ghosh, K. K. Soundararajaperumal, S., et al. 1997, *Astrophys. J. Suppl.*,  
**112**, 271.  
"Steps toward determination of the size and structure of the broad-line region  
in active galactic nuclei. X. Variability of Fairall 9 from optical data"
7. Dietrich, M., Ghosh, K. K. Soundararajaperumal, S., et al. 1998, *Astrophys. J. Suppl.*,  
**115**, 185.  
"Steps toward determination of the size and structure of the broad-line region in active  
galactic nuclei. XII. Ground-Based Monitoring of 3C390.3"

## References

- Adams, T. F. 1977, *Astrophys. J. Suppl.*, 33, 19
- Agrawal, P. C. 1996, in 'Proc. of the International Colloq. on Perspectives in High Energy Astron. & Astrophys.' TIFR, Mumbai, India, Aug 12-17, 1996, (eds. P. C. Agrawal & R. Vishvanath : Universities Press), p408
- Alef, W., et al. 1996, *Astron. Astrophys.*, 308, 376
- Aller, H. D., et al. 1985, *Astrophys. J. Suppl.*, 59, 513
- Alloin, D., et al. 1994, in *Frontiers of Space and Ground based Astronomy - The Astrophys. of the 21st Century*, (eds. W. Wamsteker, M. S. Longair, & Y. Kondo : Dordrecht: Kluwer Academic Publishers) p 423
- Alloin, D., et al. 1995, *Astron. Astrophys.*, 293, 293
- Angel, J. R. P., & Stockman, H. S. 1980, *Ann. Rev. Astron. Astrophys.*, 18, 321
- Antonucci, R.R.J. 1993, *Ann. Rev. Astron. Astrophys.*, 31, 473
- Antonucci, R.R.J. & Miller, J. S. 1985, *Astrophys. J.*, 297, 621
- Apparao, K. M. V. et al. 1978, *Nature*, 273, 450
- Arakelian, M. A., et al. 1971, *Astrophys.*, 7, 102
- Arnaud, K. A., et al. 1985, *Mon. Not. Roy. Astron. Soc.*, 217, 105
- Awaki, H. 1991, PhD thesis at Nagoya University
- Baade, W., & Minkowski, R. 1954, *Astrophys. J.*, 119, 221
- Baath, L. B. 1987, in 'Superluminal Radio Sources', Proc. of a workshop in honour of Prof. Marshall H. Cohen, held at Big Bear Solar Obs., California, USA, 28-30 Oct.1986 (eds. J. A. Zensus et al.: Cambridge University Press) p 206
- Baath, L. B., et al. 1981, *Astron. Astrophys.*, 96, 316
- Band, D. L., & Grindlay, G. E. 1985, *Astrophys. J.*, 298, 128
- Barbieri, C., et al. 1990, *Astrophys. J.*, 359, 63
- Barr, P., Giommi, P., & Maccagni, D., 1988, *Astrophys. J.*, 324, L11
- Barthel, P.D. 1989, *Astrophys. J.*, 336, 606
- Barvainis, R. 1990, *Astrophys. J.*, 353, 419
- Bell-Burnell, S. J., & Chiappetti, L. 1984, *Astron. Astrophys. Suppl.*, 56, 415

- Bell-Burnell, S. J., & Culhane, J. L. 1979, *Mon. Not. Roy. Astron. Soc.*, 188, 1p
- Bersanelli, M., et al. 1992, *Astron. J.*, 104, 28
- Blandford, R. D. & Rees, M. J. 1978, in Pittsburg Conference on BL Lac objects, ed, A.N.Wolfe (Pittsburg, Univ. of Pittsburg Press) p 328
- Blandford, R. D. 1990, Lecture Notes 1990, Swiss Society for Astrophysics and Astronomy (eds. T.J.-L. Courvoisier & M. Mayor : Springer-Verlog), p161
- Blandford, R. D. 1994, ASP Conf. Series, 54, 23
- Blandford, R. D., & McKee, C. F. 1982, *Astrophys. J.*, 255, 419
- Blandford, R. D., & Rees, M. J. 1978, in Pittsburgh Conf. on BL Lac objects, ed. A. M. Wolfe (Pittsburgh: Univ. of Pittsburgh Press), p 328
- Blandford, R. D., 1987, in 'Superluminal Radio Sources', Proc. of a workshop in honour of Prof. Marshall H. Cohen, held at Big Bear Solar Obs., California, USA, 28-30 Oct.1986 (eds. J. A. Zensus et al.: Cambridge University Press), p310
- Boksenberg, A., et al. 1978, *Nature*, 275, 404
- Boller, Th., Brandt, W. N., & Fink, H. 1996, *Astron. Astrophys.*, 305, 53
- Bowyer, S. 1994, in Frontiers of Space and Ground based Astronomy - The Astrophys. of the 21st Century, (eds. W. Wamsteker, M. S. Longair, & Y. Kondo : Kluwer Academic Publishers) p67
- Bradt, H, & Margon, B. 1978, *Sky & Telescope*, 56, 499
- Bradt, H. V. D. , Ohashi, T., & Pounds, K. A. 1992, *Ann. Rev. Astron. Astrophys.*, 30, 391
- Bregman, J. N., et al. 1982, *Astrophys. J.*, 253, 19
- Bregman, J. N., et al. 1988, *Astrophys. J.*, 331, 746
- Bregman, J. N., et al. 1990, *Astrophys. J.*, 352, 574
- Brindle, C., et al. 1990, *Mon. Not. Roy. Astron. Soc.*, 244, 577
- Brissenden, R. J. V., et al. 1990, *Astrophys. J.*, 350, 578
- Brown, L. M. J., et al. 1989, *Astrophys. J.*, 340, 129
- Burbidge, E. M., & Strittmatter, P. A. 1972, *Astrophys. J. Lett.*, 172, 37
- Burbidge, G., & Hewitt, A. 1992, in Variability of Blazars, ed. E. Valtaoja & M. Valtonen (Cambridge: Cambridge Univ. Press), p4
- Bushouse, H. A. 1987, *Astrophys. J.*, 320, 49

Catanese, M., et al. 1997, *Astrophys. J. Lett.*, 487, 143  
 Cellotti, A., et al. 1993, *Astrophys. J.*, 416, 118  
 Celotti, A., et al. 1993, *Astrophys. J.*, 416, 118  
 Claval, J., et al. 1991, *Astrophys. J.*, 336, 64  
 Claval, J., et al. 1992, *Astrophys. J.*, 392, 113  
 Clavel, J., Wamsteker, W., & Glass, I. S. 1989, *Astrophys. J.*, 337, 236  
 Cohen, R. D., et al. 1987, *Astrophys. J.*, 318, 577  
 Collin-Souffrin, S. 1991, *AIP Conf. Proc.* 254, (eds. S. Holt, S. G. Neff and C. M. Urry) p119  
 Cooke, B. A., et al. 1976, *Mon. Not. Roy. Astron. Soc.*, 177, 121p  
 Cooke, B. A., et al. 1978, *Astrophys. J.*, 222, L91  
 Courvoisier, T. J. L., Bell Burnell, J., & Blécha, A. 1986, *Astron. Astrophys.*, 169, 43  
 Courvoisier, T. J. L., et al. 1990, *Astron. Astrophys.*, 234, 73  
 Cruz-Gonzalez, I. & Huchra, J. P. 1984, *Astron. J.*, 89, 441  
 Cruz-Gonzalez, I., & Huchra, J. P. 1984, *Astron. J.*, 89, 441  
 Curtis, H. D. 1918, *Pub. Lick Obs.*, 13, 31  
 Danziger, I. J., et al. 1979, *Mon. Not. Roy. Astron. Soc.*, 188, 415  
 Davidson, P. J. N., et al. 1975, *Astrophys. J. Lett.*, 196, 23  
 de Bruyn, A. G., Wilson, A. S. 1976, *Astron. Astrophys.*, 53, 93  
 De Grijp, M. H. K., et al. 1985, *Nature*, 314, 240  
 de Korte, P.A.J. et al. 1981, *Space Sci. Rev.*, 30, 495  
 de Ruiter, H. R., Lub., J. 1986, *Astron. Astrophys. Suppl.*, 63, 59  
 Denisyuk, E. K., & Lipovetsky, V. A. 1974, *Astrophys.* 10, 195  
 Denisyuk, E. K., & Lipovetsky, V. A. 1977, *Soviet Astron. J. Lett.*, 3, 3  
 Dietrich, M., Ghosh, K. K., Soundararajaperumal. S., et al. 1998, *Astrophys. J. Suppl.*, 115, 185  
 Done, C., et al. 1992, *Astrophys. J.*, 400, 138  
 Dower, R. G., et al. 1980, *Astrophys. J.*, 235, 355  
 Doxey, R., et al. 1983, *Astrophys. J.*, 264, L43  
 Edelson, R. A. 1987, *Astron. J.*, 94, 1150  
 Edelson, R. A., et al. 1992, *Astrophys. J. Suppl.*, 83, 1  
 Edelson, R. A., Malkan, M. A., & Ricke, G. H. 1987, *Astrophys. J.*, 321,233



- Efstathiou, G., & Rees, M. J. 1988, *Mon. Not. Roy. Astron. Soc.*, 230, 5P
- Elvis, M., et al. 1978, *Mon. Not. Roy. Astron. Soc.*, 183, 129
- Elvis, M., Lockman, F. J., & Wilkes, B. J. 1989, *Astron. J.*, 97, 777
- Elvis, M. et al. 1994, *Astrophys. J. Suppl.*, 95,1
- Fabian A. C., et al., 1995, *Mon. Not. Roy. Astron. Soc.*, L11
- Fabian, A. C., et al. 1989, *Mon. Not. Roy. Astron. Soc.*, 238, 729
- Fabian, A. C., et al. 1995, *Mon. Not. Roy. Astron. Soc.*, 277, L11
- Fairall, A. P. 1977, *Mon. Not. Roy. Astron. Soc.*, 180, 391
- Fanaroff, B., & Riley, J. M. 1974, *Mon. Not. Roy. Astron. Soc.*, 167, 31p
- Feigelson, E. D., Maccacaro, T., Zamorani, G. 1982, *Astrophys. J.*, 255, 392
- Feigelson, E.D. et al. 1986, *Astrophys. J.*, 302, 337
- Fenimore, E., et al. 1988, *Astrophys. J. Lett.*, 335, 71
- Fiore, F., et al., 1994, *Astrophys. J.*, 431, 515
- Fraser, G. W. 1989, 'X-Ray Detectors in Astronomy', Cambridge Astrophysics Series, Cambridge University Press
- French, H. B., & Miller, J. S. 1980, *Pub. Astron. Soc. Pacific*, 92, 753
- Fugmann, W., & Meisenheimer, K. 1988, *Astron. Astrophys. Suppl.*, 76, 145
- Garilli, B., & Maccagni, D. 1990, *Astron. Astrophys.*, 229, 88
- Garington, S. T., et al. 1988, *Nature*, 331, 147
- Gear, W. K., et al. 1986, 304, 295
- George, I. M., Warwick, R.S., & Bromage, G. E. 1988a, *Mon. Not. Roy. Astron. Soc.*, 232, 793
- George, I. M., Warwick, R.S., & McHardy, I. M. 1988b, *Mon. Not. Roy. Astron. Soc.*, 235, 787
- George, I.M. & Fabian, A.C. 1991, *Mon. Not. Roy. Astron. Soc.*, 249, 352
- Ghisellini, G., & Maraschi, L. 1989, *Astrophys. J.*, 340, 181
- Ghisellini, G., Maraschi, L. & Treves, A. 1985, *Astron. Astrophys.*, 146, 204
- Ghosh, K. K. & Soundararajaperumal. S. , 1991a, *Astron. J.*, 102, 1298
- Ghosh, K. K. & Soundararajaperumal. S. , 1991b, *Astron. Astrophys.*, 252, 53
- Ghosh, K. K. & Soundararajaperumal. S. , 1992a, *Astron. Astrophys.*, 265, 413
- Ghosh, K. K. & Soundararajaperumal. S. , 1992b, *Astrophys. J.*, 398, 501
- Ghosh, K. K. & Soundararajaperumal. S. , 1992c, *Mon. Not. Roy. Astron. Soc.*, 259, 175

- Ghosh, K. K. & Soundararajaperumal. S. , 1993, *Astron. Astrophys.*, 273, 397
- Ghosh, K. K. & Soundararajaperumal. S., Kalai Selvi,M. & Sivarani,T, 1992,  
*Astron. Astrophys.*, 255, 119
- Ghosh, K. K. & Soundararajaperumal. S., 1991b, *Astrophys. J.*, 383, 574
- Ghosh, K. K. & Soundararajaperumal. S., 1992a, *Astrophys. J.*, 389, 179
- Ghosh, K. K. & Soundararajaperumal. S., 1992c, *Mon. Not. Roy. Astron. Soc.*, 254, 563
- Ghosh, K. K. & Soundararajaperumal. S., 1992f, *Pub. Astron. Soc. Pacific*, 104, 258
- Ghosh, K. K. & Soundararajaperumal. S., 1995, *Astrophys. J. Suppl.*, 100, 37
- Giacconi, R. 1976, *Am. J. Phys.* 44, 121
- Giacconi, R., & Colomb, F. R. 1988, *Astron. Astrophys. Suppl.*, 76, 15
- Giacconi, R., et al. 1974. *Astrophys. J. Suppl.*, 27, 34
- Giacconi, R., et al. 1979, *Astrophys. J.*, 230, 540
- Giommi, P., et al. 1986, *Astrophys. J.*, 303, 596
- Giommi, P., et al. 1987, *Astrophys. J.*, 322, 662
- Giommi, P., et al. 1990, *Astrophys. J.*, 356, 432
- Glass, I. S. 1985, *Mon. Not. Astron. Soc. S. Afr.*, 44, 60
- Goodrich, R. W. 1989, *Astrophys. J.*, 342, 224
- Grandi, P., et al. 1992, *Astrophys. J. Suppl.*, 82, 93
- Greenstein, J. L., & Matthews, T. A. 1963, *Nature*, 197, 1041
- Griffiths, R. E., et al. 1989, *Mon. Not. Roy. Astron. Soc.*, 240, 33
- Guilbert, P. W., Rees, M. J. 1988, *Mon. Not. Roy. Astron. Soc.*, 233, 475
- Halpern, J. P., et al. 1986, *Astrophys. J.*, 302, 711
- Halpern, J. P., et al. 1991, *Astron. J.*, 101, 818
- Hartman, R. C. 1997, *private communication*
- Hartman, R. C. et al. 1993, *AIP Conf. Proc.* 304, 563
- Hayakawa, S., 1991, *Nature*, 351, 214
- Hayes, M. J. C., et al. 1981, *Space Sci. Rev.* 30, 39
- Hayes, M. J., C., Culhane, J.L., & Bell Burnell,S. J. 1980, *Mon. Not. Roy. Astron. Soc.*, 192, 1p
- Hazard, C., et al. 1963, *Nature*, 197, 1037
- Heckman, T. M. , et al. 1990, *Astrophys. J. Suppl.*, 74, 833

- Heiles, C. 1975, *Astron. Astrophys. Suppl.*, 20, 37
- Hewitt, A., & Burbidge, G., 1993, *Astrophys. J. Suppl.*, 87, 451
- Holt, S. S., et al. 1989, in , in 'Proc. 23rd ESLAB Symp. on Two Topics in X-ray Astronomy. ESA SP-296, ESA, Noordwijk (eds. J. Hunt, & B. Battrick), p1105
- House, L. L. 1968, *Astrophys. J.*, 154, 1172 (suppl.)
- Hummel, E. 1981, *Astron. Astrophys.*, 93, 91
- Impey, C. D. 1987, in 'Superluminal Radio Sources', Proc. of a workshop in honour of Prof. Marshall H. Cohen, held at Big Bear Solar Obs., California, USA, 28-30 Oct.1986 (eds. J. A. Zensus et al.: Cambridge University Press), p 231
- Impey, C. D., & Neugebauer, G. 1988, *Astron. J.*, 95, 307
- Impey, C. D., & Tapia, S. 1988, *Astrophys. J.*, 333, 666
- Jannuzi, B. T., Smith, P. S., & Edelson, R. 1994, *Astrophys. J.*, 428, 130
- Jennison, R. C., & Das Gupta, M. K. 1953, *Nature*, 172, 996
- Jones, T. W., & O'Dell, S. L. 1977, *Astrophys. J.*, 215, 236
- Jones, T., et al. 1974, *Astrophys. J.*, 188, 353
- Kaastra, J. S., Kunieda, H., & Awaki, H. 1991, *Astron. Astrophys.*, 242, 27
- Kawai, N., Bregman, J. N., & Matsuoka, M. 1989, 'Proc. 23rd ESLAB Symp. on Two Topics in X-ray Astronomy. ESA SP-296, ESA, Noordwijk (eds. J. Hunt, & B. Battrick), p 957
- Kennicutt, R. C., et al. 1986, *Astrophys. J.*, 306, 130
- Kinman, T. D. 1975, in Variable Stars and Stellar Evolution, ed. E. Sherwood & L. Plaut (Boston:Reidel), p 573
- Kniffen, D. A., et al. 1994, in Frontiers of Space and Ground-Based Astronomy (eds W.Wamsteker et al.: Kluwer Academic Publishers), p5
- Konigl, A. 1981, *Astrophys. J.*, 243, 700
- Kriss, G. A., Canizares, C. R., Ricker, G. R. 1980, *Astrophys. J.*, 242, 492
- Kriss, G., A., & Doxsey, R. 1983, *Pub. Astron. Soc. Pacific*, 95, 133
- Kristian, J., & Sandage, 1970, *Astrophys. J.*, 162, 391
- Krolik, J. H. & Begelman, M. 1986, *Astrophys. J.*, 308, L55
- Krolik, J. H. & Begelman, M. 1988, *Astrophys. J.*, 329, 702
- Krolik, J. H., & Kallmann, T. R. 1987, *Astrophys. J.*, 320, L5

- Kruper, J. S., et al. 1990, *Astrophys. J. Suppl.*, 74, 347
- Kuhr, H., et al. 1981a, *Astron. J.*, 86, 854
- Kuhr, H., et al. 1981b, *Astron. Astrophys. Suppl.*, 45, 367
- Kunieda, H., et al. 1990, *Nature*, 345, 789
- Lampton, M., Margon, B., & Bowyer, S. 1976, *Astrophys. J.*, 208, 177
- Landau, R., Epstein, E. E., & Rather, J. D. G. 1980, *Astron. J.*, 85, 363
- Landau, R., et al. 1983, *Astrophys. J.*, 268, 68
- Laor, A. 1991, *Astrophys. J.*, 376, 90
- Large, M. I., et al. 1981, *Mon. Not. Roy. Astron. Soc.*, 194, 1013
- Lawson, A. J., & Turner, M. J. L. 1997, *Mon. Not. Roy. Astron. Soc.*, 288, 920
- Lawson, A. J., et al. 1992, *Mon. Not. Roy. Astron. Soc.*, 259, 743
- Leahy, J. P., & Perley, R. A. 1995, *Mon. Not. Roy. Astron. Soc.*, 277, 1097
- Ledden, I. E., Aller, H. D., & Dent, W. A. 1976, *Nature*, 260, 752
- Ledden, J. E., & O'Dell, S. L. 1985, *Astrophys. J.*, 298, 630
- Leighly, K. M., et al. 1989, in 'Proc. 23rd ESLAB Symp. on Two Topics in X-ray Astronomy. ESA SP-296, ESA, Noordwijk (eds. J. Hunt, & B. Battrock), p 961
- Leonard, P. J. T. 1996, *Nature*, 383, 394
- Liang, R. A. 1988, *Nature*, 331, 149
- Lightman, A.P. & White, T. R. 1988, *Astrophys. J.*, 335, 57
- Lynden-Bell, D. 1969, *Nature*, 223, 690
- Maccacaro, T., Garilli, B., & Mereghetti, S. 1987, *Astron. J.*, 93, 1484
- Maccagni, D., et al. 1987, *Astron. Astrophys.*, 178, 21
- Maccagni, D., et al. 1989, in BL Lac Objects, ed. L. Maraschi, T. Maccacaro, & M. H. Ulrich (Berlin: Springer), p 281
- MacDonald, G.H., Kenderdine, S., & Neville, A.C. 1968, *Mon. Not. Roy. Astron. Soc.*, 236, 39P
- Mackay, C. D. 1986, *Ann. Rev. Astron. Astrophys.*, 24, 255
- MacLeod, J. M., Andrew, B.H., & Harvey, G. A. 1976, *Nature*, 260, 751
- Makino, F., 1989, in 'Proc. 23rd ESLAB Symp. on Two Topics in X-ray Astronomy. ESA SP-296, ESA, Noordwijk (eds. J. Hunt, & B. Battrock), p 803
- Makino, F., et al. 1997, *IAU Circ.* 6702

- Makino, F., et al., 1987, *Astrophys. J.*, 313, 662
- Makino, F., et al., 1989, *Astrophys. J. Lett.*, 347, 9
- Makino, F., et al., 1991, in *Variability of Active Galactic Nuclei*, ed. H. Richard Miller & Paul J. Wiita (Cambridge: Cambridge Univ. Press), p 13
- Makishima, K. 1986, In 'The Physics of Accretion onto Compact Objects' (eds. K. O. Mason, M.G. Watson, N. E. White), (Berlin: Springer-Verlog), p249
- Malaguti, G., Bassani, L., Caroli, E. 1994, *Astrophys. J. Suppl.*, 94, 517
- Malkan, M. A. & Sargent, W. L. W. 1982, *Astrophys. J.*, 254, 22
- Malkan, M. A., Alloin, D., & Shore, S. 1989, in 'Exploring the Universe with the IUE Satellite' (ed. Y. Kondo : Dordrecht:Reidel) p 753
- Manzies, J. W., Feast, M. W. 1983, *Mon. Not. Roy. Astron. Soc.*, 203, 1p
- Marar, T. M. K. 1996, in 'Proc. of the International Colloq. on Perspectives in High Energy Astron. & Astrophys.' , TIFR, Mumbai, India, Aug 12-17, 1996, (eds: P. C. Agrawal & P. R. Vishvanath : Universities Press) p150
- Maraschi, L., et al. 1991, *Astrophys. J.*, 368, 138
- Markarian, B. E. 1969, *Astrophys.*, 5, 286
- Markarian, B. E., & Lipovetsky, V. A. 1971, *Astrophys.*, 7, 299
- Markarian, B. E., & Lipovetsky, V. A. 1972, *Astrophys.*, 8, 89
- Markarian, B. E., & Lipovetsky, V. A. 1976, *Astrophys.*, 12, 241
- Marscher, A. P. 1988, *Astrophys. J.*, 334, 552
- Marshall, F. E. et al. 1978, *Nature*, 275, 624
- Marshall, F. E. et al. 1979, *Astrophys. J. Suppl.*, 40, 657
- Marshall, F. E. et al. 1993, *Astrophys. J. Lett.*, 414, L27
- Marshall, N. et al. 1981, *Mon. Not. Roy. Astron. Soc.*, 194, 987
- Matt, G., et al. 1992, *Astron. Astrophys.*, 257, 63
- Matt, G., Perola, G. C. & Piro, L. 1991, *Astron. Astrophys.*, 247, 27
- Mayer-Hasselwander, H. A. 1996, in 'Proc. of the International Colloq. on Perspectives in High Energy Astron. & Astrophys.' TIFR, Mumbai, India, Aug 12-17, 1996, (eds. P. C. Agrawal & P. R. Vishvanath : Universities Press) p169
- McAlary, C. W., et al. 1983, *Astrophys. J. Suppl.*, 52, 341

- McHardy, I. M. 1989, in 'Proc. 23rd ESLAB Symp. on Two Topics in X-ray Astronomy. ESA SP-296, ESA, Noordwijk (eds. J. Hunt, & B. Battrock), p111
- McHardy, I. M., et al. 1981, *Mon. Not. Roy. Astron. Soc.*, 197, 893
- Mead, A.R.G., et al. 1990, *Astron. Astrophys. Suppl.*, 83, 183
- Miller, J. S., & Goodrich, B. F. 1990, *Astrophys. J.*, 355, 456
- Miller, J. S., French, H. B., & Hawley, S. A., 1978, in Pittsburgh Conf. on BL Lac objects, ed. M. Wolfe (Pittsburgh: Univ. of Pittsburgh Press), p176
- Moore, R. L., & Stockman, H. S. 1981, *Astrophys. J.*, 243, 60
- Moore, R. L., & Stockman, H. S. 1984, *Astrophys. J.*, 279, 465
- Morini, M., et al. 1986, *Astrophys. J. Lett.*, 306, 71
- Morris, S. L., et al. 1991, *Astrophys. J.*, 380, 49
- Morrison, R. & McCammon, D. 1983, *Astrophys. J.*, 270, 119
- MPE Report 1992, (Max-Planck-Institut Fur Extraterrestrische Physik : MPE Report 240, September 1992) p 61
- Mufson, S. L., et al. 1984, *Astrophys. J.*, 285, 571
- Mukherjee, R., et al. 1996, *Astrophys. J.*, 470, 831
- Murakami, T., et al. 1988, *Nature*, 335, 234
- Mushotzky, R. F. 1984, *Adv. Space Res.*, 3, 157
- Mushotzky, R. F., Done, C., & Pounds, K. A. 1993, *Ann. Rev. Astron. Astrophys.*, 31, 717
- Mushotzky, R. F., et al. 1976, *Astrophys. J. Lett.*, 206, 45
- Mushotzky, R. F., et al. 1978, *Astrophys. J.*, 226, 65
- Mushotzky, R. F., et al. 1995, *Mon. Not. Roy. Astron. Soc.*, 272, L9
- Mutel, R. L. 1989, in NRAO Parsec-Scale Radio Jet Workshop (Socorro)
- Nandra, K., & Pounds, K. A. 1994, *Mon. Not. Roy. Astron. Soc.*, 268, 405
- Nandra, K., et al. 1997, *Astrophys. J.*, 477, 602
- Nandra, K., Pounds, K. A., & Stewart, G. C. 1990, *Mon. Not. Roy. Astron. Soc.*, 242, 660
- Netzer, H. 1990, Lecture Notes 1990, Swiss Society for Astrophysics and Astronomy (eds. T.J.-L. Courvoisier & M. Mayor : Springer-Verlog), p57
- Neugebauer, G., et al. 1984, *Astrophys. J.*, 278, L1
- Neugebauer, G., et al. 1986, *Astrophys. J.*, 308, 815

- Norman, C., & Scoville, N. 1988, *Astrophys. J.*, 332, 124
- O'Dea, C. P., Barvainis, R., & Challis, P. M. 1988, *Astron. J.*, 96, 435
- O'Dell, S. L., et al. 1978, *Astrophys. J.*, 219, 818
- Oda, M. 1994, in *Frontiers of Space and Ground-Based Astronomy* (eds W. Wamsteker et al.: Kluwer Academic Publishers), p53
- Oke, J. B., Readhead, A. C. S., & Sargent, W. L. W. 1980, *Pub. Astron. Soc. Pacific*, 92, 758
- Osmer, P. S., Smith, M. G., & Weedman, D. W. 1974, *Astrophys. J.*, 189, 187
- Osterbrock, D. E. 1977, *Astrophys. J.*, 215, 733
- Osterbrock, D. E., & De Robertis, M. M. 1985, *Pub. Astron. Soc. Pacific*, 97, 1129
- Osterbrock, D. E., Koski, A. T., & Philips, M. M. 1975, *Astrophys. J. Lett.*, 197, 41
- Osterbrock, D. E., Koski, A. T., & Philips, M. M. 1976, *Astrophys. J.*, 206, 898
- Owen, F. N., Spangler, R., & Cotton, W. D. 1980, *Astron. J.*, 85, 351
- Padovani, P., & Urry, C. M. 1992, *Astrophys. J.*, 387, 449
- Paul, B., et al. 1997, *Astron. Astrophys.*, 320, L37
- Pauliny-Toth, I. I. K., & Kellermann, K. I. 1968, *Astron. J.*, 73, 953
- Pauliny-Toth, I. I. K., & Kellermann, K. I. 1972, *Astron. J.*, 77, 797
- Pauliny-Toth, I. I. K., et al. 1972, *Astron. J.*, 77, 265
- Penfold, J. E. 1979, *Mon. Not. Roy. Astron. Soc.*, 186, 297
- Perley, R. A. 1982, *Astron. J.*, 87, 859
- Perlman, E. S., & Stocke, J. T. 1993, *Astrophys. J.*, 406, 430
- Peterson, B. M. 1988, *Pub. Astron. Soc. Pacific*, 100, 18
- Peterson, B. M. 1993, *Pub. Astron. Soc. Pacific*, 105, 247
- Peterson, B. M., et al. 1994, *Astrophys. J.*, 425, 622
- Petre, R., et al. 1984, *Astrophys. J.*, 280, 499
- Pian, E., et al. 1998, *Astrophys. J. Lett.*, 492, L17
- Pica, A. J., et al. 1980, *Astron. J.*, 85, 1142
- Pica, A. J., et al. 1988, *Astron. J.*, 96, 1215
- Piro, L., Yamauchi, M., & Matsuoka, M. 1990, *Astrophys. J. Lett.*, 360, 35
- Planck, M. 1901, *Ann. Physik*, 4, 533
- Pohl, M., et al. 1995, *Astron. Astrophys.*, 303, 383

- Porcas, R. W., in 'Superluminal Radio Sources', Proc. of a workshop in honour of Prof. Marshall H. Cohen, held at Big Bear Solar Obs., California, USA, 28-30 Oct.1986 (eds. J. A. Zensus et al.: Cambridge University Press), p 12
- Pounds, K. A. 1989, in 'Proc. 23rd ESLAB Symp. on Two Topics in X-ray Astronomy. ESA SP-296, ESA, Noordwijk (eds. J. Hunt, & B. Battrock), p753
- Pounds, K. A., et al. 1989, *Mon. Not. Roy. Astron. Soc.*, 240, 769
- Pounds, K. A., et al. 1990, *Nature*, 344, 132
- Preuss, E., & Fosbury, R. A. E. 1983, *Mon. Not. Roy. Astron. Soc.*, 204, 783
- Puschell, J. J. 1981, *Astron. J.*, 86, 16
- Qian, S. J., et al. 1991, *Astron. Astrophys.*, 241, 15
- Quin et al. 1996, *Astrophys. J. Lett.*, 456, 83
- Ramsey, B. D., in 'Proc. of the International Colloq. on Perspectives in High Energy Astron. & Astrophys.' TIFR, Mumbai, India, Aug 12-17, 1996, (eds. P. C. Agrawal & P. R. Vishvanath : Universities Press), p 336
- Rao, A. R., et al. 1997, Submitted to *Astron. Astrophys.*
- Recondo-Gonzalez, M. C., et al. 1997, *Astron. Astrophys. Suppl.*, 121, 461
- Rees, M. J. 1966, *Nature*, 211, 468
- Rees, M. J. 1971, *Nature*, 229, 312
- Rees, M. J. 1984, *Ann. Rev. Astron. Astrophys.*, 22, 471
- Rees, M. J., et al. 1969, *Nature*, 223, 788
- Reichert, G. A., et al. 1985, *Bull. Am. Astron. Soc.*, 17, 578
- Remillard, R. A., et al. 1989, *Astrophys. J.*, 345, 140
- Reynolds, C. S. & Fabian, A. C. 1997, *Mon. Not. Roy. Astron. Soc.*, 290, L1
- Reynolds, C. S. 1997, *Mon. Not. Roy. Astron. Soc.*, 286, 513
- Rich, et al. 1984, *Astrophys. J.*, 286, 517
- Rieke, G. H., et al. 1976, *Nature*, 260, 754
- Rodriguez-Pascual, P. M. et al. 1997, *Astrophys. J. Suppl.*, 110, 9
- Roelling, T. L., et al. 1986, *Astrophys. J.*, 304, 646
- Ross, R. R., & Fabian. A. C. 1993, *Mon. Not. Roy. Astron. Soc.*, 261, 74
- Rush, B., et al. 1996, *Astrophys. J.*, 471, 190



- Rybicki, G. B., & Lightman, A. P. 1979, 'Radiation Processes in Astrophysics', (Wiley-Interscience Publication)
- Sambruna, R. M., et al. 1993, *Astrophys. J.*, 408, 452
- Sandage, A. 1960, *Sky and Telescope*, 21, 148
- Sandage, A., & Tammann, G. A. 1981, 'A Revised Shapley-Ames Catalog of Bright Galaxies (Washington, D. C.: Carnegie Institution of Washington), p 34
- Santos-Lleo, M., Ghosh, K. K., Soundararajaperumal. S., et al. 1997, *Astrophys. J. Suppl.*, 112, 271
- Schiels, G. A. 1978, *Nature*, 272, 706
- Schmidt, M. 1963, *Nature*, 197, 1040
- Schmidt, M. 1968, *Nature*, 218, 663
- Schneider, D. P., Schmidt, M., & Gunn, J. E. 1989a, *Astron. J.*, 98, 1507
- Schneider, D. P., Schmidt, M., & Gunn, J. E. 1989b, *Astron. J.*, 98, 1951
- Schneider, D. P., et al. 1991, *Bull. Am. Astron. Soc.*, 23, 1450
- Sembay, S., et al. 1985, *Mon. Not. Roy. Astron. Soc.*, 216, 121
- Seyfert, C. K. 1943, *Astrophys. J.*, 97, 28
- Shafer, R. A., Haberl, F., Arnaud, K. A., & Tennant, A. F. 1991, esa TM-09, 'XSPEC User's Guide', (ESA:Noordwijk)
- Shakura, N.I., & Sunyaev, R. A. 1973, *Astron. Astrophys.*, 24, 337
- Shimmins, A. J., & Bolten, J. G. 1972, *Aust. J. Phys. Astrophys. Suppl.*, 23, 1
- Shimmins, A. J., & Bolten, J. G. 1974, *Aust. J. Phys. Astrophys. Suppl.*, 32, 1
- Shuder, J. M., & Osterbrock, D. E. 1981, *Astrophys. J.*, 250, 55
- Siemiginowska, A., & Elvis, M. 1994, *Astrophys. J. Suppl.*, 92, 603
- Sillanpaa, A., et al. 1988, *Astrophys. J.*, 325, 628
- Simkin, S. M., Su, H. J., & Schwarz, M. P. 1980, *Astrophys. J.*, 237, 404
- Singh, K. P., Rao, A. R., & Vahia, M. N. 1990, *Astrophys. J.*, 365, 455
- Sitko, L. M. 1989, in BL Lac Objects, eds. L. Maraschi, T. Maccacaro, & M. H. Ulrich (Berlin:Springer), p 119
- Sitko, L. M., & Junkkarinen, V. T. 1985, *Pub. Astron. Soc. Pacific*, 97, 1158
- Smith, F. G., & Hoffleit. 1963, *Nature*, 198, 650

- Smith, P. S., et al. 1987, *Astrophys. J. Suppl.*, 64, 459
- Soltan, A. 1982, *Mon. Not. Roy. Astron. Soc.*, 200, 115
- Stark, J. P., Bell Burnell, S. J., & Culhane, J. L. 1978, *Mon. Not. Roy. Astron. Soc.*, 182, 23p
- Stark, J. P., et al. 1992, *Astrophys. J. Suppl.*, 79, 77
- Staubert, R., et al. 1986a, *Astron. Astrophys.*, 162, 16
- Staubert, R., et al. 1986b, *Astrophys. J.*, 310, 694
- Stein, W. A., 1978, in Pittsburgh Conf. on BL Lac objects, ed. A. M. Wolfe (Pittsburgh: Univ. of Pittsburgh Press), p 328
- Stein, W. A., O'Dell, S. L., & Strittmatter, P. A. 1976, *Ann. Rev. Astron. Astrophys.*, 14, 173
- Steppe, H., et al. 1988, *Astron. Astrophys. Suppl.*, 75, 317
- Stetson, P. B. 1987, *Pub. Astron. Soc. Pacific, Bull. Am. Astron. Soc.* 19, 745
- Stetson, P. B. 1990, *Pub. Astron. Soc. Pacific*, 102, 654
- Stickel, M., et al. 1991, *Astrophys. J.*, 374, 431
- Stoche, J. T., et al. 1985, *Astrophys. J.*, 298, 619
- Stoche, J. T., et al. 1988, in Optical Surveys for Quasars, eds. P. Osmer, et al. (San Francisco:ASP), p 311
- Stoche, J. T., et al. 1990, *Astrophys. J.*, 348, 141
- Stoche, J. T., et al., 1989, in BL Lac Objects, eds. L. Maraschi, T. Maccacaro, & M. H. Ulrich (Berlin:Springer), p 209
- Strittmatter, P. A., et al. 1974, *Astrophys. J.*, 190, 509
- Tadhunter, C. N., Perez, E., & Fosbury, R. A. E. 1986, *Mon. Not. Roy. Astron. Soc.*, 219, 555
- Taylor, B. G., et al. 1981, *Space Sci. Rev.*, 30, 479
- Takalo, L. O. 1994, *Vistas in Astron.*, 38, 77
- Tanaka, Y., et al. 1995, *Nature*, 375, 659
- Tananbaum, H., et al. 1978, *Astrophys. J.*, 223, 74
- Tau, et al. 1996, *Science*, 271, 142
- Tennant, A. F., & Mushotzky, R. F. 1983, *Astrophys. J.*, 264, 92
- Treves, A., et al. 1989, *Astrophys. J.*, 341, 733
- Trumper, J. 1994, in Frontiers of Space and Ground-Based Astronomy (eds W. Wamsteker et al.: Kluwer Academic Publishers), p 47

- Tsunemi, H., et al. 1989, *Pub. Astron. Soc. Jap.*, 41, 391
- Tucker, W., et al. 1973, *Astrophys. J.*, 180, 715
- Turner, T. J., & Pounds, K. A. 1989, *Mon. Not. Roy. Astron. Soc.*, 240, 833
- Turner, T. J., et al. 1981, *Space Sci. Rev.* 30, 513
- Turner, T. J., et al. 1989, in 'Proc. 23rd ESLAB Symp. on Two Topics in X-ray Astronomy. ESA SP-296, ESA, Noordwijk (eds. J. Hunt, & B. Battrick), p 769
- Turner, T. J., et al. 1990, *Mon. Not. Roy. Astron. Soc.*, 244, 310
- Turner, T. J., et al. 1993, *Astrophys. J.*, 419, 127
- Ulmer, M. P., et al. 1983, *Astrophys. J. Lett.*, 270, 1
- Ulrich, M. H. 1990, in "Structure and Emission Properties of Accretion Disks", Proc. of the 6th IAP Meeting/IAU Colloquium No. 129 Paris, 2-6 July 1990 (eds. C. Bertout et al.) p 43
- Ulrich, M. H., et al. 1975, *Astrophys. J.*, 198, 261
- Ulvestad, J. S., & Wilson, A. S. 1984, *Astrophys. J.*, 285, 439
- Ulvestad, J. S., Johnston, K. J., & Weiler, K. W. 1983, *Astrophys. J.*, 266, 18
- Urry, C. M., & Padovani, P. 1995, *Pub. Astron. Soc. Pacific*, 107, 803
- Urry, C. M., et al. 1987, in 'Variability of Galactic & Extragalactic X-ray sources' (ed. A. Treves), Associazione per l'Avanzamento dell' Astronomia, p15
- Urry, C. M., et al. 1989, in 'Proc. 23rd ESLAB Symp. on Two Topics in X-ray Astronomy. ESA SP-296, ESA, Noordwijk (eds. J. Hunt, & B. Battrick), p 789
- Urry, C. M., Maraschi, L., & Phinney, S. E. 1991a, *Comm. Ap.*, 15, 111
- Urry, C. M., Mushotzky, R. F., & Holt, S. S. 1986, *Astrophys. J.*, 305, 369
- Urry, C. M., Padovani, P., & Stickel, M. 1991b, *Astrophys. J.*, 382, 501
- Urry, C. M., & Shafer, R.A. 1984, *Astrophys. J.*, 280, 569
- Valtaoja, L., et al. 1991, *Astron. J.*, 101, 78
- van Groningen, E., & de Bruyn, A. G. 1989, *Astron. Astrophys.*, 211, 293
- Veilleux, S., & Zheng, W. 1991, *Astrophys. J.*, 377, 89
- Veron-Cetty, M. P., Veron, P., & Tarengi, M. 1982, *Astron. Astrophys.*, 113, 46
- Veron-Cetty, M. P., & Veron, P. 1993, A Catalog of Quasars and Active Nuclei (6th ed.); ESO Sci. Rep. 5; Garching: ESO)
- von Montigny, et al. 1995a, *Astrophys. J.*, 440, 525

- Von Montigny, et al. 1995b, *Astron. Astrophys.*, 299, 680
- Vrtilek, J. M., & Carleton, N. P. 1985, *Astrophys. J.*, 284, 106
- Wagner, S. J., & Witzel, A. 1995, *Ann. Rev. Astron. Astrophys.*, 33, 163
- Walker, M. F., & Chincarini, G. 1967, *Astrophys. J.*, 147, 416
- Wall, J. V., et al. 1975, *Aust. J. Phys. Astrophys. Suppl.*, 34, 55
- Wall, J. V., et al. 1986, *Mon. Not. Roy. Astron. Soc.*, 219, 23P
- Wallinder, F. H., et al. 1992, *Astron. Astrophys. Rev.*, 4, 79
- Walter, R., & Fink, H. H. 1993, *Astron. Astrophys.*, 274, 105
- Wamsteker, W., & Colina, L. 1986, *Astrophys. J.*, 311, 617
- Wamsteker, W., et al. 1997, *Mon. Not. Roy. Astron. Soc.*, 288, 225
- Ward, M., et al. 1987, *Astrophys. J.*, 315, 74
- Wardle, J. F. C., & Roberts, D. H. 1988, *IAU Symposium* 124, 143
- Webb, J. R., et al. 1988, *Astron. J.*, 95, 374
- Weedman, D. W. 1973, *Astrophys. J.*, 183, 29
- Weedman, D. W. 1986, 'Quasar Astronomy', Cambridge Astrophysics Series, Cambridge University Press
- Weiler, K. W., & Johnston, K. J. 1980, *Mon. Not. Roy. Astron. Soc.*, 190, 269
- West, R. M. 1979, *IAU Circ.*, No. 3415
- West, R. M., Grosbol, P., Sterken, C. 1980, *ESO preprint* No. 101
- White, N. E., & Giommi, P. 1991, in *Database and On-line Data in Astronomy*, eds. D. Egret & M. Albrecht (Dordrecht:Kluwer), p 11
- White, N. E., & Peacock, A. 1988, *Mem. Soc. Astron. Ital.*, 59, 7
- Wilkes, B. J. 1986, *Mon. Not. Roy. Astron. Soc.*, 218, 331
- Wilkes, B. J., & Elvis, M. 1987, *Astrophys. J.*, 323, 243
- Wilkes, B. J., et al. 1989, in 'Proc. 23rd ESLAB Symp. on Two Topics in X-ray Astronomy. ESA SP-296, ESA, Noordwijk (eds. J. Hunt, & B. Batrick), p1081
- Wills, D., & Wills, B. J. 1976, *Astrophys. J. Suppl.*, 31, 143
- Winkler, P., & White, A. 1975, *Astrophys. J.*, 199, L139
- Wierick, G., Westerlund, B., & Garnier, R. 1979, *Astron. Astrophys.*, 72, 277

- Wolfe, A. M., 1978, in Pittsburgh Conf. on BL Lac objects, ed. A. M. Wolfe  
(Pittsburgh: Univ. of Pittsburgh Press), p 1
- Wolter, A., et al. 1994, *Astrophys. J.*, 433, 29
- Woltjer, L. 1990, in Lecture Notes 1990, Swiss Society for Astrophysics and Astronomy (eds.  
T.J.-L. Courvoisier & M. Mayor : Springer-Verlog), p 1
- Wood, K. S., et al. 1984, *Astrophys. J. Suppl.*, 56, 507
- Worrall, D. M., et al. 1984a, *Astrophys. J.*, 278, 521
- Worrall, D. M., et al. 1984b, *Astrophys. J.*, 286, 711
- Worrall, D. M., et al. 1987, *Astrophys. J.*, 313, 596
- Yaqoob, T., Warwick, R. S., & Pounds, K. A. 1989, *Mon. Not. Roy. Astron. Soc.*, 236, 153
- Zamorani, G., et al. 1981, *Astrophys. J.*, 245, 357
- Zensus, J. A. 1989, in BL Lac Objects, ed. L. Maraschi, T. Maccacaro, & M. H. Ulrich  
(Berlin: Springer), p 3
- Zhang, Y. F., et al. 1994, *Astrophys. J.*, 432, 91
- Zheng, W., et al. 1995, *Astron. J.*, 109, 2355